University of Strathclyde

Department of Physics

Characterising Computational Models and Evaluation Methods: Using Macroscopic Quantities to Gain Confidence in Microscopic Phenomena

by

Tom Kirchner

A thesis presented in fulfilment of the
requirements for the degree of

Doctor of Philosophy

2013

This thesis is the result of the author's original research. It has been composed by the author and has not been previously submitted for examination which has led to the award of a degree.

Signed:  Date: July 5, 2013

Acknowledgements

I wish to thank Professor Maxim V. Fedorov for giving me the opportunity to perform research at the German Max-Planck-Institute for Mathematics in the Sciences and the Institute of Physics at the University of Strathclyde, the British University of the Year 2012/13. I appreciate his advice and support.

This work is part of an industrial collaboration of the University of Strathclyde and Schlumberger Limited: The Schlumberger Grant "Molecular Simulations of Aqueous Salt Solutions" by the Schlumberger R&D Institute in Daharan, Saudi Arabia. I want to thank my collaborators from Schlumberger: Wael Abdallah, Aldi Asmadi and Stephen Dyer. Special thanks goes to Mikhail Stukan for introducing me to the field of polarizable force fields and his guidance during the project.

I thank my colleagues Andrey Frolov, Nikolaj Georgi, Vladislav Ivaništšev, Ekaterina Ratkova, Anastasia Romanova and Volodymyr Sergiievskyi for fruitful discussions.

This work wouldn't have been possible without super computing facilities. I acknowledge the supercomputing support from the von Neumann-Institut für Computing, FZ Jülich (Project ID ESMI11). Additional computing power was provided by the Academic and Research Computer Hosting Industry and Enterprise in the West of Scotland, ARCHIE-WeSt. Moreover I thank the Max Planck Institut für Mathematik in den Naturwissenschaften and the whole administrative and EDV team for hospitality during the stay there and for access to the local computing facilities. This work was supported by Grant FE 1156/2-1 of the Deutsche Forschungsgemeinschaft (DFG), which I want to acknowledge for the high standards of parental rights and the support they provide.

I want to thank my my parents, my siblings, my grandparents and my whole family for their patience and confidence.

Most of all, I wish to thank my wife Kathleen for all of her support throughout my PhD and my son Sebastian for the countless hours of joy and for pulling me home from work.

Contributions

This work would not have been possible without the assistance from other scientists. Here we want to acknowledge these contributions.

Simulation Setup and Parameter Mikhail Stukan from Schlumberger Limited contributed the force field parameter of the SW10e water model and provided initial simulation parameter for the first simulations. In addition, he prepared the modification of the Gromacs code to allow osmotic pressure simulations using the membrane method. We profited from the experience of Mikhail Stukan when simulating the surface tension, as he provided us with the results of his rigorous system tests.

NaRIBaS - a Sophisticated Tool for Automatising Simulations During the work on the thesis, numerous simulations were performed. The calculation of the hydration free energy required for example hundreds of simulations to be processed, most of them similar in the setup apart from one or two single parameters. Usually in such cases, self written scripts are used to do most of the work. However, they have the disadvantage to be very specific in their tasks.

In this work, simple automatised scripts are replaced by a more general task managing framework using template data files, parameter lists and directory trees. Still, this framework is specifically build for the calculation of hydration free energies and potential of mean force functions with Gromacs.

The concept was used by Kathleen Kirchner and vastly developed, creating the simulation framework NaRIBaS – A scripting framework for computational modelling of Nanomaterials and Room Temperature Ionic Liquids in Bulk and Slab [1]. The main task of NaRIBaS is the automatised handling of simulation files, but in a much more general and powerful way. The structure allows every computational scientist to adapt the framework to his specific problem of data creation and evaluation in a fast and efficient manner.

This work highly profited from the use of the NaRIBaS framework. Recently, it finished its alpha status and opened for public, see

`http://sourceforge.net/projects/naribas/`.

Abstract

Polarizable force fields are a new and promising way of modelling water solutions using molecular dynamic computer simulations. In this work, we discuss the general workflow of characterising new water and ion models and apply this scheme on the SW10e water model with polarizable ions. We thereby investigate several physico-chemical properties in terms of physical meaningfulness, experimental characteristics, simulation methods and performance of the polarizable model under test, namely the density, hydration enthalpy and Gibbs free energy, structural properties, residence time, the potential of mean force, surface tension and the osmotic pressure.

Recently, the osmotic pressure was discovered as a new and reliable method to characterise the quality of a model for aqueous solutions. Therefore, we thoroughly investigated one computational way of calculating the osmotic pressure: the membrane method.

In a novel approach, we use the polarizability of ions to adjust the model to fit to experimental values at high salt concentrations. We are able to create a consistent ion and water model reproducing bulk properties and interfacial properties at low and high salt concentrations.

Graphical abstract

Developing a water-ion model for reproducing physico-chemical properties of high concentrated salt solutions at interfaces

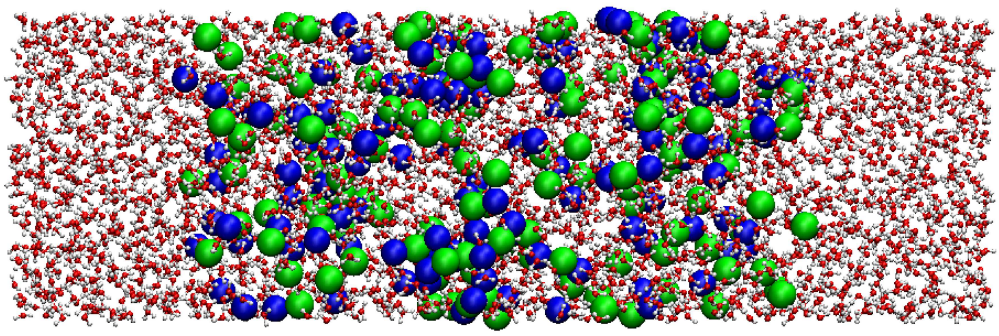

PART 1:
Understanding
Criterias and Methods

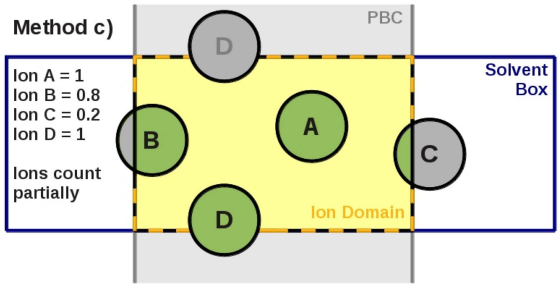

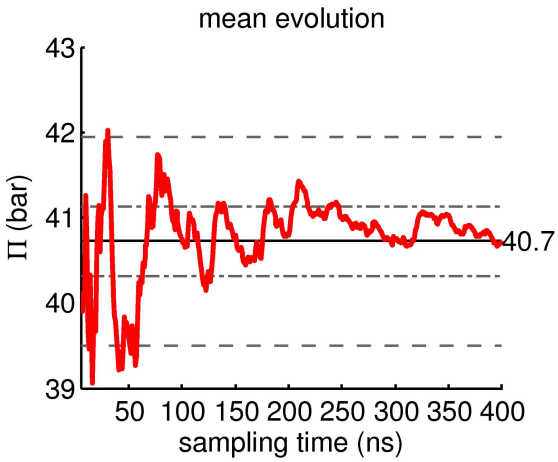

PART 2: Understanding the Model Parameter

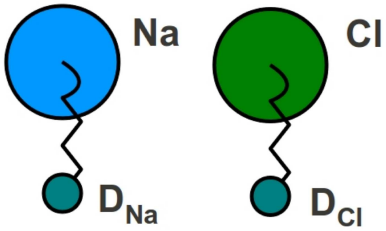

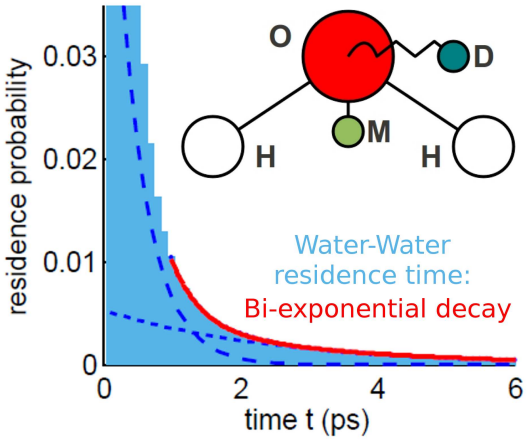

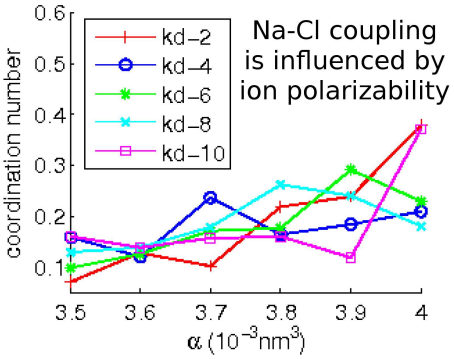

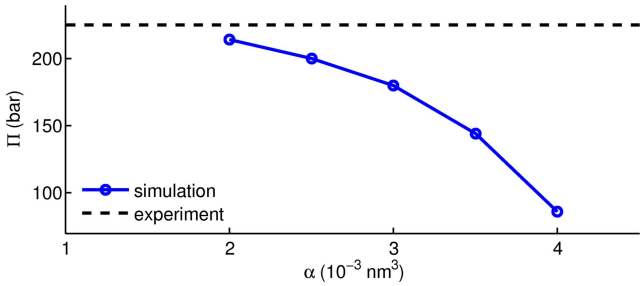

Variation of the Ion polarizability allows tuning of physical properties

PART 3: Tuning the model parameter

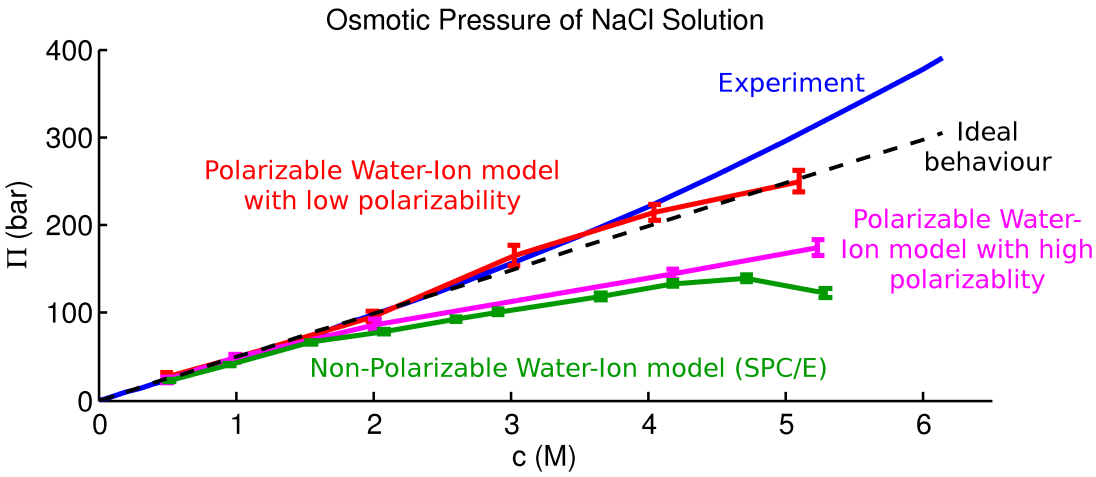

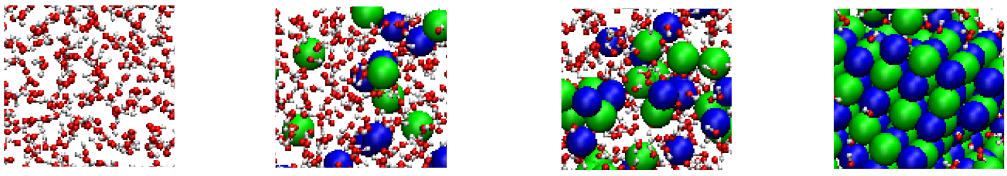

The polarizable Water-Ion Model SW10e with Ions modelled as Drude Oscillators is capable of reproducing interfacial properties of Brines.

Contents

Chapter 1

Introduction

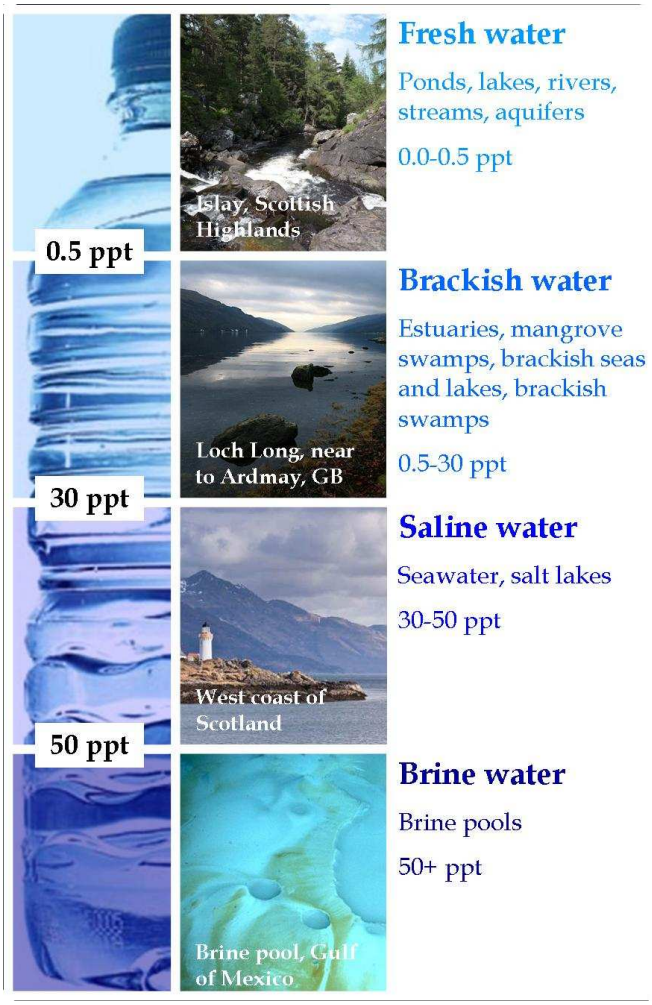

Figure 1.1: Salinity bottle with Scottish influence. From top to bottom the salt content increases. Starting with the world purest water, which can be found in the Scottish highlands.

1.1 Research Motivation: Water and Brines are a Source of Life - Understanding is Critical

Our introducing figure of a salinity bottle with Scottish influence represents a key substance in our daily life: Water and salty water or brine. Whereas Scotland is richly blessed with springs and rivers containing fresh water of high quality, the access to clean fresh water is critical in an emerging part of the world. Advances on purification and desalination processes are highly demanded [2, 3, 4]. New ways of general waste water treatment, desalination, water purification, but also power generation became applicable through the understanding of osmosis based effects - the movement of ions through membranes [5, 6].

Every year, considerable amounts of money are spent by governments and industrial concerns on improving existing application that include the treatment of sea water under normal and extreme conditions. Recently, a new approach for enhancing oil recovery rates involves the flooding of oil fields with desalinated water, which means brine that contains a lower salt content than normal sea water [7].

The influence of aqueous salt solutions on interfaces results in a wide range of phenomena including also chemical and biological applications such as osmosis in cells, micelle and membrane formation, protein folding, chemical separation, nano-particle formation, and interfacial polymerisation [8].

The driving physical phenomena for this large set of applications is concentrated in effects of hydrated ions at interfaces and hydrophobic segregation [9, 8, 10]. Molecules are either individually hydrated or found to combine into macromolecular structures [9]. The effects are microscopic in nature, thus measurements of macroscopic quantities do not resolve the microscopic origin of the observed effects [11, 12]. The surface tension is a sample macroscopic quantity, that varies under the inclusion of additives in pure water. As known for a long time, the precise measurement of the surface tension allows the usage of this physical quantity in quality control of chemical reactions and industrial processes. The presence of solvents or surfactants in liquids during chemical reactions can be monitored by continuous measuring of the surface tension. However, the knowledge of the surface tension itself does not lead to an understanding of the water and impurity structuring at the surface, that leads to the variation of the interfacial tension.

Experiments in the microscopic regime are often difficult, costly and/or inaccurate, and mostly not applicable under extreme conditions [13, 14]. Such

conditions occur in drill holes of offshore oil platforms, where very high pressures and temperatures are encountered. Especially in deep, oil rich and porous rock, experimental measurements are difficult to perform.

By using computer simulations we are able to reduce the number of participating interactions and possible artificial factors, thereby precisely analysing sub-parts of the whole and collecting pieces of the puzzle for the final picture [15]. Moreover, we can combine microscopic features of a system with macroscopic properties. Thereby we open new paths for tailoring application specific substances [16] or engineer new applications.

The hydrophobic effect is qualitatively well understood, however few theoretical approaches have been made to explain and quantify the assembly of hydrophobic molecules. This gap is to be filled by computer simulation of molecular models of the included species. These models are defined by the forces acting between the particles, coining the term force field. Results of computational experiments highly depend on the models they are founded on, in terms of accuracy and reliability. The development of such models requires a state-of-the-art knowledge of physical effects, simulation methods and quantum effects.

1.2 Problem Statement: The Current Molecular Description Fails to Reproduce Macroscopic Phenomena of Brines

The current force fields used in computational experiments for understanding aqueous solutions at interfaces are insufficient, as has been shown by several authors [17, 18]. The discrepancies are already apparent in the comparison of structural parameters such as water-water distribution functions with scattering structure factors from neutron and X-ray diffraction [17]. Indeed, the current set of water and ion models has been developed to reproduce bulk properties of water [19, 20, 21, 22, 23]. However, surface properties of water and brines are of major importance in a vast number of environments.

Water and ions at an interface are characterised by a distortion of their original boundary formed by the solution. Especially the inclusion of polarization effects in the water-ion models is considered as a useful approach in modelling their interfaces [18, 24].

Polarizable force fields are the state of the art in computational science using molecular dynamic simulations. The SWM4-NDP created by Lamoureux et al

[25] in conjunction with the ion force field developed by Yu et al [26] is the most recent. A number of recent publications [27, 28, 12, 29, 30] shows its great success.

Our goal is the further development of water and ion models to predict interfacial properties of brines. There is no well defined way to improve computational models. We will present a route to tackle this problem in the upcoming section.

1.2.1 Making Predictions of the Real World - on Developing and Testing Models

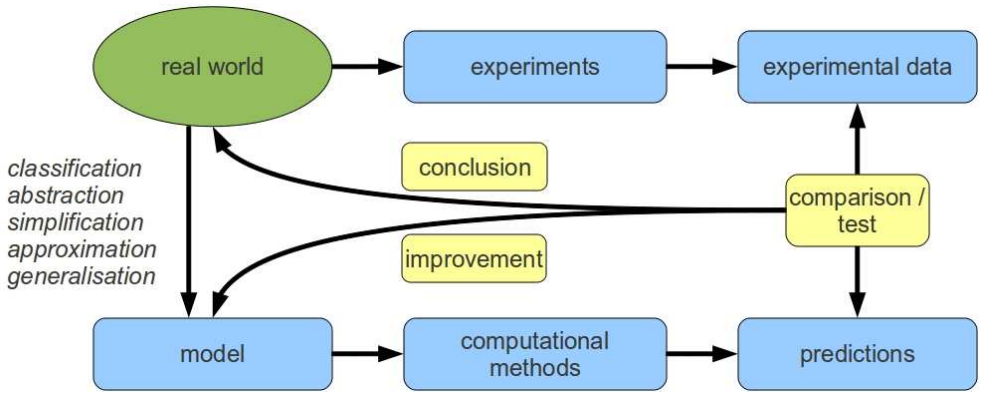

Figure 1.2: Flow-chart demonstrating the work of computational physics and chemistry by modelling the real world and comparing the predictions of the model with experimental data. The flow-chart is taken and modified from van Gunsteren and Berendsen [31].

The flow-chart presented in Fig. 1.2.1 shows the view of van Gunsteren and Berendsen on model development in computer simulation: A model is designed from the real world and predictions on the behaviour of the model are made by using computational methods. These predictions are compared with experimental data extracted by experiments on the real world. We want to expand the original scheme. First, by comparing experiments and predictions we are able to draw conclusions on the construction and working of the real world. Secondly, by the same way we can try to improve our computational model.

We already discussed the importance of computer simulations in modern science and the necessity to improve our computational models. When discussing model development, many scientists neglect the entity of the model with the computational methods in use and the interplay with the real world.

Models act as input for computational methods. An ion/water model might serve as input for various mathematical routines to treat the molecular interactions and allow conclusions on physical properties. Among the mathematical

routines, classical molecular dynamics based on solving Newton's equation of motion and integral equation theory based on the theory of Ornstein-Zernike are very popular [32]. The six-dimensional Ornstein-Zernike equation [33] can be reduced to a one-dimensional form, the 1D reference interaction site model (RISM) [34]. The RISM theory was expanded to 3D by Cortis et al [35] and recently, Sergiievsky et al [36, 37] developed an efficient multi-grid solver for the 3DRISM equation system. We tried to utilise this new method for the investigation of charged interfaces. As Kuharski and Chandler [38] note in their paper using the 1DRISM equation and the hypernetted-chain approximation, the method is not optimised for interfaces. The authors determined the coordination number of an artificially charged Iron ion in water and found a nearly linear dependency of the hydration number from the charge of the ion. The coordination number increased up to 15, which is unreasonable.

Our own tests with 3DRISM and charged surfaces revealed a similar behaviour: At high interaction energies, liquid densities increase unlimited. The discrepancies of the integral equation theory in conjunction with electrified interfaces make them at the current state not applicable. Thus, we choose to use more complex and expensive methods based on molecular dynamics simulations.

In a recent paper, Gereben and Pusztai [39] state the fact, that they are not able to find systematic data about the dependency of physical quantities on simulation parameter. The authors do not speak about a new model using a newly developed simulation method, but about the extensively used SPC/E water model and the well defined structure factor.

When reading recent publications about computational model development, it becomes apparent, that there is no general consensus about the way on how to quantify and test the model performance. For instance, whereas former model development concentrated on bulk properties of water and ion models at low concentrations, more recent publications discovered the importance of surface effects of high concentrated solutions [40, 41, 42, 30]. We want to give the reader an explanation on the route we choose to tackle the problem of model evaluation.

As in Fig. 1.2.1 indicated, we can choose from a wide variety of physicochemical properties to test our model. The first question to answer is the meaningfulness of the property. This step is mostly done unconsciously but a very important one. The answer strongly depends on the tasks of the model. If it should reproduce the dielectric properties of water we might want to look on the vibrational modes of the oxygen-hydrogen bonds. If our model is rigid or adapted to other properties, we cannot expect it to well reproduce vibrational

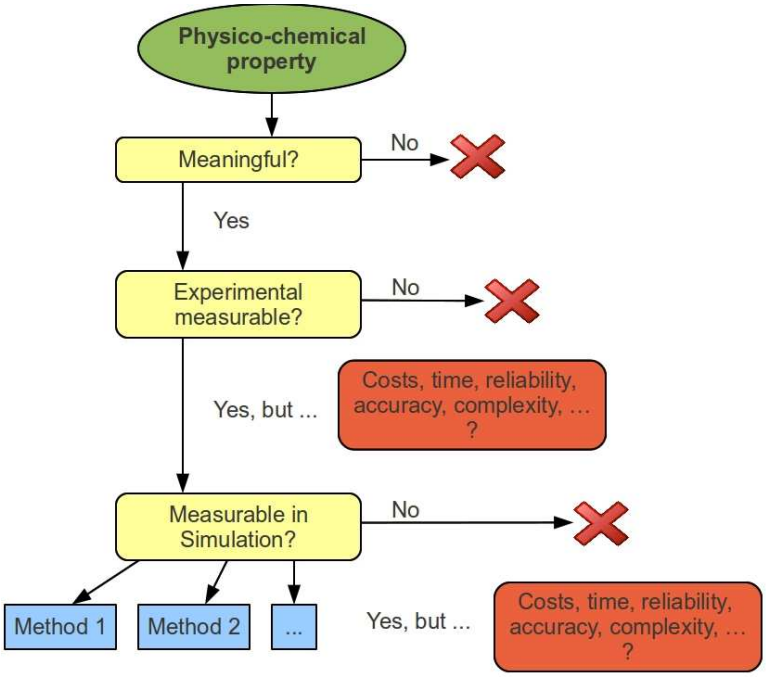

Figure 1.3: Flow-chart on the working scheme used in this work for testing a new computational model.

modes. Usually, we have to decide about important features the model should reproduce before we construct it.

The meaningfulness of a model-quantity is primarily defined by its area of application.

It should be noted, that this statement might seem obvious, but in reality it is often ignored. There is a wide variety of publications where water solution models are built to reproduce bulk properties and are used to investigating proteins or interfacial phenomena, see for example Frolov et al [43]. It is not necessarily unreasonable to extend models beyond the original scope of application, nevertheless one should always keep the risks of such untested model-method combinations in mind.

New models are created to reproduce certain properties. In some cases, the question about the possibility to measure them experimentally is not posed. Two very commonly measured quantities of ions in solution is the hydration free energy and the hydration number. But experimentally the hydration free energy is not measurable without major assumption done on the system. Thus results are highly speculative, as seen by the large deviation of approx. 30 kJ/mol for the hydration free energy of sodium [40]. As for the hydration number, Karttunen and Patra pointed to the fact, that "reported experimental coordination numbers for sodium are between 4 and 8" [44]. It becomes apparent, that only such quantities

should be used for calibrating model quantities, that are measurable with high accuracy and reliability.

On top, experimentalists naturally prefer experiments that are cheap in terms of money and time, easy to perform and with low risks to the equipment and staff.

Answering about experimental possibilities, the same questions arise for the simulation methods. Many macroscopic properties cannot be simulated at all, mostly for the difference in timescale, seconds or longer in real life to nanoseconds in computer simulation, and differences in system size. For example the forming of a water drop takes place at the scale of millimetre, a cell is of the size of micrometre, computer simulation boxes are in the range of nanometre.

Even if the quantity of choice is measurable in computer simulation, the question raised by Gereben and Pusztai still maintains: what are the specific parameters of the simulation method in terms of equilibration time, accuracy, reliability, effort, etc [39]. Whereas safety is no issue in computer simulation, economical considerations are also important in terms of human time and computational effort and costs.

We try to calibrate our new water model on reasonable, justified quantities. Thereby we provide insight into the meaningfulness, the quality and availability of experimental data and we provide specifications about the simulation methods we use. Where no data on the method itself is available, we aim to test the method using a cheap and well known reference model.

1.2.2 Research Outline

Using molecular dynamic simulations, we tested and, if necessary, calibrated ion parameters used in conjunction with a modified SWM4-NDP model. Our final goal is the reliable calculation of the surface tension of brines, using the osmotic pressure as an important milestone.

For many physical predictions the interfaces water/air, water/solid or rock and water/oil play an outstanding role. In this context, the polarizable water force field SW4-NDP shows surprising behaviour at the brine/air interfaces as the sodium and chloride ions seem to crystallise at the interface [1]. This behaviour is neither necessarily non-physically nor contradicted by experiment, but it needs further investigation. The osmotic pressure of ions in water is measured experimentally with great certainty and is very sensible to ion-ion and ion-water correlation. If we are able to well reproduce the experimental osmotic pressure

[1] Personal communication with Mikhail Stukan, Schlumberger Limited

using computer simulations, this would give us great confidence in our results of other interfacial properties like the surface tension.

1.3 Research Contributions

The research presented in this thesis pertains to the academic fields of electrochemistry, water and salt properties and computational physical chemistry. The principle contributions made by this thesis are:

A A critical discussion of methodological concepts for force field design.

B Characterising computational methods for calculation of potential of mean force.

C Extensive testing of a method for osmotic pressure calculation using the well established SPC/E water model.

D Characterising and screening of a polarizable ion and water force field, thereby

1. validating the good performance of the SW10e water model, and
2. calibrated the polarizable ion force fields to meet specific bulk and interfacial properties of brines.

This work is part of an industrial collaboration of the University of Strathclyde and Schlumberger Limited: The Schlumberger Grant "Molecular Simulations of Aqueous Salt Solutions" by the Schlumberger R&D Institute in Daharan, Saudi Arabia.

1.4 Thesis Outline

The text is organised in the following way:

In conclusion to the research motivation presented in this introduction, we review structuring of water and ions at interfaces in Chapter 2. Thereby we emphasise the necessity of calibrating a force field model for water and ions by calculating its interfacial properties such as osmotic pressure.

In Chapter 3 we introduces the reader to the description of molecules in modern computational physics by so called force fields including their extension to account for polarization effects. We will comment on the force field development

of water and ions in the past years in both directions: non-polarizable and polarizable force field approaches. A synopsis on the models under study will finalise the chapter.

Chapter 4 contains a collection of physico-chemical properties of water solutions including a short introduction on their physical meaning and a description of experimental methods with comments on the accuracy. The simulation methods are described in detail and – if necessary – a benchmark on performance and accuracy is provided using the cheap and well documented SPC/E water model as input and reference. As many measurement methods are system dependent, we documented the work-flow and characterised the methods in detail. Every section contains the application of the documented simulation methods on the polarizable force field model. Force field parameters and salt concentrations are varied. Finally, a short conclusion is drawn on the presented methods and models.

The following properties are discussed

1. **Density.**
2. **Energetic properties.**
3. **Radial distribution function.**
4. **Residence time.**
5. **Potential of mean force.**
6. **Osmotic Pressure.**
7. **Surface tension.**

The thesis is concluded by three separate summaries and a brief outlook. The summaries aim to provide the reader a general overview on (i) values of measured quantities of our most successful model, (ii) experimental and computational methods for determining brine properties and (iii) scientific results obtained from the performed force field screening.

Chapter 2

Surface Properties of Water are Widely Affected by the Purity of Water

Ions, surfactants and other particles are known to drastically change interfacial properties of water such as the surface tension. The specific segregation of hydrophobic molecules and water at a combined interface is still a topic of expanded research [9, 8, 10]. Depending on the very principle of molecular hydrophobicity, molecules are either individually hydrated or found to combine into macromolecular structures [9]. The hydrophobic effect is qualitatively well understood, however few theoretical approaches have been made to explain and quantify the assembly of hydrophobic molecules.

The weak interactions between water molecules at the surface and between water and hydrophobic molecules result in interfacial structuring and molecular orientation on both sides of the interface [10]. The structures are drastically influenced by ions, surfactants and other bio-molecules.

Among possible impurities or additives, we concentrate our effort on reviewing ion and salt effects at the interface. The influence of ions on the water interface is expressed through their ability to stabilise the water structure or to destabilise it. Ions that are known to stabilise the water structure and therefore salt-out proteins, are called *Kosmotropes*, whereas ions, that result in a better solubility of proteins are called *Chaotropes* [45].

The initial work describing the strength of ion interactions in a very simple form was performed by Hofmeister in 1888 [46]. Today the large number of review articles based on the so-called *Hofmeister series* of ions shows its importance [47, 48, 49, 45, 50, 24]. Hofmeister found that the interaction strength of ions

in various processes follows a well-defined order. Moreover the order does not depend on the counter-ion involved.

The nature of the topic under discussion - structural properties of molecular salt solutions - makes the necessity of the usage of computer simulations apparent [15, 14]. Considering, for example, the discussion of forces operating between phospholipid bilayer membranes in water and aqueous solutions, the interpretation of experimental results proofed extremely difficult [51]. However computer simulations allow clear and direct evaluation of the forces between the membranes including the structuring of confined water and ions and their influence. A similar discussion on the usefulness of combining experimental methods with computer simulations was made by Moore et al [8]. The authors compared spectroscopic studies with molecular dynamics simulations to describe molecular structure and interactions between water and hydrophobic surfaces.

Within the following section we will explain the interest in ion effects in water especially at various interfaces such as the liquid/vapour interface, at protein surfaces and at other hydrophobic surfaces. Such effects are mostly accessible in computer simulations, but hardly observable on a microscopical scale by experiments. We conclude the necessity of developing a new water-ion model due to discrepancies in the current description of water and ions at interfaces in computer experiments.

2.1 The Interfacial Structure of Pure Water at Various Interfaces is Dominated by Hydrogen Bonds

The dynamics of water near a hydrophobic surface was ed by Bagchi [52]. Because of the missing possibility to form hydrogen bonds the interaction of water molecules near a hydrophobic surface will differ a lot from that near a hydrophilic surface. A hydrophobic surface can modify the water dynamics significantly because it can induce a structure in the surrounding layer. Water dynamics are also predicted to be slow both near hydrophobic and near hydrophilic surfaces but more slow near hydrophilic ones.

The Liquid/Vapour Interface of Pure Water As suggested by the current research [53], the surface structure of water at the liquid/vapour interface is caused by strong hydrogen bonds between water pairs.

The Liquid/Solid Interface of Pure Water Stacchiola et al [54] observed the water structuring at Au(111) surfaces. The surface was found to be hydrophobic as only weak interaction of water with Gold atoms were found. Interestingly, the authors report the formation of a unique double bilayer. The water molecules separating the Gold surface from the bulk water is itself hydrophobic as all water molecules in this interfacial layer are strongly bound to each other and thereby lack the ability to form hydrogen bonds with the bulk water molecules.

Water Outside and Inside of Carbon Nanotubes Thomas et al [55] investigated the effect of tube diameter on the density, molecular distribution and molecular orientation of water inside and outside carbon nanotubes. The density of water molecules outside the tube is enhanced and the molecular distribution is non-uniform near the carbon surface as expected. The hexagonal carbon surface forms low-energy potential wells, that are occupied by water molecules. The behaviour of unconfined water molecules is invariant with the carbon nanotube diameter and the orientation of water molecules close to a carbon nanotube of any diameter are likely to point towards either a circumferential or axial aligned carbon atom.

Hummer et al [56] were early in investigating electrostatic interactions in solution and made molecular dynamics simulations of water inside carbon nanotubes. The results show spontaneous and continuous filling of a non-polar carbon nanotube with a one-dimensionally ordered chain of water molecules. The molecules are observed to move pulse-like through the nanotube. The tight hydrogen-bonding network inside the tube [57] ensures that density fluctuations in the surrounding bath lead to a rapid motion of water molecules along the tube axis. Hydrophobic channels can have significant water occupancy despite a reduction in the number of hydrogen bonds compared to the bulk fluid.

2.2 The Interfacial Structure of Salt Solutions: The Influence of Ions on the Interfacial Structure of Water at Various Surfaces is Considerable

The Liquid/Vapour Interface The discussion of salt effects on the interfacial ordering of water is a long standing one. Common sense in the past suggested that ions are usually repelled from the liquid/vapour interface to maximise the

interaction surface with water. However, in the last decade the structural picture of ions at the interface has been drastically refined through computer simulations [58].

Jungwirth and Tobias [59] simulated in 2001 sodium halides in water at the liquid/vapour interface. Small, non-polarizable anions, e.g. Fluoride, are repelled from the surface as it was suggested earlier. However, the authors found an enrichment of large, polarizable halide anions, e.g. Bromide and Iodide, at the surface. By suggesting specific hydrogen bonding between ions and water, the authors explained the unexpected ion concentration increase in the interfacial region.

As discussed by Eggimann and Siepmann [60], the ionic size plays a key role in the processes that drive monovalent inorganic ions to the surface. The authors modelled aqueous solutions containing a mixture of anions of varying size. As a result, the number of anions at the interface increases with their size.

Following the spirit of the Hofmeister series, recent advances have been made in describing interactions of ions in combination with specific counter-ions by using simple ion-combining rules [50]. The ion description is based on the varying affinity of ions to a solution interface.

Caleman et al [27] discussed the energetics of ion solvation of alkali halides by molecular simulations. The preferred adsorption of ions either at the liquid/-vapour interface or in the bulk water is based on the water-water interaction energy when the ions are partially desolvated.

Salt Effects on Proteins The stabilising and destabilising effect of salts on the folding of proteins in aqueous solution was shown nearly two decades ago by Baldwin [61]. A recent wave of interest in the topic was induced by the work of Fedorov et al [62, 63, 64, 65, 66]. Salts in aqueous solution are not only known to induce conformational changes of macromolecules, but also to induce protein crystallisation [67, 68].

Fedorov, Goodman and Schumm [63, 64] explained the influence of sodium chloride and potassium chloride on the preferential conformation of poly-L-glutamate. In the pure aqueous solution, the peptide has an extended conformation. The addition of a small amount of sodium ions affects the interaction between the negatively charged carboxylate groups of the peptide, thereby reducing the repulsion between the groups that cause the extended conformation. With reduced repulsion poly-L-glutamate prefers the conformation of an α-helix. On the addition of potassium to the dissolved peptide, no conformational changes are found. The

reason is suggested in the occurrence of Potassium ions in the second and third solvation shells of poly-L-glutamate instead of the first solvation shell. The low charge density of Potassium makes it impossible for the ion to compete with the water of the first hydration shell, resulting in a negligible influence of Potassium on the interaction of peptide groups.

As shown by Fedorov et al [64], a discussion of the Hofmeister effects shall include the consideration of direct ion-macromolecule or ion-surface interactions. The bulk water structuring plays a minor role, whereas the interactions with water molecules in the first solvation shell are of high importance.

Thus we understand, that poorly solvated ions are attracted to hydrophobic surfaces. However, ion/counter-ion interaction need to be considered for the full picture as shown by Lund et al [69]. Strongly solvated ions might reach hydrophobic surfaces simply through attraction of weakly solvated ions that approached the surface earlier.

Salt Effects on Micelle Systems The mechanisms of conformational changes and protein crystallisation are found to be similar to the mechanisms of micelle formation of surfactants in salt solutions [67, 68]. The properties of sodium dodecyl sulfate (SDS) aggregates in saline solutions of excess sodium chloride or calcium chloride ions were studied by Sammalkorpi et al.[70] through molecular dynamics simulations. One of the most important issues is found to be the electrostatics as many molecules become ionised in aqueous solutions, and ions and the ionic strength of the solution largely control the association and dissociation of molecules in micelles. The ionic strength of the solution affects not only the aggregate size of the resulting anionic micelles but also their structure. Specifically, the presence of $CaCl_2$ induces more compact and densely packed micelles with a significant reduction in gauche defects in the SDS hydrocarbon chains in comparison with NaCl. Furthermore, more stable salt bridges between the charged SDS head groups mediated by Ca_2^+ than Na^+ had been observed. The presence of these salt bridges helps to stabilise the more densely packed micelles.

Salt Effects on Nanotube Solutions The most of technical and biological aqueous environments of carbon nanotubes contain different salts and, as it has been recently reported by several groups, the salt ions have significant effects on physical-chemical properties of single-wall carbon nanotubes in water solutions [71, 72, 73, 74]. The solvation properties of carbon nanotubes were monitored by absorption, photo luminescence and Raman spectroscopy via investigation of resonance features for specific nanotube chiralities [72, 73]. The salt addition

manifests itself in modification of the electric field around nanotubes, resulting in the quenching of photoluminescence [72, 73, 74]. The nanotube's photoluminescence is of vital importance for realisation of carbon nanotube sensor applications using the fluorescence resonance energy transfer between carbon nanotubes and its biological/chemical surroundings and for the development of ultrafast photonic carbon nanotube-based devices [75, 76, 77, 78]. Importantly, Brege et al [73, 74] reveal that the strength of photo luminescence quenching effect has strong correlation with the ionic radius of the quenching ions, showing the increase in quenching with increase in the ionic radius of ions.

Frolov et al [43] analysed the ion distribution outside of carbon nanotubes by molecular dynamics simulations. Small ions with high surface charge density (e.g. Li^+, F^-) make no direct contacts with the carbon nanotube surface. These ions are strongly hydrated, and therefore the ions are unable to approach the carbon nanotube surface closer than the size of one water molecule. Big ions with low surface charge density (Cs^+, Br^-, I^-) are weakly hydrated and can make a significant amount of direct contacts with the carbon nanotube surface. Caused by the low surface charge density, the ionic hydration shells can easily loose one water molecule that allows the ions to make direct contacts with the carbon nanotube surface.

Liu et al [79] prepared MD simulations to investigate the permeation of ions and water through a membrane. The membrane consists of single wall carbon nanotubes connecting two reservoirs. Analysing the trajectories lead to the interesting result, that hydrated ions of the same charge and ions of opposite charge can pass each other in the tube. In the confined space of a 0.90 nm wide nanotube, Na^+ and Cl^- ions pass each other by sharing an expanded hydration shell which re-forms around each ion as they move away from each other. The transport of ions together with water molecules through a carbon nanotube is thereby possible [80].

2.3 Why Developing new Water and Ion Models? Current Models are Insufficient at Interfaces!

The presented literature review provides a non-exhaustive overview of recent findings concerning water structure at interfaces, ion effects in water, and the combination of hydrophobic surfaces and hydrated ions. The topic is under active research.

As has been shown by several authors [17, 18], the current force fields used in computer experiments for understanding aqueous solutions at interfaces are insufficient. The discrepancies are already apparent in the comparison of structural parameters such as water-water distribution functions with scattering structure factors from neutron and X-ray diffraction [17].

Current water models have been developed to reproduce bulk properties of water such as density and enthalpy of vaporisation [81]. Similarly, the current set of ion models is adjusted to perform well in the aqueous-phase [82].

Water and ions at an interface are characterised by a distortion of their original boundary formed by the solution. To account for this changed surrounding, especially the inclusion of polarization effects in the water-ion models is considered as a useful approach [18, 83, 24].

Chapter 3

Force Field Construction in Modern Computational Physics

Within this chapter we introduce the description of molecules in modern computational physics by so called force fields. Force fields are a mathematical description of intra- and inter-molecular forces between atoms. The simplicity or complexity of the mathematical model determines the computational costs for any preceding experiment, but might also drastically influence the achieved accuracy and reliability of the results. Due to their complex nature, polarization effects have only recently been introduced in the field of computational simulations. However, their influence appeared to be important and the reliability of the results improved for some physical properties drastically. Especially interfacial phenomena are considered to be influenced by local polarization effects and thus might be predicted accurately upon implementing polarizable force fields for their calculation. We will comment on the force field development of water and ions in the past years in both directions: non-polarizable and polarizable force field approaches. A synopsis on the models under study will finalise the chapter.

3.1 Describing Molecules in Computer Simulations: Designing a Force Field

In molecular dynamics simulations the motion of particles (e.g. hard spheres, atoms, molecules) is calculated by solving Newton's equation of motion [84]: A force $\vec{F}$ acting on a particle with mass m causes an acceleration $\vec{a}$

$$\vec{a} = \frac{\vec{F}}{m} = -\frac{1}{m}\frac{\partial \vec{U}}{\partial \vec{r}}.$$

The force $\vec{F}$ is calculated through the interaction potential U specifying the inter- and intra-molecular energies. Molecular models contain parametric potential forms to fit the electronic energies to experimental or higher level computational data [85]. These mathematical constructions are called *force fields*.

The essence of a force field construction is the description of potentials through a mathematical form containing a number of parameters. These parameters are calculated and adjusted to allow a reasonable reproduction of a set of experimentally measured physico-chemical properties.

3.1.1 Mathematical Description of Intra- and Intermolecular Forces

The classical force field models consist of bonded and non-bonded interaction

$$U^{\text{total}}(r) = U^{\text{bonded}}(r) + U^{\text{non-bonded}}(r).$$

Bonded Interaction Bonded interactions are the sum of intramolecular interaction terms, e.g. covalent bonds, angles, dihedrals, and can be further extended by multi-body terms

$$U^{\text{bonded}} = \sum_{\text{bonds}} K_r(r - r_{eq})^2 + \sum_{\text{angles}} K_\theta(\theta - \theta_{eq})^2 + \sum_{\text{dihedrals}} \frac{V_n}{2}\left[1 + \cos(n\varphi - \gamma)\right].$$

Specific parameter for bonded interaction are fitted to results of X-ray crystallography, vibrational analysis, or (cross-polarization magic-angle-spinning) nuclear magnetic resonance.

In current models the application of rigid bonds has been proven useful due ta a decrease of computational costs. A rigid bond is considered to be invariant thereby reflecting the missing possibility to model vibrational modes in classical molecular dynamics. The computational implementation of a rigid bond between atoms is done using specific algorithms, called SHAKE [86], RATTLE [87] or LINCS [88]. All algorithms are based on an artificial repositioning of particles to meet the required bond lengths. Thus, all algorithms contain advances and drawbacks, as discussed in their provided references.

Intra- and Intermolecular Non-Bonded Terms Intra- and intermolecular non-bonded interactions is composed of Van der Waals and Coulomb terms.

$$U^{\text{non-bonded}}(r) = U^{\text{Coulomb}}(r) + U^{\text{Van der Waals}}(r).$$

The Coulomb term describes the direct interaction of position-fixed point charges and decays with r^{-1}

$$U^{\text{Coulomb}}(r) = \frac{1}{4\pi\varepsilon_0}\frac{q_1 \cdot q_2}{r}.$$

For describing the pairwise Van der Waals interactions, it was found that they mainly consist of a repulsive part due to compact overlapping of electron clouds and an attractive part due to permanent / induced dipole - dipole interaction (pairwise, quadrupole, etc.). Due to the complicated nature, the Van der Waals interaction was originally modelled with simple potential forms.

The first potential form merged the idea of a harmonic bond potential and a dissociation energy and was derived by Philip Morse in 1929 and is called Morse potential.

$$U_{ij}^{\text{Morse}}(r) = D_e \cdot \left(1 - \mathrm{e}^{-a(r-r_e)}\right)^2.$$

Later assumptions on the form of the repulsive and attractive parts of the Van der Waals potential were performed by Buckingham, Lennard-Jones and Tosi-Fumi. All used an exponential e^r or potential r^{-12} term for modelling the repulsion and a single r^{-6} term for the dispersion or r^{-6} in combination with r^{-8} for including quadrupole interaction.

$$U_{ij}^{\text{Buckingham}}(r) = A_{ij}\mathrm{e}^{-B_{ij}r} - \frac{C_{ij}}{r^6},$$

$$U_{ij}^{\text{Lennard-Jones}}(r) = 4 \cdot \varepsilon_{ij}\left[\left(\frac{\sigma_{ij}}{r}\right)^{12} - \left(\frac{\sigma_{ij}}{r}\right)^{6}\right],$$

$$U_{ij}^{\text{Tosi-Fumi}}(r) = B_{ij}\mathrm{e}^{-\alpha_{ij}r} - \frac{C_{ij}}{r^6} - \frac{D_{ij}}{r^8}.$$

The most popular potential form was derived by Lennard-Jones [89] (see Figure 3.1, 3.2 and 3.3). The explanation for the wide usage lies in the good performance in terms of computational costs. The calculation speed of the energy is directly increased by avoiding the square root of the distance r and calculating an exponential term e^r. In addition the 12-6 Lennard-Jones type allows to simply square the first calculated power-of-six term r^{-6} to obtain the full potential.

The description of the interaction between particles of the same kind is straightforward. However, within mixtures of particles every combination of particles needs to be described, resulting in $n \cdot (n-1)/2$ interaction terms. For the Lennard-Jones potential, a variety of combination rules have been tested to ease the effort of definition the interaction between unlike particles, however the two simplest

THE PROCEEDINGS OF
THE PHYSICAL SOCIETY

VOL. 43, PART 5 *September* 1, 1931 NO. 240

COHESION

BY J. E. LENNARD-JONES, The University, Bristol

A Lecture delivered before the Society on May 1, 1931.

§ 1. INTRODUCTION: NEW IDEAS IN PHYSICS

THERE are in nature, as in politics, two opposing forces. One of these aims at a peaceful consolidation and the other at a more active and probably more spectacular disruptive process. In nature it is cohesion between atoms which tends to produce condensation and solidification, and temperature which tends to produce dissociation, first of solids into liquids and then into isolated molecules, then of molecules into atoms and finally into electrons and protons (as in the hotter stars).

Figure 3.1: First notice of the 12-6 Lennard-Jones potential form $U_{ij}^{\text{Lennard-Jones}}(r) = 4 \cdot \varepsilon_{ij} \left[\left(\frac{\sigma_{ij}}{r} \right)^{12} - \left(\frac{\sigma_{ij}}{r} \right)^{6} \right]$. Taken from [89].

if the square roots be expanded, as they can for large R. This indicates that the energy of interaction of the dipoles, or the

$$\textit{van der Waals polarization energy} = -h\nu_0 e^4/2k^2R^6,$$

and that there is an attractive *force* proportional to the inverse seventh power of the distance.

Figure 3.2: The r^{-6} term for modelling dispersion directly results from theoretical calculations. Taken from [89].

force of the type λR^{-7}, may appropriately be given here‡. The repulsive field, which comes into play at short distances, is represented by a force of the type $\lambda_{(\text{rep.})}\, R^{-n}$. Theoretical calculations of the type discussed in the next paragraph show that the repulsive field is more complicated than this and contains terms of the form $e^{-\alpha R}$, but it falls off very rapidly with distance and can (in the case of helium at any rate) be represented, over the range which is most effective in atomic collisions, by a term of the type $\lambda_{(\text{rep.})}\, R^{-n}$.

Figure 3.3: The r^{-12} term for repulsion was obtained by optimised fitting of the experimental values of crystal spacing of the solidified gas or its heat of sublimation for gases like Argon. Taken from [89].

one are most widely used.

The Lorentz-Berthelot rules [84] apply an arithmetic combination rule for σ

$$\sigma_{ij} = \frac{\sigma_i + \sigma_j}{2}$$

and a geometric combination for ε

$$\varepsilon_{ij} = \sqrt{\varepsilon_i \cdot \varepsilon_j}.$$

Other force fields apply geometric combination rules for both parameter σ and ε

$$\sigma_{ij} = \sqrt{\sigma_i \cdot \sigma_j},$$

$$\varepsilon_{ij} = \sqrt{\varepsilon_i \cdot \varepsilon_j}.$$

Along with force field specifications, a suitable combination rule should always be provided. A variation of the combination rules may drastically influence physico-chemical properties of the system, as discussed since years [90, 91]. However, not all computational scientists pay attention to this force field parameter and provide the used combination rule.

Unfortunately the nature of electrostatic interactions is far away from being simple, and many recent works have shown the disadvantages of the simplified models for Van der Waals interaction like overestimation of dynamic properties such as the diffusion constant [19, 20, 21, 22, 23]. Therefore the next section will introduce the Van der Waals force and its origin more in detail.

3.1.2 The Physical Concept of Permanent/Induced Dipole-Dipole Interaction and Charge Fluctuations: the Van der Waals Force

According to the modern atomic model, an atom has a small positively charged nucleus surrounded by a large region occupied by electrons. The phrase "electron cloud" describes literally this region. As the electrons do not have fixed positions but rather probabilities of presence, the electron cloud consistently fluctuates. In addition, nearby atoms lead to deformations of the electron cloud and thereby to the formation of dipoles, which can be permanent or spontaneously.

The different possible combinations of permanent and induced dipoles that lead to the Van der Waals force are related to different researcher who first reported them:

- Keesom force: force between two permanent dipoles;
- Debye force: force between a permanent dipole and a corresponding induced dipole;
- London dispersion force: force between two instantaneously induced dipoles.

3.1.3 Computational Implementation of Polarization Effects: Polarizable Force Fields

A brief summary of possible methods for inclusions of polarization effects in classical force fields is given by Cieplak et al. in the review article "Polarization effects in molecular mechanical force fields" [20]. There are three general approaches, namely fluctuating charges, Drude oscillator and induced point dipole, which are explained more in detail below. For the sake of completeness, it should be mentioned, that two further methods exist for implementing polarization effects in molecular simulations. The methods are based on implementing the electronic polarization via quantum mechanical treatment in explicitly modelling electrons [92], or in modelling a polarizable continuum solvent.

- **Fluctuating charge** A basic physical principle is the electronegativity equalisation. Until the electronegativities of all atoms is equalised, charges will flow between the atoms. Within the fluctuating charge model the atomic charge is described through a Taylor expansion, which is truncated after terms of second order; a neutral atomic state is chosen as a reference

point

$$E(q) = E_0 + q\left(\frac{\partial E}{\partial q}\right)_0 + \frac{1}{2}q^2\left(\frac{\partial^2 E}{\partial q^2}\right)_0.$$

Thereby the term $\left(\frac{\partial E}{\partial q}\right)_0$ equals the electronegativity and $\left(\frac{\partial^2 E}{\partial q^2}\right)_0$ reflects the resistance to electron flow to or from an atom. The optimum charge distribution requires a minimisation of the energy with respect to the charges on the atoms.

- **Drude oscillator**

  Using the concept of the Drude oscillator, a polarizable atom is modelled as a system of two particles: a charged core particle and a charged shell particle are connected through a harmonic spring. Therefore, Drude oscillator models are also called shell models. The magnitude of the shell charges q_D is fixed, however the electronic polarization may change through the distance variation of core and shell particle. The force constant k_D for the spring, that binds the particles, is used to implement the polarizability α

$$\alpha = \frac{1}{4\pi\varepsilon_0}\frac{q_D^2}{k_D}.$$

- **Induced point dipole**

  In force fields that employ the point dipole model, an additional energy term, E_{pol}, is added to the total energy:

$$E_{pol} = -\frac{1}{2}\sum_i \mu_i E_i = -\frac{1}{2}\sum_i \alpha_i E_i^{(0)} E_i.$$

  An extension of this point dipole model was done by Thole and is called "smearing dipole model" [22].

$$U^{\text{polarizable}}(r) = U^{\text{non-polarizable}}(r) - \sum_i \mu_i \cdot E_i - \sum_i \sum_{j>i} \mu_i \mu_j : T_{ij} + \sum_i \frac{\mu_i \mu_i}{2 \cdot \alpha_i^2}.$$

  The first term is already described above, the second term represents charge-dipole interactions, the third term represents dipole-dipole interactions and the last term is the energy required to induce the dipole. E_{ij}^f is the fractional electric field on atom i generated by the partial charges of all other atoms except the intra-molecular atoms within the same ion, T_{ij} is the dipole field tensor and μ_i and μ_j are the induced atomic dipoles.

3.2 Force Field Development for Brines Without Polarization Effects

The first water and ion models have been developed on the basis of simple considerations concerning bond lengths, angles and atomic diameters. Throughout the last decades, a variety of improvements have been made, resulting in several water and ion models capable to reproduce specific physico-chemical properties. The widely used SPC/E water model and two ion models are described below.

3.2.1 The Cheap Non-polarizable SPC/E Water Model

The Extended Simple Point Charge (SPC/E) water model [93] is a widely used and computational cheap water model [41]. The SPC/E water model is rigid and consists of 3 sites, the oxygen atom and two hydrogen atoms. Whereas all three atoms carry a point charge and thereby introducing a permanent dipole in the molecule, only the oxygen atom shows Lennard-Jones interaction with its surrounding. More details and a schematic representation of the SPC/E model are shown in Tab. 3.1 and Fig. 3.4.

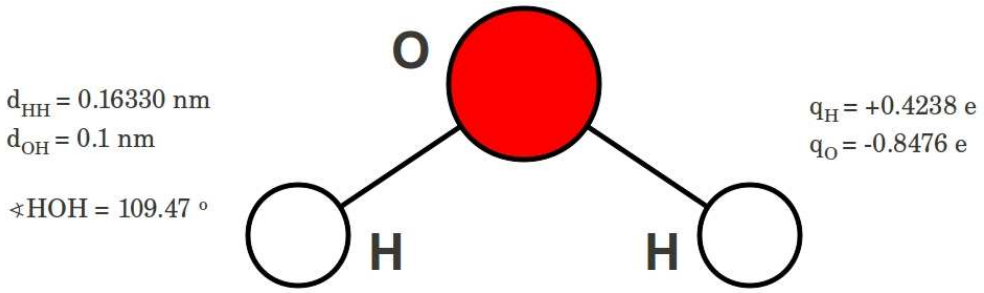

Figure 3.4: Schematic representation of the SPC/E water model.

3.2.2 Non-Polarizable Models for Hydrated Ions

The ion models chosen to be used in conjunction with the SPC/E water model are simple Lennard-Jones spheres with a point charge at the centre of mass. They do not show a dipole or polarizability. Beside their simplicity, they were used with great success.

The Kirkwood-Buff ion Force Field (KBFF) developed by Weerasinghe and Smith [94] was designed to be used for the study of salt effects on peptides, proteins or DNA. In their study, the authors report a good performance of the

model in reproducing experimentally determined Kirkwood-Buff integrals as well as density, isothermal compressibility and ion diffusion constants.

A second approach was made by Joung, Cheatham and co-workers (JCFF) [95]. In their work the models are tuned to balance crystal and solution properties such as the hydration free energies of the solvated ions and lattice energies and lattice constants of alkali halide salt crystals. The optimisation across the entire monovalent series avoids systematic deviations. In addition to well reproducing the solution and crystal properties, the new ion parameters well reproduce binding energies of the ions to water and the radii of the first hydration shells.

The development of simple ion force fields is still in progress and many more models are used in the scientific community: e.g. the popular OPLS/AA force field by Jensen and Jorgensen [82] based on the work of Jorgensen [96], the AMBER FF [97] and the Dang FF [98] to name just a few.

We choose to use the JCFF as reference for energetic properties and the KBFF as reference for the osmotic pressure, as the KBFF performs best in a study by Hess et al [40]. The most important ion FF parameter can be found in Tab. 3.1.

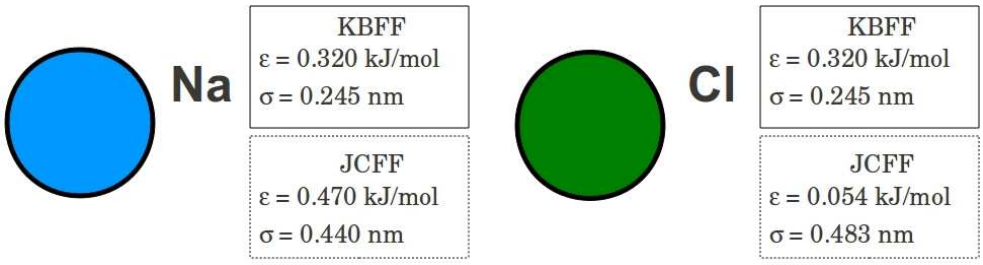

Figure 3.5: Schematic representation of the KBFF and SPC/E water model.

Table 3.1: Parameter of SPC/E water, JCFF and KBFF ions. Geometric combination rules are applied for KBFF. The JCFF was developed in conjunction with the Lorentz-Berthelot combination rules.

model	atom	σ (nm)	ϵ (kJ/mol)	q (e)
SPC/E	O	0.3166	0.6506	-0.8476
	H	0.0	0.0	0.4238
JCFF	Na^+	0.222	1.476	1.0
	Cl^-	0.483	0.053	-1.0
KBFF	Na^+	0.245	0.320	1.0
	Cl^-	0.440	0.470	-1.0

3.3 Force Field Development for Brines Including Polarization Effects

3.3.1 Development of a Polarizable Water and Ion Model - The Origin of SW10e

In a recent article, Dyer et al [41] were able to improve the results of solubility calculation of small solutes in water by introducing a polarization effect in the ion FF. Using a Drude oscillator [99], the group of Lamoureux and Roux developed and improved a full set of polarizable ions with a polarizable water model, the SWM4-DP model [100, 101] and the SWM4-NDP model [25, 102]. This new model proved successful in a number of recent publications [27, 28, 12, 29, 30].

The implementation in Gromacs is described in a work of Maaren and van der Spoel [103].

Beside the great success of the model, development still goes on. In a recent work, Luo et al [30] pointed out a shortcoming of the model in reproducing solution quantities at high salt concentration. The problem is well known also for classical ion models, see a comparative work by Luo and Roux [42].

Luo and co-workers were able to improve the performance of the model by tuning the ion-ion interaction, leaving the ion-water interaction unchanged. This method is feasible in computer simulation, but can become cumbersome when used in conjunction with other ions and atoms. Most force field are built in conjunction with a combination rule which allow to calculate all pair interaction from this combination rule. If this is not used, all pair interactions have to be listed and tuned manually. For n atoms in the force field this amounts to $\frac{n(n-1)}{2}$ combinations, leading for 8 different atoms already to 28 pair interaction potentials.

A different attempt to optimise the SWM4-NDP water and ion model was made by Mikhail Stukan from Schlumberger Limited and in this work. By reason of the fact that the polarizability of ions in solution and in vacuum can differ considerably [1], the polarizability of sodium and chloride is altered. In addition, the spring constant of the Drude particle is modified for the water model and for both ion models. The new water model is coined SW10e.

The Drude constant is changed for two reasons: 1) to investigate possible influences of the spring constant on physical properties and 2) enhance the simulation stability. An explanation on point 2) as well as a detailed description of the

[1] personal communication with Maxim Fedorov

water and ions model and the parameter to screen are provided in the upcoming sections.

3.3.2 The Polarizable Water Model SW10e

The SW10e water model is a 5 point rigid water model with a shell particle harmonically bound to the oxygen site to introduce polarizability. A schematic representation is shown in Fig. 3.6, more details can be found in Tab. 3.3. The oxygen site O carries the polarizability, but no net-charge. The polarizability is introduced by a massless shell particle D harmonically bound to the oxygen site. The shell particles mimics the electron cloud around the oxygen atom. This system was introduced by Drude and consequently called Drude oscillator [104]. Similar to the TIP4P model [105], the permanent dipole of the molecule is introduced by a massless auxiliary site M located along the HOH bisector. Like most water models, Lennard-Jones interaction takes place only for the oxygen site. A comparison with the original model SW4-NDP developed by Lamoureux et al [25] is presented in Tab. 3.2.

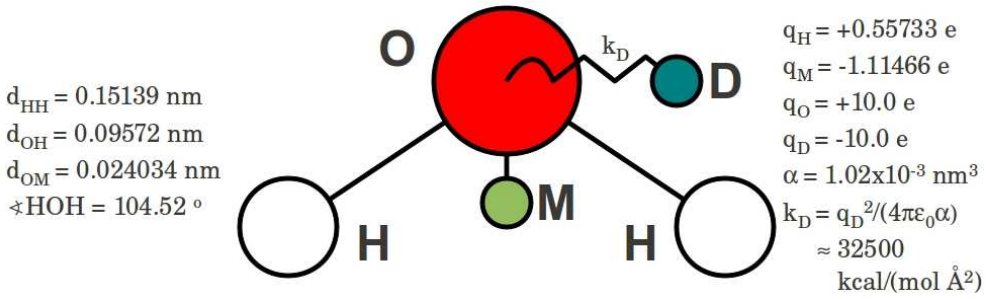

Figure 3.6: Schematic representation of the SW10e water model developed by Lamoureux et al [25] and modified by Mikhail Stukan.

Table 3.2: Summary of the differences between the SW10e model and its predecessor, the SW4-NDP, developed by Lamoureux et al [25].

Characteristic	SW4-NDP	SW10e
q_O (e)	1.71636	10
q_D (e)	-1.71636	-10
α (10^{-3}nm^3)	0.97825	1.02
k_D (kcal/(mol Å^2))	1000	$\approx$ 32500

The polarizability α_p determines the size of a dipole $\vec{p}$ induced by an external

electric field $\vec{E}$:

$$\vec{p} = \alpha_p \vec{E} = q \cdot \vec{r}, \tag{3.1}$$

with $\vec{r}$ being the displacement of the charge q. In most publications, when speaking of the polarizability, the polarizability volume α_{pv} is meant:

$$\alpha_{pv} \quad \left[\mathrm{cm}^3\right] = \frac{10^6}{4\pi\varepsilon_0}\alpha_p \quad \left[\mathrm{C} \cdot \mathrm{m}^2 \cdot \mathrm{V}^{-1}\right].$$

We will follow this nomenclature and call the polarization volume from now on polarization α and provide it in units of volume.

The Drude particle D is bound to the oxygen site O by a harmonic spring with the force constant k_D. The force balance on the Drude particle then reads:

$$\vec{E} \cdot q = k_\mathrm{D} \cdot \vec{r} \quad \longrightarrow \quad \vec{E} = \frac{k_\mathrm{D} \cdot r}{q}.$$

Using Equ. 3.1, the polarizability α introduced by the Drude particle calculates:

$$\alpha = \frac{1}{4\pi\varepsilon_0}\frac{q_\mathrm{D}^2}{k_\mathrm{D}}, \tag{3.2}$$

with q_D denoting the charge on the Drude particle. It should be emphasized, that the Drude particle is excluded from interaction within the molecule, especially no Coulomb interaction with the oxygen site or the permanent dipole of the water molecule takes place. The only force counteracting the external field is the harmonic spring with the force constant k_D. As the Drude particle exhibits no Lennard-Jones interaction, only the external electric field introduced by surrounding molecules acts on the Drude particle. The spring constant k_D is equal in all three spatial directions, therefore the polarizability α is also isotropic in contrast to real water. The error is estimated to be small, as the anisotropy is small [103].

Following Equ. 3.2, the polarization α can be introduced with a free variable: q_D or k_D. The size of the spring constant k_D determines the amplitude of the displacement of the Drude particle and consequently, how close the model is to the point-dipole approximation. In addition, a small spring constant can influence the run stability of the simulation. As the Drude particle exhibits no Lennard-Jones repulsion, it might approach a charged particle and cause a so called Coulomb-catastrophe. Yu et al state for the SWM4-NDP model, this might occur as soon as one introduces a divalent ion [102].

To illustrate this influence of the force constant, we investigated an additional

water model similar to the SW10e model but with a different Drude particle charge, and consequently different spring constant k_{D}. Histograms of the displacement of the shell particles for the two models are shown in Fig. 3.7. As the bulk properties of the two models do not differ, we decided to use the high charged SW10e model for upcoming studies, as it promises to be more stable.

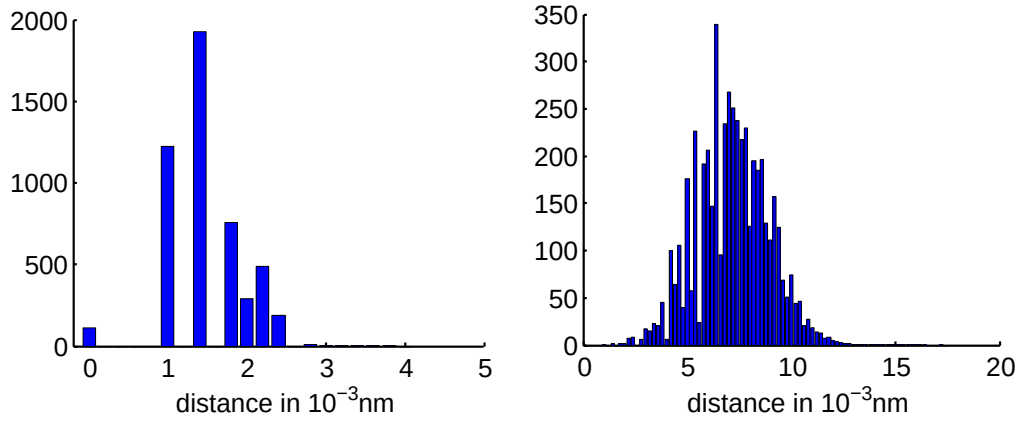

(a) $q_{\mathrm{D}} = 10.0\,\mathrm{e}$ (b) $q_{\mathrm{D}} = 1.88\,\mathrm{e}$

Figure 3.7: A histogram representation of the distance of the Drude particle to its oxygen host atom for a) SW10e water and b) a similar water model with a lower Drude particle charge in bulk. As the Drude particles are excluded from the interaction within the molecule, a distance of 0 indicates the compensation of external fields.

3.3.3 Polarizable Ion Models Based on a Drude Oscillator

Polarizable ions are constructed similar to the polarizable water model: A Drude particle is harmonically bound to the host atom. To charge the ions, a charge of $\pm 1\,e$ was added to the host atom. As the host atom and the Drude particle are excluded from each other, the charging of the host atom does not influence the polarization behavior.

To learn more on the influence of the spring constant k_{D} and to assure stable simulation runs, we investigated several models exhibiting different spring constants, ranging from 2000 to 10000 $\mathrm{kcal}/\left(\mathrm{mol}\cdot\mathrm{\AA}^2\right)$ (equals 836'000 to 4'180'000 $\mathrm{kJ}/(\mathrm{mol\,nm}^2)$) for both ions under study: sodium and chloride.

Some efforts are made to improve the performance of polarizable ion models at high concentration [30]. We try to avoid the manipulation of combination rules and instead change the polarizability values. This is reason by the fact that polarizabilities of ions in solution and in vacuum can differ considerably and are not well known in solution. But even if they would be exactly known, different

polarizabilities than in real water might prove suitable for the ion models used in computer simulation.

As the polarizability of chloride is one magnitude larger than of sodium, in a first step the polarizability α_{Cl} of chloride is changed in a range from 3.5 to $4.0 \cdot 10^{-3}\,\mathrm{nm}^3$ whereas the polarizability of sodium is held constant at $0.157 \cdot 10^{-3}\,\mathrm{nm}^3$. See Fig. 3.8 for a summary of the ion force field parameter used.

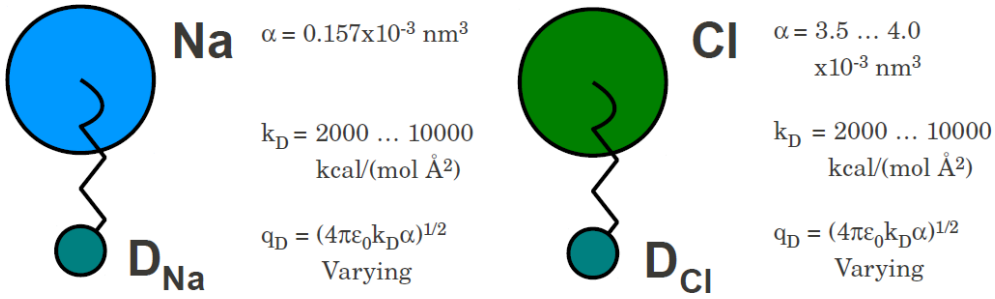

Figure 3.8: Schematic representation of the polarizable ion models introduced by Yu in the group of Lamoureux and Roux [102] and modified in this work as they will be used in the first stage of the study.

Table 3.3: Lennard-Jones parameter of SW10e water and polarizable ions. Lorentz-Berthelot combination rules are applied.

model	atom	σ (nm)	ϵ (kJ/mol)	q (e)
NaCl	Na^+	0.260	0.132	1.0
	Cl^-	0.442	0.301	-1.0
SW10e	O	0.318	0.883	+10.0
	D	0.0	0.0	-10.0
	M	0.0	0.0	-1.11
	H	0.0	0.0	0.56

During the study it proved useful to sample even a greater range of polarizabilities. In the second part of the study about ions, the polarizability of chloride α_{Cl} ranges from 2.0 to $4.0 \cdot 10^{-3}\,\mathrm{nm}^3$.

3.4 Synopsis of the Systems under Study: A Comment on the Variation of Force Field Parameter

For method testing we refer to the widely used and well documented SPC/E water model. The two non-polarizable ion models under study are the Joung-Cheatham force field (JCFF) and the Kirkwood-Buff force field (KBFF).

We vary the polarizable water model SW10e, developed by Mikhail Stukan, to test the influence of the spring constant k_D.

- Spring constants k_D for both water models vary between 1150 and $32500\,\mathrm{kcal}/\left(\mathrm{mol}\cdot\mathrm{\AA}^2\right)$ (equals 480'000 and 13'600'000 $\mathrm{kJ}/(\mathrm{mol}\,\mathrm{nm}^2)$).

For modelling polarizable ions we apply the Drude oscillator method. Thereby we screen a variety of spring constants k_D for both ions and the polarizability α_Cl for the chloride ion.

- Spring constants k_D for both ions varies between 2000 and $10000\,\mathrm{kcal}/\left(\mathrm{mol}\cdot\mathrm{\AA}^2\right)$ (equals 836'000 and 4'180'000 $\mathrm{kJ}/(\mathrm{mol}\,\mathrm{nm}^2)$).
- Polarizability α_Cl of chloride vary between
  - 3.5 and $4.0\cdot10^{-3}\,\mathrm{nm}^3$ in steps of $0.1\cdot10^{-3}\,\mathrm{nm}^3$, and
  - 2.0 and $4.0\cdot10^{-3}\,\mathrm{nm}^3$ in steps of $0.5\cdot10^{-3}\,\mathrm{nm}^3$.

Chapter 4

Characterising of the Models and Methods: Physico-Chemical Properties of Brine Solutions

4.1 Density

4.1.1 Introduction: the Density is an Elementary Macroscopic Quantity

The density ρ of a fluid is a macroscopic quantity. Microscopic structures such as bond lengths and angles, hydrogen bonds or cavities influence the density as well as the molecular dynamics. However, the knowledge of the density does not allow any conclusions about the quantitative behaviour of the molecular structure and dynamics. Still, as a first estimate, the density is widely used to declare the usability of a given molecular model as large deviation from the aimed density is an elimination criterion for a model.

The density is experimentally known with great precision. Similar it is cheap and easy to measure in computer simulation, therefore the density is usually the first quantity that is analysed to detect possible errors in the model or the simulation setup. Unreasonable dynamics of a model, or improper ion-water interactions may be directly visible in a wrong density or density behaviour when heating the system or increasing the ion concentration.

The density ρ of aqueous salt solutions is known to be depending on three physical quantities, namely

- salt content or salt concentration expressed as molality m or salinity S,
- temperature T, and
- pressure p.

The density of salty water decreases with increasing temperature. If the salt content is increased, the density increases as well.

In the following section we will comment on the accuracy of the experimental method used to measure the density. We describe the simulation method and finalise with the actual performance of the polarizable model under study. As we are interested in the ion-water interaction, we measured the density as function of ion concentration and the temperature, which is shown in the last section. The section is completed by an discussion and an outlook.

4.1.2 The Experimental Method: Vibrating Tube Densimeter and an Empirical Formula

The density of water and brine under various conditions can be precisely measured using a vibrating tube densimeter [106, 107, 108]. The error for the density estimation of water even under high pressure and high temperature is in the range of 0.01 to 0.03 % [108]. Based on the high quality results for the density an empirical expression is estimated combining the salinity, temperature and pressure.

It is under common usage by scientists in the fields of solution chemistry, geochemistry and oceanography as well as engineers to estimate the density of 'real' aqueous salt solutions by measuring the pressure, temperature and conductivity of the water using Conductivity-Temperature-Depth (CTD) instruments. The measurement of the electrical conductivity allows the calculation of the salinity of water. As the CTD instrument is constructed to sink into the ocean water, the hydrostatic pressure allows estimation of the distance between the instrument and the water surface ("depth").

According to the Alfred-Wegner-Institut für Polar- und Meeresforschung, current CTD instruments are capable of reaching 6000 m depth [109]. By using double sensor pairs for data quality checks, an accuracy of ± 0.001 K for temperature and ± 0.002 for salinity can be reached.

In 1980 Millero and co-workers [106, 107] performed precise measurements of NaCl, $MgCl_2$, Na_2SO_4 and $MgSO_4$ aqueous solutions at ambient pressure but different salt concentrations and temperatures. Their work resulted in empirical formulas for density calculations. The standard error of the density calculation is given as $\pm 3.3 \cdot 10^{-6}$ g/cm^3 for temperatures between 0 and 40 ° C and 0 to 40 ppm for the salinity.

It has been stated, that "the present international standard for the representation of the properties of seawater is the 1980 International Equation of State of Seawater (EOS-80), released by JPOTS and published by Millero et al. (1980) [...] and until 2009 no more recent standard EOS has been officially adopted for the calculation of the thermodynamic properties of standard seawater." [108]. Thus, we use the density reference values supplied by Millero et al [106] in this work.

4.1.3 Description of the Simulation Method

A simulation box with N particles is created and allowed to relax its volume V under controlling temperature T and pressure p. Within the so called NPT ensemble, the density can be calculated by multiplying the number of molecules N_i with their respective atomic mass m_i and dividing by the volume:

$$\rho = \frac{\sum_i N_i m_i}{V}.$$

If a good starting configuration is provided, the density of water equilibrates in a few ps of simulation time. The fluctuations around the mean value are below 2 % and 1.2 ns long trajectories vary below 0.6 % in their mean density.

4.1.4 Performance of the Polarizable Model

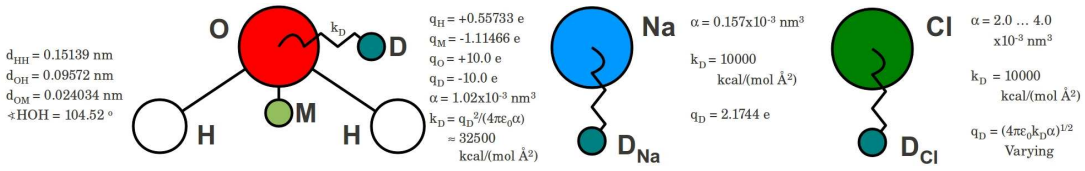

Figure 4.1: Schematic representations of the SW10e water and ion models developed by Lamoureux et al [25] and modified by Mikhail Stukan.

Simulation Setup

The simulations are performed with Gromacs 4.5.5 [110] in double precision.

Three different simulation series are performed: neat water, low concentrations and high concentrations with different temperatures.

Neat water The tool Packmol [111] is used with 6 different random seeds to create 6 starting configurations with 1024 SW10e molecules. The energy is minimised for all 6 systems using the steepest decent algorithm.

A simulation within the NPT ensemble is performed for 4 ns for each replica. For evaluation, the first 400 ps of simulation are omitted to ensure good equilibration. The pressure is kept at 1 bar and the temperature maintained at 298.15 K.

In addition a neat water box with a variation of the SW10e model with a small Drude charge $q_D = 1.88\,e$ is simulated.

Low concentrations The influence of salt concentration is investigated by adding 1 to 18 NaCl ion pairs to the water box. The resulting concentrations range from 0.054 M to 1.0 M. The polarizability of chloride is set to $\alpha_{Cl} = 4.0 \cdot 10^{-3}\text{nm}^3$ and a spring constant of $k_D = 10 \cdot 10^3\,\text{kJ}/\,(\text{mol} \cdot \text{nm}^2)$ is applied. The ion solution simulations are performed similar to the neat water simulations with a simulation time of 1 ns.

High concentrations - different temperatures For simulations at different concentrations and different temperatures, boxes including 1024 SW10e water molecules and 0, 10, 19, 38, 76 and 94 ion pairs are created. The ion model with a Drude force constant $k_D = 10 \cdot 10^3\,\text{kcal}/\left(\text{mol} \cdot \text{Å}^2\right)$ and a polarizability of chloride $\alpha_{Cl} = 2.0 \cdot 10^{-3}\text{nm}^3$ is used.

The boxes are equilibrated in the NPT ensemble for 300 ps at 4 different temperatures: 298.15 K, 313.15 K, 333.15 K and 353.15 K.

Periodic boundary conditions are applied in all directions. The cutoff of the Lennard-Jones interactions is taken to be 1.2 nm with shifted potential taken

from 1.0 nm. The long-range Coulomb interactions are handled by the Particle-Mesh Ewald method [112] with a cutoff of 1.5 nm and a grid spacing of 0.1 nm. The neighbour list for non-bonded interactions is updated every 10th integration step. We use the leap-frog algorithm for integrating Newton's equations of motion with 0.001 ps time step. All simulations are performed at fixed temperature. Velocity rescaling is used with a temperature coupling constant of 0.1 ps [113]. The pressure is held constant using the Berendsen barostat [114] with a pressure constant of 0.5 ps. We store the atomic coordinates of the ions each 5 ps for further analysis.

Matlab [115] was applied for mathematical operations and plotting.

Results and Conclusion

Pure water The density of the neat SW10e water box varies with $\rho = 1001.3\,\mathrm{kg/m^3}$ by 0.4 % from the experimental value of $997.1\,\mathrm{kg/m^3}$. The water model with a lower Drude charge (SW4 LC) overestimates the density slightly more, as shown in Tab. 4.1.

Table 4.1: Simulation results of pure SW10e water and a modification with a Drude particle charge of 1.88 e (Low Charge) in comparison with results obtained by computer simulation by Lamoureux et al [25] and experimental values, taken from [106]. The temperature is 298.15 K. Results at higher temperatures are presented in Tab. 5.2.

	Low Charge	SW10e	Lamoureux et al [25]	experiment [106]
ρ (kg/m^3)	1002.5	1001.3	998	997.1

Solution Results for the density of salt solutions at two different polarizabilities α_{Cl} at $T = 25\,^{\circ}\mathrm{C}$ are presented in Tab. 4.2. The difference between the polarizabilities compared with each other and with experimental references are marginal.

Table 4.2: Density of NaCl SW10e solution at two salt concentrations with two different polarizabilities α_{Cl} at $T = 25\,^{\circ}\mathrm{C}$.

α 10^{-3}nm^3	c (M)	ρ (kg/m^3)	experiment [106] (kg/m^3)
4.0	0.5364	1021.55	1020.860
2.0	0.5362	1019.70	1020.603
4.0	0.9555	1035.11	1039.226
2.0	1.0112	1040.09	1041.720

Densities at different salt concentrations and different temperatures are shown in Fig. 4.2. For $\alpha_{\mathrm{Cl}} = 2.0 \cdot 10^{-3}\mathrm{nm}^3$, the values are available in Tab. 5.2.

During the whole range of all concentrations, the density does not increase as strongly with the salt concentration as the reference data. The deviation becomes only apparent at higher concentrations greater than 1 M. Whereas at ambient temperature the pure SW10e water shows a larger density than the real one, at concentrations higher than 4 M the density is underestimated by nearly 5 %.

The diminished brine density points to less strongly hydrated ions at higher concentrations. This is an interesting fact, as not only the density, but also the hydration enthalpy of the ions is in good agreement with experiment at low ion concentration, see Sec. 4.2. It seems, that the hydration is weakened while increasing the salt concentration, possibly, by an disturbance of the hydration shell through other ions in the vicinity. A possible explanation might be a too high ion-ion interaction energy.

The concentration dependence of the density is basically the same for the temperatures under investigation, see Fig. 4.2(b).

The decrease in density upon heating is reasonable, but too large, see Fig. 4.2(c). To measure the influence of the temperature on the density, the volumetric thermal expansion coefficient γ_V of pure water is estimated for the temperature interval of 25 to 80 °C as

$$\gamma_V = \frac{\Delta V}{V} \cdot \frac{1}{\Delta T} = \left(1 - \frac{\rho_{25\,\mathrm{K}}}{\rho_{80\,\mathrm{K}}}\right) \frac{1}{\Delta T} = 0.81 \cdot 10^{-3}\,1/\mathrm{K}.$$

The expansion coefficient γ_V^{ref} calculated in the same way for the same temperature range of experimental values is less: $\gamma_V^{\mathrm{ref}} = 0.46 \cdot 10^{-3}\,1/\mathrm{K}$ [106]. The increased simulated volumetric thermal expansion coefficient γ_V might be explained with the reduced interaction energy between the SW10e water molecules compared to real water. This reduced energy becomes visible in the hydration enthalpy of $\Delta H = -34.2\,\mathrm{kJ/mol}$ for SW10e instead of $\Delta H = -41.5\,\mathrm{kJ/mol}$. (Note: Please mind, that the volumetric thermal expansion coefficient is generally temperature dependent and the change in volume thereby has to be an integral. One experimental expansion coefficient at $T = 20\,°\mathrm{C}$ is at $\gamma_V^{\mathrm{ref}} = 0.2 \cdot 10^{-3}\,1/\mathrm{K}$ [116].)

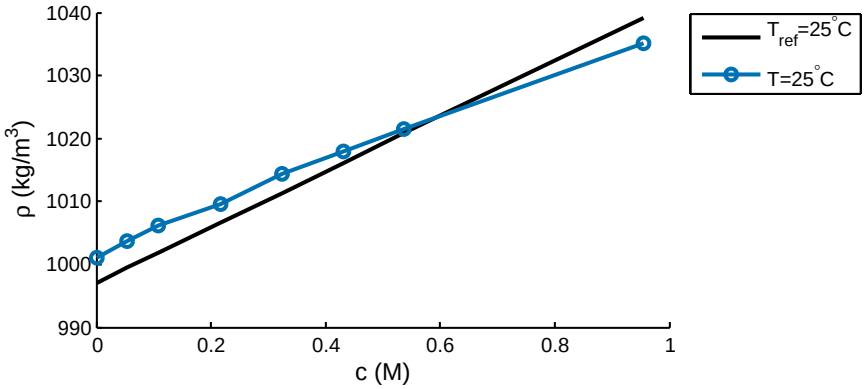

(a) $\alpha_{\mathrm{Cl}} = 4.0 \cdot 10^{-3}\mathrm{nm}^3$

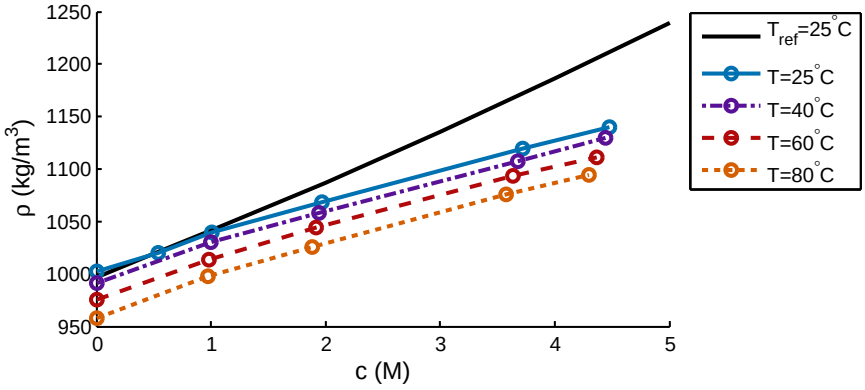

(b) $\alpha_{\mathrm{Cl}} = 2.0 \cdot 10^{-3}\mathrm{nm}^3$

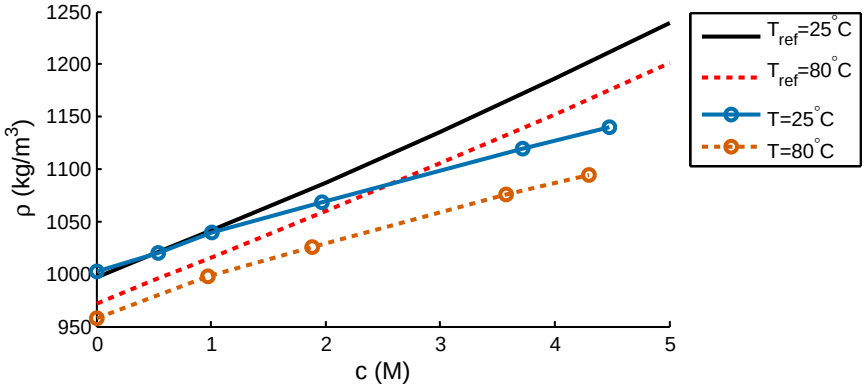

(c) $\alpha_{\mathrm{Cl}} = 2.0 \cdot 10^{-3}\mathrm{nm}^3$

Figure 4.2: Density of a sodium-chloride solution in SW10e. The simulations are performed at different concentrations and different temperatures. Experimental reference data is taken from Millero et al [106]. For $\alpha_{\mathrm{Cl}} = 2.0 \cdot 10^{-3}\mathrm{nm}^3$, the values are available in Tab. 5.2. a) Low concentration at $T = 25\,^{\circ}\mathrm{C}$ with $\alpha_{\mathrm{Cl}} = 4.0 \cdot 10^{-3}\mathrm{nm}^3$. b) High concentration at several temperatures with $\alpha_{\mathrm{Cl}} = 2.0 \cdot 10^{-3}\mathrm{nm}^3$. The solid black line marks the experimental reference at $T_{\mathrm{ref}} = 25\,^{\circ}\mathrm{C}$. c) High concentration at two temperatures with $\alpha_{\mathrm{Cl}} = 2.0 \cdot 10^{-3}\mathrm{nm}^3$. The solid black line marks the experimental reference at $T_{\mathrm{ref}} = 25\,^{\circ}\mathrm{C}$, the red dotted line marks the experimental reference at $T_{\mathrm{ref}} = 80\,^{\circ}\mathrm{C}$.

4.1.5 Conclusion: Quality of the Method and Performance of the Model

The density can be measured experimentally with great accuracy and confidence. The same is true for simulations. Therefore the quick estimation of the density provides a valuable tool for testing the simulation setup and force field before expanding the computational effort for the analysis of more sophisticated quantities.

At ambient conditions, the deviation of the neat water density of the polarizable model SW10e from the experimental density is in the order of 0.4 %. Upon adding sodium and chloride ions the density increases with ion concentration. Further, the polarizability has only marginal effects.

Upon heating, the density decreases stronger than anticipated by experiment and at higher salt concentrations, the density is more and more exceeded by the experimental reference values. These effects point to a weakened ion hydration at higher ion concentration with a too large ion-ion interaction energy and too small water-water interaction energy.

4.2 Gibbs Free Energy and Enthalpy of Hydration

We provide a short introduction on energetic quantities used for understanding solvation processes. After discussing the experimental methods for measuring the hydration free energy, we present the computational methods for enthalpy and free energy calculation.

We calculate the hydration free energy and investigate the influence of different sets of λ parameter with the JCFF ion model in SPC/E water. We present the enthalpy for polarizable ion pairs with different polarizabilities and at different salt concentrations to investigate possible influences on the interaction energy. Finally, we calculate the hydration free energy for one polarizable model. The section is completed by a conclusion on the method and model performance.

4.2.1 Introduction: Foundation for Understanding Solvation Processes

The free energy is fundamental for the understanding of thermodynamic properties in aqueous solutions [117]. Ben-Naim [118] states two main reasons for investigating the solvation energy of solutes: first, the solvation free energy provides us with the solubility of the solute, and second, the solvation free energy plays an important role in determining the equilibrium constant of chemical reactions in the solvent.

A pictorial understanding of the solution free energy could be obtained by understanding the thermodynamic cycle, that allows the calculation of the free energy of solution $\Delta G^*_{\mathrm{sol}}$ [119]. One cycle would transfer the solute molecule from the crystal phase to vacuum and to solution. The free energy of solution $\Delta G^*_{\mathrm{sol}}$ would then be the sum of the two contributions from the sublimation free energy $\Delta G^*_{\mathrm{sub}}$ (crystal to vacuum) and the hydration free energy $\Delta G^*_{\mathrm{hydr}}$ (vacuum to solution)

$$\Delta G^*_{\mathrm{sol}} = \Delta G^*_{\mathrm{sub}} + \Delta G^*_{\mathrm{hydr}} = -RT \ln S_0 V_{\mathrm{m}}, \tag{4.1}$$

where R is the molar gas constant, T the temperature, S_0 the intrinsic solubility and V_{m} the molar volume of the crystal. The superscript * denotes the usage of the Ben-Naim terminology [119].

For a discussion and determination of the solubility, we have to evaluate the hydration free energy $\Delta G_{\mathrm{hydr}} = \Delta H_{\mathrm{hydr}} - \Delta ST$. Enthalpy and Entropy of solvation are thermodynamic state functions [120] and experimentally measurable

[121]. The hydration enthalpy $\Delta H_{\text{hydr}} = \Delta U + p \cdot \Delta V$ is derived from the the internal energy of the system U and the product of pressure p and volume V.

Energetic properties such as the enthalpy play an outstanding role in force field calibration performed in the past decades, as many authors donate a lot of efforts in determining these properties and comparing them with experimental references or with higher order computational methods, see for example Joung and Cheatham [95] for an discussion on non-polarizable ion force fields and Lamoureux et al [25] and Yu et al [102] for polarizable force fields.

4.2.2 Experimental Methods: Strong Assumptions for Single Ions

Hydration free energies are determined through experimentally measured hydration enthalpies and entropies. Heats of solution are measured with calorimetric instruments, that are constantly improved to allow wider applications and increased accuracy [122].

A review of Gibbs free energies, hydration enthalpies and entropies of ions in water is given by Fawcett [121]. Whereas instruments are cheap and accurate, one has to keep in mind that they only allow the measurement of energetic properties of *ion pairs*. The solvation of single ions cannot be studied experimentally. Instead, assumptions about the absolute size of hydration enthalpies of single ions are made and subsequently the hydration enthalpies of other ions are estimated [123].

4.2.3 Description of the Simulation Methods

Hydration Enthalpy ΔH_{hydr} The Enthalpy $H = U + pV$ of a simulation box can easily derived from the system as the inner energy U is the sum of all Lennard-Jones interaction energies E_{LJ}, Coulomb interaction energies E_{Coulomb} and kinetic energies E_{kin}:

$$H = U + pV = E_{\text{kin}} + E_{\text{Coulomb}} + E_{\text{LJ}} + pV, \tag{4.2}$$

with p being the pressure and V the volume of the box.

We will define the hydration enthalpy ΔH_{hydr} of an ion or ion pair as the change in enthalpy between a pure solvent box and a solution box with the same amount of solvent molecules but including the respective ion or ion pair.

Hydration Free Energy ΔG_{hydr} The enthalpy H does not include entropic effects. For a discussion and determination of the solubility, we have to evaluate the hydration free energy $\Delta G_{\text{hydr}} = \Delta H_{\text{hydr}} - \Delta ST$. The hydration free energy cannot be calculated directly from a simulation, but more advanced methods have to be applied.

Such an advanced method is the thermodynamic integration (TI) method for determining the hydration free energy ΔG_{hydr} of ions. Knight and Brooks provide a recent review on this method [117]. The TI method is often referred to as 'slow-growth-method', as the ions are decoupled from the system and the interactions are slowly turned on, thereby the ion 'grows' inside the solution. Also possible is the vanishing of the ion from solution. This route is similar to the slow-growth-method but promises to be computationally more stable.

To determine the change in free energy of a system with and without an incorporated ion, we couple the ion-solvent interactions with a λ parameter: at $\lambda = 0$ the system is fully coupled to the ion, at $\lambda = 1$ the ion is fully decoupled from the system. We perform the decoupling in two steps: first we decouple the Coulomb interaction, including polarizability effects, and secondly, we will decouple van der Waals interactions.

The free energy is then calculated by

$$\Delta G_{\lambda=0\to\lambda=1} = -\int_0^1 \left\langle \frac{\partial H(\lambda)}{\partial \lambda} \right\rangle \mathrm{d}\lambda. \tag{4.3}$$

A Comment on the Direct Estimation of the Solubility Palmer et al [119] discuss the numerous difficulties for calculating the solubility of small drug-molecules. Beside recent proceedings in this field reported by the same authors [124], the estimation of solubility is still far from being a standard method in computational physics. A recent work of Karamertzanis et al [125], still engaged in the topic of predicting hydration free energy of neutral solutes, illustrates this.

In a short estimation of the solubility of the ion models under study, we performed simulations of ion crystals and used solution data. We neglected entropic effects for the sublimation energy and this already lead to the unphysical result, that most of the ion models tested are completely insoluble. This is contradicted by bulk simulations with well dissolved ions and emphasises the need for an accurate and carefully executed simulation routine.

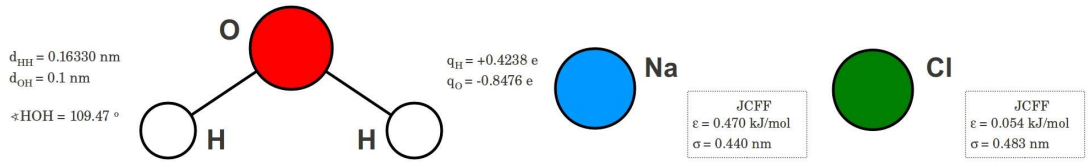

Figure 4.3: Schematic representation of the SPC/E water and JCFF ion model.

4.2.4 Performance of the Method

Simulation Setup

The JCFF ion force field [95] is applied and the SPC/E water model [93] used.

The simulations are performed with Gromacs 4.5.5 [110] in single precision. A pre-equilibrated box of 1000 SPC/E water molecules and the specific ion is used as starting configuration for all simulations.

The Coulomb and Van der Waals (vdW) interactions are decoupled from the system separately, the Coulomb interactions first. For decoupling vdW interactions, soft-core potentials are applied [126]. For decoupling Coulomb interaction, λ_{Coulomb} values from 0 to 1.0 in steps of 0.05 are applied with intermediate steps at 0.025 and 0.075 (23 values in total). For decoupling vdW interaction, the same λ values are used but with intermediate steps at 0.575 and 0.625. Additional sets for λ_{Coulomb} with seven steps

$$(0.0; 0.167; 0.333; 0.5; 0.667; 0.833; 1.0)$$

and 13 steps

$$(0.0; 0.083; 0.167; 0.250; 0.333; 0.417; 0.5; 0.583; 0.667; 0.750; 0.833; 0.917; 1.0)$$

and additional sets for λ_{vdW} with seven steps

$$(0.0; 0.167; 0.333; 0.5; 0.667; 0.833; 1.0)$$

and nine steps

$$(0.0; 0.11270; 0.24180; 0.37090; 0.5; 0.62910; 0.75820; 0.88729; 0.94365)$$

are applied.

Several equilibration steps are done for every λ value. First, the steepest descent algorithm is applied. The NVT ensemble and the NPT ensemble are applied for 40 ps, respectively. The production run is performed in the NPT

ensemble for 1 ns. The pressure is kept at 1 bar and the temperature maintained at 298.15 K.

Periodic boundary conditions are applied in all directions. The cutoff of the Lennard-Jones interactions is taken to be 1.0 nm with shifted potential taken from 0.9 nm. The long-range Coulomb interactions are handled by the Particle-Mesh Ewald method [112] with a cutoff of 1.3 nm and a grid spacing of 0.112 nm. The neighbour list for non-bonded interactions is updated every 10th integration step. We use leap-frog stochastic dynamics integrator algorithm for integrating Newton's equations of motion with a 0.002 ps time step. All simulations are performed at fixed temperature. The integrator functions as thermostat with a temperature coupling constant of 0.1 ps. We store the atomic coordinates of the ions each 5 ps for further analysis.

The Gromacs tool g_bar is used for evaluation and error estimation based on the Bennetts Acceptance Ratio (BAR) method [127].

Matlab [115] is applied for mathematical operations and plotting.

To handle the amount of individual simulations, nearly 100 for one value of the hydration free energy, the whole procedure is automatised.

Result: Agreement with References

The results of free energy of hydration ΔG_{hyd} calculations are presented in Tab. 4.3. The different sets of λ parameter show only slight deviations of less than 0.2 kcal/mol from the presented result. This deviation is larger than the errors estimated by the BAR method [127].

The results are in very good agreement with simulation references by Joung and Cheatham [95].

Table 4.3: Free energy of de-hydration $-\Delta G_{\mathrm{hyd}}$ for chloride and sodium ions in water. As computational reference, the hydration free energy results of Joung and Cheatham are used [95]. Experimental references are taken from the same paper, initially they were performed by Schmidt et al [128] and Marcus [129]. The errors in this work are estimated with the BAR method [127].

ion species	$-\Delta G_{\mathrm{hyd}}$ (kcal/mol)			
	this work	Joung [95]	Schmidt [128]	Marcus [129]
Sodium	88.4 ± 0.1	89.0	88.7	87.2
Chloride	89.0 ± 0.1	89.3	89.1	81.3

Conclusion

We are able to calculate the hydration free energy with the same method/model combination as used by Joung and Cheatham [95]. The thermodynamic integration method excels through high accuracy, but also considerable effort and computational costs through the large number of single simulations that have to be performed.

We tested the influence of the coupling parameter λ, with the expected result that within a reasonable choice of the number of λ-values the dependency is negligible. Possible influences of other simulation parameter like the system size have not been investigated and have been to our knowledge not yet considered in any reference.

4.2.5 Performance of the Polarizable Model

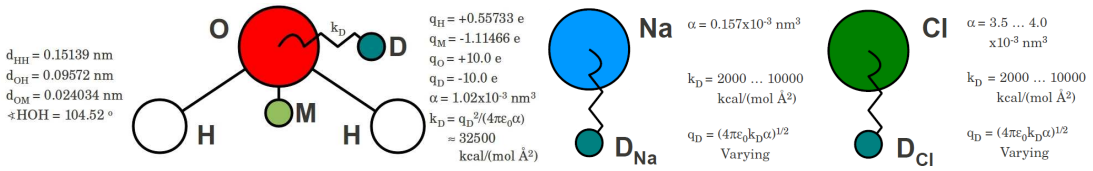

Figure 4.4: Schematic representations of the SW10e water and ion models developed by Lamoureux et al [25] and modified by Mikhail Stukan.

A Comment on the Implementation in Gromacs

State-of-the-art simulation software such as Gromacs contain an interface for λ coupling and an advanced evaluation and error estimation routine based on the Bennetts Acceptance Ratio (BAR) method [127].

Upon using Gromacs 4.5.5 [110] with the free energy framework and the tool g_bar for the evaluation, we encountered two bugs. First, the tool g_bar was not able to process all input data as the temperature seemed to change for different λ values. An error in the source code concerning the variable definition caused the problem and we were able to point the developers to the source of the error which was fixed subsequently.

The second bug concerns the usage of the free energy framework in conjunction with polarizability effects. This is not possible, as the code is not able to scale the polarizability correctly. We informed the developers, but they were not able to fix this issue yet.

For this reason, the setup and evaluation of the free energy calculation of polarizable ions needs to be done manually by scaling of the atom and Drude particle charge and polarizability α of the ion. The evaluation can be performed by using Equ. 4.3.

Simulation Setup

The simulations are performed with Gromacs 4.5.5 [110] in double precision.

The force field of sodium and chloride is sampled by using six different polarizabilities of chloride

$$\alpha_{\mathrm{Cl}} = 3.5,\ 3.6,\ 3.7,\ 3.8,\ 3.9,\ 4.0 \cdot 10^{-3}\mathrm{nm}^3$$

and five different spring constants of the Drude particles of sodium and chloride

$$k_{\mathrm{D}} = 2,\ 4,\ 6,\ 8,\ 10 \cdot 10^3\,\mathrm{kJ}/\left(\mathrm{mol}\cdot\mathrm{nm}^2\right),$$

resulting in 30 separate force field parameter sets. A pre-equilibrated simulation box consisting of 1024 SW10e molecules and 10 NaCl ion pairs serves as starting configuration. The setup results in a concentration of roughly 0.5 M. The same starting configuration is used for every model.

For every model, a simulation within the NPT ensemble is performed for 1 ns. The pressure is kept at 1 bar and the temperature maintained at 298.15 K.

Periodic boundary conditions are applied in all directions. The cutoff of the Lennard-Jones interactions is taken to be 1.2 nm with shifted potential taken from 1.0 nm. The long-range Coulomb interactions are handled by the Particle-Mesh Ewald method [112] with a cutoff of 1.5 nm and a grid spacing of 0.1 nm. The neighbour list for non-bonded interactions is updated every 10th integration step. We use the leap-frog algorithm for integrating Newton's equations of motion with 0.001 ps time step. All simulations are performed at fixed temperature. Velocity rescaling [113] is used with a temperature coupling constant of 0.1 ps. The pressure is held constant using the Berendsen barostat [114] with a pressure constant of 0.5 ps. We store the atomic coordinates of the ions each 5 ps for further analysis.

The influence of salt concentration is investigated with a similar setup except for a reduction of the number of ions pairs to 1, 2, 4, 6 and 8. The resulting concentrations range from 0.054 M for 1 ion pair to 0.54 M for 10 ion pairs in the box. For this additional simulations, the polarizability of chloride is set to $\alpha_{\mathrm{Cl}} = 4.0 \cdot 10^{-3}\mathrm{nm}^3$ and a spring constant of $k_{\mathrm{D}} = 10 \cdot 10^3\,\mathrm{kJ}/\left(\mathrm{mol}\cdot\mathrm{nm}^2\right)$ is applied.

Reference values for the Enthalpy are determined by evaluating 6 replica simulations of pure SW10e water molecules, each 4 ns long.

For the same model and with the same simulation parameters, a hydration free energy calculation is performed. A box with 1024 SW10e water molecules and one ion is equilibrated for 40 ps in the NVT and NPT ensemble respectively. The data is sampled for 500 ps in the NPT ensemble. For decoupling the Coulomb interactions, all charges q and the polarizability α of the ions are scaled by λ.

The Gromacs tool g_bar is used for evaluation and error estimation based on the Bennetts Acceptance Ratio (BAR) method [127].

Matlab [115] is applied for mathematical operations and plotting.

To handle the amount of individual simulations, nearly 100 for one value of

the hydration free energy, the whole procedure is automatised.

Results

Hydration Enthalpy ΔH A summary of the hydration enthalpy results for different ion models is presented in Tab. 4.4.

Two experimental values for the hydration enthalpy ΔH of one sodium-chloride ion pair are $-783\,\mathrm{kJ/mol}$ [123] and $-843.4\,\mathrm{kJ/mol}$ [130]. For all screened parameters and ion concentrations, the measured values lie in the reported range.

Increasing the polarizability α_{Cl} of chloride leads to an increase of the hydration enthalpy ΔH by roughly 1 %. Increasing the spring constant k_{Drude} does not give a clear tendency. The results are in agreement with structural properties extracted from the same simulations, see Sec. 4.3.5. The radial distribution functions exhibit no influence of the spring constant and indicate an increased interaction of chloride ions and water molecules.

Table 4.4: Summary of the de-hydration enthalpy $-\Delta H$ of one sodium-chloride ion pair in SW10e water with different polarizabilities α_{Cl} of chloride and different spring constants k_{D} of sodium and chloride. Two experimental values for the hydration enthalpy ΔH of one sodium-chloride ion pair are $-783\,\mathrm{kJ/mol}$ [123] and $-843.4\,\mathrm{kJ/mol}$ [130]. 10 sodium-chloride ion pairs are dissolved in a box with 1024 SW10e water molecules, resulting in a salt concentration of roughly 0.5 M. The enthalpy is normalised to one sodium-chloride ion pair.

$-\Delta H$ (kJ/mol)	α_{Cl} ($10^{-3}\mathrm{nm}^3$)					
k_{D} ($10^3\,\mathrm{kcal}/\left(\mathrm{mol\,\AA^2}\right)$)	3.5	3.6	3.7	3.8	3.9	4.0
2	784.2	783.4	784.2	786.0	787.4	790.0
4	781.2	784.5	784.5	785.8	786.8	788.9
6	783.4	783.6	783.9	785.5	784.5	788.1
8	780.9	784.6	785.0	785.5	786.9	788.1
10	781.7	783.4	785.0	784.8	787.7	790.3

Concentration Dependency of the Hydration Enthalpy The influence of the salt concentration is summarised in Tab. 4.5. Using 4 to 10 ion pairs does not effect the de-hydration enthalpy. The simulations with 1 and 2 pairs exhibit a 1.3 % increase from the mean value of the other simulations of $790\,\mathrm{kJ/mol}$. This deviations might be due to insufficient sampling. The effect might also arose from better hydration of the ions, due to the lack of other ions to disturb the water molecules in the solvation shell. Anyway, the small influence of the

concentration on the hydration enthalpy indicates well dissolved and separated ions in the solution up to a salt concentration of 0.5 M.

Table 4.5: Summary of the de-hydration enthalpy $-\Delta H$ of one sodium-chloride ion pair in SW10e water with different salt concentrations. The number of ion pairs in 1024 SW10e water molecules is 1, 2, 4, 6, 8 and 10, corresponding to roughly 0.05 M to 0.5 M salt concentration. The de-hydration enthalpy $-\Delta H$ is normalised to one sodium-chloride ion pair. The simulations are performed for the ion model with $\alpha_{\mathrm{Cl}} = 4.0 \cdot 10^{-3}\mathrm{nm}^3$ and $k_{\mathrm{D}} = 10 \cdot 10^3\,\mathrm{kcal}/\left(\mathrm{mol} \cdot \mathrm{\AA}^2\right)$.

# ion pairs	c (M)	$-\Delta H$ (kJ/mol)
1	0.054	799.5
2	0.108	800.3
4	0.216	788.8
6	0.324	790.2
8	0.432	789.9
10	0.540	790.3

Hydration Free Energy ΔG The free energy of hydration for sodium and chloride is calculated for the ion model with

$$\alpha_{\mathrm{Cl}} = 4.0 \cdot 10^{-3}\mathrm{nm}^3$$

and

$$k_{\mathrm{D}} = 10 \cdot 10^3\,\mathrm{kcal}/\left(\mathrm{mol} \cdot \mathrm{\AA}^2\right),$$

see Tab. 4.6. As anticipated before, the decoupling of the Coulomb interaction including polarizability effects is done manually.

The results of the calculations in this work are too small compared with experimental data and with a simulation reference. Because of the high computational costs of the simulation, we are not able to point the reason for this deviation with great confidence. One reason might be insufficient sampling (only 0.5 ns for every λ value), which adds to the lack of a sophisticated evaluation routine. On the other hand, the hydration free energy of a chloride ion with a different polarizability results in a similar value: 69.2 kcal/mol instead of 70.3 kcal/mol, see Tab. 5.3.

Table 4.6: The de-hydration free energy $-\Delta G$ for chloride and sodium in SW10e water. The simulations are performed for the ion model with $\alpha_{\mathrm{Cl}} = 4.0 \cdot 10^{-3}\mathrm{nm}^3$ and $k_{\mathrm{D}} = 10 \cdot 10^3\,\mathrm{kcal}/\left(\mathrm{mol} \cdot \mathrm{\AA}^2\right)$. As computational reference, the hydration free energy results of Yu et al are used [102]. Experimental references are taken from Schmidt et al [131] and Marcus [129].

ion species	$-\Delta G_{\mathrm{hyd}}$ (kcal/mol)			
	this work	Yu et al [102]	Schmidt [131]	Marcus [95]
Sodium	64.4	96.3	88.7	87.2
Chloride	70.3	78.4	89.1	81.3

Conclusions

The hydration enthalpy has been estimated for several force field parameter and various salt concentrations. For all screened parameter and ion concentrations, the measured values lie in the range of experimental references. The influence of the spring constant of the Drude particle is negligible.

Using the same methodological approach for calculating the hydration free energy as for the non-polarizable reference model, we encountered difficulties in the computational implementation of the method but were able to solve or circumvent them.

The tested model seems to underestimate the hydration free energy. However, the origin of the deviation from experimental and simulated references might have multiple reasons, among them

- Inappropriate sampling time: The method especially in combination with polarizable force fields is computational expensive and thus we simulated only 0.5 ns for every λ value. Some computational scientists use several hundred nanoseconds of simulation time to sample energetic properties [132].
- Influence of simulation setup, e.g. system size.
- Missing correction terms, see [102].
- Erroneous computational implementation of the simulation or calculation routines.

4.2.6 Conclusion: Quality of the Method and Performance of the Model

The quantification of the hydration process in terms of energetic properties might provide physical insights. However, experimental references are based on strong assumptions, that influence the resulting values. Large deviations between reported values for the hydration free energies of ions are found [40]. Thus a comparison of experimental references and simulated quantities is difficult.

However, very accurate methods for computational calculating the hydration enthalpy have been developed in the past years. Among the methods we tested the thermodynamic integration with the Bennetts Acceptance Ratio evaluation method. Although the comparison with experimental references might not be reasonable, discussion of the influence of model parameter or different models on solvation properties is promising. The determination of energetic properties is still a useful way for describing and characterising the solution model under study.

Among the various possibilities to calculate the hydration free energy, we concentrated purely on reproducing the method Joung and Cheatham applied. We were able to successfully reproduce the values for SPC/E and JCFF ions.

Upon applying the same procedure to the polarizable model, we encountered various difficulties starting with the implementation in the simulation software. Final results underestimate the free energy by 20 kcal/mol. The reason for this underestimation might be found ether in the model or in the method. Research needs to be done on the application of possible correction terms [102] and on possible influences of the simulation setup. Moreover, the computational implementation of the thermodynamic integration method in combination with polarizable force fields appeared not fully tested.

Our conclusions are in agreement with the recent focus changes that are made concerning the force field development. In the past decades, models have been calibrated to reproduce energetic properties of solutions such as enthalpies. Newer publications focus on other benchmark quantities such as the osmotic pressure [30, 42, 40].

4.3 Structural Properties: Radial Distribution Functions and Coordination/Hydration Numbers

4.3.1 Introduction: The Concept of the Hydration Shell

Introducing an ion into bulk water disturbs the water structure and therefore has immediate influence on the physical properties of the solution [118]. The strong ion-water correlations are found to not only break the original bulk water structure but to lead to specific new structures of water molecules around the ion [118]. This creates the picture of an ionic nucleus surrounded by a shell of water molecules - the so called hydration shell. The behaviour of the hydration shell varies with the ion, for simple ions dominantly with the size and sign of the charge [118, 133, 134]. Relevant thermo-physical properties of ions in solution are strongly affected by the molecular structure of the solvation shell [118].

Structural properties of ions in solution can be described by ion-water, ion-ion and water-water radial distribution functions $g(r)$, abbreviated as RDF [84]. The correlation function $g(r)$ presents the probability of finding a pair of particles i and j at the distance $\vec{r}_{ij}$ relative to the probability for a completely random distribution at the same density [84, 135], leading to the definition including the number of particles N and the volume V:

$$g(r) = \frac{V}{N^2} \langle \sum_i \sum_{j \neq i} \delta(\vec{r} - \vec{r}_{ij}) \rangle. \tag{4.4}$$

Bearing the concept of the hydration shell in mind, a discussion of the number of molecules in the respective shells, the so called coordination number is widely accepted [136]. In case of water, the term "hydration number" also occurs in the scientific discussion. However, neither the precise meaning nor the usefulness of the coordination number is clearly defined. Moreover, calculation of the coordination number depends largely on the method used for their determination [136, 137].

In this work, we will use a definition by Chialvo et al [137]: The running coordination number $n(R)$ results from the integration of the radial distribution function

$$n(R) = 4\pi\rho \int_0^R r^2 g(r) \mathrm{d}r, \tag{4.5}$$

with ρ being the number density of the solvent.

With R being the position of the first minimum in the RDF ($R = r_{\min}$), the running coordination number $n(r_{\min})$ is referred to as the coordination number c_n.

In the following section we will comment on the technical capabilities and accuracy of experimental methods used to measure the RDF of ions in solution. We provide a brief review about the knowledge of the hydration shell of ions. We describe the simulation method and finalise with the actual performance of the polarizable model under study. In this section, we screen 30 different ion models and compare them in terms of structural data. As the simulations are performed at a finite concentration of roughly 0.5 M, we verify our results at lower concentrations.

4.3.2 The Experimental Method: Data Reconstruction by Diffraction Experiments Combined with Computer Simulations

Structural changes in the solvent, as occur by the presence of ions, cause density fluctuations. These fluctuations are related to the structure factor $S(k) = 1/N\langle\rho(k)\rho(-k)\rangle$ and may be measured by diffraction experiments [134]. The radial distribution function $g(r)$ is connected with the experimentally measurable structure factor $S(k)$ through a three dimensional Fourier transformation [84]:

$$S(k) = 1 + \rho\hat{g}(k) = 1 + 4\pi\rho \int_0^\infty r^2 \frac{\sin kr}{kr} g(r)\mathrm{d}r.$$

Structural properties of ions in water are experimentally measured by neutron scattering and X-ray diffraction [138, 44, 45]. One important drawback of the method is that the full set of site-site correlation functions cannot be calculated upon using the Fourier transform of the diffraction data. The reason is found in the low signal strength obtained for ion-ion correlations. Even for ion-water radial distribution functions, the peak heights can only be measured with great uncertainty. This fact results in a wide spread of reported coordination numbers, ranging from 4 to 8 for sodium and from 6 up to 11 for chloride in aqueous solution [44]. The peak positions of the ion-water radial distribution functions on the other hand can be determined with reasonable precision as they are related to the wave length of the peak of the structure factor.

Neutron diffraction in combination with Monte-Carlo simulations allows to investigate the water structure in the presence of ions as well as their solvation shell

[139, 17, 140, 141]. The combination of diffraction measurements with computer simulations is a form of **data reconstruction**.

Such methods are always prone to uncertainties as they require initial datasets of high quality and high quantity. In the example of Botti et al [139], the authors used only 3 datasets obtained from diffraction experiments to estimate 15 site-site correlation functions of a concentrated HCl solution - which might be a source of uncertainty. Only a sensible choice of the diffraction measurements and the method of interpreting the measurements allows to obtain meaningful ion-water and water-water partial radial distribution functions [141].

4.3.3 Review: Structure of Water Around Ions

By combining diffraction measurements with Monte-Carlo simulations, Botti et al [139] analysed the microscopic structure of a concentrated HCl solution. Thereby the interaction of the water molecules with the solutes is found the be a disturbance similar to the application of an external pressure to neat water. Water usually forms a tetrahedral network of hydrogen bonds, which is reordered by dissociated hydrogen and chloride ions and non-dissociated HCl. The chloride ion is covered by a strong hydration layer, whereas the H_3O^+ complex - resulting from hydrated H^+ ions - participates in three strong and short hydrogen bonds.

Mile et al [17] used a similar approach by combining diffraction measurements with Monte-Carlo simulations and molecular dynamics simulations upon studying the structure of aqueous caesium chloride solutions. The authors showed that upon increasing the salt concentration the average number of water molecules around the ions decreases as water molecules in the hydration shell are substituted by counter-ions (see also [141]). In addition, the average number of water molecules around a given water molecule decreases from approximately 4 to about 3 as concentration increases.

It is already a known phenomena, that the hydration shell of some ion species is rather diffuse, whereas water molecules around other ions seem to be strongly bound and neatly oriented [17, 43]. Mähler and Persson [142] studied recently the hydration of the alkali metal ions in aqueous solution by large angle X-ray scattering and double difference infrared spectroscopy. Sodium and potassium are found to be weakly hydrated with only a single water shell. Lithium is more strongly hydrated thereby having a second hydration shell. The explicit statement of the authors should be noted, that determining the coordination numbers of water molecules around the ions is very difficult using the given experimental methods.

4.3.4 Description of the Evaluation Method

To calculate the RDF for a particle pair i and j, the distance r_{if} is calculated for every pair i,j in the simulation box and for every time-frame. The distances are binned in a histogram with a bin-width of $\Delta r = 0.002\,\mathrm{nm}$. The histogram is normalised by the factor V/N^2 resulting in a finite size version of Equ. 4.4:

$$g(r) = \frac{V}{N^2}\langle \sum_i \sum_{j \neq i} (\vec{r} - \vec{r}_{ij}) < \frac{1}{2}\Delta r \rangle.$$

The position of the first maximum of the RDF is taken from the raw dataset. At this position, the RDFs exhibits good statistics.

At the position of the first minimum, few sampling takes place. In addition, the RDF curves are flat at this point. To increase the quality of results, the RDF is interpolated with a spline and the position of the first minimum taken from the fit. The peak of the first maximum is not fitted, as sharp peaks tend to be artificially altered by fitting routines.

The cumulative or hydration number c_n of the first shell is obtained by integrating the RDF $g(r)$ from 0 to the position of the first minimum of the RDF r_{min} as described in Equ. 4.5.

The RDFs and cumulative numbers are calculated for the atom site of sodium, the atom site of chloride and the atom site of oxygen, thereby excluding the Drude particles attached to the atoms.

Ion-ion RDFs generally have a lower quality than ion-water RDFs because of the worse sampling. Reducing the concentration of ions, the effect on the sampling quality is drastic as the number of ion pairs decreases with the second order of the concentration.

Moreover, some parts of the ion-ion RDFs exhibit large errors, as the ions are well separated from each other by their hydration shells [83].

4.3.5 Performance of the Polarizable Model

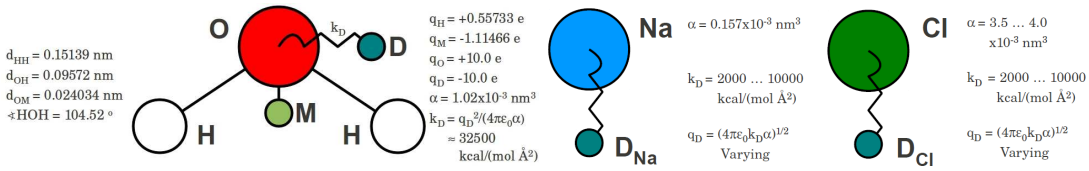

Figure 4.5: Schematic representations of the SW10e water and ion models developed by Lamoureux et al [25] and modified by Mikhail Stukan.

Simulation Setup

The simulations are performed with Gromacs 4.5.5 [110] in double precision.

The force field of sodium and chloride is sampled by using six different polarizabilities of chloride

$$\alpha_{\mathrm{Cl}} = 3.5,\ 3.6,\ 3.7,\ 3.8,\ 3.9,\ 4.0 \cdot 10^{-3}\mathrm{nm}^3$$

and five different spring constants of the Drude particles of sodium and chloride

$$k_{\mathrm{D}} = 2,\ 4,\ 6,\ 8,\ 10 \cdot 10^3\,\mathrm{kJ}/\left(\mathrm{mol}\cdot\mathrm{nm}^2\right),$$

resulting in 30 separate force field parameter sets. A pre-equilibrated simulation box consisting of 1024 SW10e molecules and 10 NaCl ion pairs serves as starting configuration. The setup results in a concentration of roughly 0.5 M. The same starting configuration is used for every model.

For every model, a simulation within the NPT ensemble is performed for 1 ns. The pressure is kept at 1 bar and the temperature maintained at 298.15 K.

Periodic boundary conditions are applied in all directions. The cutoff of the Lennard-Jones interactions is taken to be 1.2 nm with shifted potential taken from 1.0 nm. The long-range Coulomb interactions are handled by the Particle-Mesh Ewald method [112] with a cutoff of 1.5 nm and a grid spacing of 0.1 nm. The neighbour list for non-bonded interactions is updated every 10th integration step. We use the leap-frog algorithm for integrating Newton's equations of motion with 0.001 ps time step. All simulations are performed at fixed temperature. Velocity rescaling [113] is used with a temperature coupling constant of 0.1 ps. The pressure is held constant using the Berendsen barostat [114] with a pressure constant of 0.5 ps. We store the atomic coordinates of the ions each 5 ps for further analysis.

The influence of salt concentration is investigated with a similar setup except for a reduction of the number of ions pairs to 1, 2, 4, 6 and 8. The resulting concentrations range from 0.054 M for 1 ion pair to 0.54 M for 10 ion pairs in the box. For this additional simulations, the polarizability of chloride is set to $\alpha_{\mathrm{Cl}} = 4.0 \cdot 10^{-3}\mathrm{nm}^3$ and a spring constant of $k_{\mathrm{D}} = 10 \cdot 10^3\,\mathrm{kJ}/\left(\mathrm{mol} \cdot \mathrm{nm}^2\right)$ is applied.

For the neat SW10e simulations, a simulation setup as described in Sec. 4.1.3 is used.

Matlab [115] is applied for mathematical operations and plotting.

Results of the Force Field Screening

Example RDF plots, coordination numbers c_n and positions of the first maximum r^1_{max} and second maximum r^2_{max} of sodium-oxygen, chloride-oxygen and sodium-oxygen RDFs are provided in Fig. 4.6, 4.7 and 4.8. Figure 4.9 shows the oxygen-oxygen RDF of neat SW10e water. Table 4.7 provides a summary of the structural results.

Table 4.7: Structural properties of sodium and chloride ions in SW10e water at a salt concentration of 0.5 M and of neat SW10e water. Presented are the positions of the first maximum and first minimum of the indicated RDFs in conjunction with experimental values taken from Patra and Karttunen [44] for ions and from Soper [143] for neat water. For the sodium-chloride RDF no experimental data with reasonable accuracy is available. The qualitative influence of the screened force field parameter is summarised in the bottom of the table. The simulation results for all screened force field parameter are summarised in respective intervals.

RDF	maximum r^1_{max} (nm)	exp. maximum r^1_{max} (nm)	minimum r_{min} (nm)	exp. minimum r_{min} (nm)
O-O	0.280	0.2878	0.334	0.3325
Na-O	0.236	0.23-0.24	0.316-0.318	0.305-0.340
Cl-O	0.316	0.30-0.32	0.368-0.386	0.375-0.440
Na-Cl	0.264-0.256	—	0.362-0.363	—

FF variation	influence
k_{D}	negligible
α_{Cl}	increases Na-Cl coupling and Cl-O interaction

Neat Water Neat SW10e water reproduces experimental properties of the oxygen-oxygen RDF [143].

Ion Solution For all screened force field parameter, the values of $r^1_{\max}$ and $r_{\min}$ of Na-O and Cl-O RDFs are in agreement with experimental references [44]. For different polarizabilities α_{Cl}, $r_{\min}$ exhibits a wider spread than $r^1_{\max}$. This is a consequence of the flatness of the curves at the minima.

As mentioned above, experimental data for ion-ion RDFs cannot be obtained with reasonable accuracy. A comparison with reported data from other simulations using popular force fields shows consistence with all models under study, see Jensen and Jorgensen [82].

Influence of the Force Field Parameter In general, the spring constant k_{D} has no influence on the results. Although there is some scattering of results for different k_{D}, there is no general trend visible.

For the Na-O RDF, the position of the peaks do not depend on the polarizability α_{Cl}, which is natural, as only the polarizability of chloride is altered. There is a slight decrease in the coordination number as the polarizability α_{Cl} increases. As the sodium-oxygen interaction is not affected by the altered polarizability α_{Cl}, this effect must arise from a stronger sodium-chloride coupling.

For the Cl-O RDF, the position of the peaks is shifted to smaller distances (by 3%) on increasing the polarizability α_{Cl}. There is a pronounced decrease in the coordination number with increasing polarizability α_{Cl} as the water molecules in the proximity of chloride are replaced by sodium ions. In conclusion, less water stays around the chloride ion, however it is closer attached.

In a similar way, the distance between sodium and chloride is reduced with increasing polarizability α_{Cl} but the coordination number increases by a factor of 2!

Decreasing the polarizability further to $\alpha_{\mathrm{Cl}} = 2.0 \cdot 10^{-3}\mathrm{nm}^3$ the discussed trends are continued: the Cl-O coordination number increases whereas the Na-Cl coordination number decreases; $r^1_{\max}$ of the Cl-O RDF and $r^1_{\max}$ of the Na-Cl RDF increase further and the Na-O interaction is not changed, see Tab. 5.5.

In conclusion, the increasing polarizability of chloride does affect the (induced) dipole-dipole interaction between 1) the chloride ion and the SW10e molecule and 2) between the chloride ion and the sodium ion. The effect on sodium surpasses the effect on water, thus leading to a replacement of water in the proximity of chloride by sodium ions. The decreased hydration of chloride has an immediate influence on the osmotic pressure, see Sec. 4.6.

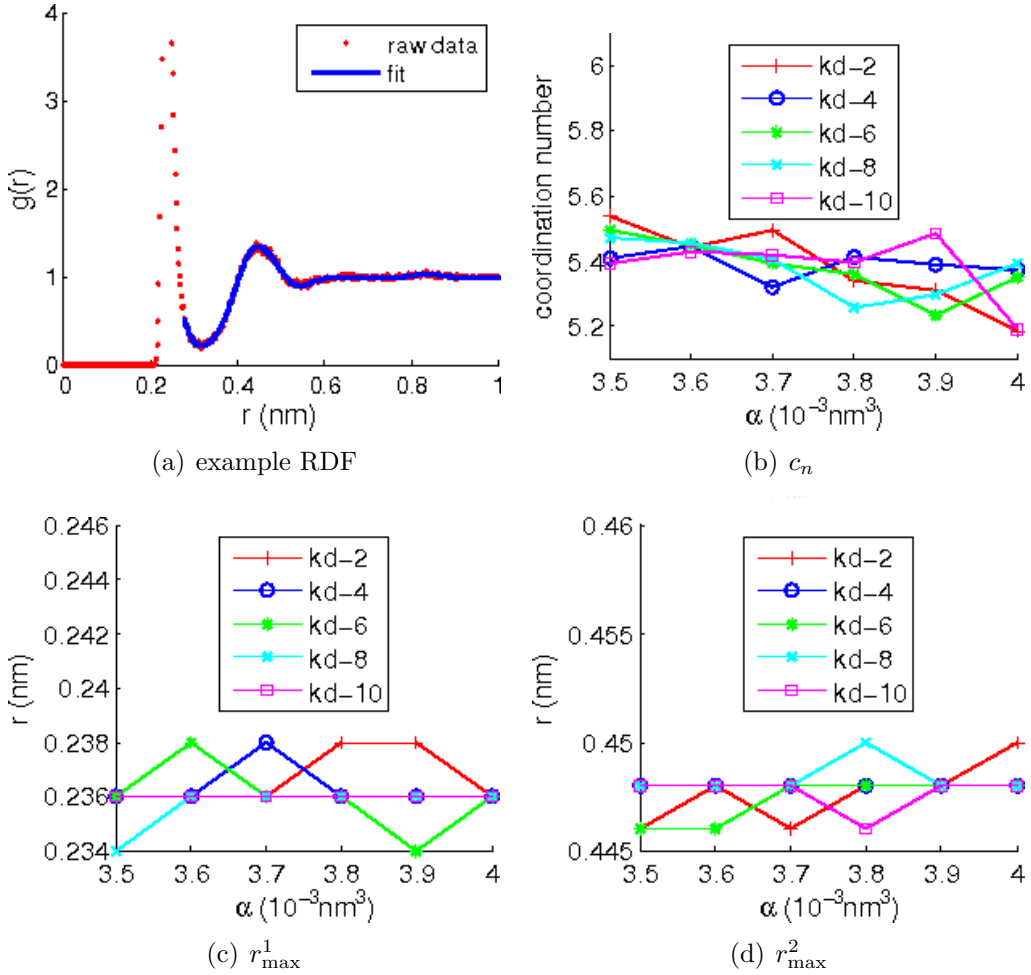

(a) example RDF

(b) c_n

(c) $r^1_{\max}$

(d) $r^2_{\max}$

Figure 4.6: **Na-O RDF** Summary of structural parameters of sodium ions in SW10e water gained from the sodium-oxygen radial distribution function (RDF). The simulations are performed with 10 sodium-chloride ion pairs in a box with 1024 SW10e water molecules, with different polarizabilities α_{Cl} of chloride and different spring constants k_{D} of sodium and chloride. a) Example RDF. The simulation is performed for the ion model with $\alpha_{\mathrm{Cl}} = 4.0 \cdot 10^{-3}\mathrm{nm}^3$ and $k_{\mathrm{D}} = 10 \cdot 10^3\,\mathrm{kJ}/\,(\mathrm{mol} \cdot \mathrm{nm}^2)$. The red dots represent the simulated data and the blue line a splinefit. b) First coordination number c_n. c) Peak position of the first maximum of the RDF $r^1_{\max}$. d) Peak position of the second maximum of the RDF $r^2_{\max}$.

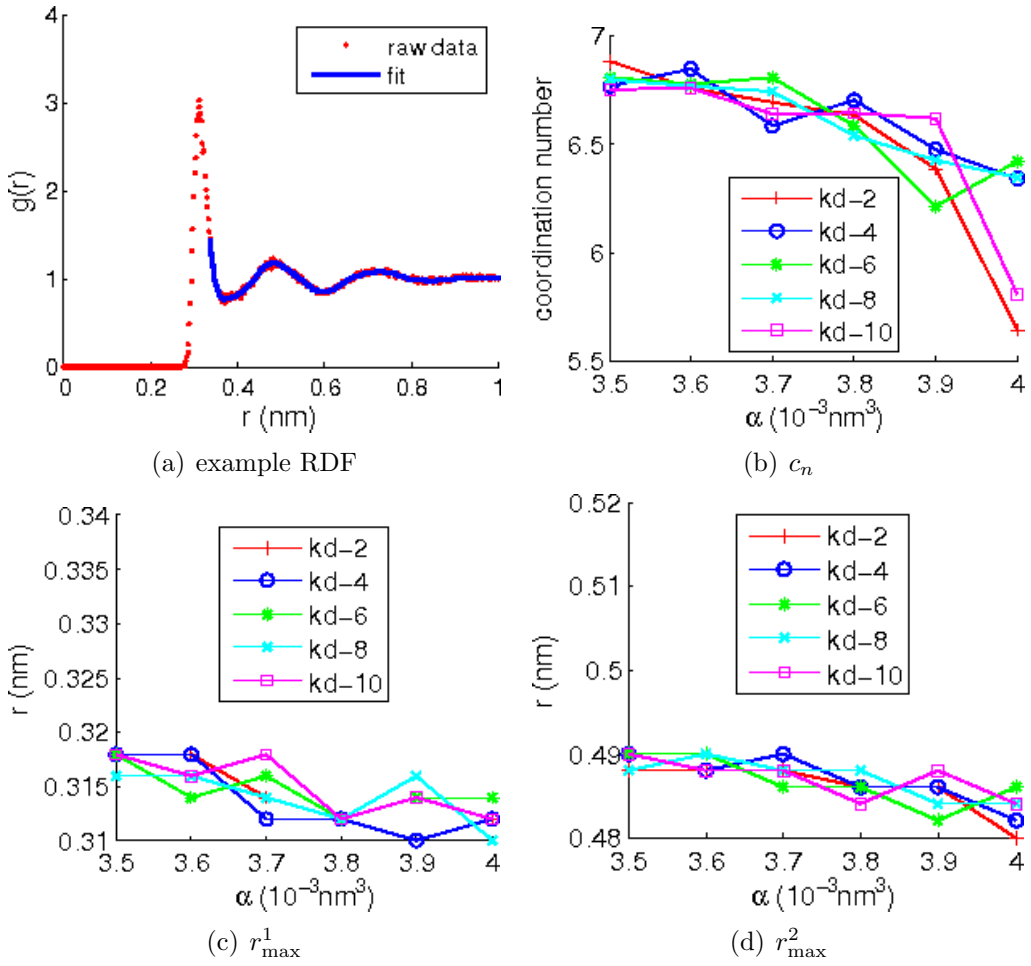

(a) example RDF (b) c_n

(c) $r^1_{\max}$ (d) $r^2_{\max}$

Figure 4.7: **Cl-O RDF** Summary of structural parameters of chloride ions in SW10e water gained from the chloride-oxygen radial distribution function (RDF). The simulations are performed with 10 sodium-chloride ion pairs in a box with 1024 SW10e water molecules, with different polarizabilities α_{Cl} of chloride and different spring constants k_{D} of sodium and chloride. a) Example RDF. The simulation is performed for the ion model with $\alpha_{\mathrm{Cl}} = 4.0 \cdot 10^{-3}\mathrm{nm}^3$ and $k_{\mathrm{D}} = 10 \cdot 10^3\,\mathrm{kJ}/\,(\mathrm{mol} \cdot \mathrm{nm}^2)$. The red dots represent the simulated data and the blue line a splinefit. b) First coordination number c_n. c) Peak position of the first maximum of the RDF $r^1_{\max}$. d) Peak position of the second maximum of the RDF $r^2_{\max}$.

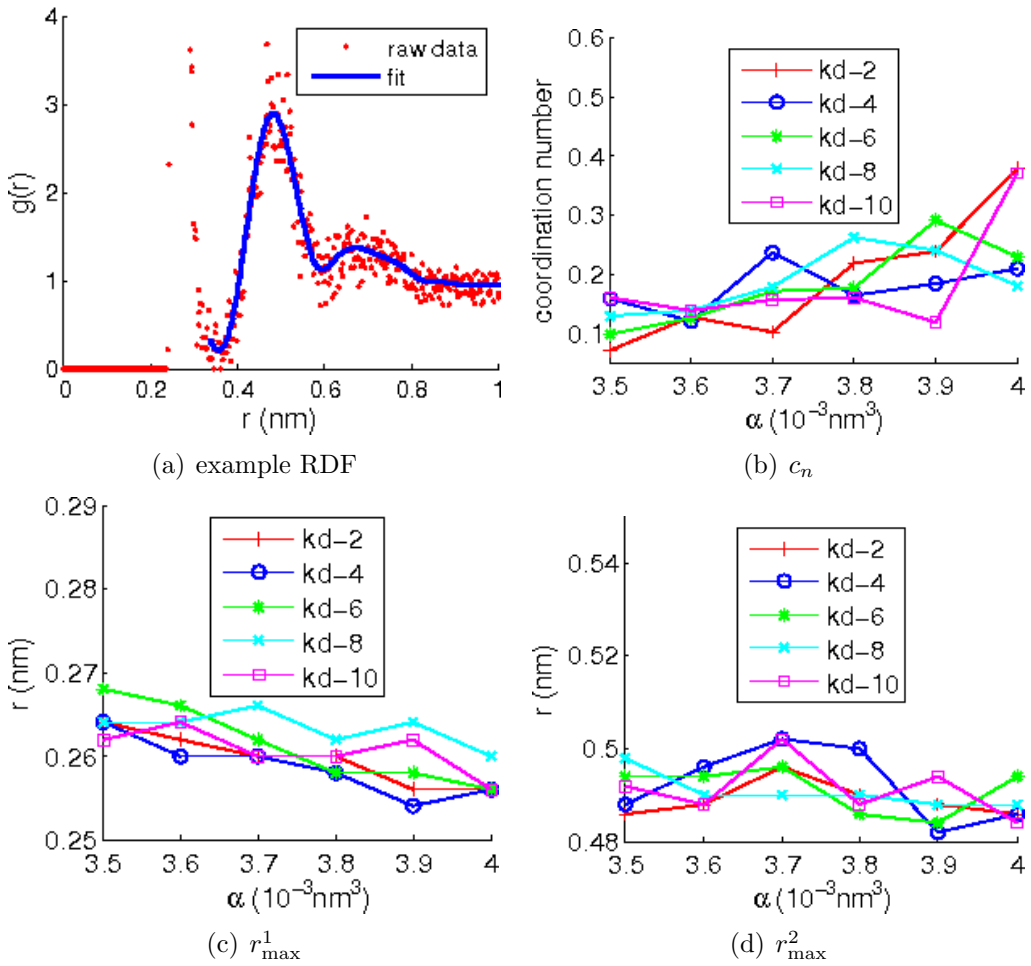

(a) example RDF (b) c_n

(c) $r^1_{\max}$ (d) $r^2_{\max}$

Figure 4.8: **Na-Cl RDF** Summary of structural parameters of sodium-chloride ions in SW10e water gained from the sodium-chloride radial distribution function (RDF). The simulations are performed with 10 sodium-chloride ion pairs in a box with 1024 SW10e water molecules, with different polarizabilities α_{Cl} of chloride and different spring constants k_{D} of sodium and chloride. a) Example RDF. The simulation is performed for the ion model with $\alpha_{\mathrm{Cl}} = 4.0 \cdot 10^{-3}\mathrm{nm}^3$ and $k_{\mathrm{D}} = 10 \cdot 10^3\,\mathrm{kJ}/\,(\mathrm{mol} \cdot \mathrm{nm}^2)$. The red dots represent the simulated data and the blue line a splinefit. b) First coordination number c_n. c) Peak position of the first maximum of the RDF $r^1_{\max}$. d) Peak position of the second maximum of the RDF $r^2_{\max}$.

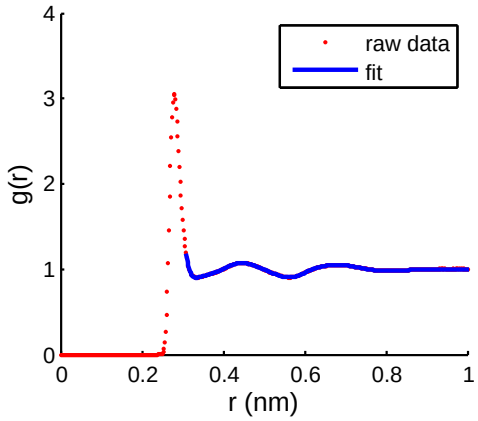

Figure 4.9: **O-O RDF** Oxygen-oxygen radial distribution function in neat SW10e water.

Concentration Dependence of the Pair Distribution Maximum

As the structural data for ion pairing and hydration number depends on the salt concentration, the RDF is defined for infinite dilution. Real experiments and our simulations are performed at finite concentration to obtain sufficient sampling. However, at low concentration, the results are expected to differ only slightly from infinite dilution, as the ions are well separated by the hydration shell [83].

Characteristic quantities of the RDFs at salt concentrations of $c = 0.054\,\mathrm{M}$ to $0.54\,\mathrm{M}$ are presented in Tab. 4.8.

For all but one concentrations we find the peak positions of the sodium-oxygen, chloride-oxygen and sodium-chloride RDF to be equal. For the lowest concentration we have, as expected, difficulties in sampling the Na-Cl distribution function as only two ions are found in the whole simulation box. The value of $0.674\,\mathrm{nm}$ for the position of the maximum in the sodium-chloride RDF measured at $c = 0.054\,\mathrm{M}$ is therefore an artificial result.

Table 4.8: Concentration dependency of the position of the first maximum of Na-O, Cl-O and Na-Cl RDFs for sodium-chloride in SW10e. 1, 2, 4, 6, 8 and 10 ion pairs are dissolved in a box with 1024 SW10e water molecules, corresponding to a salt concentration of $c = 0.054\,\mathrm{M}$ to $0.54\,\mathrm{M}$. The simulations are performed for the ion model with $\alpha_{\mathrm{Cl}} = 4.0 \cdot 10^{-3}\mathrm{nm}^3$ and $k_{\mathrm{D}} = 10 \cdot 10^3\,\mathrm{kJ}/\,(\mathrm{mol} \cdot \mathrm{nm}^2)$.

		r^1_{max} (nm)		
# ion pairs	c (M)	Na-O	Cl-O	Na-Cl
1(*)	0.054	0.234	0.312	0.674
2	0.108	0.238	0.32	0.256
4	0.216	0.236	0.316	0.258
6	0.324	0.236	0.312	0.268
8	0.431	0.236	0.312	0.258
10	0.536	0.236	0.312	0.256

(*) result is artificial - sampling is insufficient

4.3.6 Conclusion: Performance of the Method and the Model

We presented a method for sampling RDFs using bulk simulations of water molecules and ions. Whereas the method is cheap and straightforward, it exhibits difficulties in sampling the ion-ion RDFs. This problem becomes more pronounced at low ion concentrations and at ion-ion distances of low probability. We will present a method to circumvent this problem in Sec. 4.5.

At the given concentration of ions, reasonable water-water and ion-water RDFs can be expected from a 1 ns long simulation. The position of maxima and minima are well distinguishable. On the other hand, the position of the first minimum is afflicted with a relative large error as the curve is usually flat at this point. The error in the position of the first minimum together with the general error in the amplitude of the RDF combine to uncertainties in the cumulative number.

To benchmark ion and water models on the real world, ion-ion RDFs are of minor interest, as they are not measurable by experiments. In terms of peak position, water-ion RDFs can be measured experimentally with good accuracy and show good agreement with simulated results. We improved the computational performance by simulating at a finite concentration and confirmed the validity of our results, by crosschecking with results obtained at high dilution.

To characterise our water and ion models, we measured and characterised structural data for a variety of 30 polarizable ion models. We analysed RDFs in terms of peak and valley position and cumulative number.

In general, the spring constant k_{D} has a negligible influence on the results.

Whereas the polarizability of chloride has a minor influence on the chloride-water interaction, it plays a dominant role in the sodium-chloride coupling: while increasing the polarizability from $\alpha_{\mathrm{Cl}} = 3.5$ to $\alpha_{\mathrm{Cl}} = 4.0 \cdot 10^{-3}\mathrm{nm}^3$ the coordination number increases by a factor of 2(!) thereby replacing the water molecules in the proximity of chloride by sodium ions. Due to this behaviour, we expect a noticeable influence of the polarizability on the osmotic pressure, see Sec. 4.6.

4.4 Residence Time

4.4.1 Introduction - the Dark Side of the Hydration Shell

The discussion of the hydration shell is not complete without investigating the dynamic properties of the hydration shell. Typically, the hydration shell is described by means of the (static) hydration number and the radial distribution function. Impey et al [144] were among the first, to describe the *persisting coordination*. That means the characteristic time the water molecules stay in the hydration shell. For a precise definition of this characteristic time called *residence time* τ, they introduced the function $P_j(t, t_n; t^*)$. Whereas Impey et al use a slightly different definition, P_j basically provides the probability of an water molecule j to stay in the hydration shell after entering at t_n till $t_n + t$ without leaving the shell longer than t^*. As the residence probability P only depends on the duration of the stay in the hydration shell and is in the mean identical for all water molecules, we can write:

$$\langle P_j(t, t_n; t^*)\rangle = P(t; t^*).$$

Naturally, $P(t = 0) = 1$ and $P(t = \infty) = 0$.

The concept can easily be applied to the coordination number n, thereby introducing a time dependent persistent coordination number $n(t)$:

$$n(t) = n(0)P(t; t^*).$$

The tolerance time t^* is chosen by Impey et al and others to be 2 ps [144, 145, 146, 147, 43]. Impey et al estimate t^* to be the time necessary for water molecules to enter a new hydration shell. For this, they calculate the residence time of water around water with $t^* = 0$ and obtain $\tau_{OO} = 1.8\,\text{ps}$.

According to Impey et al, the function $n(t)$ follows an exponential decay $n(t) \approx n(0)\exp(-t/\tau)$ with τ being the *residence time*. The exponential decay is not valid at "short times" [144].

Authors as Guàrdia and Padró [145], Smith and Dang [146] and Lee et al [147] used the residence time for characterising ionic solutions in the 1990s. In these works, the authors agree about two general trends: The residence time increases with decreasing temperature and increases with decreasing ion radius. Beside agreement in these general observations, the absolute reported values vary strongly. In recent years, papers discussing the residence time became rare.

A recent paper including the discussion of residence times in aqueous solution

is published by Joung and Cheatham [148] in 2009. The authors use the residence time to compare different ions and different force fields. Alas, beside of the great increase in computational power since the 1990s, the authors are not able to determine the residence time for all ionic species, either because it exceeds the simulation time or the ensemble size is insufficient. As for the other ions and force fields "consistent trends in the cation-anion residence time [...] (as function of ion size) are not observed" [148].

Frolov et al [43] use the residence time as means of describing the kinetic behaviour of different ions in a solution with a carbon surface. The residence time is calculated for ions and water in the vicinity of a carbon nanotube to determine the tendency of molecular species to stay close to the nanotube. Frolov et al [43] found a strong dependency of the residence time with the ion size, the smaller the ions, the shorter they stay at the carbon surface, whereas water stays the longest.

Koneshan et al [133] describe the ion solvation of neutral and charged ions in terms of residence times and observe the formation of a solvent cage around the ions upon charging or discharging.

The upcoming sections act as fundamental study on the usability and meaningfulness of the residence time and as means to identify possible applications and obstacles. First, we discuss available experimental data. Then, we will provide a brief description of the evaluation routine of the residence time. We will calculate the tolerance time t^* for SW10e water and investigate the influence of the fitting parameter on the result. The residence probabilities and residence times for water around water, water around ions and ions around ions are presented and their reliability is discussed. We will conclude the study with a discussion on drawbacks of the evaluation method and a discussion on possible future work.

4.4.2 Experimental Method: Order of Magnitude through Nuclear Magnetic Resonance and Quasi-Elastic Neutron Scattering

The interpretation of the residence time of water in the hydration shell of ions relies heavily on computational experiments [149, 134]. A comparison of the quantity of published references considering simulation results [144, 145, 146, 147, 133, 148, 43] and experimental studies [134] of the dynamics of the hydration shell shows a severe unbalance.

The reason is to be found in the accuracy of the results, as the experimental

methods Nuclear Magnetic Resonance (NMR) and Quasi-Elastic Neutron Scattering (QENS) only provide the *order of magnitude* of the residence time [134]. Fortunately, simulation results are in agreement with the observed orders of magnitudes and thus are considered as reliable source for further discussion of the subject.

The only estimate for the water-water residence time is mentioned by Impey et al [144] and is done by Hertz: Hertz estimates the residence time of pure water by correlating the diffusivity of water with the mean distance between two water molecules. This very crude estimate provides a residence time of 2 ps, which is in surprisingly good agreement with simulation data.

4.4.3 Description of the Simulation Method

We use the definition of residence time provided by Impey et al [144]. Therefore a NPT simulation is performed and the trajectory saved with a high frequency for further processing.

For an easier explanation, we assume to calculate the residence of water molecules around a specific ion. The procedure can easily be extended to any desired pair of molecules and number of ions in the box. We identify all water molecules in the first hydration shell around the ion by their residue numbers. In the next frame, the relative position of water molecules is determined and it is checked, if they are a) still in the hydration shell or b) have left the hydration shell. If they are still in the hydration shell, their individual counter is increased by 1 frame. If they left the hydration shell, a second timer is started. If the molecule reenters the hydration shell during a period smaller than t^*, the time outside the hydration shell is added to the stay time. If a molecule stays longer than t^* outside the hydration shell, the duration inside the hydration shell t is printed out.

The individual residence times are plotted in a histogram and fitted to an exponential function. As the residence time is defined at long times, the short time parts of the residence probability is omitted. Tests reveal, that a good starting point for the fit is at 1 ps. Fits are applied on time intervals with reasonable statistics, for water-water residence times typically up to 15 ps. To elude remnants of the fast declining parts in the probability function, a bi-exponential function

$$f(t) = a \cdot \exp(-t/\tau_a) + b \cdot \exp(-t/\tau_b)$$

is used for fitting and the larger time-constant taken as residence time.

4.4.4 Performance of the Polarizable Model

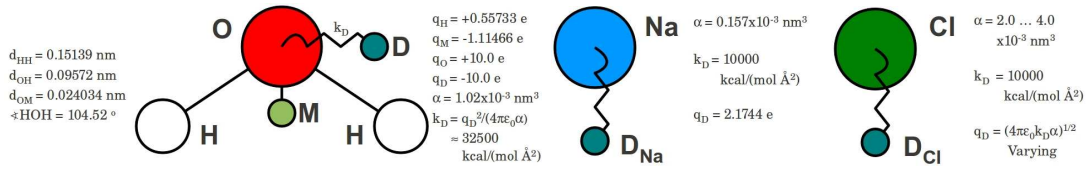

Figure 4.10: Schematic representations of the SW10e water and ion models developed by Lamoureux et al [25] and modified by Mikhail Stukan.

Simulation Setup

The simulations are performed with Gromacs 4.5.5 [110] in double precision.

For chloride different force fields with a polarizabilities of chloride between $\alpha_{\mathrm{Cl}} = 2.0 \cdot 10^{-3}\mathrm{nm}^3$ and $\alpha_{\mathrm{Cl}} = 4.0 \cdot 10^{-3}\mathrm{nm}^3$ are used.

For pure SW10e water, a simulation with 1024 SW10e water molecules is performed within the NPT ensemble for 1 ns. We store the atomic coordinates of the ions each 0.1 ps for further analysis.

Simulations with ions are performed at different concentrations for different times. The coordinates are stored every 1.0 ps.

The pressure is kept at 1 bar and the temperature maintained at 298.15 K.

Periodic boundary conditions are applied in all directions. The cutoff of the Lennard-Jones interactions is taken to be 1.2 nm with shifted potential taken from 1.0 nm. The long-range Coulomb interactions are handled by the Particle-Mesh Ewald method [112] with a cutoff of 1.5 nm and a grid spacing of 0.1 nm. The neighbour list for non-bonded interactions is updated every 10th integration step. We use the leap-frog algorithm for integrating Newton's equations of motion with 0.001 ps time step. Velocity rescaling [113] is used with a temperature coupling constant of 0.1 ps. The pressure is held constant using the Berendsen barostat [114] with a pressure constant of 0.5 ps.

Matlab function [115] are developed for mathematical operations and plotting.

Results of the Water-Water Residence Time

Figure 4.11 shows the residence probability $P_{OO}(t)$ of water around water for the SW10e model.

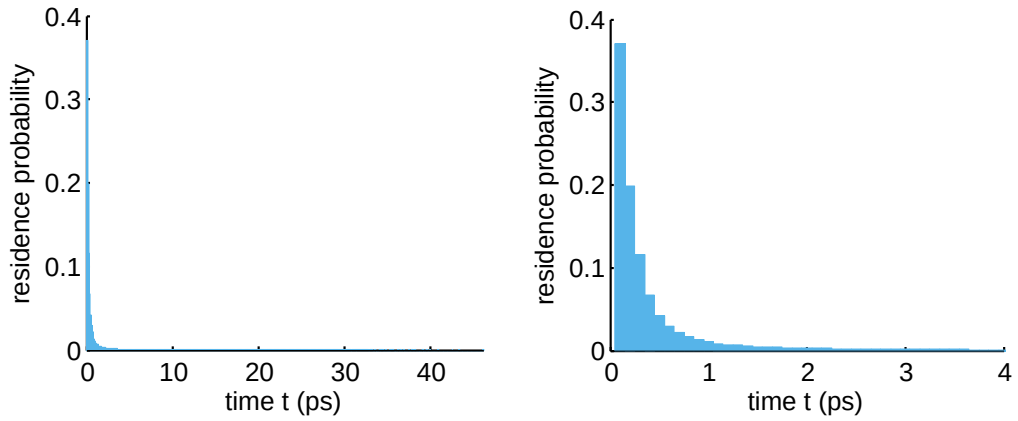

(a) $P(t)$ O-O (b) $P(t)$ O-O

Figure 4.11: Residence probability $P_{OO}(t)$ of water around water for the SW10e model with $t^* = 0$. The oxygen atom is taken to represent the whole water molecule. The bin size of the probability function is 0.1 ps. a) $P_{OO}(t)$ over the full range of measured stays up to over 40 ps. b) Close-up of $P_{OO}(t)$.

A bi-exponential function is fitted to $P_{OO}(t)$ for different time intervals. The results are presented in Tab. 4.9, Fig. 4.12 and Fig. 4.13.

The short time part can not be approximated by a mono or bi-exponential function. This time regime is attributed to water molecules not participating in the formation of a hydration shell but of colliding with, passing by or touching the shell.

For intermediate time intervals, we exclude the short time part and the tail of the probability function with bad statistics. Thus we obtain high quality fits and also mono-exponential fits are possible. Taking the slow diminishing contributions from the bi-exponential fits or the mono-exponential fit, we can estimate the water-water residence time of SW10e to be 2.5 to 2.6 ps. For residence time calculations of water around ions and ions around ions we will use a tolerance time of $t^* = 2$ ps in agreement with Impey et al [144].

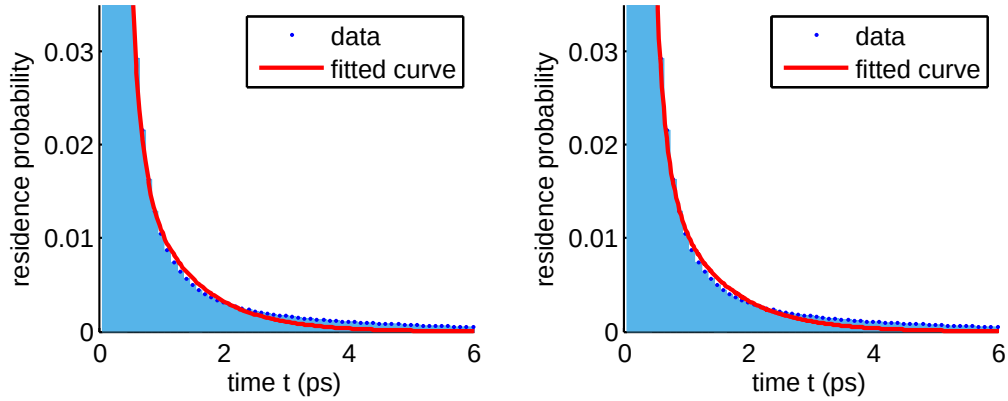

(a) 0.1 ps-end

(b) 0.1-25 ps

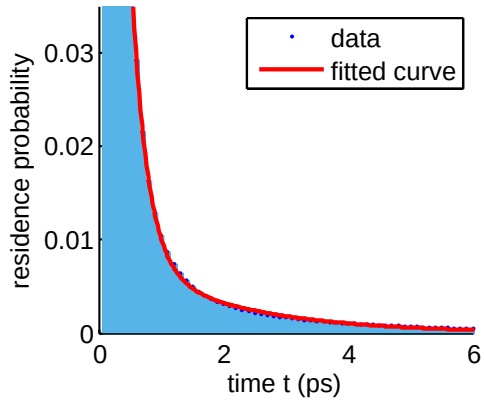

(c) 0.5-25 ps

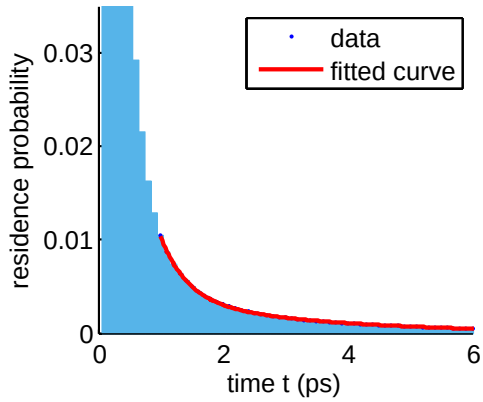

(d) 1.0-25 ps

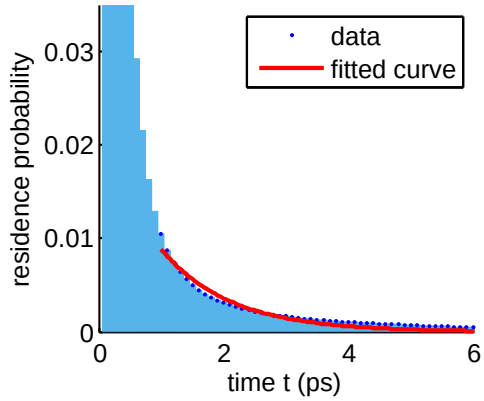

(e) 1.0 ps-end

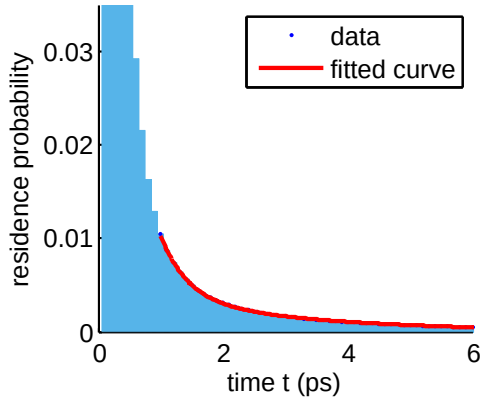

(f) 1.0-15 ps

Figure 4.12: Residence probability $P_{\mathrm{OO}}(t)$ of water around water for the SW10e model with $t^* = 0$ and bi-exponential fits for different time intervals. The bin size of the probability function is 0.1 ps. The oxygen atom is taken to represent the whole water molecule. a), b) and c) Good quality fits are not possible if the time interval for fitting starts too early, nor when e) the tail of the probability function $P_{\mathrm{OO}}(t)$ is taken into account. d) and f) At intermediate time intervals, good fits are possible and show a similar shape. For details see Tab. 4.9.

Table 4.9: Bi-exponential fits of the residence probability $P_{OO}(t)$ of water around water for the SW10e model with $t^* = 0$ ps for different time intervals as indicated in the second column. The bin size of the probability function is 0.1 ps. The oxygen atom is taken to represent the whole water molecule. Good quality fits are not possible if the time interval for fitting starts too early, nor when the tail of the probability function $P_{OO}(t)$ is taken into account. At intermediate time intervals, good fits are possible and show a similar shape. For the fit in Fig. 4.13(b) a mono-exponential function is used.

Fig.	time interval (ps)	τ_a (ps)	τ_b (ps)
4.12(a)	0.1 - end	0.89	0.15
4.12(b)	0.1 - 25	0.91	0.15
4.12(c)	0.5 - 25	1.81	0.25
4.12(d)	1.0 - 25	2.49	0.42
4.12(e)	1.0 - end	5.55	1.12
4.12(f)	1.0 - 15	2.49	0.43
4.13(b)	3.0 - 15	2.58	—

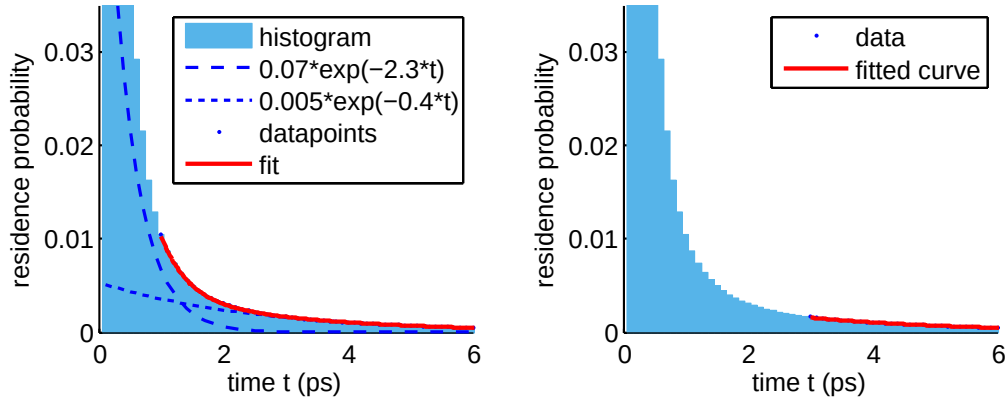

(a) 1.0-15 ps (b) 3.0-15 ps

Figure 4.13: Residence probability $P_{OO}(t)$ of water around water for the SW10e model with $t^* = 0$ and exponential fits for different time intervals. The bin size of the probability function is 0.1 ps. The oxygen atom is taken to represent the whole water molecule. a) Bi-exponential fit for the time interval of 1.0 to 15 ps (red line). The two dashed lines represent the two exponential parts of the fit with $\tau_a = 2.49$ ps and $\tau_b = 0.43$ ps. The fast decaying part vanishes after 3 ps. b) Consequently, the residence probability $P_{OO}(t)$ can be fitted with a mono-exponential fit $a \exp(-t/\tau_a)$ in the time interval 3.0 to 15 ps with $\tau = 2.58$ ps.

Results of the Ion-Water and Ion-Ion Residence Time

To evaluate the ion-water and ion-ion residence time, simulations with a storage frequency of once every 1.0 ps are performed. The tolerance time t^* is set to 2 ps. Three different simulations are evaluated: 300 ps at 1 M ion concentration, 1 ns at 0.5 M and 4 ns at 0.5M. The probability functions $P_{\mathrm{NaO}}(t, t^*)$, $P_{\mathrm{ClO}}(t, t^*)$, $P_{\mathrm{NaCl}}(t, t^*)$ and fits are presented in the Fig. 4.14, 4.15 and 4.16. A summary of residence times is provided in Tab. 4.10. Residence times for ions around ions are not given, as not enough statistics are available. Anyway, a very long residence time is suspected, see Fig. 4.16(e).

Beside reasonable looking fits of the probability functions, the actual residence times τ vary greatly for the different simulations. We suspect, that more statistics are necessary to determine the ion-water residence time with confidence. We want to emphasise the point, that for a reliable determination of an exponential coefficient high quality data is necessary. Reasonable fits of the ion-ion probability functions are not possible at all. Also, the reported correlation between the residence time of water around sodium and chloride [144] is not supported by our data: the residence time of sodium is either equal or lower than the residence time of chloride, see Tab. 4.10.

Table 4.10: Mono- and bi-exponential fits of the residence probability $P_{\mathrm{NaO}}(t, t^*)$ and $P_{\mathrm{ClO}}(t, t^*)$ of water around Na and Cl, respectively, with $t^* = 2$ ps. Three different simulations times are used to create three sets of data. The bin size of the probability function is 1.0 ps. The oxygen atom is taken to represent the whole water molecule.

	$P_{\mathrm{NaO}}(t, t^*)$				$P_{\mathrm{ClO}}(t, t^*)$		
Fig.	sim. time (ns)	τ_a (ps)	τ_b (ps)	Fig.	sim. time (ns)	τ_a (ps)	τ_b (ps)
4.14(b)	0.3	3.46	—	4.14(d)	0.3	9.21	—
4.15(b)	1.0	11.1	—	4.15(d)	1.0	22.7	2.60
4.16(b)	4.0	20.0	3.0	4.16(d)	4.0	20.0	2.7

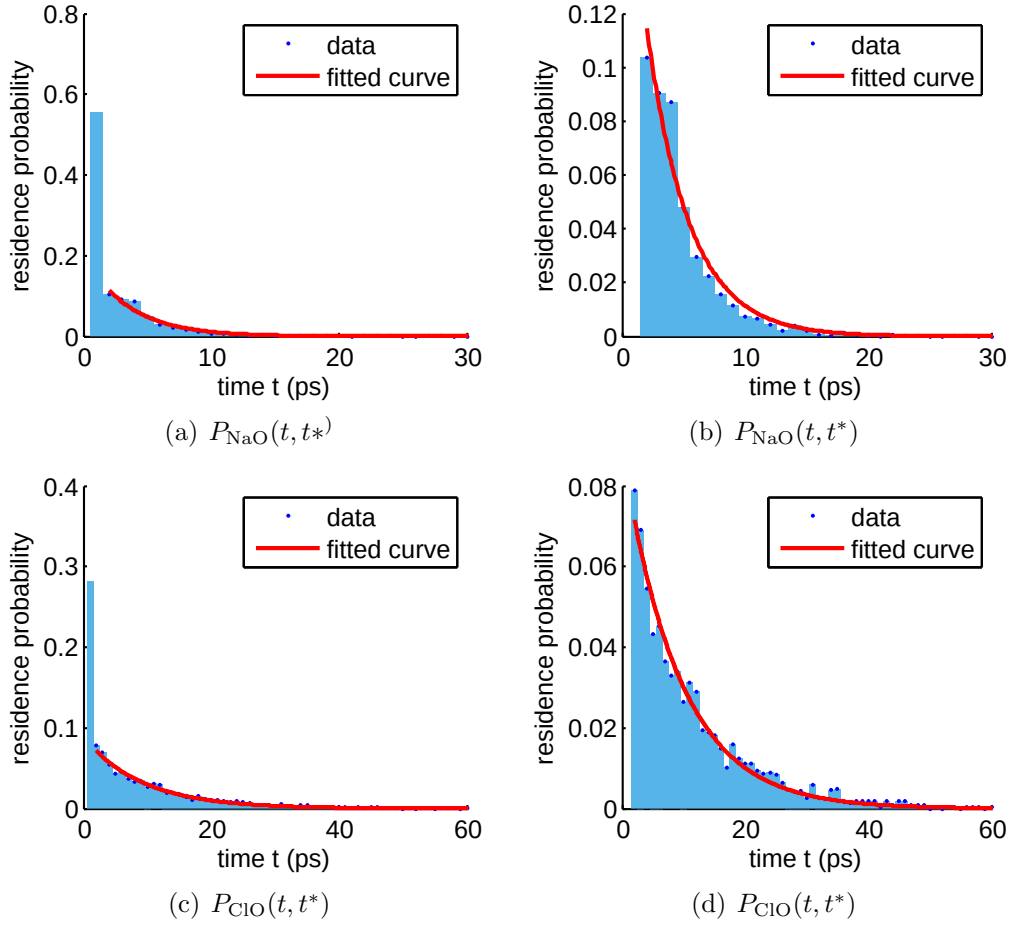

(a) $P_{\mathrm{NaO}}(t, t*)$ (b) $P_{\mathrm{NaO}}(t, t^*)$

(c) $P_{\mathrm{ClO}}(t, t^*)$ (d) $P_{\mathrm{ClO}}(t, t^*)$

Figure 4.14: **1.0 M, 0.3 ns** Residence probability $P_{\mathrm{NaO}}(t, t^*)$ and $P_{\mathrm{ClO}}(t, t^*)$ for water around Na and Cl, respectively, with $t^* = 2\,\mathrm{ps}$ and exponential fits. The bin size of the probability function is 1.0 ps. The oxygen atom is taken to represent the whole water molecule. a) Mono-exponential fit for $P_{\mathrm{NaO}}(t, t^*)$ with $\tau = 3.46\,\mathrm{ps}$. b) Closeup of a). c) Mono-exponential fit for $P_{\mathrm{ClO}}(t, t^*)$ with $\tau = 9.21\,\mathrm{ps}$. d) Closeup of c). For the residence probability of Na around Cl only one datapoint is available.

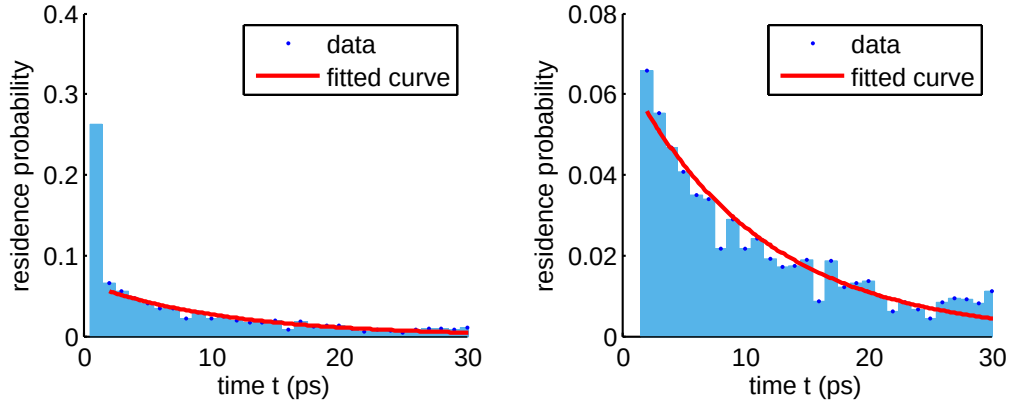

(a) $P_{\mathrm{NaO}}(t, t*)$ (b) $P_{\mathrm{NaO}}(t, t^*)$

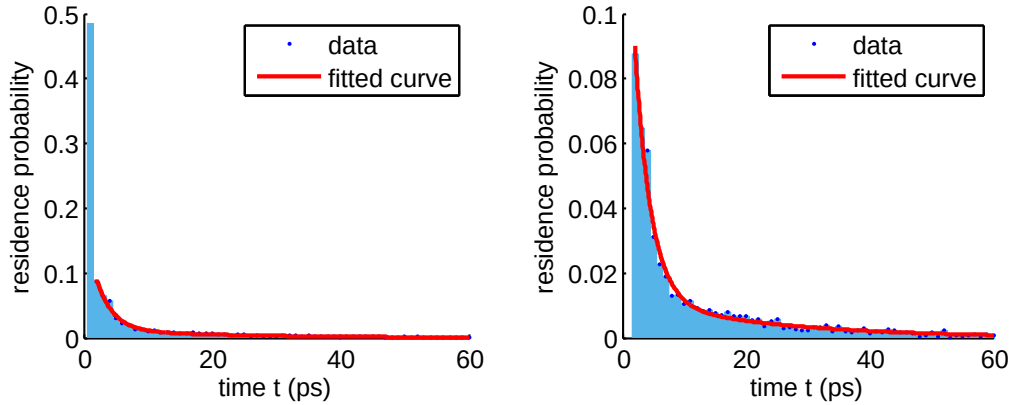

(c) $P_{\mathrm{ClO}}(t, t^*)$ (d) $P_{\mathrm{ClO}}(t, t^*)$

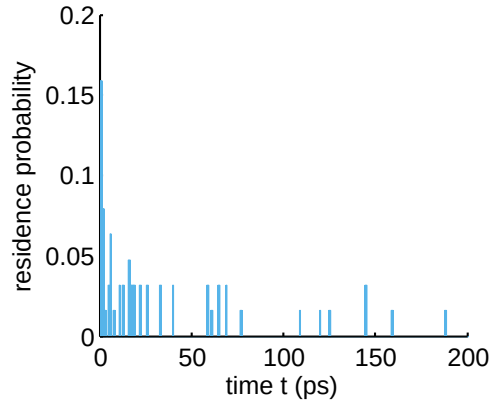

(e) $P_{\mathrm{NaCl}}(t, t^*)$

Figure 4.15: **0.5 M, 1 ns** Residence probability $P_{\mathrm{NaO}}(t, t^*)$, $P_{\mathrm{ClO}}(t, t^*)$ and $P_{\mathrm{NaCl}}(t, t^*)$ for water around Na and Cl and for Na around Cl, respectively, with $t^* = 2\,\mathrm{ps}$ and exponential fits. The bin size of the probability function is 1.0 ps. The oxygen atom is taken to represent the whole water molecule. a) Mono-exponential fit for $P_{\mathrm{NaO}}(t, t^*)$ with $\tau = 11.1\,\mathrm{ps}$. b) Closeup of a). c) Bi-exponential fit for $P_{\mathrm{ClO}}(t, t^*)$ with $\tau_a = 22.7\,\mathrm{ps}$ and $\tau_b = 2.60\,\mathrm{ps}$. d) Closeup of c). e) Residence probability of Na around Cl $P_{\mathrm{NaCl}}(t, t^*)$.

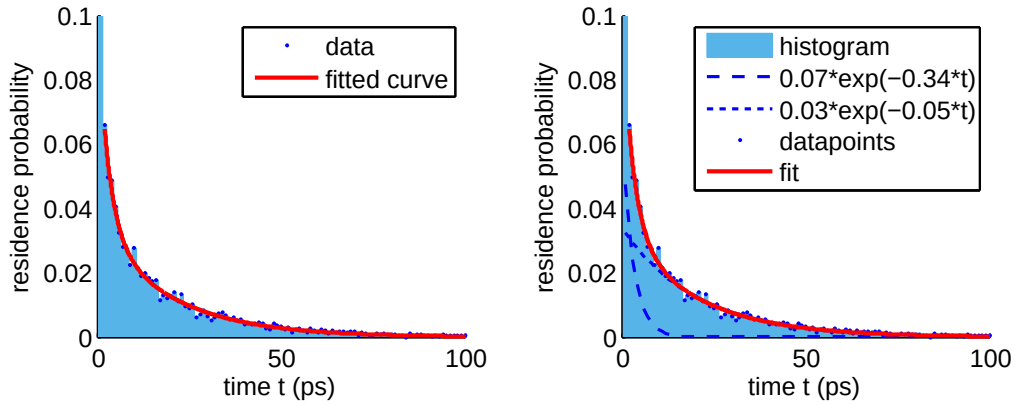

(a) $P_{\mathrm{NaO}}(t, t*)$

(b) $P_{\mathrm{NaO}}(t, t^*)$

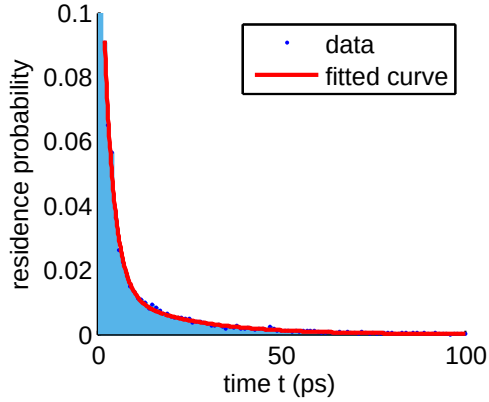

(c) $P_{\mathrm{ClO}}(t, t^*)$

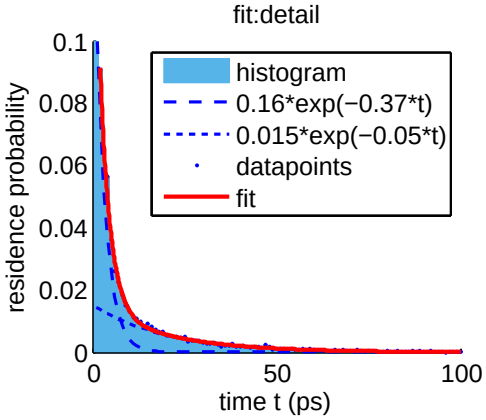

(d) $P_{\mathrm{ClO}}(t, t^*)$

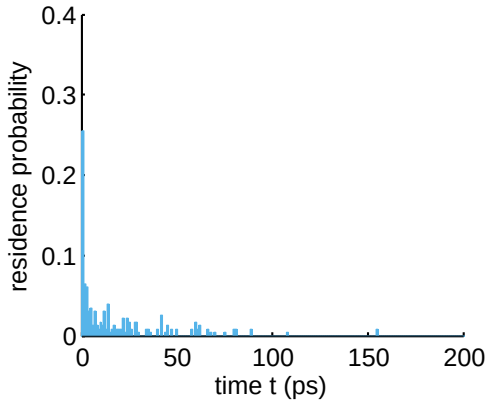

(e) $P_{\mathrm{NaCl}}(t, t^*)$

Figure 4.16: **0.5 M, 4 ns** Residence probability $P_{\mathrm{NaO}}(t, t^*)$, $P_{\mathrm{ClO}}(t, t^*)$ and $P_{\mathrm{NaCl}}(t, t^*)$ for SW10e water around Na and Cl and for Na around Cl, respectively, with $t^* = 2\,\mathrm{ps}$ and exponential fits. The bin size of the probability function is 1.0 ps. a) Bi-exponential fit for $P_{\mathrm{NaO}}(t, t^*)$ with $\tau_a = 20.0\,\mathrm{ps}$ and $\tau_b = 3.0\,\mathrm{ps}$. b) Closeup of a). c) Bi-exponential fit for $P_{\mathrm{ClO}}(t, t^*)$ with $\tau_a = 20.0\,\mathrm{ps}$ and $\tau_b = 2.7\,\mathrm{ps}$. d) Closeup of c). e) Residence probability of Na around Cl $P_{\mathrm{NaCl}}(t, t^*)$.

4.4.5 Conclusion

The residence time is a promising quantity in revealing dynamic properties of ion solvation and ion interaction with interfaces [144, 145, 146, 147, 133, 148, 43, 149, 134]. In our opinion, the residence time is underutilised in modern computational science. Anyway, the method of determining the residence time needs more rigorous investigation before it can be used.

Performance of the Method We are able to provide reasonable data for the water-water residence time consistent with the work by Impey et al [144].

We are not able to calculate reliable ion-water and ion-ion residence times. Especially for ion-ion interactions, the residence time is so long and the event of parting ions so rare, that a sound statement of the residence time would need a huge amount of data.

Beside the need for good statistics, there are other variables which need a more thoroughly investigation. Laage and Hynes [150] raised the issue, that residence times are sensitive to the value of the tolerance time t^*. We did not test the influence of the t^* parameter, nor the influence of a small variation of the hydration shell radius or a different definition for a hydration shell as proposed by Northrup and Hynes [151]. The influence of the bin size of the residence probability on the residence time has yet to be determined, or in other words, the minimum frequency of saving the trajectory is unknown.

In general, the necessity of using fit functions introduces many arbitrary variables, as starting and end time of the fit, form of the fit function, initial guess and more. Without dispelling these obstacles by providing rigorous definitions and thoroughly investigations, identical trajectories easily lead to a variation of residence times.

A possibility to modify the calculation of the residence time would be to take the arithmetic mean or the meridian of the residence probability P. In this way, we might decrease the amount of necessary data while maintaining physical meaningfulness and avoiding the use of a fit function. A possible shortcoming of this approach is the high influence of the short time regime on the result. Arithmetic means of the residence probability over all data result in very short residence times.

Results for the Model We are able to provide a reasonable value for the SW10e water-water residence time of 2.5 ps. This result is consistent with the work by Impey et al [144] and provided experimental estimations. As for ion-water and ion-ion residence time, we need better statistics for reliable results. We estimate ion-water residence times of 20 ps with a deviation of 10 ps between independent simulations. Thus, we cannot compare the residence time of different ion species nor can we securely discuss an observed decrease of the residence time with increasing salt concentration.

We conclude, that the estimation of the residence time requires further research on the method as proposed above and thus no physical interpretation of our model performance can be done by now.

4.5 Potential of Mean Force

4.5.1 Introduction: Describing the Solution in a Nut Shell

In 1935 Kirkwood [152] has been the first scientist to describe *the potential of intermolecular forces with reference to the relative coordinates of molecular pairs.* The potential can be expressed through "simple integrals in the configurational space associated with the relative motion of molecular pairs". Within the integrals, pair distribution functions are used to describe the molecular structuring in the configurational space. These days the *Potentials of Mean Force (PMF)* are still of great interest [153, 154, 155, 156, 157, 158, 159, 160, 161, 162, 163, 164].

The PMF and radial distribution functions (RDF) play a dominant role in the description of a wide number of physico-chemical properties of solutions [152, 84, 165]. The Kirkwood-Buff theory of solutions developed in 1951 by Kirkwood and Buff describes the relationships between thermodynamic quantities and molecular distribution functions for multi-component systems in the (T,V,μ)-ensemble [166]. By correlating thermodynamic properties such as compressibility, partial molar volumes and derivatives of the chemical potentials with pair correlation functions, the Kirkwood-Buff theory proved to be extremely powerful [167]. Since today, publications on protein-salt interactions such as protein hydration are based on the Kirkwood-Buff theory [168, 169, 170].

It becomes apparent that a precise knowledge of the PMF and molecular distribution functions is crucial for understanding ion effects in nature. For developing force fields of ions in aqueous solution, the description of the PMF proved to be a valuable tool [94, 40, 171].

In this study, we will focus on ions in solutions. It should be noted, that PMFs can also be calculated for ions approaching or pushing through interfaces [164]. We aim to calculate the potential of mean force of dissolved sodium-chloride, sodium-sodium and chloride-chloride ion pairs. The calculation of the PMF via molecular dynamics simulations can be performed in two independent ways:

(a) by applying Boltzmann inversion of the RDF: $PMF(r) = -k_{\mathrm{B}}T\ln(g(r))$, using a simulation trajectory, or

(b) via the biased potential approach using a collection of trajectories with distance restrained ions and evaluate the data by

  i calculating the time average of the force for separate distances r, or

  ii using Bennets Acceptance Ratio (BAR) for evaluation [127].

Method (a) has the advantage of being straight forward but maintains all the disadvantages of the RDF calculation, see Sec. 4.3. Dominantly, the sampling of diluted ions is poor, especially ion-ion distances with low probability. However, we will use method (a) as reference at 1 M concentration, where the sampling is much improved due to the relative high salt concentration. Even then, a 400 ns trajectory is necessary for good quality data.

We will concentrate in the methodical part on method (b). Both evaluation methods (i) and (ii) are compared in terms of error estimation. Independent from the evaluation method, the biased potential method is based on assumptions. The validity of the assumptions will be discussed in the method section, see Sec. 4.5.3.

As a first step we reproduce simulation results obtained by Hess et al [40] using the simple and cheap SPC/E water and KBFF ion model. We will extend the method to finite concentrations and compare the results with the ones given by Hess et al and with results extracted from RDF calculations.

Our special interest lies in the development of a polarizable force field for aqueous ions. Therefore we present an estimation of the costs for performing calculations of the PMF for the polarizable model with the same accuracy as for the simple non-polarizable model. We conclude with a discussion on the performance of the biased potential method.

4.5.2 Experimental Method

The reconstruction of PMFs from atomic force microscopy (AFM) is described by Gullingsrud et al [172]. The authors facilitate the unbinding of a protein ligand complex by pulling the particles apart with the tip of an elastic cantilever. By monitoring the position of the tip, the applied force can be measured and thus a PMF constructed. However, the analysis of the ligand unbinding on an atomistic time scale is still not resolved, as 'real' experiments are performed in milliseconds or seconds, whereas computational experiments take place in orders of nanoseconds. Therefore, most authors only refer to the peak force or rupture force instead of providing the whole PMF.

The PMF between small single ions is not experimentally accessible by the current state-of-the-art methods. Attempts to correlate simulated PMFs with experimental data are based on Samoilovs work from 1957 [173, 174, 175] and other methods [157]. Kalyuzhnyi et al [175] compare the difference between the first minimum and the first maximum of the calculated ion-water PMF with the activation energy as provided by Samoilov.

4.5.3 Description of the Simulation Method: the Biased Potential

Well dissolved ions as sodium chloride in water tend to stay separated from each other. Even if they happen to be in the proximity of each other, they will tend to avoid ion-ion distances at the energy barriers. These energy barriers are characterised by an energy penalty as opposed to adjacent positions. For the calculation of the PMF, the knowledge of the mean force between the ions at *every* distance is necessary with high accuracy.

Artificial potentials acting on the ions can be used to enable good sampling at ion-ion distances of choice. Those artificial potentials cause a biased ion-ion potential. Most prominently, the so called umbrella sampling utilise a harmonic potential for restraining the particle positions. The particular form of the harmonic potential reminds of an open umbrella.

We use the LINCS algorithm [88] to maintain the distance (r) between the ions. The mean force on the ions in the simulation is then identical to the negative constraining force $-\langle f_\mathrm{c}(r)\rangle$.

It should be noted, that only the distance between the ions is constraint, thus the ion pair can move freely through the simulation box. Even then, by constraining the distance between the two ions, we reduce the available phase space to the surface of a sphere with radius r. This results in an entropic force $f_S(r)$

$$f_S(r) = -\frac{\mathrm{d}}{\mathrm{d}r}\left[k_\mathrm{B}T\ln\left(4\pi r^2\right)\right] = \frac{2k_\mathrm{B}T}{r},$$

with k_B being the Boltzmann constant and T the temperature. The entropic force is necessary to keep two non-interacting particles in vacuum at a fixed distance. As the entropic force is artificially introduced by the simulation setup, it has to be subtracted from the measured mean force.

Consequently, the mean force f_m acting on two ions in solution calculates as the negative restraining force f_c minus the entropic force

$$f_\mathrm{m}(r) = -\langle f_\mathrm{c}(r)\rangle - f_S(r).$$

The PMF at the distance r is the difference in free energy V at distance r and between the state of the ions at infinite separation

$$PMF(r) = V(r) - V(\infty).$$

We are free to set $V(\infty) = 0$. The PMF can be calculated by integrating the

mean force f_m when approaching infinity

$$PMF(r) = \int_r^\infty f_\mathrm{m}(s)\mathrm{d}s = -\int_r^\infty \left[\langle f_\mathrm{c}(s)\rangle + f_S(s)\right]\mathrm{d}s.$$

In computer simulation, we are limited by a maximum distance r_m, therefore the formula reads

$$PMF(r) = -\int_r^{r_\mathrm{m}} \left[\langle f_\mathrm{c}(s)\rangle + f_S(s)\right]\mathrm{d}s + C.$$

The constant C is thereby defined as the free energy at distance r_m.

Hess' Implementation Hess et al [40] choose r_m to be 1.2 nm. At this distance, they estimated the PMF to be dominated by Coulomb interaction

$$PMF(r) = \frac{q_1 q_2}{4\pi\varepsilon_0\varepsilon_r^{c=0}}\frac{1}{r} \qquad r \geq r_\mathrm{m},$$

with ε_0 being the vacuum permittivity and $\varepsilon_r^{c=0}$ the relative permittivity of the neat water model.

This determines C as

$$C = \frac{q_1 q_2}{4\pi\varepsilon_0\varepsilon_r^{c=0}}\frac{1}{r_\mathrm{m}}.$$

Error Estimation The error of the PMF at distance r is calculated by assuming independent errors at every distance $s > r$ and integrate the error backwards from 1.2 nm to r. The individual errors are estimated by block-averages.

The error in the offset C origins from the error in the dielectric constant and adds to the error of the PMF.

Coulomb Scaling at Finite Salt Concentration At a finite salt concentration c, the PMF of ions will differ from the PMF at infinite dilution. Hess et al [40] suppose to quantify this effect by assuming a scaling of the Coulomb interaction between the ions due to an altered dielectric constant of the solution $\varepsilon_r(c \neq 0)$. The change in the dielectric constant origins from the disturbance of the water structure due to the ions. The PMF then calculates

$$PMF(r,c) = PMF(r) + \frac{q_1 q_2}{4\pi\varepsilon_0}\left(\frac{1}{\varepsilon_r(c)} - \frac{1}{\varepsilon_r^{c=0}}\right)\frac{1}{r}. \tag{4.6}$$

The scaling is applied for all distances, thereby also altering the offset C at r_m

$$C = \frac{q_1 q_2}{4\pi\varepsilon_0\varepsilon_r(c)}\frac{1}{r_\mathrm{m}}. \tag{4.7}$$

Reasoning of the Assumptions The presented method uses several assumptions on the system. At infinite dilution, the main assumptions are

(a) the interaction between ions at distances equal or greater than 1.2 nm is dominated by Coulomb interaction and

(b) at a distance of 1.2 nm, the separating water molecules behave like bulk water.

Point (a) is reasoned, because the shape of the PMF is very close to the shape of Coulombic interaction at large distances. Point (b) is highly speculative, as the water structure between the ions is strongly perturbed. The dielectric constant of water around a charged species differs greatly from the bulk value, see the paper of Fedorov and Kornyshev for a detailed description [176]. The offset C is therefore afflicted with an unknown systematic error.

At finite concentration, more assumption are added:

(c) the only influence of additional ions on the ion-ion PMF is the altered dielectric constant of the solution,

(d) the change in the interaction can be captured by scaling of the Coulomb interaction and

(e) the Coulomb interaction is scaled by the concentration dependent dielectric constant of the solution.

The influences of ions are manifold. Point (c) may be reasoned by the fact, that ions are well separated from each other by their hydration shells and therefore do not interfere with the molecules involved in the PMF calculation. Assumption (d) on the other hand seems to be too strong. At small distances, there are no, or only one, water molecules between the ions to screen the Coulomb interactions. In addition, ions will screen the Coulomb interaction stronger than water. Due to the free moving, charge carrying ions in the simulation box, the solution becomes conducting and the static dielectric constant infinity.

Boltzmann Inversion The PMF can be calculated via Boltzmann inversion

$$PMF(r) = -k_{\mathrm{B}}T \ln(g(r)),$$

where $g(r)$ is the RDF. The RDF is extracted from a trajectory as described in Sec. 4.3.

4.5.4 Performance of the Method

To characterise the method more thoroughly, we calculate the PMF at infinite dilution and at a finite salt concentration of 1 M. At 1 M we calculate the PMF in three different ways (i) by scaling of the initial PMF, (ii) by calculating the PMF the same way as for infinite dilution with a scaled offset C and (iii) by Boltzmann inversion of the RDF extracted from an equilibrium bulk simulation.

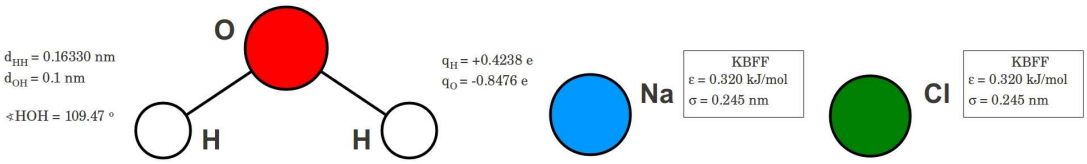

Figure 4.17: Schematic representation of the SPC/E water and KBFF ion model.

Simulation Setup

The KBFF ion force field [94] was applied and the SPC/E water model [93] used.

The simulations are performed with Gromacs 4.5.5 [110] in single precision. The tool Packmol [111] is used to create boxes of 1024 SPC/E water molecules and the specific ion pair.

Every ion pair is simulated at several fixed distances. The distance is maintained using the LINCS algorithm [88]. For every distance, a single simulation within the NPT ensemble is performed for 4 ns. For evaluation, the first 400 ps of the simulation are omitted to ensure good equilibration. The pressure is kept at 1 bar and the temperature maintained at 298.15 K.

Following distances for the ion pairs are applied: the smallest distance is taken to be 0.23 nm for Na^+-Cl^-, 0.29 nm for Na^+-Na^+ and 0.35 nm for Cl^--Cl^-. Intervals of 0.01 nm are applied below a distance of 0.4 nm, intervals of 0.02 nm till a distance of 1.00 nm and a spacing of 0.04 nm till the maximum distance at 1.2 nm equal for all ion pairs. For the Na^+-Cl^- ion pair, additional distances were chosen at 0.345, 0.355, 0.365 and 0.375 nm.

Periodic boundary conditions are applied in all directions. The cutoff of the Lennard-Jones interactions is taken to be 0.9 nm. The long-range Coulomb interactions are handled by the Particle-Mesh Ewald method [112] with a cutoff of 0.9 nm and a grid spacing of 0.1 nm. The neighbour list for non-bonded interactions is updated every 5th integration step. We use the leap-frog algorithm for integrating Newton's equations of motion with a 0.004 ps time step. All simulations are performed at fixed temperature. Velocity rescaling is used with a temperature coupling constant of 0.1 ps [113]. The ion pair for PMF calculation was decoupled from the thermostat. We store the atomic coordinates of the ions each 4 ps for further analysis.

An initial relaxation step is done by applying a time step of 0.1 fs for 0.8 ps.

For simulations at 1 M concentration, 17 sodium-chloride ion pairs are added to the box. The additional ion pairs are coupled to the thermostat and can move freely.

In Gromacs, the restraining force of the LINCS algorithm is extracted using the free energy terminology.

In total, 155 production simulations of 4 ns length each have to be performed for one set of PMFs, amounting to 620 ns.

The RDF simulation is performed with an identical setup of 1024 SPC/E water molecules and 18 ion pairs but without distance constrained ions and for a total duration of 400 ns.

The NaRIBaS framework [1] is used for preparation and analysis of the simulations. Matlab [115] is applied for mathematical operations and plotting.

PMF via the Biased Potential Method: Mean Force for Every Distance r vs. Bennetts Acceptance Ratio The PMF calculation using a biased potential approach allows two different analysis paths. First a collection of trajectories with distance restrained ions is produced as explained above. The direct analysis way would be the calculation of the mean force between two particles at a specific distance. Fluctuations in force and distance caused by particle movement lead to relative large errors for this method. The error can be drastically reduced by using a more sophisticated evaluation approach named Bennetts Acceptance Ratio (BAR) implemented in the Gromacs tool g_bar [127].

In the following paragraph we compare the error estimation for the two analysis paths.

Figure 4.18 is presented for comparison of the results of the two different analysis paths for the PMF. The qualitative and quantitative appearance of the

calculated PMFs is similar. However the difference between the methods becomes apparent by comparing the error bars. For the direct method of calculating the mean force for every distance r separately, the error varies with a maximum value of approx. 1.5 kJ/mol. The error for the PMF calculated with the BAR method is below 0.03 kJ/mol. The error introduced by the uncertainty of the dielectric constant is in the range of 0.2 kJ/mol and adds to the error of the PMF. For the BAR method of evaluation, the line thickness corresponds to the given error estimate.

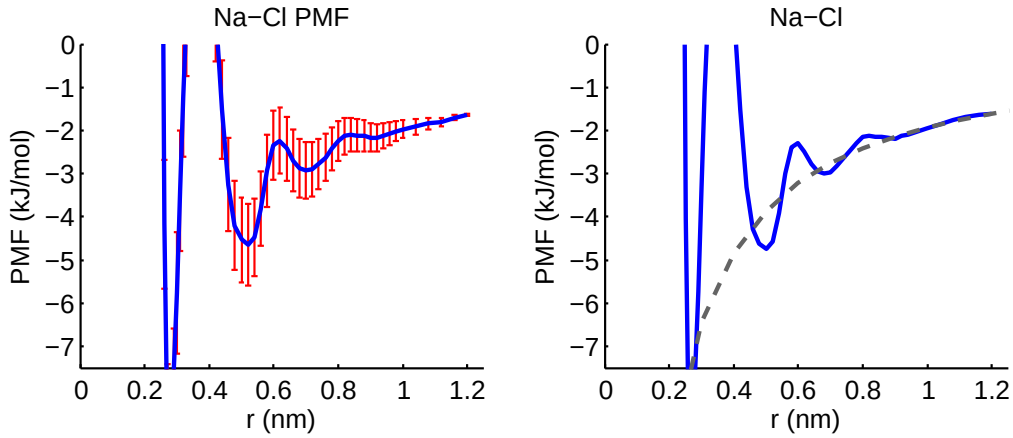

(a) Direct evaluation method.

(b) BAR evaluation method.

Figure 4.18: **(Na^+-Cl^- PMF) Comparison of evaluation methods.** Potential of mean force for the Na^+-Cl^- ion pair in 1024 water molecules. a) Direct evaluatin method. The blue line corresponds to the PMF, the red bars show the estimated error of max. 1.5 kJ/mol. b) BAR evaluation method. The blue line corresponds to the PMF, the grey dashed line shows the electrostatic interaction. The error for the PMF due to fluctuations is below 0.03 kJ/mol. The error introduced by the uncertainty of the dielectric constant is in the range of 0.2 kJ/mol and adds to the error of the uncorrected PMF. The line thickness corresponds to the given error estimate.

Considering the given error estimates, we use in all upcoming calculations the BAR evaluation method.

PMF at Infinite Dilution Graphical representations of the calculated PMFs are shown in comparison with reference graphs in the Fig. 4.19, 4.20 and 4.21. The curves match each other qualitatively and mostly also quantitatively. Deviations become apparent when investigating the minima, see Tab. 4.11: The position of the minima are the same, whereas the depths for the first minima are not. Seemingly, Hess et al [40] used a fitting routine for their PMF that is not described in the paper. Spline fits tend to reduce peak heights, especially if the peaks are very sharp. Some way of data extrapolation would also explain why the first peak is at 0.268 nm, a position, where no data points from simulations are available.

The errors are below 0.03 kJ/mol. The error introduced by the uncertainty of the dielectric constant alone is in the range of 0.2 kJ/mol and adds to the error of the uncorrected PMF. Hess et al [40] provide an error estimation with the same procedure of less than 0.2 kJ/mol.

Table 4.11: Comparison of the PMF calculation results for the Na^+-Cl^- ion pair between this work and Hess et al [40]. Given are the position and depth of the first (r_1) and second (r_2) minimum of the PMF.

	r_1 (nm)	PMF(r_1) (kJ/mol)	r_2 (nm)	PMF(r_2) (kJ/mol)
This work	0.27	-9.5	0.50	-4.7
Hess et al	0.268	-6.7	0.50	-5.0

Using the method introduced by Hess et al [40], we are able to reproduce the given results within the same error range.

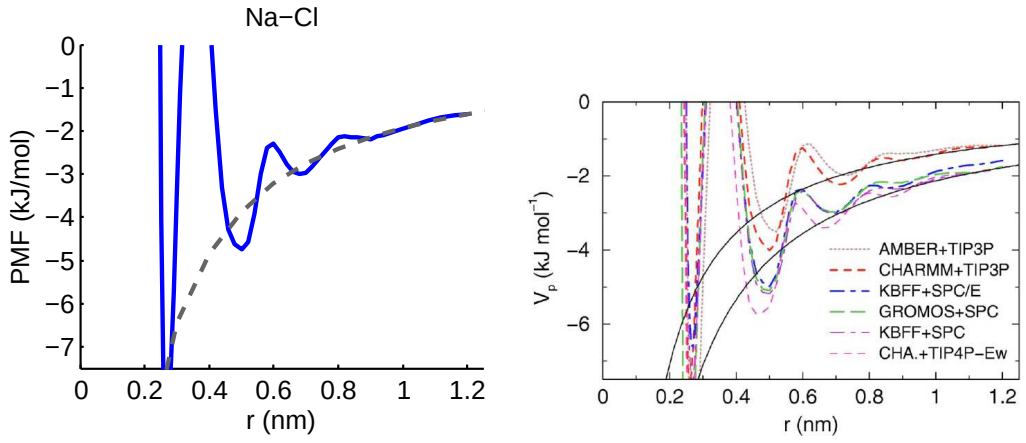

(a) This work. (b) Hess et al [40].

Figure 4.19: **(Na^+-Cl^- PMF) Comparison with reference.** Calculated PMF for the Na^+-Cl^- ion pair in 1024 SPC/E water molecules. a) This work. The blue line corresponds to the PMF of the ions. The grey dashed line shows the electrostatic interaction. b) Reference taken from Hess et al [40]. The blue dashed line shows the data for the KBFF ion model in SPC/E water.

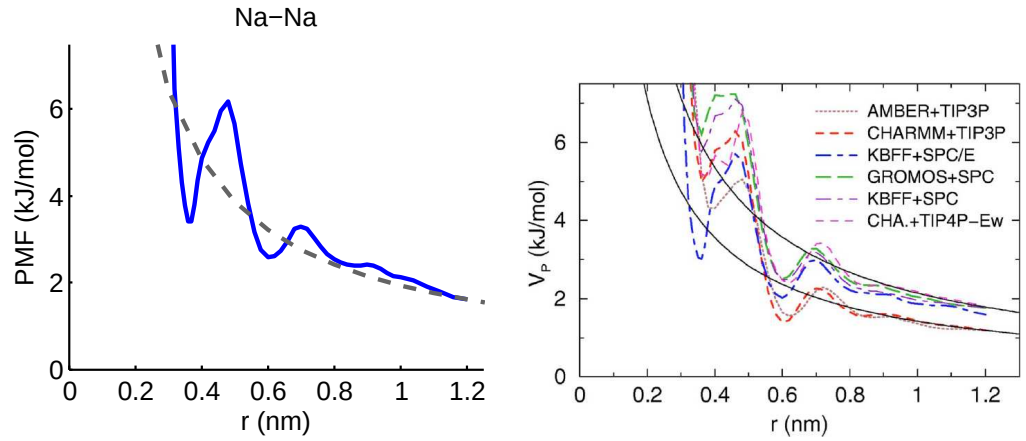

(a) This work. (b) Hess et al [40].

Figure 4.20: **(Na^+-Na^+ PMF) Comparison with reference.** Calculated PMF for the Na^+-Na^+ ion pair in 1024 SPC/E water molecules. a) This work. The blue line corresponds to the PMF of the ions. The grey dashed line shows the electrostatic interaction. b) Reference taken from Hess et al [40]. The blue dashed line shows the data for the KBFF ion model in SPC/E water.

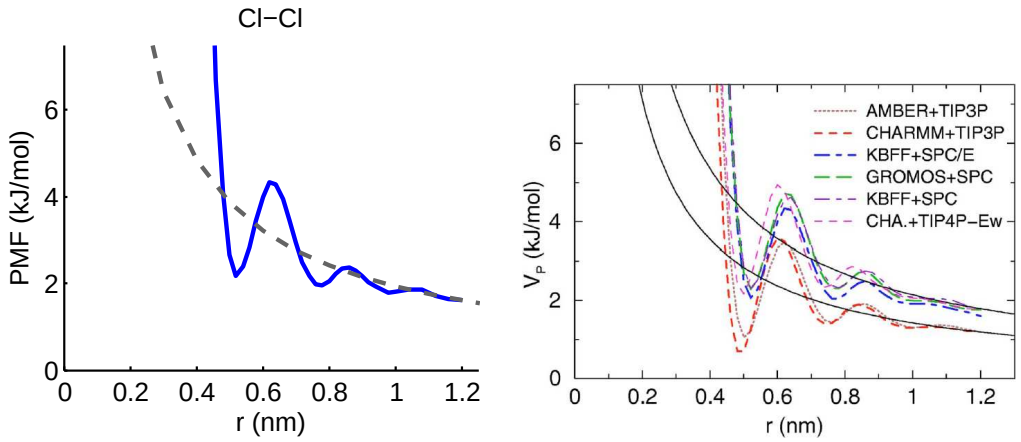

(a) This work.

(b) Hess et al [40].

Figure 4.21: **(Cl^--Cl^- PMF) Comparison with reference.** Calculated PMF for the Cl^--Cl^- ion pair in 1024 SPC/E water molecules. a) This work. The blue line corresponds to the PMF of the ions. The grey dashed line shows the electrostatic interaction. b) Reference taken from Hess et al [40]. The blue dashed line shows the data for the KBFF ion model in SPC/E water.

Calculating the PMF at Finite Concentration The dielectric constant $\varepsilon_r(c)$ at 1 M salt concentration was calculated using the 400 ns RDF simulation as input. For estimating the dielectric constant the Kirkwood formula [40, 177] is applied:

$$\varepsilon_r(c) = 1 + \frac{4\pi}{3Vk_BT}\langle M^2_{\text{total}}\rangle,$$

where V is the volume of the simulation box, k_B is the Boltzmann constant, T the absolute temperature and $\vec{M}_{\text{total}}$ is the collective, or total dipole, of the box

$$\vec{M}_{\text{tot}}(t) = \sum_i \sum_\alpha q_{i,\alpha} \cdot \vec{r}_{i,\alpha}(t),$$

with q the charge and $\vec{r}$ the position of site α of molecule i.

A discussion about calculating the frequency dependent dielectric function is provided in the appendix A.

At 1 M salt concentration, the dielectric constant is reduced to $\varepsilon_r(c) = 58.6$, which is in agreement with Hess et al [40].

Using Equ. 4.6, the PMF at infinite dilution is scaled to a finite dilution of 1 M. A comparative result is created by simulating the PMF at 1 M salt concentration and scaling of the offset C, see Equ. 4.7. The results are compared in Fig. 4.22, 4.23 and 4.24.

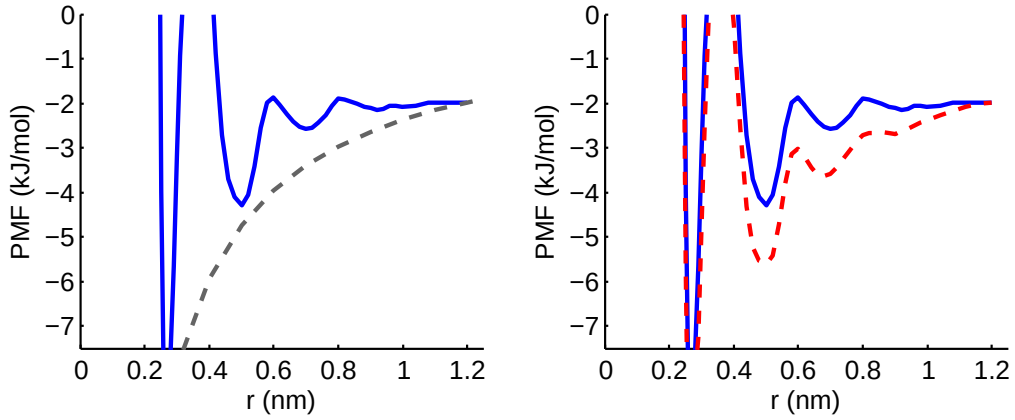

(a) PMF, scaled offset C.

(b) Scaled PMF (red-dashed) and PMF with scaled offset C (blue).

Figure 4.22: **(Na^+-Cl^- PMF) Comparison of Methods.** Calculated PMF for the Na^+-Cl^- ion pair in 1024 SPC/E water molecules at 1 M salt concentration. a) Scaled offset C. The blue line corresponds to the PMF of the ions calculated with explicit simulations and scaled offset C. The grey dashed line shows the electrostatic interaction. b) The blue line corresponds to the PMF with scaled offset C as in a). The red dashed line represents the PMF calculated using a scaling of the PMF at infinite dilution as Hess et al [40] proposed.

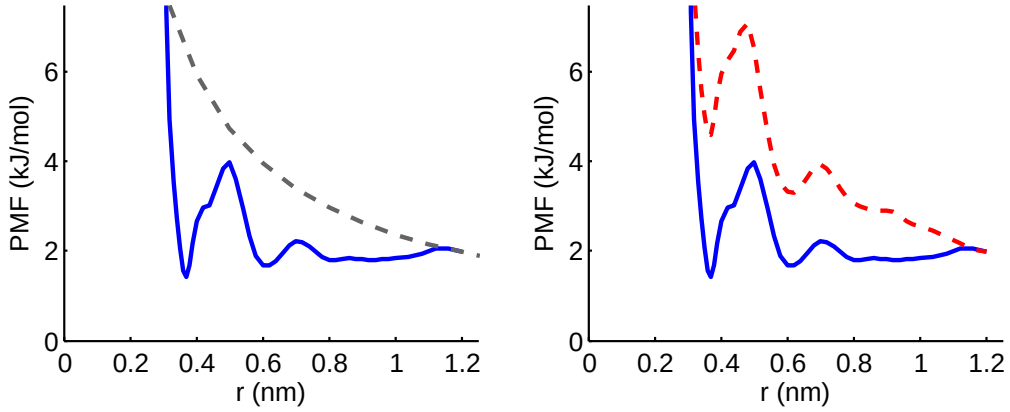

(a) PMF, scaled offset C.

(b) Scaled PMF (red-dashed) and PMF with scaled offset C (blue).

Figure 4.23: **(Na^+-Na^+ PMF) Comparison of Methods.** Calculated PMF for the Na^+-Na^+ ion pair in 1024 SPC/E water molecules at 1 M salt concentration. a) Scaled offset C. The blue line corresponds to the PMF of the ions calculated with explicit simulations and scaled offset C. The grey dashed line shows the electrostatic interaction. b) The blue line corresponds to the PMF with scaled offset C as in a). The red dashed line represents the PMF calculated using a scaling of the PMF at infinite dilution as Hess et al [40] proposed.

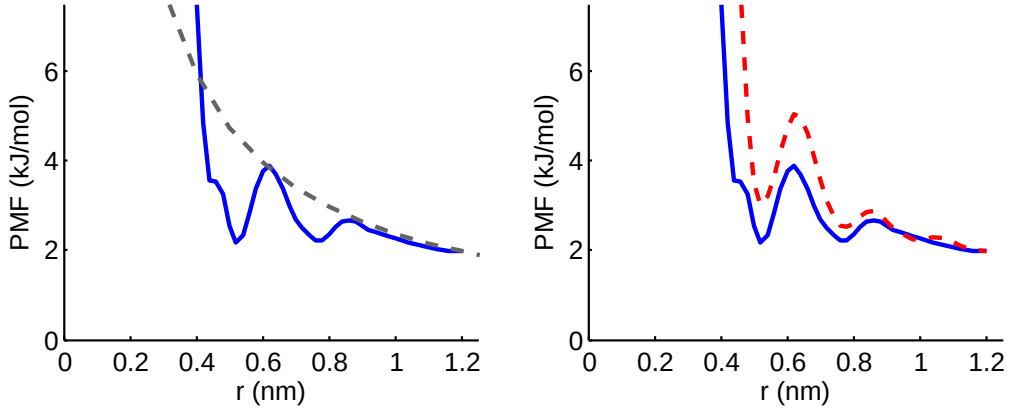

(a) PMF, scaled offset C.

(b) Scaled PMF (red-dashed) and PMF with scaled offset C (blue).

Figure 4.24: **(Cl^--Cl^- PMF) Comparison of Methods.** Calculated PMF for the Cl^--Cl^- ion pair in 1024 SPC/E water molecules at 1 M salt concentration. a) Scaled offset C. The blue line corresponds to the PMF of the ions calculated with explicit simulations and scaled offset C. The grey dashed line shows the electrostatic interaction. b) The blue line corresponds to the PMF with scaled offset C as in a). The red dashed line represents the PMF calculated using a scaling of the PMF at infinite dilution as Hess et al [40] proposed.

The error estimate of the PMF calculation is below 0.03 kJ/mol and the error introduced by the uncertainty in the dielectric constant roughly 0.2 kJ/mol.

Comparing the results from PMF scaling with the results from explicit simulations, a pronounced deviation becomes apparent. Whereas the overall shape of the curves is similar, the amplitude of the scaled PMFs is larger. Also, the explicitly simulated Na^+-Na^+ PMF shows no Coulombic behaviour at distances greater than 1 nm, the explicitly simulated Cl^--Cl^- PMF does and the explicitly simulated Na^+-Cl^- PMF shows a diminished slope. As anticipated before, the ions at finite dilution enhance the screening of the Coulomb interaction. The effect is differently pronounced for the ion species: whereas the Coulomb interaction of sodium is strongly diminished and the deviation to the scaled PMF large, the Coulomb interaction of chloride is nearly undisturbed and thereby the deviation to the scaled PMF small. The sodium-chloride PMF exhibits a behaviour somehow in between the two extrema.

Motivated by the missing Coulombic behaviour of the explicitly simulated PMF at finite dilution, we compare the PMF from the biased potential with a PMF extracted from a bulk simulation by Boltzmann inversion of the RDF, see Fig. 4.25. When assuming the Coulombic interaction to be declined to zero at 1.2 nm, the offset C becomes also zero. The agreement is apparent.

Conclusion The biased potential method is a viable tool for determining the PMF of ions in infinite and finite solutions with great precision. The usability of the method is determined by the validity of certain assumption. Whereas the assumptions at infinite dilution seem reasonable, the PMF scaling at finite solution proved unsuccessful.

It should be mentioned, that beside the apparent problems of the method, Hess et al [40] used this method with success for osmotic pressure calculations. As the constant C does not alter the force calculations, the implicit solvent simulations of Hess et al are not influenced by this source of error. Also the calculation of activation energies are not affected by errors of C.

The PMF at finite concentration can be calculated by explicit simulations using either Boltzmann inversion or a biased potential. But at infinite dilution only the biased potential method is applicable.

In any case, the biased potential method highly depends on the assumption on the strength of interaction at the maximum distance, so namely the determination of the offset C. A better insight into the method might be achieved by simulating larger distances.

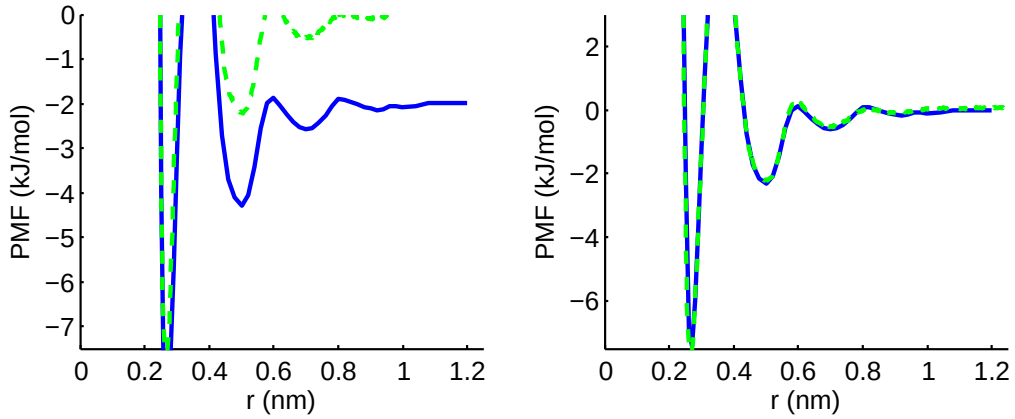

(a) PMF with a scaled offset C (blue) and PMF from Boltzmann inversion (green-dashed).

(b) PMF with offset $C = 0$ (blue) and PMF from Boltzmann inversion (green-dashed).

Figure 4.25: **(Na^+-Cl^- PMF)** Calculated PMF for the Na^+-Cl^- ion pair in 1024 SPC/E water molecules at 1 M salt concentration. a) Scaled offset C. The blue line corresponds to the PMF of the ions extracted from explicit simulation with a biased potential and scaled offset C. The green dashed line shows the PMF extracted from a bulk simulation by Boltzmann inverting the RDF. b) PMF with offset $C = 0$. The blue line corresponds to the same PMF as in a), but without adding an offset C. The green dashed line shows the PMF extracted from a bulk simulation by Boltzmann inverting the RDF. Please mind the altered range of the y axis.

Estimation of the Computational Costs for Testing the Performance of the Polarizable Model

Very few and fast equilibration steps are necessary. In total, 155 production simulations of 4 ns length need to be performed, amounting to 620 ns. For the cheap non-polarizable model, 2400 core-h in total have been spent.

A single 4 ns simulation with a polarizable FF would cost 4300 core-h. To simulate all pairs of PMF we would have to invest 660'000 core-h.

There are some possibilities to decrease the computational costs:

1. If only the Na^+-Cl^- PMF is of special interest, than roughly a third of the simulations will do.

2. The accuracy with the BAR evaluation method is very good. Depending on the aimed accuracy, we could decrease the sampling time.

3. Further optimisation of the simulation setup might be possible.

4. We could use the NVT ensemble instead of NPT. This would be not the optimal ensemble, but the influence on a well equilibrated box should be small and the performance increases.

4.5.5 Conclusion: Quality of the Method and Performance of the Model

The full form of the PMF is experimentally not accessible, however features of the PMF curve like the difference between maxima and minima might be associated with experimentally measurable energies. Still, from a molecular point of view it provides a useful tool to characterise intermolecular interaction.

Using advanced sampling techniques based on the Bennetts Acceptance Ratio, the PMF between infinitely diluted ions can be obtained with high accuracy - errors are within the line width of a drawn PMF. At finite salt concentration, a number of assumptions may lead to unpredictable errors in the PMF - results for the PMF differ drastically depending on the chosen assumptions.

For simple non-polarizable water models, the calculation of the PMF is doable with reasonable costs. However, the inclusion of polarization effects in the model force field increases drastically the computational costs. Therefore, results for the polarizable model are not produced.

4.6 Osmotic Pressure

The concept of the osmotic pressure and osmotically driven membrane processes opens the door to the construction of a wide set of important technologies and for understanding several basic phenomena that are crucial for life in general. Among the technologies one finds water and waste water treatment, desalination, and power generation [178, 5, 6]. Reverse osmosis is the basis of filtering (nanofiltration, ultrafiltration and microfiltration), a process commonly used to purify water, but shows also potential for the recycling process of ionic liquids [179]. Induced-charge electro-osmosis and electrophoresis are among possible applications [180].

Whereas membranes in plant cells and other living cells are build out of proteins, the current technological state-of-the-art allows the preparation of membranes composed of polymeric, organo-mineral, ceramic or metallic compounds. Also depending on the filtration techniques and usage different pore sizes can be constructed [178]. For further discussion of the membrane techniques and applications, we refer to the review article of Bruggen et al [178].

Following the discussion of Hess et al [40], the osmotic pressure is not only of vital importance in biological and industrial applications, but also capable of proving the quality of a computational model for ion/solvent interactions. However, accurate measurements of the osmotic pressure are still under development and of increasing interest in the computational scientific community [181, 40, 42].

In the upcoming sections we will provide the definition of the osmotic pressure and open the discussion of possible computational implementations of osmotic pressure calculations. Two methods are described in more detail, namely the combination of the potential of mean force calculation with implicit solvent simulations [181, 40, 182] and the newly developed membrane method [42, 30]. We review current experimental standards in the measurement of the osmotic pressure.

The membrane method was invented by Lou and Roux [42] in 2010, however a detailed methodological description of the method in terms of simulation parameter, initial box configuration and membrane setup is still missing. In addition to the discussion of the influence of the named properties, we will comment on the equilibration time and the accuracy of the membrane method. Both parameter influence the final costs for the calculation of the osmotic pressure, which is especially important for the application of the method on expensive polarizable force field models for water and ions. Finally, we estimate the osmotic pressure using polarizable water and ions and discuss the usability of the membrane method.

4.6.1 Introduction: The Definition of the Osmotic Pressure and Concentration Terms

According to the IUPAC definitions [183], the osmotic pressure Π is the excess pressure required to maintain osmotic equilibrium between a solution and the pure solvent separated by a membrane permeable only to the solvent

$$\Pi = -RTV_{\text{solvent}} \ln a_{\text{solvent}},$$

where V_{solvent} is the partial molar volume and a_{solvent} the activity of the solvent for an incompressible fluid. R is the universal gas constant and T the temperature. For ideal dilute solutions, the osmotic pressure is expressed in solute properties by the Van't Hoff equation

$$\Pi = c^*_{\text{solute}} RT = \rho_{\text{solute}} \frac{RT}{M_{\text{solute}}}. \tag{4.8}$$

Here the solute refers to individually moving molecules or ions with the concentration c^*_{solute} or mass concentration ρ_{solute} and average molar mass M_{solute}. To avoid misunderstanding, it should be emphasised, that the total concentration c^*_{solute} does refer to every single solute molecule in the solution. If the solute is a salt, we call the total concentration ion concentration c^*_{ion} counting every single ion.

In contrast to the solute concentration c^*_{solute} we will use the term salt concentration c_{salt}. The salt concentration refers to the number of particles which combine to a neutral salt. If the salt contains two ions per neutral group, as for Na^{1+}-Cl^{1-}, the salt concentration and the ion concentration are connected by a factor of 2: $c^*_{\text{ion}} = 2 \cdot c_{\text{salt}}$. All terms are summarised in Tab. 4.12.

4.6.2 The Experimental Method

A variety of experimental methods for measuring the osmotic pressure and the related activity coefficients have been developed in the past century. The deviation between *membrane osmometers* [184, 185], *vapour pressure osmometers* [186] and *freezing point osmometers* [187] accounts for the solution properties that are used to determine the osmotic pressure [188].

A quick and accurate membrane method was developed in 1904 by Berkeley and Hartley [184, 185]. Their apparatus contains a porcelain tube and a copper ferrocyanide membrane surrounded by a metallic container. Whereas the porcelain tube is filled with pure solvent, the metallic container contains the salt

Table 4.12: Concepts and definitions of the term "concentration" when referring to salt solutions.

Term	Symbol	Explanation	Connection to other terms
Salt concentration	c or c_{salt}	Concentration counting the smallest neutral ion groups in the solution	
Ion concentration	c^* or c^*_{ion}	Concentration counting every single ion in the solution	$c^*_{\text{ion}} = 2 \cdot c_{\text{solute}}$ if the salt contains two ions per smallest neutral ion group
Total concentration	c^* or c^*_{solute}	Concentration counting every solute particle in the solution	
Mass concentration	ρ_{solute}	Total concentration multiplied by the molar mass	$\rho_{\text{solute}} = M_{\text{solute}} \cdot c^*_{\text{solute}}$

solution. Due to osmosis, the pure solvent tends to flow into the solution jar. An external pressure is applied on the solution e.g. by a piston to counteract the flow of the solvent. The applied pressure is easily measured and equals the osmotic pressure. Advantageously the concentration of the solution does not change during the whole procedure as the solvent flow is permitted. Furthermore the method is applicable to high osmotic pressures as the osmotic pressure is compensated by an external pressure and the membrane is kept unperturbed.

Typically, experimental data of the osmotic pressure Π is given using the osmotic coefficient ϕ, see Robinson [186], Hamer and Wu [189] and Archer [190]. The Van't Hoff equation $\Pi = \phi c^*_{\text{solute}} RT$ with $\phi = 1$ is only applicable for an ideal solution. Deviations in real solutions from the ideas behaviour are provided through the "correction term" $\phi \neq 1$.

For NaCl the osmotic coefficient ϕ appears as a parabolic curve with a minimum of 0.920 at a salt concentration of 0.4 M and ambient temperature and pressure, see Fig. 4.30 later in the section. The accuracy of the osmotic pressure calculations is extremely high. The probable error of the osmotic coefficient is estimated to be below 0.2 % [186]. Generally, the osmotic coefficient is temperature dependent, see Liu and Lindsay [191].

4.6.3 Simulation Methods Reviewed

The development of methods to calculate the osmotic pressure of ions in solution is still in progress. In the 90's Lyubartsev and Laaksonen [192, 193, 181, 194] have

been the first to estimate the osmotic pressure using implicit solvent simulations. The method called "reverse Monte Carlo approach" is based on

Step 1 the estimation of the ion-ion interaction potential at a specific salt concentration;

Step 2 the usage of the ion-ion interaction potential as input for advanced simulations or calculations of the potential of mean force (PMF) with extremely high accuracy;

Step 3 the final calculation of the osmotic pressure Π based on the following equation

$$\Pi = \frac{N k_B T}{V} - \frac{1}{3V} \left\langle \sum_{i,j} \frac{\partial U}{\partial r_{ij}} r_{ij} \right\rangle .$$

For calculating the osmotic pressure, the pair interaction potential is differentiated with respect to the ion distance - therefore as less noise as possible in the PMF is a prerequisite for the accurate calculation of the osmotic pressure.

Initially, Lyubartsev and Laaksonen [181] calculated the ion-ion interaction potential through a Boltzmann inversion of the ion-ion radial distribution function for finite concentrations obtained by classical simulations of water and ions. The calculation of the PMF with high accuracy was then performed via implicit solvent simulations using the pre-calculated ion-ion interaction potential. This method combination was modified by two groups either by changing the routine for calculating the initial ion-ion interaction potential [195, 40] or by applying the integral equation theory for the calculation of the osmotic coefficient [182, 83].

As the correct calculation of the PMF is a key step for estimating the osmotic pressure accurately, we refer to a more detailed discussion on the PMF and especially the method used by Hess et al [40] in Chapter 4.5.

In 2010 the PMF based methods for calculating the osmotic pressure of ions in solution has been extended by the *membrane method* described by Luo and Roux [42]. The membrane method allows to calculate directly the osmotic pressure by introducing a potential wall or 'membrane' into the simulation setup. The results of Lou and Roux are promising, however a detailed description of the simulation methodology and analysis procedure is missing. Rigorous method testing in terms of simulation parameter and membrane implementation/configuration is required.

In the following sections we will describe the simulation method in detail. After developing an efficient simulation and evaluation routine, we used the KBFF

ion model in conjunction with the SPC/E water model to answer questions about convergence, performance optimisation, possible artefacts because of thermodynamic coupling, influence of the wall "hardness" and the domain and box size. The work of Hess et al [40] provides a computational reference for the system.

4.6.4 Description of the Simulation Method: the Membrane Method

The membrane method is first reported by Luo and Roux [42]. The method is based on the concept of introducing a semi-permeable membrane into the simulation setup. The membrane is simulated as a harmonic potential $V(r)$ acting only on the solute molecules outside an ion domain $r_0 < r < r_1$:

$$V(r) = \frac{1}{2}k\,(r - r_0) \qquad r < r_0;$$

$$V(r) = 0 \qquad r_0 < r < r_1;$$

$$V(r) = \frac{1}{2}k\,(r - r_1) \qquad r > r_1,$$

with k being the force constant of the membrane.

Leaving the ion domain, a force F will act on the ions, pushing them back into the ion domain:

$$F = -\frac{\mathrm{d}}{\mathrm{d}r}V(r).$$

The osmotic pressure Π is identical to the pressure or force per area applied by the membrane:

$$\Pi = \frac{\langle \sum_i F \rangle_t}{A},$$

where A is the membrane area, $\langle\rangle_t$ the mean over time frames and $\sum_i$ the sum over all i solute particles.

Implementation in Gromacs The Gromacs code is modified by Mikhail Stukan to introduce the membrane. In detail, the restraining routine is modified. Position restrained particles start to feel the restraining potential only after a specified displacement d. If all solute particles are restrained to the position r_{centre}, the setup results in a $2d$ wide ion domain around r_{centre}.

The restraining potential works only in z-direction, the solute molecules can move freely in x- and y-direction. Periodic boundary conditions are applied in all three spatial directions, resulting in a continuous solution slab in xy-direction of $r_{\mathrm{id}} = r_1 - r_0$ width separated from its images by a pure solvent domain in

z-direction. If the pure solvent bulk domain is large enough, all interactions between the solute molecules and their images in z directions are screened.

A snapshot of an example simulation is provided in Fig. 4.26.

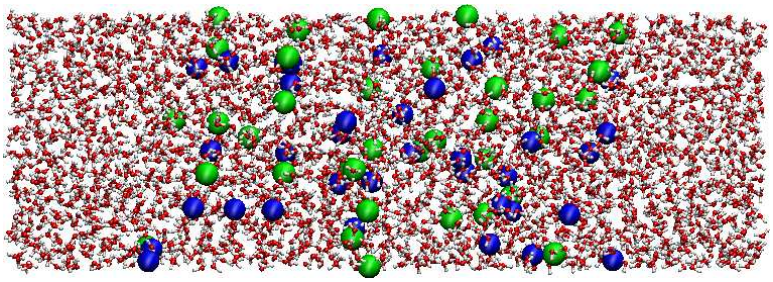

Figure 4.26: A snapshot of an osmotic pressure simulation box. Water molecules are printed in red and white, sodium and chloride ions are shown in blue and green, respectively. The ion domain is in the centre of the simulation box, on the left and right border is the solvent bulk domain.

Determining the Real Concentration Due to the limited amount of water molecules and ions in the simulation box, it is not always possible to set the concentration exactly to a given value. Furthermore, and much more important, the membrane walls are soft in the used simulation setups, allowing ions to leave the ion domain, be it under an energy penalty. Because of the limited size of the ion domain, this effect on the boundaries can alter the original concentration by up to 10 %.

To define a meaningful concentration, the ions in the ion domain and the volume of the ion domain is taken for calculating the concentration. Because the walls react only on the centre of mass of ions, thereby allowing the ions to cross the membrane with their outer parts, a volume corrections has to be applied. Right handling of boundary conditions is a necessity.

Rigorously, the concentration c is defined as the mean number of particles N in a volume V infinitely away from the boundaries

$$c = \frac{N}{V} = \frac{\langle \sum_i n_i \rangle_t}{V}.$$

In real world experiments, the volume is commonly determined using a kind of a measuring cup. This is not totally correct, as this method neglects the influence of the border or interfaces of the fluid with the cup. In other words, if the measured volume of the liquid would be doubled, the mass of the liquid would not increase in the same rate, as the influence of the interfaces changes. Because of the small

size of atoms and molecules, the amount of molecules disturbed at the interface is extremely small in comparison to the amount of bulk molecules.

For an illustrative discussion of the influence of the boundaries on the volume definition, we consider a hard box filled with 3 particles as shown in Fig. 4.27. There are at least three possible ways of defining the accessible volume of the balls:

1. The accessible volume equals the volume the balls are able to cover.
   Closely related to the picture of a molecule as bulky object.

2. The accessible volume is defined through the geometric centre of the balls. The box boundaries are expected to interact with the surface of the balls.
   Used by most evaluation programs.

3. The accessible volume is defined through the geometric centre of the balls. However, the box boundaries are expected to interact with the geometric centre of the balls.
   Applies best to the case, when the molecule is hindered in his movement by a potential exclusively acting on its geometric centre.

Obviously, the density or concentration depends on the chosen or applicable definition.

The membrane setup is due to partial periodic boundary conditions *and* soft walls more complex than our initial picture (see Fig. 4.27) for defining accessible volume and ion counting. In computationalsurf science, periodic boundary conditions (PBC) are applied to mimic a bulk fluid without interfaces [84]. In the simulation setup for measuring the osmotic pressure, the PBC for ions are only applicable in 2 dimension: x and y. In z-direction, the ions encounter the membrane. Figure 4.28 shows the handling of ions in xy-direction by PBC.

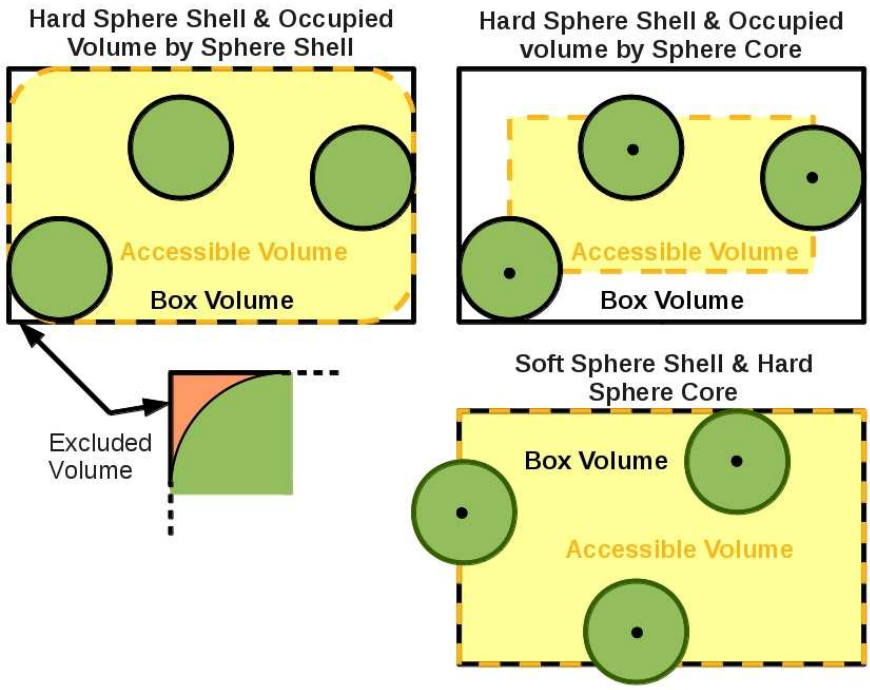

Figure 4.27: Different definitions of the accessible volume of three balls in a hard box. (Left) The accessible volume equals the volume the balls are able to cover. (Top-Right) The accessible volume is defined through the geometric centre of the balls. The box boundaries are expected to interact with the surface of the balls. (Bottom-Right) The accessible volume is defined through the geometric centre of the balls. However, the box boundaries are expected to interact with the geometric centre of the balls.

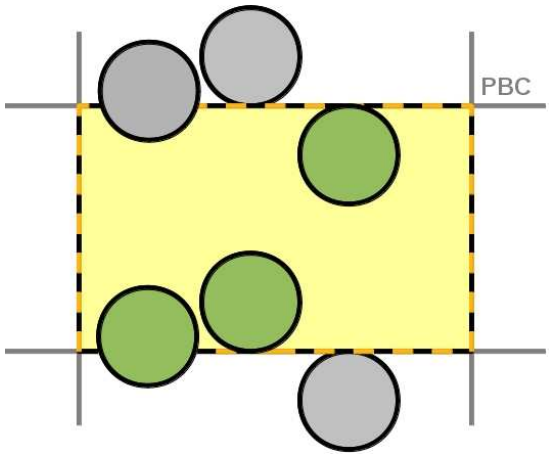

Figure 4.28: Application of periodic boundary conditions (PBC). Green spheres represent ions in the simulation box, grey spheres their periodic images.

Figure 4.29 illustrates three different algorithms for the calculation of the ion concentration within the membrane system. The algorithms can be distinguished by applied volume definitions and estimation of the ion numbers.

Figure 4.29(a) shows the counting of ions based on the position of their centre. The volume of the ion domain is defined through the box boundaries and the position of the membranes. Ions with a centre of mass inside the ion domain contribute fully to the ion concentration. Within a simulation box with 3D PBC, this method provides correct ion concentrations. However, with soft membranes in the xy-plane ions may partially leave the ion domain (ion B in the sketch). Thus the accessible volume is underestimated. The ions gain considerable space in z-direction upon partially leaving the ion domain. Due to the diminished ion concentration outside the ion domain, this effect is not compensated by ions outside the ion domain as ion C.

One possible correction for this effect is illustrated in Fig. 4.29(b): the extra volume that is seemingly available for the ions is added to the ion domain. Still, only ions with a centre of mass inside the original ion domain contribute to the ion concentration. This definition overestimates the accessible volume for the ions as ion C is not added to the ion number but occupies a considerable amount of space within the volume. The difference between the two definitions is far from negligible. It can alter the calculated concentration by more than 10 %.

To circumvent such implications and apply a more realistic calculation algorithm, we consider a partial contribution of ions according to their volume inside the ion domain, see Fig. 4.29(c). The volume of the ion domain is again defined through the box boundaries and the position of the membranes. The position of the ions with respect to the membrane position determines their contribution. An ion in the middle of the membrane box counts fully to the ion number, an ion close to the membrane counts proportional to its spherical cap volume[1] V_{cap} inside the ion domain

$$V_{\mathrm{cap}} = \frac{\pi h^2}{3}(3r - h).$$

Thereby h refers to the maximum distance between ion surface and membrane within the ion domain volume and r describes the ion radius. This method proved to deliver the most robust results.

[1] The volumetric portion of a sphere cut off by a plane.

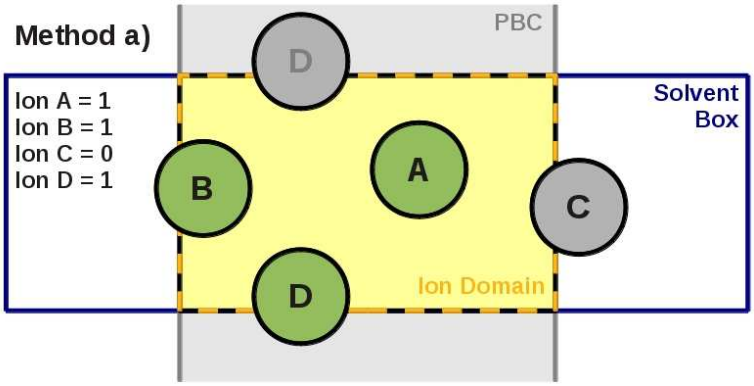

(a) Centre of ions

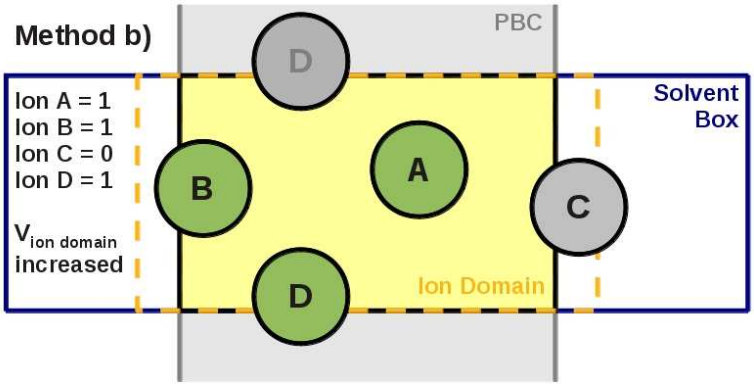

(b) Increased ion domain

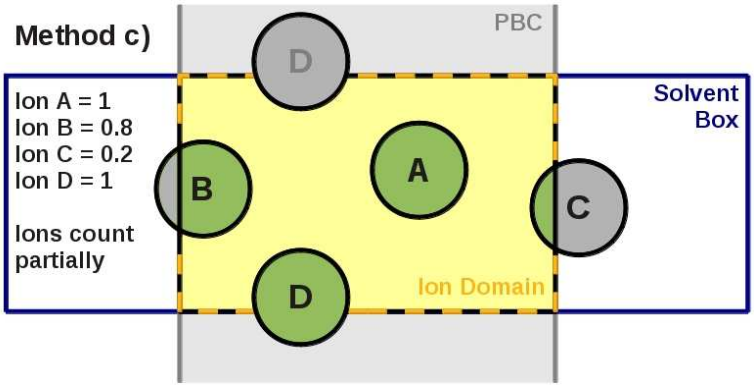

(c) Partially contributing

Figure 4.29: Models for counting of ions inside the ion domain including the handling of periodic boundary conditions (PBC). Green spheres represent ions inside the ion domain, grey spheres ions outside the ion domain. The image of ion D in z-direction is also printed in grey. a) Counting the ions (centre-of-mass) within the ion domain. b) Counting the ions (centre-of-mass) between the membranes. Estimating an increased ion domain as an effective volume. c) Partial contribution of ions according to their volume inside the ion domain.

Extracting Reference Data In references, the osmotic coefficients ϕ are given for specific concentrations. To extract the osmotic coefficients for the simulated concentrations, a linear regression between the points of known concentrations is performed, see Tab. 4.13 for computational references of the KBFF ion model in SPC/E water and Fig. 4.30 for experimental reference by Hamer and Yung-Chi [189].

Generally, the osmotic coefficient is temperature dependent [191]. As the slope of the osmotic coefficient $\phi(T)$ is flat in the range of 298.15 to 253.15 K, we can assume a constant osmotic coefficient for this temperature range. Experimental reference values of the osmotic pressure $\Pi(T)$ therefore increase linear with the temperature as described by the Van't Hoff equation.

Table 4.13: Osmotic coefficients ϕ of the KBFF ion model in SPC/E water at different concentrations, taken from Hess et al [40]. The osmotic coefficients ϕ for concentrations c_{NaCl} not given in the table are calculated assuming a linear dependency $\phi(c_{\mathrm{NaCl}}) = A \cdot c_{\mathrm{NaCl}} + B$. For concentrations above 2.8 M an ideal gas behaviour is assumed, namely, $\phi = 1$.

salt concentration c_{NaCl} (M)	osmotic coefficient ϕ	A (1/M)	B
0.1	0.920		
0.5	0.905	-0.0375	0.92375
0.5	0.905		
1.0	0.924	0.038	0.886
1.0	0.924		
2.8	0.998	0.041	0.883
>2.8	1.000	0.000	1.000

Evaluating the Trajectory The force on the membrane wall F is related to the restraining energy E by the relation

$$F = \sqrt{2 \cdot k \cdot E}. \tag{4.9}$$

The mean restraining energy $\langle E \rangle$ is provided by the Gromacs tool g_energy. However, this quantity is the average over (i) the number of ions that feel a restraining potential and (ii) the different energies of the ions. Calculating the square root makes it impossible to use this property in an osmotic pressure calculation as

$$\langle F \rangle = \langle \sqrt{2kE} \rangle \neq \sqrt{2k\langle E \rangle}.$$

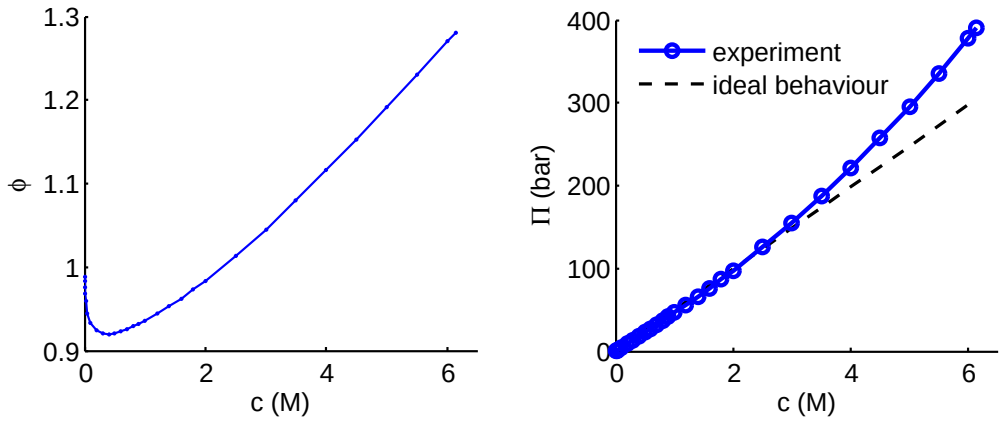

(a) Osmotic coefficient ϕ

(b) Osmotic pressure Π

Figure 4.30: Experimental data of NaCl in water at 298.15 K from 0.001 M to a saturated solution as provided by Hamer and Yung-Chi [189]. a) Osmotic coefficient ϕ. b) Osmotic pressure Π (blue curve with circles) and the behaviour of an ideal solution described by the Van't Hoff equation (black dashed line).

To extract the restraining force per ion per frame, a Tcl script is written utilising the software VMD [196]. The script identifies all ions outside the ion domain for every frame and prints the actual position. A Matlab [115] script then calculates the forces and takes the mean. As a side effect, the osmotic pressure on each surface and for each ion species can be evaluated separately.

4.6.5 Performance of the Method

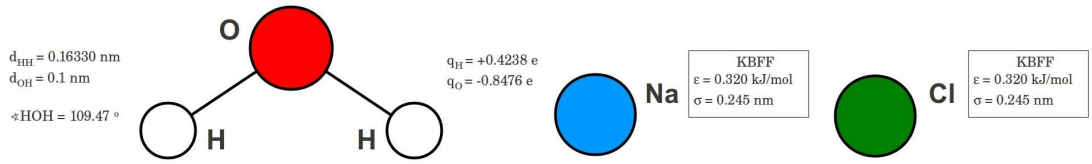

Figure 4.31: Schematic representation of the SPC/E water and KBFF ion model.

To characterise the method thoroughly, we are especially interested in the following questions:

- **(Equilibration Behaviour)** How much time does the osmotic pressure need to converge?
- **(Barostat Coupling)** What influence has the simulated ensemble, precisely, is there a difference in using the NPAT or the NVT ensemble?
- **(Thermostat Coupling)** Does the thermostat coupling of ions has an effect on the osmotic pressure?
- **(Size effects)** Does the measured osmotic pressure depend on the ion domain size r_{id}?
- **(Membrane Hardness)** Does the measured osmotic pressure depend on the force constant k of the membrane wall?
- **(Starting configuration)** What is the influence of an unfavourable starting configuration on the equilibration behaviour of the osmotic pressure simulation?
- **(Crystallisation)** How does the osmotic pressure simulation react on salt crystallisation?
- **(Concentration dependence)** Are results for the osmotic pressure at different concentrations comparable to results for the same model but different methods?

The given number of questions determines the construction of the simulation setup and its variations.

Simulation Setup

The KBFF ion force field [94] is applied and the SPC/E water model [93] used.

The simulations are performed with Gromacs 4.5.5 [110] in single precision. The tool Packmol [111] is used to create the simulation boxes.

The simulation boxes are roughly 3 nm long in x and y-direction and 9 nm in z-direction with 3072 water molecules inside the box. The ion domain size r_{id} is 3 or 6 nm in z-direction. The ion domain expands in x and y-direction and is limited in z-direction by a neat water domain. The number of ions in the ion domain varies with the simulation setup.

The simulations are equilibrated at a pressure of 1 bar in the NPT ensemble for 300 ps. Some boxes are equilibrated using the NPAT ensemble, thereby leaving the value of the cross-section A constant. Few exceptional simulations are performed in the NPAT ensemble during the whole simulation. For all simulations, the first 1 ns of the production run is neglected to ensure good equilibration.

The temperature is maintained at 298.15 K. In some simulation, the ions are decoupled from the thermostat.

The force constant k of the membrane varies between 50 and 50'000 $\mathrm{kJ/(mol{\cdot}nm^2)}$.

Periodic boundary conditions are applied in all directions. The cutoff of the Lennard-Jones interactions is taken to be 0.9 nm. The long-range Coulomb interactions are handled by the Particle-Mesh Ewald method [112] with a cutoff of 0.9 nm and a grid spacing of 0.1 nm. The neighbour list for non-bonded interactions is updated every 5th integration step. We use the leap-frog algorithm for integrating Newton's equations of motion with a 0.004 ps time step. All simulations are performed at fixed temperature. Velocity rescaling is used with a temperature coupling constant of 0.1 ps [113]. We store the atomic coordinates of the ions each 4 ps for further analysis.

The NaRIBaS framework [1] is used for preparation and analysis of the simulations. Matlab [115] is applied for mathematical operations and plotting.

Results

A summary of the simulations applying different *simulation setups* can be found in Tab. 4.14. Namely, the influence of the ensemble, NVT versus NPAT, the ion domain size r_{id} and the thermostat acting on the ions is investigated and compared with a reference simulation run (NPAT ensemble, 400 ns run time).

In Tab. 4.15 results for different *membrane force constants* acting on the ions are presented.

Simulations with different *salt concentrations* are summarised in Tab. 4.16, a graphical overview is shown in Fig. 4.36.

Further details are provided in the appendix.

- **(Equilibration Behaviour)** How much time does the osmotic pressure need to converge?

  To answer this question, a simulation with 400 ns simulation time is performed, see Tab. 4.14, Fig. 4.32 and Fig. 4.33. A maximum of 5 % deviation from the mean value is reached after 42 ns sampling time, 3 % deviation after 59 ns sampling time and 1% deviation after 335 ns. With confidence, it can be assumed, that the results of the 160 ns long simulations lay within a 3 % deviation from the real value. Most simulations converge in a 5 % interval to the mean value in the first 80 ns. For $k = 1'000\,\mathrm{kJ/(mol \cdot nm^2)}$ there is a 25 ns regime with strong reduced osmotic pressure, see Fig. B.9 from 75 ns to 100 ns.

  Our block average error estimate gives a 3 % confidence interval for the 400 ns simulation. With 95 % confidence, the 'real' value lies within this interval. For the 180 ns simulation the confidence interval is 5 %.

  The long equilibration time is reflected in the large standard deviation of the osmotic pressure S_N of approximately 25 % of the mean osmotic pressure.

  These estimates are done for simulations with a salt concentration of roughly 1 M inside the ion domain. At higher concentrations, the osmotic pressure is expected to converge faster as more ions interact with the membrane. For the same reason, at lower concentrations the osmotic pressure is expected to converge slower.

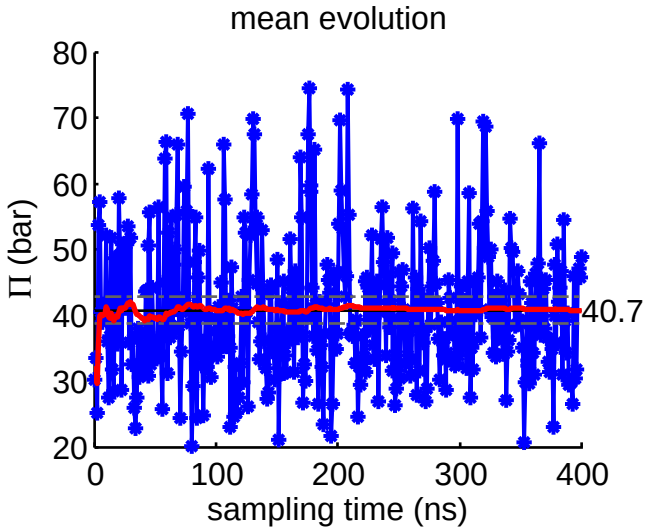

Figure 4.32: **(Long – Fluctuations & Block Averages)** Block average of the osmotic pressure with 1 ns sampling time (blue line with asterisks) and running average of the osmotic pressure (red line). The horizontal lines mark the mean osmotic pressure (solid) and a ±5 % interval around it (grey dashed lines). The 5 % interval is finally entered after 42 ns sampling time. The membrane walls have a force constant k of 100 kJ/(mol·nm^2). 36 NaCl ion pairs are dissolved in 3072 SPC/E water molecules and are confined in a 6 nm slab, resulting in a salt concentration of 0.95 M inside the ion domain. The box is allowed to change its size in z-direction to maintain the pressure, namely a NPAT ensemble is applied. Further results are shown in Tab. 4.14. The total duration of the simulation is 400 ns including 1 ns equilibration time.

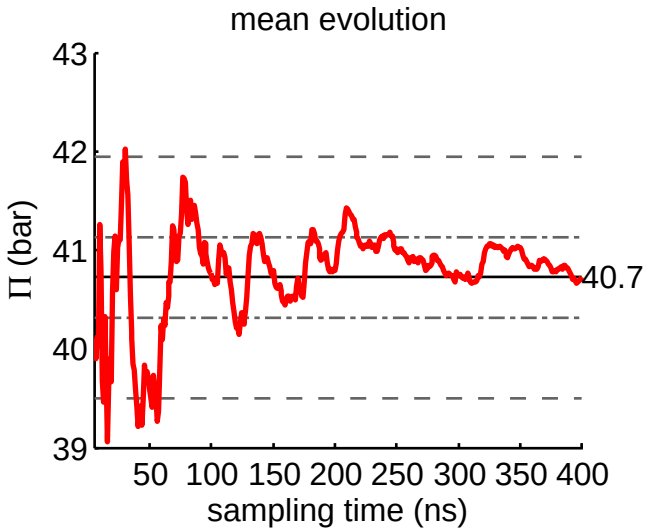

Figure 4.33: **(Long – Running Average & Confidence Intervals)** Running average of the osmotic pressure (red line). The horizontal lines mark the mean osmotic pressure (solid), a ±3 % interval around it (outer grey dashed lines) and a ±1 % interval (inner grey dash-dotted line). The 3% interval is finally entered after 59 ns sampling time, the 1 % interval is finally entered after 335 ns sampling time. The membrane walls have a force constant k of 100 kJ/(mol·nm^2). 36 NaCl ion pairs are dissolved in 3072 SPC/E water molecules and are confined in a 6 nm slab, resulting in a salt concentration of 0.95 M inside the ion domain. The box is allowed to change its size in z-direction to maintain the pressure, namely a NPAT ensemble is applied. Further results are shown in Tab. 4.14. The total duration of the simulation is 400 ns including 1 ns equilibration time. The first 10 ns are not shown in the graph.

- **(Barostat Coupling)** What influence has the simulated ensemble, precisely, is there a difference in using the NPAT or the NVT ensemble?

  As it is visible in Tab. 4.14, the measured osmotic pressures for the 400 ns NPAT simulation and the 80 ns NVT simulation are identical within their error margins. An equilibration time of 300 ps in the NPT ensemble seems to be enough to ensure a good performance of the NVT simulation. The NPAT ensemble ensures a constant pressure over the whole simulation time, however the computational costs increase considerable. Only 70 % of the performance of the NVT simulations is reached in the NPAT ensemble.

- **(Thermostat Coupling)** Does the thermostat coupling of ions has an effect on the osmotic pressure?

  Upon leaving the ion domain, the ions are accelerated towards the ion domain. The acceleration leads to an increased temperature of the ions.

  As the thermostat artificially alters the velocity of the particles, the thermostat is suspected to influence the ion-membrane interaction. As visible from Tab. 4.14, the result for a system with ions coupled to the thermostat compared to a system with ions decoupled from the thermostat differ by less then 1.5 bar. The influence of the thermostat is therefore estimated to be small and within the order of random fluctuations. The temperature of decoupled ions is the same as of the water molecules due to the strong coupling between solute and solvent. To avoid even slight influences of the thermostat, we suggest a decoupling of ions from the thermostat in the simulations.

- **(Size effects)** Does the measured osmotic pressure depend on the ion domain size r_{id}?

  For a comparison of different domain sizes see Tab. 4.14, simulation a) and c). In a small domain size the salt concentration is more diminished than in a big domain as the 'surface effect' of the membrane has a proportional larger influence. Anyway, with 86% of the reference value, the result is in reasonable agreement with other simulations. In addition, the ion density profile shows a pronounced plateau in the middle of the ion domain pointing to a good separation of the two membrane walls. The 3 nm wide ion domain is therefore preferable over the 6 nm wide ion domain size as it is computational cheaper.

Table 4.14: **(Simulation Setups – KBFF NaCl Ions in SPC/E Water)** Summary of osmotic pressure Π calculations for KBFF NaCl ions in SPC/E water. When not mentioned otherwise in the abbreviation 'Abb.' column as NVT, the simulations are performed in a NPAT ensemble leaving the cross-section of the box constant and varying the length of the box to maintain pressure. The ion domain r_{id} is 6 nm long, for the simulation c) named 'small domain' the ion domain is only 3 nm long. The ions are not coupled to the thermostat, except simulation d) named coupled ions. The force constant of the membrane k is set to 100 kJ/(mol·nm^2). The concentration refers to the ion-pair concentration inside the ion-domain. The reference osmotic pressure Π_{ref} is calculated as described in Sec. 4.6.4 using the data from Hess et al [40] for the same model. The measured osmotic pressure is given with an error estimate from block averages with 95% confidence. Further details are shown in the appendix. S_{N} denotes the standard deviation of the measured osmotic pressure Π_{measured}.

	Abb.	Fig.	t (ns)	c (M)	Π_{ref} (bar)	Π_{measured} (bar)	S_{N} (bar)
a)	long	B.1	400	0.952	44.1	40.7 ± 1.0	10.3
b)	NVT	B.2	80	0.954	44.2	39.9 ± 2.2	9.9
c)	small domain	B.3	80	0.903	41.7	37.7 ± 1.6	7.2
d)	coupled ions	B.4	160	0.953	44.1	39.4 ± 1.5	10.0

- **(Membrane Hardness)** Does the measured osmotic pressure depend on the force constant k of the membrane wall?

  In Tab. 4.15 results for different membrane force constants acting on the ions are presented. As the membranes are modelled as repulsive walls, they act on the ions according to a certain hardness (high force constant k) or softness (low force constant k). Hard walls keep nearly all ions inside the ion domain whereas in simulations with soft walls the density of ions slowly declines at and behind the membrane walls. The membrane hardness has two effects on the simulation: (i) decreasing salt concentration in the ion domain with decreasing force constant and (ii) with increasing force constant the number of ions interacting with the wall is reduced.

  The salt concentration inside the ion domain depends on the force constant k, thereby influencing the measured osmotic pressure. The change in the salt concentration has to be taken into account during the calculation of the reference values of the osmotic pressure.

  With high membrane force constants less ions are outside the ion domain. The sampling is reduced and consequently the error increases. For too high force constants ($k = 50'000\,\mathrm{kJ/(mol \cdot nm^2)}$) the simulations even become unstable.

  We conclude, that an optimized membrane force constant shall be low enough to enable good sampling. However the higher the force constant, the easier is the calibration of the simulation setup in terms of target concentrations. We prefer an intermediate value for the membrane force constant of $k = 100\,\mathrm{kJ/(mol \cdot nm^2)}$.

Table 4.15: **(Membrane Hardness – KBFF NaCl Ions in SPC/E Water)** Summary of osmotic pressure Π calculations for KBFF NaCl ions in SPC/E water. The simulations are performed in a NPAT ensemble leaving the cross-section of the box constant and varying the length of the box to maintain pressure. The ion domain is 6 nm big. The force constant of the membrane k is varied in a range from 50 to 50'000 kJ/(mol·nm^2). The simulation with $k = 50'000\,\mathrm{kJ/(mol \cdot nm^2)}$ crashed. The concentration refers to the ion-pair concentration inside the ion-domain. The reference osmotic pressure Π_{ref} is calculated as described in Sec. 4.6.4 using the data from Hess et al [40] for the same model. The simulation time of the calculation is 160 ns. The measured osmotic pressure is given with an error estimate from block average with 95% confidence. Further details are shown in the appendix. S_{N} denotes the standard deviation of the measured osmotic pressure Π_{measured}.

k (†)	Fig.	c (M)	Π_{ref} (bar)	Π_{measured} (bar)	$\mathrm{S_N}$ (bar)
50	B.5	0.93	43.0	40.5 ± 1.7	10.7
100	B.6	0.95	44.0	39.6 ± 1.7	10.8
200	B.7	0.97	45.0	41.1 ± 1.4	9.0
500	B.8	0.98	45.4	41.9 ± 1.8	11.3
1'000	B.9	0.99	45.9	40.6 ± 1.6	10.2
5'000	B.10	0.99	45.9	41.7 ± 1.8	11.5
10'000	B.11	0.99	45.9	42.6 ± 2.0	12.6
50'000			crashed		

(†) (kJ/(mol·nm^2))

- **(Starting configuration)** What is the influence of an unfavourable starting configuration on the equilibration behaviour of the osmotic pressure simulation?

  To estimate the dynamics of the system and the time scale for relaxation, the influence of a non-equilibrated starting configuration is investigated. Instead of distributing the ions evenly over the 6 nm ion domain, all ions are restrained in a 3 nm domain at the beginning of the simulation, see Fig. 4.34(c) for an example with a salt concentration of $c = 3.7\,\mathrm{M}$. Surprisingly, it takes up to 50 ns for the system to evolve from this starting configuration to an equilibrium configuration which reproduces the correct equilibrated osmotic pressure Π, see Fig. 4.34(a). Averaged over the whole trajectory of 160 ns, the density profile shows a well equilibrated behaviour, see Fig. 4.34(b).

  In general, the systems need much longer to relax from the perturbation than expected.

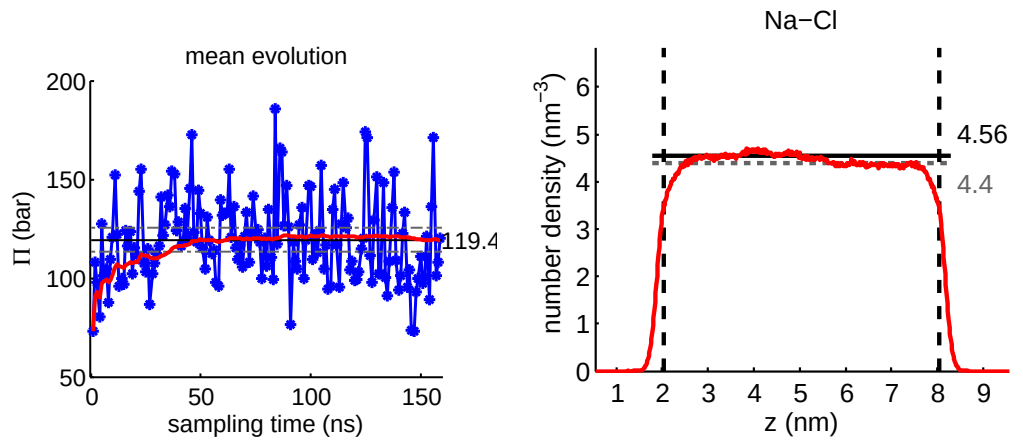

(a) Osmotic pressure Π.

(b) Number density distribution ρ_N.

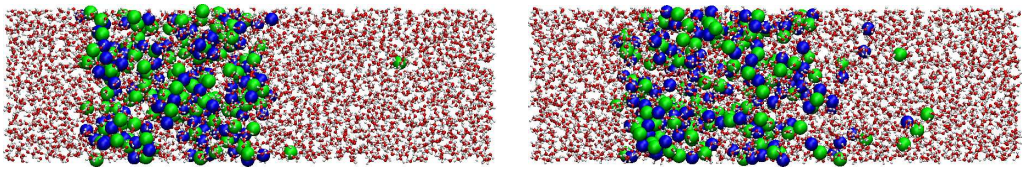

(c) Snapshot $t = 64$ ps.

(d) Snapshot $t = 1$ ns.

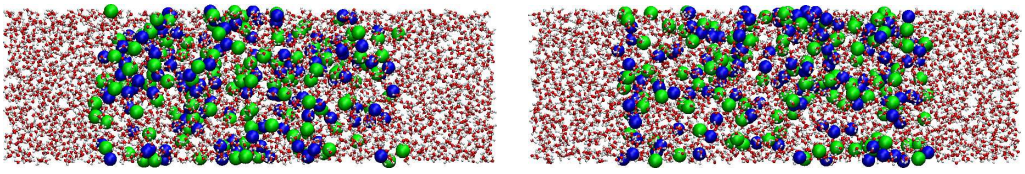

(e) Snapshot $t = 10$ ns.

(f) Snapshot $t = 50$ ns.

Figure 4.34: **(Influence of the Starting Configuration)** Illustration of the influence of the starting configuration on the osmotic pressure calculation. 133 NaCl ion pairs are dissolved in 3072 SPC/E water molecules and are confined in a 6 nm slab, resulting in a salt concentration of 3.7 M inside the ion domain. In the initial configuration, the ions are restricted to a 3 nm slab. The volume of the box is kept constant (NVT ensemble) after a 300 ps equilibration time in a NPAT ensemble at 1 bar. The temperature is 298.15 K. The total duration of the simulation is 160 ns including 1 ns equilibration time. a) Block average of the osmotic pressure with 1 ns sampling time (blue line with asterisks) and running average of the osmotic pressure (red line). The horizontal lines mark the mean osmotic pressure (solid) and a ±5 % interval around it (grey dashed lines). b) Number density distribution of ion species in the box. The vertical dashed lines mark the position of the membrane. The horizontal lines mark the position of the target concentration with 'hard' membrane walls (black solid), and the actual concentration between the membrane walls (grey dashed line). c) Snapshot of the simulation box after 64 ps of the production run. Sodium ions are printed in blue, chloride ions in green, oxygen atoms in red and hydrogen atoms in white, respectively. More snapshots are shown after 1 ns simulation time (d), 10 ns simulation time (e) and 50 ns simulation time (f).

- **(Crystallisation)** How does the osmotic pressure simulation react on salt crystallisation?

  In the osmotic pressure calculation at very high concentrations, the solubility limit $K_{\max}$ of KBFF NaCl in SPC/E water is reached. This is the case for the simulation with a salt concentration of $c = 5.3\,\mathrm{M}$. The precipitation of NaCl is visible in the snapshot in Fig. 4.35.

  The NaCl crystal behaves as one particle in the aqueous solution, thereby reducing the number of dissolved ion species. This is immediately visible in the reduced number of ions at the membrane walls, see Fig. B.20(c) and Fig. B.20(d). As the osmotic pressure depends on the number of particles acting on the membrane walls, the crystallisation and the reduced concentration of ion species result in a drop in the osmotic pressure, see Tab. 4.16 and Fig. 4.36(a).

  The stated osmotic pressure of 122.7 bar does not represent the equilibration value of the system. The formation of the crystal increases the equilibration time drastically, see Fig. B.20(a).

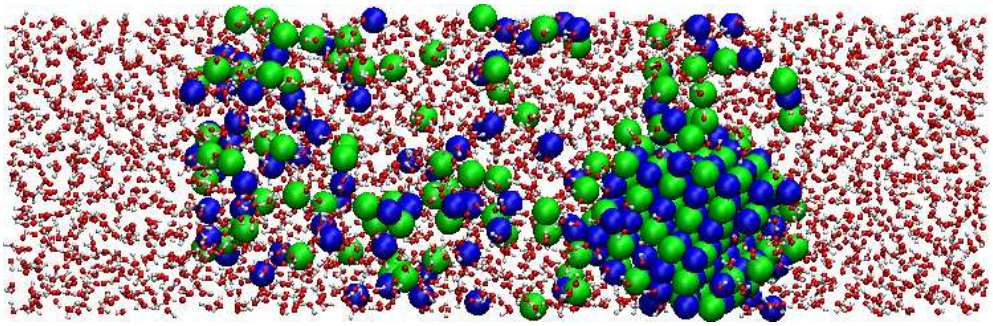

Figure 4.35: Snapshot of an osmotic pressure simulation of KBFF NaCl in SPC/E water. 190 NaCl ion pairs are dissolved in 3072 SPC/E water molecules and confined in a 6 nm slab, resulting in a salt concentration of 5.3 M inside the ion domain. A crystal is forming well visible on the bottom right side.

- **(Concentration dependence)** Are results for the osmotic pressure at different concentrations comparable to results for the same model but different methods?

  How to understand the concentration dependence of the osmotic pressure observed for the KBFF NaCl and the SPC/E water model as observed in Fig. 4.36(a)? The drop of the osmotic pressure at $c = 5.3\,\mathrm{M}$ can be attributed to crystallisation of NaCl, see above. Beside that, the results for KBFF NaCl in SPC/E water equals the result for the unmodified CHARMM FF by Luo and Roux [42], see Fig 4.36(b). For the KBFF ion model, the deviation of simulated data to experimental data becomes pronounces at a concentration of 2 M, whereas for the CHARMM FF the results are in reasonable agreement up to 3 M. In the calculation from Hess et al [40], the KBFF ions in SPC/E water also tend to underestimate the osmotic pressure compared to the experimental value, this trend becomes more pronounced when reaching salt concentrations larger than 2.8 M.

  The main question that remains is: Can the failure of reproducing correct osmotic pressure at high concentrations be attributed to the model or the method?

  The results reported by Hess et al [40] for the model used in this study are roughly 10 % larger than our results obtained by the membrane method. Hess et al used implicit solvent simulations with an estimated potentials of mean force for the ion-solvent interactions. Luo and Roux [42] state, that the usage of implicit solvents and PMFs is limited to low concentrations. This is comprehensible, as the influence of higher salt concentrations on the ion-ion interaction is only valued by Hess et al by adjusting the macroscopic dielectric constant of the system[2]. Thus, it cannot be stated with certainty, which method provides results closer to the real osmotic pressure of the model.

  Furthermore, many ion models are created for low concentrations. At high concentrations most models, especially where chloride is involved, tend to overestimate the ion-ion coupling, thereby reducing the osmotic pressure and the ion solubility.

[2] Drawbacks of the PMF calculations are discussed in Chapter 4.5

Table 4.16: **(Salt Concentration – KBFF NaCl Ions in SPC/E Water)** Summary of osmotic pressure Π calculations for KBFF NaCl ions in SPC/E. 19 to 190 NaCl ion pairs are dissolved in 3072 SPC/E water molecules, resulting in a concentration of roughly 0.5 to 5.0 M. After a 300 ps equilibration in the NPAT ensemble, simulations are performed for 160 ns in the NVT ensemble. The ion domain is 6 nm long, the whole box is roughly 9 nm long. The ions are not coupled to the thermostat. The force constant of the membrane k is set to 100 kJ/(mol·nm^2). The concentration refers to the ion-pair concentration inside the ion-domain. The reference osmotic pressure Π_{ref} is calculated as described in Sec. 4.6.4 using the data from Hess et al [40] for the same model. The measured osmotic pressure is given with an error estimate from block averages with 95% confidence. All simulations are run for 160 ns, except for the production run of the simulation with $c = 1.0$ M, which is performed in the NPAT ensemble for 400 ns. Further details are shown in the appendix. S_{N} denotes the standard deviation of the measured osmotic pressure Π_{measured}.

Fig.	c (M)	Π_{ref} (bar)	Π_{measured} (bar)	S_{N} (bar)
B.12	0.515	23.5	23.2 ± 1.2	7.7
B.1	0.952	44.1	40.7 ± 1.0	10.3
B.13	1.548	73.6	66.2 ± 2.1	13.4
B.14	2.075	101.7	78.6 ± 2.3	14.7
B.15	2.601	131.5	92.7 ± 2.5	16.3
B.16	2.906	149.7	100.7 ± 3.1	20.0
B.17	3.655	197.7	118.3 ± 3.4	21.6
B.18	4.178	233.9	133.3 ± 3.6	23.2
B.19	4.715	273.3	139.0 ± 3.6	23.1
B.20	5.288	318.3	122.7 ± 5.2	33.7

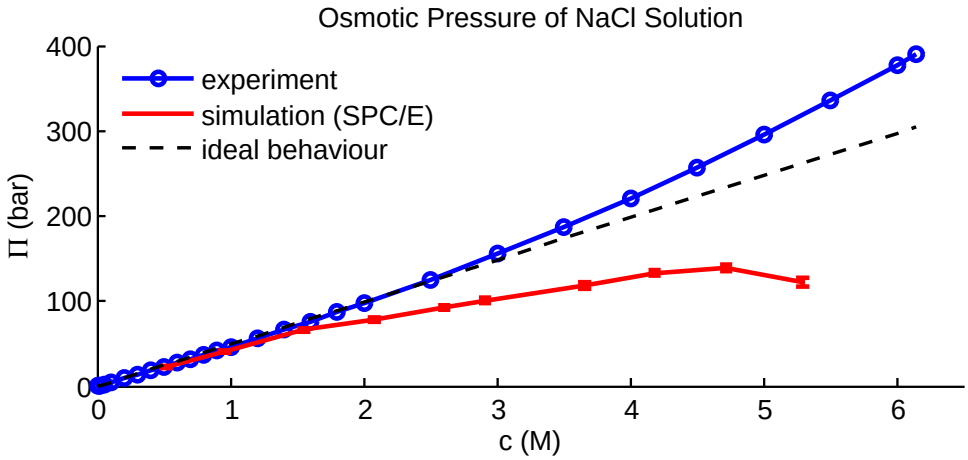

(a) SPC/E + KBFF.

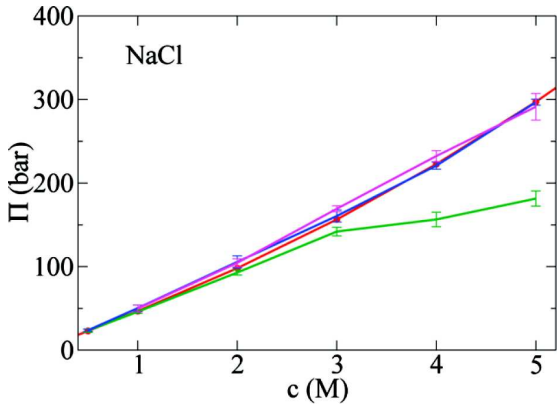

(b) CHARMM

Figure 4.36: **(Salt Concentration & Reference – KBFF NaCl Ions in SPC/E Water)** Overview of the results of osmotic pressure calculations for NaCl in water. a) NaCl ions modelled with the KBFF in SPC/E water (red line with error bars). Reference values are calculated as described in 4.6.4 and approximate experimental values (blue, circled line). b) The graph is taken from Luo and Roux [42]. The results for the CHARMM force field (green line with error bars) are presented together with experimental values (red line). Additional lines show results for a modified force field.

Conclusion of the Method We put the membrane method for determining the osmotic pressure of aqueous solutions to a thoroughly methodological investigation. This includes the effects of simulation parameters as the applied thermostat or ensemble, the simulation box size and setup and the membrane hardness. The method is also characterised in terms of equilibration time and influence of the starting configuration. Special emphasis is set to the calculation of the salt concentration inside the ion domain with anisotropic periodic boundary conditions, an issue often neglected in scientific literature.

The membrane method proved to be a robust and straightforward method. Most simulation parameter have only very minor effects on the result. The functionality is very similar to the experimental setup and can be directly evaluated. In contrast to other methods presented, the membrane method is applicable without further assumptions or corrections to the full range of salt concentrations, from high degree of dilution to the solubility limit. As our main aim is to describe the behaviour of solutions at high concentrations, the applicability at high salt concentrations is emphasised.

In contrast to implicit simulation techniques, the explicit full atom simulation of the water and ion model guarantees to reproduce the osmotic pressure of the model. The disadvantage of such a simulation lies in the high computational costs and the slow equilibration behaviour. Anyway, by our rigorous testing, we are able to identify the computational cheapest setup. The knowledge of the equilibration behaviour allows us to estimate the necessary simulation time for a given target accuracy with confidence in our results.

4.6.6 Performance of the Polarizable Model

The method is tested in detail with the KBFF ion model and the SPC/E water model, see Sec. 4.6.5. As the osmotic pressure is of great importance in this work, we do most of the testing again for the polarizable model. As the SW10e model is computational very expensive, we are not able to produce very long trajectories and the results are afflicted with a larger error as indicated in the respective tables.

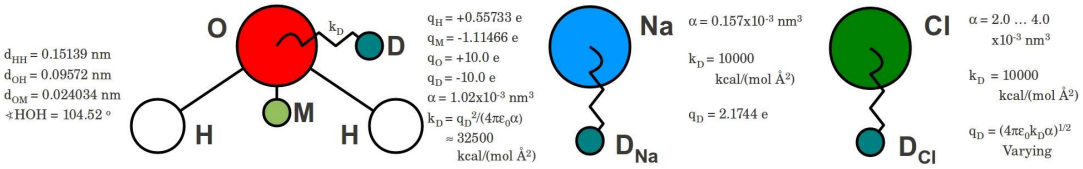

Figure 4.37: Schematic representations of the SW10e water and ion models developed by Lamoureux et al [25] and modified by Mikhail Stukan.

Simulation Setup

The simulations are performed with Gromacs 4.5.5 [110] in double precision. The tool Packmol [111] is used to create the simulation boxes.

The force field of sodium and chloride is sampled by using five different polarizabilities of chloride

$$\alpha_{\mathrm{Cl}} = 2.0,\ 2.5,\ 3.0,\ 3.5,\ 4.0 \cdot 10^{-3}\mathrm{nm}^3.$$

The simulation boxes are roughly 3 nm long in x and y-direction and vary in length in the z-direction from 6 nm with 2048 water molecules to 12 nm with 4096 water molecules. The ion domain size r_{id} is 3 or 6 nm in z-direction. The ion domain expands in x and y-direction and is limited in z-direction by a neat water domain. The number of ions in the ion domain varies with the simulation setup.

The simulations are equilibrated at a pressure of 1 bar in the NPT ensemble for 300 ps. Some boxes are equilibrated using the NPAT ensemble, thereby leaving the value of the cross-section A constant. For all simulations, the first 1 ns of the production run is neglected to ensure good equilibration.

If not explicitly mentioned, the temperature is maintained at 298.15 K. In some simulation, the ions are decoupled from the thermostat. Some simulations are run at higher temperatures: 313.15 K, 333.15 K and 353.15 K.

The force constant k of the membrane varies between 100 and 10'000 kJ/(mol·nm^2).

Periodic boundary conditions are applied in all directions. The cutoff of the Lennard-Jones interactions is taken to be 1.2 nm with shifted potential taken from 1.0 nm. The long-range Coulomb interactions are handled by the Particle-Mesh Ewald method [112] with a cutoff of 1.5 nm and a grid spacing of 0.1 nm. The neighbour list for non-bonded interactions is updated every 10th integration step. We use the leap-frog algorithm for integrating Newton's equations of motion with 0.001 ps time step. All simulations are performed at fixed temperature. Velocity rescaling [113] is used with a temperature coupling constant of 0.1 ps. The pressure is held constant using the Berendsen barostat [114] with a pressure constant of 0.5 ps. We store the atomic coordinates of the ions each 5 ps for further analysis.

The NaRIBaS [1] framework is used for preparation and analysis of some the simulations. Matlab [115] is applied for mathematical operations and plotting.

Results

In the upcoming section, we will present the results for the polarizable ion model in conjunction with SW10e water. We present the influence of the general simulation setup in Tab. 4.17 and Fig. 4.38, the influence of the polarizability of chloride ions in Tab. 4.18 and Fig. 4.39, the evolution of the osmotic pressure at different concentration in Tab. 4.19 and Fig. 4.40 and finally we give an overview about all osmotic pressure simulations performed with the model with a polarizability of chloride of $\alpha_{\mathrm{Cl}} = 2.0 \cdot 10^{-3}\mathrm{nm}^3$ in Tab. 4.20. The last table also includes different temperatures at 4 and 5 M salt concentrations.

The reference osmotic pressure Π_{ref} is calculated as described in Sec. 4.6.4 using experimental data provided by Hamer and Yung-Chi [189].

As some simulations fit to several discussion, they can be found in several tables. We accept this redundancy as necessary to enhance the overview.

Simulation Setup & Wall Hardness – Polarizable Ions and SW10e Water The influence of different simulation setups and different ion models are summarised in Tab. 4.17 for a salt concentration of roughly 0.5 M. Beside one, all simulations are rather short and the errors large. Still, the results can be used to evaluate trends. As shown for the non-polarizable model the influence of the ion domain size r_{id}, solvent domain size r_{sd}, wall constant k and thermostat coupling is negligible.

Table 4.17: **(Simulation Setup & Wall Hardness – Polarizable Ions and SW10e Water)** Summary of results obtained from an osmotic pressure calculation using different setups. 10 to 20 NaCl ion pairs are dissolved in a water box consisting of SW10e water molecules and are confined in a slab, resulting in a salt concentration of roughly 0.5 M inside the ion domain. The NVT ensemble is applied after 300 ps of equilibration in a NPT ensemble at a pressure of 1 bar. Further results are shown in the indicated figures. The polarizability of chloride α_{Cl} is indicated in the second column. The error of the osmotic pressure Π is estimated using block averages with 1 ns sampling time. S_{N} denotes the standard deviation of the measured osmotic pressure Π_{measured}. The ions marked with (*) are decoupled from the thermostat. r_{id} and r_{sd} mark the size of the ion domain and the solvent domain, respectively.

k (†)	α_{Cl} (‡)	r_{id} (nm)	r_{sd} (nm)	Fig.	t (ns)	c (M)	Π_{ref} (bar)	Π_{measured} (bar)	S_{N} (bar)
100	4.0	6	6.5	B.21	15	0.531	24.3	22.8 ± 3.9	6.8
100	4.0	3	9.5	B.22	8	0.511	23.3	19.1 ± 2.3	2.6
100	4.0	3	3.3	B.23	8	0.497	22.7	23.6 ± 5.2	6.0
100	3.5	3	9.5	B.24	8	0.498	22.7	23.6 ± 3.0	3.4
100	3.5	3	3.3	B.27	8	0.502	22.9	22.7 ± 7.2	8.2
1'000	3.5	3	3.3	B.28	8	0.541	24.7	19.1 ± 3.3	3.8
10'000	3.5	3	3.3	B.29	8	0.544	24.9	36.8 ± 13.2	15.2
100	3.5(*)	3	3.3	B.30	8	0.502	22.9	22.5 ± 3.9	4.5
1'000	3.5(*)	3	3.3	B.31	8	0.536	24.5	26.3 ± 3.7	4.3
10'000	3.5(*)	3	3.3	B.32	8	0.548	25.0	21.0 ± 5.6	6.4

(†) $(\mathrm{kJ/(mol{\cdot}nm^2)})$
(‡) $(10^{-3}\,\mathrm{nm^3})$

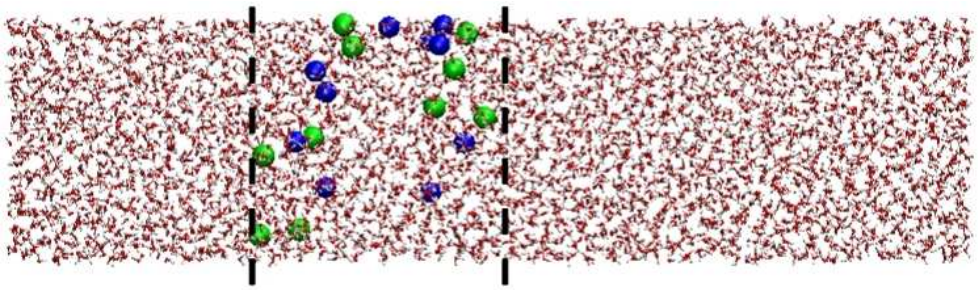

(a) Small ion domain.

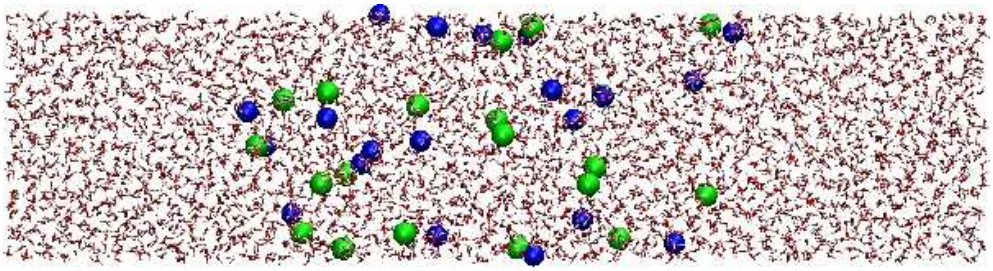

(b) Big ion domain.

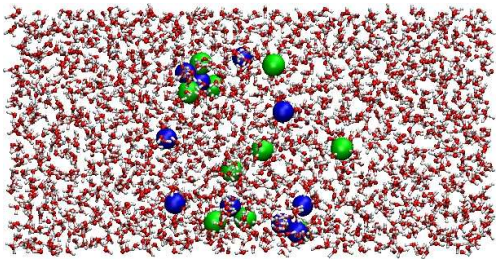

(c) Small box.

Figure 4.38: Snapshots of SW10e simulations with sodium chloride ion pairs. For SW10e only the oxygen (red) and hydrogen (white) sites are shown, for sodium and chloride only the atom sites are shown in blue and green, respectively. The target concentration is 0.5 M inside the ion domain. a) 12.5 nm long box with a 3 nm wide ion domain. 10 ion pairs are dissolved. The vertical dashed lines mark the position of the membrane. b) 12.5 nm long box with a 6 nm wide ion domain. 20 ion pairs are dissolved. c) 6.3 nm long box with a 3 nm wide ion domain. 10 ion pairs are dissolved.

Polarizability – Polarizable Ions and SW10e Water The numerical results for the osmotic pressure upon increasing the polarizability α_{Cl} from 2.0 to $4.0 \cdot 10^{-3}\,\mathrm{nm}^3$ at three different salt concentrations (0.5, 4.0 and 5.0 M) are provided in Tab. 4.18 and Fig. 4.39.

For a salt concentration of 0.5 M we observe an agreement with the experimental reference value. However due to the short sampling time, we do not feel secure to discuss a dependency of the osmotic pressure on the polarizability.

Our special interest lies in the performance of the model at high salt concentration. For high salt concentrations and variable polarizability, two distinctive trends are visible: (i) the osmotic pressure increases with decreasing polarizablity α and (ii) with higher polarizability α the ions are more likely to precipitate.

At the highest concentration ($c = 5.0\,\mathrm{M}$), the osmotic pressure firstly increases slightly with polarizability, followed by a continuous and pronounced decrease. The drop at high polarizabilities is attributed to a crystallisation, see for example the density profile in Fig. B.42. The Π-α_{Cl} dependency exhibits a maximum and optimum at $\alpha_{\mathrm{Cl}} = 2.5 \cdot 10^{-3}\,\mathrm{nm}^3$ but the two values at $\alpha_{\mathrm{Cl}} = 2.5 \cdot 10^{-3}\,\mathrm{nm}^3$ and $\alpha_{\mathrm{Cl}} = 2.0 \cdot 10^{-3}\,\mathrm{nm}^3$ are both in the range of their respective errors.

Considering the lower concentration ($c = 4.0\,\mathrm{M}$), the polarizability $\alpha_{\mathrm{Cl}} = 2.0 \cdot 10^{-3}\,\mathrm{nm}^3$ seems to be optimal in terms of reproducing the experimental osmotic pressure.

Table 4.18: **(Polarizability – Polarizable Ions and SW10e Water)** Results obtained from osmotic pressure calculation with different salt concentrations of NaCl. 10, 80 and 100 NaCl ion pairs are dissolved in a water box consisting of 2048 SW10e water molecules and are confined in a 3 nm wide slab, resulting in a salt concentration of roughly 0.5, 4.0 and 5.0 M inside the ion domain. The NVT ensemble is applied after 300 ps of equilibration in a NPT or NAPT ensemble at a pressure of 1 bar. Further results are shown in the indicated figures. The polarizability of chloride α_{Cl} is indicated in the second column. The error of the osmotic pressure Π is estimate using block average with 1 ns sampling time. S_{N} denotes the standard deviation of the measured osmotic pressure Π_{measured}. The ions marked with (*) are decoupled from the thermostat. r_{id} and r_{sd} mark the size of the ion domain and the solvent domain, respectively.

k (†)	α_{Cl} (‡)	r_{id} (nm)	r_{sd} (nm)	Fig.	t (ns)	c (M)	Π_{ref} (bar)	Π_{measured} (bar)	$\mathrm{S_N}$ (bar)
100	2.0	3	3.3	B.43	8	0.493	22.5	26.5 ± 4.6	4.9
100	2.5	3	3.3	B.26	8	0.519	23.7	15.3 ± 3.8	4.0
100	3.0	3	3.3	B.25	8	0.498	22.7	22.8 ± 5.2	6.0
100	3.5	3	9.5	B.24	8	0.498	22.7	23.6 ± 3.0	3.4
100	4.0	3	3.3	B.23	8	0.497	22.7	23.6 ± 5.2	6.0
100	2.0(*)	3	3.8	B.47	20	4.047	224.6	214.2 ± 9.6	20.0
100	2.5(*)	3	3.8	B.35	20	4.080	226.9	199.9 ± 12.3	25.6
100	3.0(*)	3	3.8	B.36	20	4.117	229.5	180.2 ± 6.8	14.2
100	3.5(*)	3	3.8	B.37	20	4.181	234.1	143.9 ± 5.9	12.3
100	4.0(*)	3	3.8	B.38	20	4.312	243.5	86.1 ± 7.6	15.9
100	2.0(*)	3	3.9	B.51	20	5.097	302.9	249.7 ± 12.8	26.7
100	2.5(*)	3	3.9	B.39	20	5.071	300.8	256.4 ± 11.9	25.0
100	3.0(*)	3	3.9	B.40	20	5.140	306.3	227.2 ± 10.0	21.0
100	3.5(*)	3	3.9	B.41	20	5.236	314.1	174.2 ± 8.9	18.7
100	4.0(*)	3	3.9	B.42	20	5.406	327.9	101.4 ± 8.6	18.0

(†) $(\mathrm{kJ/(mol{\cdot}nm^2)})$
(‡) $(10^{-3}\,\mathrm{nm^3})$

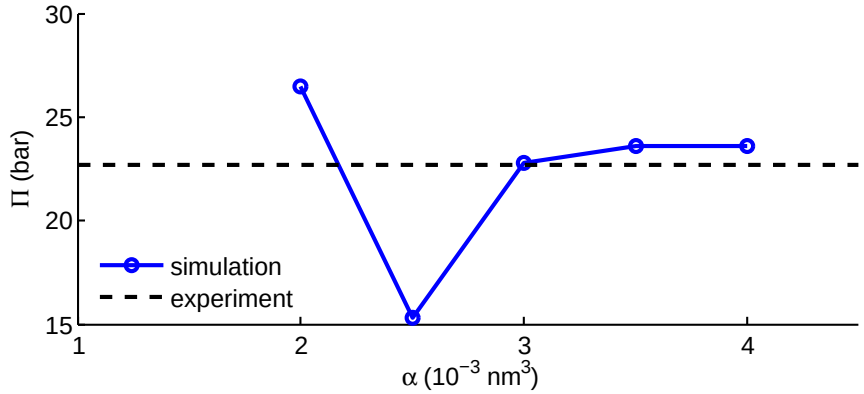

(a) Salt concentrations $c = 0.5\,\mathrm{M}$.

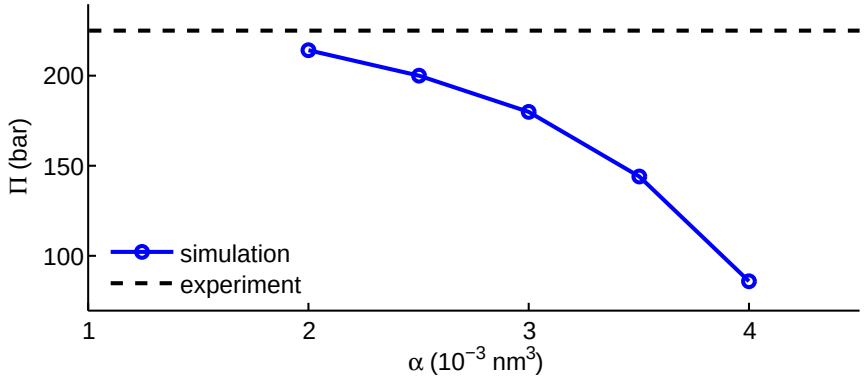

(b) Salt concentrations $c = 4.0\,\mathrm{M}$.

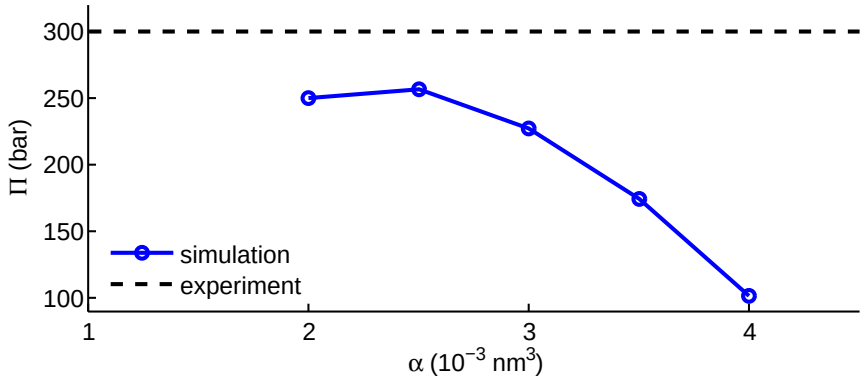

(c) Salt concentrations $c = 5.0\,\mathrm{M}$.

Figure 4.39: **(Polarizability – Polarizable Ions and SW10e Water)** Overview of the results of osmotic pressure calculations for polarizable NaCl in SW10e water with different polarizabilities α_{Cl} of chloride. The blue line with circles shows simulation results, the black dashed lines shows the experimental target value. a) Salt concentrations $c = 0.5\,\mathrm{M}$. b) Salt concentrations $c = 4.0\,\mathrm{M}$. c) Salt concentrations $c = 5.0\,\mathrm{M}$.

Salt Concentration – Polarizable Ions and SW10e Water Simulations at salt concentrations of 0.5, 1, 2, 4, 5 and 8 M with two different polarizabilities of $\alpha_{\mathrm{Cl}} = 2.0 \cdot 10^{-3}\,\mathrm{nm}^3$ and $\alpha_{\mathrm{Cl}} = 3.5 \cdot 10^{-3}\,\mathrm{nm}^3$ are presented in Tab. 4.19. The runtime is prolonged to 20 ns, thereby providing reasonable statistics. As expected, the simulation at 8 M shows crystallisation, similar as described above for the non-polarizable ion-water model at 5.3 M.

We show all osmotic pressure data for the two ion models in Fig. 4.40. The model with $\alpha_{\mathrm{Cl}} = 2.0 \cdot 10^{-3}\,\mathrm{nm}^3$ shows very good agreement with the experimental data at concentrations up to 4 M. Even at higher concentrations, the underestimation of the osmotic pressure is less drastic compared to non-polarizable models and the polarizable model with higher α_{Cl}.

In Fig. 4.40(b) a computational reference by Luo et al [30] for their polarizable water-ion with altered Lennard-Jones combination rules is shown. The uncorrected water-ion model behaves similar to our high-polarizability model.

Luo and co-workers are able to improve the performance of the model by tuning the ion-ion interaction, leaving the ion-water interaction unchanged. As we discussed in Sec. 3.3.1, this approach might prove cumbersome in the future. We show the feasibility of a different pathway to optimise the ion force field without manipulating individual pair-interaction parameter.

Table 4.19: **(Salt Concentration – Polarizable Ions and SW10e Water)** Results obtained from osmotic pressure calculation with different salt concentrations of NaCl. 10, 20, 40, 80, 100 and 160 NaCl ion pairs are dissolved in a water box consisting of 2048 SW10e water molecules and are confined in a 3 nm wide slab, resulting in a salt concentration of roughly 0.5, 1.0, 2.0, 4.0, 5.0 and 8.0 M inside the ion domain. The NVT ensemble is applied after 300 ps of equilibration in a NPT or NAPT ensemble at a pressure of 1 bar. Further results are shown in the indicated figures. The polarizability of chloride α_{Cl} is indicated in the second column. The error of the osmotic pressure Π is estimated using block averages with 1 ns sampling time. S_{N} denotes the standard deviation of the measured osmotic pressure Π_{measured}. The ions marked with (*) are decoupled from the thermostat. r_{id} and r_{sd} mark the size of the ion domain and the solvent domain, respectively.

k (†)	α_{Cl} (‡)	r_{id} (nm)	r_{sd} (nm)	Fig.	t (ns)	c (M)	Π_{ref} (bar)	Π_{measured} (bar)	S_{N} (bar)
100	3.5	3	3.3	B.27	8	0.502	22.9	22.7 ± 7.2	8.2
100	3.5	3	3.1	B.33	20	0.990	45.9	48.0 ± 4.9	9.2
100	3.5	3	3.2	B.34	20	2.010	98.1	86.6 ± 6.6	12.5
100	3.5(*)	3	3.8	B.37	20	4.181	234.1	143.9 ± 5.9	12.3
100	3.5(*)	3	3.9	B.41	20	5.236	314.1	174.2 ± 8.9	18.7
100	2.0	3	3.3	B.43	8	0.493	22.5	26.5 ± 4.6	4.9
100	2.0(*)	3	3.8	B.44	20	0.995	46.18	48.23 ± 4.0	8.35
100	2.0(*)	3	3.8	B.45	20	1.994	97.21	95.36 ± 5.9	12.4
100	2.0(*)	3	3.8	B.46	20	3.025	157.0	165.27 ± 11.4	23.8
100	2.0(*)	3	3.8	B.47	20	4.047	224.6	214.2 ± 9.6	20.0
100	2.0(*)	3	3.9	B.51	20	5.097	302.9	249.7 ± 12.8	26.7
100	2.0(*)	3	4.2	B.55	20	8.493	—	272.3 ± 18.9	39.5

(†) $(\mathrm{kJ/(mol{\cdot}nm^2)})$
(‡) $(10^{-3}\,\mathrm{nm^3})$

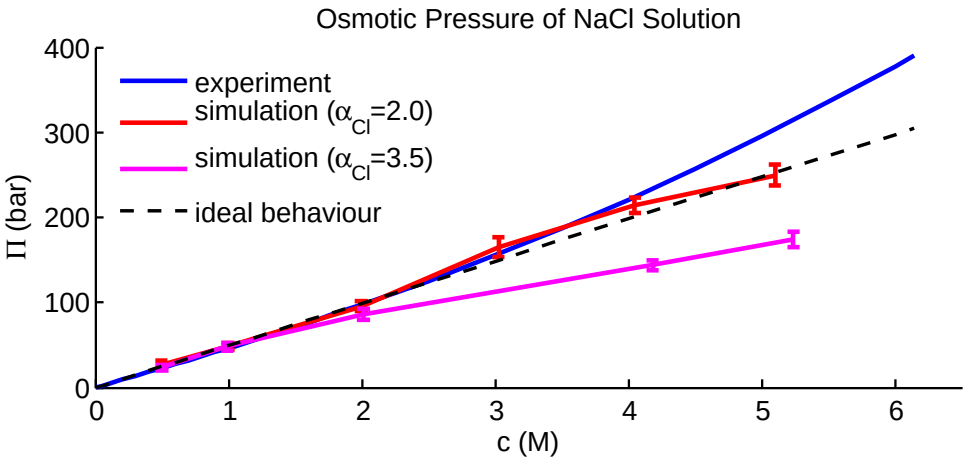

(a) this work

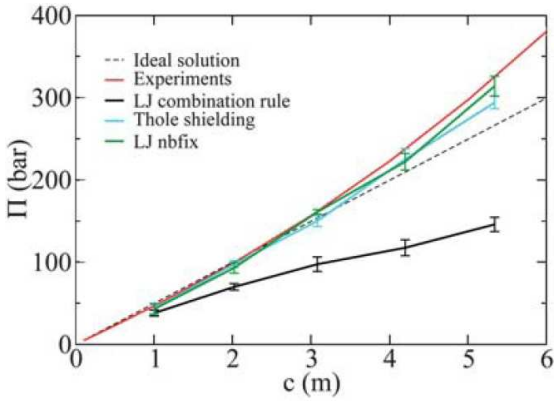

(b) Luo et al

Figure 4.40: **(Salt Concentration & Reference – Polarizable Ions and SW10e Water)** Overview of the results of osmotic pressure calculations for NaCl in water. a) Polarizable NaCl ions in SW10e water (red and magenta line with error bars). The blue line shows experimental reference values calculated as described in 4.6.4 b) The graph is taken from Luo et al [30]. The results for the unmodified polarizable force field [102, 25] (black line with error bars) are presented together with experimental values (red line). Additional lines show results for a modified force field.

Temperature – Polarizable Ions and SW10e Water Table 4.20 and Fig. 4.41 provide an overview of the performance of the polarizable ion model with polarizability of chloride α_{Cl} set to $2.0 \cdot 10^{-3}\,\mathrm{nm}^3$. A concentration range between 0.5 and 8 M is screened, at $c = 4\,\mathrm{M}$ and $c = 5\,\mathrm{M}$ different temperatures between 25 °C and 80 °C are simulated.

As it is visible in Fig. 4.41, the model is able to reproduce experimental osmotic pressure values both at low and high concentrations. At the highest concentration of 5 M the experimental osmotic pressure surpasses the simulated value. At this concentration, we suspect the model to be near or at the solubility limit. The increased ion coupling and reduced ion mobility are expected to result in a lower osmotic pressure. An ion-ion residence time analysis or a detailed RDF analysis might provide more insights in this phenomenon. More information on the calculation of the residence time can be found in Section 4.4.

The simulated osmotic pressure shows no pronounced temperature dependency. The experimental osmotic coefficient ϕ is nearly constant in the temperature regime under investigation [191]. Therefore, following the Van't Hoff equation 4.8, the osmotic pressure should increase linear with temperature. Or in other words, we expect an increase of the osmotic pressure by roughly 16 % when heating from 25 °C to 80 °C.

Upon increasing the temperature, several effects influence the osmotic pressure: increased kinetic energy of ions, decreased extend of hydration and a decreased extend of ion-ion association. The loss of ion-hydration may lead to an *increase* in ion-ion association, which would have a diminishing effect on the osmotic pressure. This explanation would coincide with discussions about the density, see Sec. 4.1. More investigations are necessary to fully describe the behaviour of our model system upon heating.

To summarise: The model with a polarizability of chloride of $\alpha_{\mathrm{Cl}} = 2.0 \cdot 10^{-3}\,\mathrm{nm}^3$ can reproduce the osmotic pressure up to a high concentration of 4 M, where the performance decreases. At concentrations above 4 M, the model underestimates the osmotic pressure compared to the experimental results.

We are *not* able to show any temperature influence on the osmotic pressure for our model.

Table 4.20: **(Temperature – Polarizable Ions and SW10e Water)** Summary of osmotic pressure simulation results under variation of temperature and salt concentration. The temperature T is varied between 298.15, 313.15, 333.15 and 353.15 K corresponding to 25, 40, 60 and 80 °C. The amount of 10, 20, 40, 80, 100 and 160 NaCl ion pairs are dissolved in a water box consisting of 2048 SW10e water molecules. The ions are confined in a $r_{\mathrm{id}} = 3.0\,\mathrm{nm}$ wide slab, resulting in a salt concentration of roughly 0.5, 1.0, 2.0, 4.0, 5.0 and 8.0 M inside the ion domain. r_{sd} marks the size of the solvent domain. The polarizability of chloride α_{Cl} is $2.0 \cdot 10^{-3}\,\mathrm{nm}^3$. The force constant of the membrane is set to $k = 100\mathrm{kJ}/(\mathrm{mol} \cdot \mathrm{nm}^2)$. The NVT ensemble is applied after 300 ps of equilibration in a NAPT or NPT ensemble at a pressure of 1.0 bar. For a visualisation of the equilibration behaviour and the concentration profile, see the respective figures indicated in the forth column. The error of the osmotic pressure Π is estimated using block averages with 1 ns sampling time. S_{N} denotes the standard deviation of the measured osmotic pressure Π_{measured}.

T (K)	α_{Cl} (‡)	r_{sd} (nm)	Fig.	t (ns)	c (M)	Π_{ref} (bar)	Π_{measured} (bar)	S_{N} (bar)
298.15	2.0	3.3	B.43	8	0.493	22.5	26.5 ± 4.6	4.9
298.15	2.0(*)	3.8	B.44	20	0.995	46.18	48.23 ± 4.0	8.35
298.15	2.0(*)	3.8	B.45	20	1.994	97.21	95.36 ± 5.9	12.4
298.15	2.0(*)	3.8	B.46	20	3.025	157.0	165.27 ± 11.4	23.8
298.15	2.0(*)	3.8	B.47	20	4.047	224.6	214.2 ± 9.6	20.0
313.15	2.0(*)	3.8	B.48	20	4.029	234.6	225.0 ± 9.6	20.1
333.15	2.0(*)	3.8	B.49	20	4.049	251.2	217.6 ± 9.5	19.8
353.15	2.0(*)	3.8	B.50	20	4.072	268.1	211.8 ± 6.4	13.5
298.15	2.0(*)	3.9	B.51	20	5.097	302.9	249.7 ± 12.8	26.7
313.15	2.0(*)	3.8	B.52	20	5.072	316.1	265.8 ± 15.2	31.9
333.15	2.0(*)	3.8	B.53	20	5.100	338.8	257.0 ± 10.3	21.5
353.15	2.0(*)	3.8	B.54	20	5.093	358.4	259.5 ± 9.3	19.5
298.15	2.0(*)	4.2	B.55	20	8.493	—	272.3 ± 18.9	39.5

(‡) $(10^{-3}\,\mathrm{nm}^3)$

(*) Thermostat coupling applies only to the water molecules, ions are excluded.

Conclusion: Performance of the Model We calculated the osmotic pressure for the polarizable SW10e water model and polarizable ion models in a wide range of salt concentrations, polarizabilities and temperatures. The original model shows the known drawback at high concentration of underestimating the osmotic pressure. This behaviour was reported by Luo et al [30] for polarizable models and by Luo and Roux [42] for non-polarizable models. We replicate the osmotic pressure slope for the non-polarizable SPC/E water and KBFF ion force field in the method section.

In a unique approach, we use the polarizability to adapt the model to the osmotic pressure at high concentration. The goal of reproducing the osmotic pressure over the whole range of concentrations is achieved and the variation of the ion polarizability proved to be a suitable tool for tuning model parameter to reproduce experimental quantities.

By using the polarizability to tune the ion force field, we ensure the compatibility between different ions with each other and the water model.

The experimental temperature behaviour is not reproduced by our model. Some possible reasons are discussed but will be further investigated in a future work.

4.6.7 Conclusion: Quality of the Method and Performance of the Model

The osmotic pressure can be measured experimentally with very high precision. As the osmotic pressure strongly depend on the ion-ion and ion-water interaction and can be measured at very high ion concentration, the quantity proved to be a valuable benchmark for force field development.

The membrane method proved to be a robust and straightforward method. The membrane method is applicable without further assumptions or corrections to the full range of ion concentrations, from high degree of dilution to the solubility limit and even beyond that. As our main aim is to describe the behaviour of solutions at high concentrations, the applicability at high ion concentrations is emphasised. For our aims, the advantages outweight the relatively high computational costs.

We calculated the osmotic pressure for the polarizable SW10e water model and polarizable ion models in a wide range of ion concentrations, polarizabilities and temperatures. The variation of the ion polarizability proved to be a suitable variable to reproduce experimental values of the osmotic pressure. The apparent underestimation of the osmotic pressure at high ion concentrations can be counteracted by a decrease of the polarizability. The maximum effect is anticipated to be at or close to $\alpha_{\mathrm{Cl}} = 2.0 \cdot 10^{-3}\mathrm{nm}^3$.

Finally, the goal of reproducing the osmotic pressure over the whole range of concentrations is achieved. The new model proved a good performance in a surface property far away from the dilution limit.

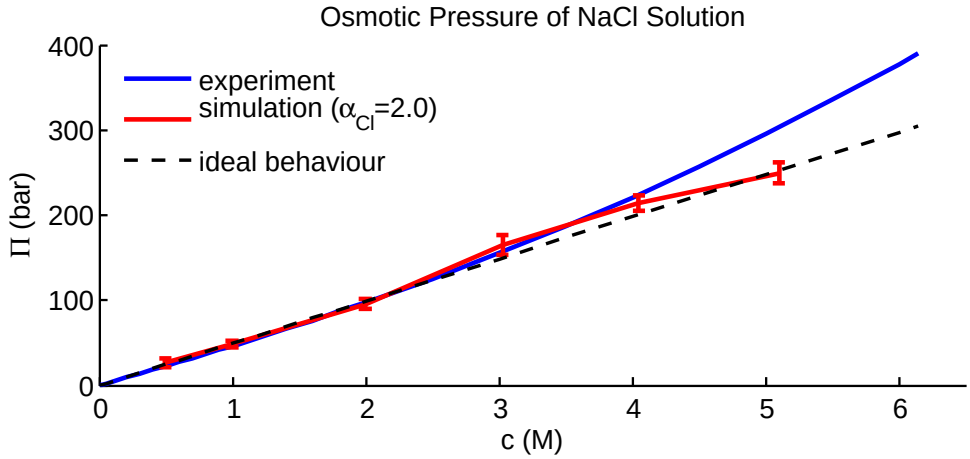

Figure 4.41: Osmotic pressure calculations of polarizable NaCl in SW10e water (red line with error-bars) for $\alpha_{\mathrm{Cl}} = 2.0 \cdot 10^{-3}\mathrm{nm}^3$. Comparison with experimental (blue line) and ideal (black line) behaviour.

4.7 Surface Tension

We introduced the great importance of water surface properties in Chapter 1 and 2.

The surface tension γ proved a valuable tool to describe the behaviour of water at interfaces [197]. On the other hand, "water is an demanding partner"[27], also in terms of surface tension. Whereas Caleman et al [27] use molecular simulations to describe the surface preferences of halides, e.g. chloride, at the water/air interface, Chen and Smith [198] describe sodium-chloride as "surface excluded solutes". We hope, that through tuning our ion model with the osmotic pressure, we are able to predict a realistic behaviour of the ions at the solution/air interface and to reproduce experimental values for the surface tension.

The feature of liquids to resist or to press an increase of surface area is expressed in the surface tension. The term *surface tension* describes the behaviour of the liquid *surface* similar to a stretched membrane that is *in tension* [199]. As the example of water with table salt and oil implies, the surface tension is a key quantity for many dissolution processes.

By describing the interface from an energetic point, the surface tension γ is defined as the work required to increase a surface area divided by that area A [183]

$$\gamma = \frac{\partial F}{\partial A}.$$

Thereby F corresponds to the Helmholtz free energy $F = E - TS$ [199] if the volume, temperature and particle number is held constant.

The term "surface tension of water" is often used as abbreviation for the surface tension of water at the water/air interface.

Ions, surfactants and particles affect the interfacial tension at water surfaces to vapour, liquid and solid surfaces drastically as shown by experiments and computer simulations [200, 27, 198]. Whereas surfactants are known to decrease the surface tension of water, some salts, e.g. NaCl, are able to increase the surface tension [200]. Among the number of potential additives to pure water, we concentrate on ion and salt effects.

A short overview about experimental methods and their accuracy is given followed by a description of the method to calculate the surface tension in computer simulations including recent results from other authors. The equilibration behaviour is investigated using a 1 M ion solution in conjunction with the SPC/E model. Results are presented for the surface tension of pure liquid water against a vapour interface obtained for two polarizable (SW10e + modified SW10e) and a non-polarizeable (SPC/E) force field. The performance of the polarizable model with $\alpha_{\mathrm{Cl}} = 2.0 \cdot 10^{-3}\mathrm{nm}^3$ is presented at different salt concentrations and temperatures.

4.7.1 The Experimental Method: the Surface Tension of Neat and Impure Water is Measurable with High Accuracy

As the surface tension of liquids varies under the inclusion of impurities, the precise measurement of the surface tension allows the usage of this physical quantity in quality control of industrial processes. For example, the presence of solvents or surfactants in liquids during chemical reactions can be monitored by continuous measuring of the surface tension. Thus, in the past century, the development of experimental methods for measuring the surface tension resulted in a considerable number of methods taking into account the varying conditions in laboratories.

A classical tensiometer as invented by Du Noüy [201] consists of a platinum ring, that is carefully pulled out of a liquid, thereby stretching the liquids "skin" or surface. The Wilhelmy plate method is used in a similar way to estimate the necessary force to lift a plate from the liquid/air surface [202].

Based on the formation of water droplets at the border of a tip, the surface tension can be estimated by analysing the shape of the liquid drop. The method is called pendant drop method. The sessile drop method origins in the formation of a specific contact angle of a liquid droplet placed on a surface [203].

The capillary rise method is based on adhesion [204]. Currently the International Association for the Properties of Water and Steam [205] uses the results of capillary rise experiments for the official estimation of the surface tension of water. The error of most experimental applications of this method are given to be between 0.3 % for 20° C and 1.7 % for 360° C [206].

4.7.2 Experimental Reference

Experimental values for NaCl solutions at different salt concentrations and temperatures are taken from the work of Horibe et al [200]. The surface tension shows a linear dependency from the salt concentration c and the temperature T and can be approximated with the following formula:

$$\gamma_{\text{ref}} = \gamma_0 + A \cdot c(wt\%) + B \cdot (T - T_0).$$

In this formula, the concentration c is expressed in weight percent ($wt\%$), $\gamma_0 = 72.0\,\text{mN/m}$, $T_0 = 298.15\,\text{K}$, $A = 1.7/5.0\,\text{mN/m}$ and $B = (-0.7)/5.0\,\text{mN/(Km)}$. Figure 4.42 illustrates the experimental surface tension for a pure water up to a NaCl concentration of 5 M and a temperature range of 25 to 80 °C.

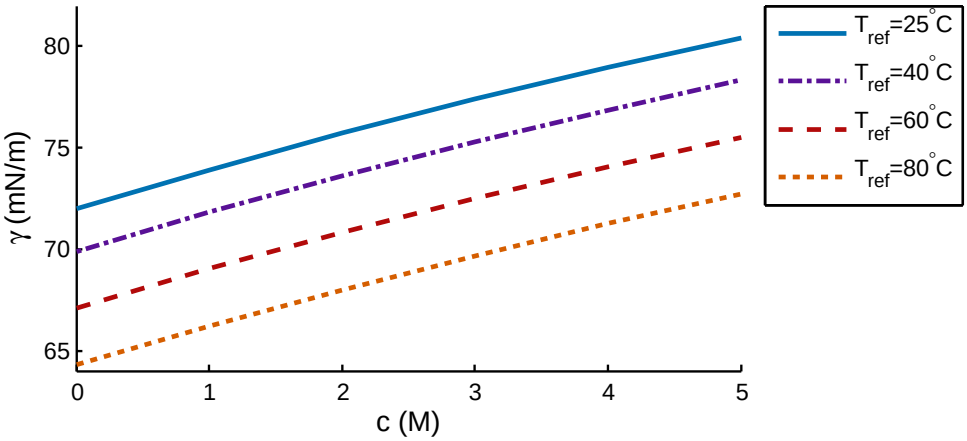

Figure 4.42: Experimental reference values taken from Horibe et al [200] for the surface tensions γ of NaCl salt solutions under variation of temperature T and salt concentration c.

4.7.3 Methods: Simulating Liquid/Vapour Interfaces

Current research on water/vapour interfaces by computer simulations has be controversial [197, 207, 208]. It has been reviewed, that results for the surface tension using the same water model in different studies vary drastically. However, the origin of the deviations is yet unknown. Suggestions are based on a variety of simulation conditions such as Lennard-Jones cutoff distance and simulation time [208], but also implementation of the long-range electrostatic interactions [207] and the algorithm of choice for the bond flexibility [197]. Spohr [209] discussed the influence of electrostatic boundary conditions and spherical truncation methods on interfacial properties.

In addition to difficulties with pure water, the behaviour of ions at the air/brine interfaces is contradictory as well [27, 198].

There are topologically different simulation methods for calculating the surface tension of liquid/air interfaces. The two most common are 1) the droplet method, based on geometric considerations [84] and 2) the slab method, based on calculating the pressure tensor [207].

We measure the surface tension according to method 2) by modelling the liquid in conjunction with a vacuum slab. Due to three-dimensional periodic boundary conditions, the simulation box contains overall two liquid/vapour interfaces. The diagonal components of the pressure tensor P_{ii} and the box length in z direction L_z can be used to calculate the surface tension:

$$\gamma_{lv} = \frac{1}{2} \cdot L_z \cdot \left[\langle P_{zz} \rangle - \frac{1}{2} \langle P_{xx} \rangle - \frac{1}{2} \langle P_{yy} \rangle \right].$$

Note that a division by two is introduced outside the square brackets to account for the simulation setup containing two liquid/vapour interfaces [207].

According to Chen and Smith [197], a long range dispersion correction $\gamma_d = 4.4\,\mathrm{mN/m}$ has to be added to the preliminary result

$$\gamma = \gamma_{lv} + \gamma_d.$$

4.7.4 Performance of the Method

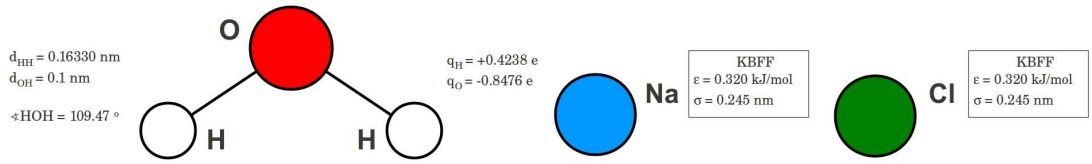

Figure 4.43: Schematic representation of the SPC/E water and KBFF ion model.

Simulation Setup

The simulations are performed with Gromacs 4.5.5 [110]. The tool Packmol [111] is used to create a box of 1024 SPC/E water molecules. The box is prolonged in z-direction by a vacuum slab of roughly 7 nm length, resulting in a box size of $x \times y \times z = 3.1 \times 3.1 \times 10.0\,\mathrm{nm}^3$.

A simulation within the NVT ensemble is performed for 4 ns. For evaluation, the first 400 ps of the simulation are omitted to ensure good equilibration.

For the simulation at 1 M salt concentration, a pre-equilibrated box with 18 KBFF ion pairs and 1024 SPC/E water molecules is used. The box size in z-direction is increased by a factor of 4 to roughly 12 nm and the simulation is run for 80 ns.

The temperature is maintained at 298.15 K.

Periodic boundary conditions are applied in all directions. The cutoff of the Lennard-Jones interactions is taken to be 0.9 nm. The long-range Coulomb interactions are handled by the Particle-Mesh Ewald method [112] with a cutoff of 0.9 nm and a grid spacing of 0.1 nm. The neighbour list for non-bonded interactions is updated every 5th integration step. We use the leap-frog algorithm for integrating Newton's equations of motion with a 0.004 ps time step. All simulations are performed at fixed temperature. Velocity rescaling is used with a temperature coupling constant of 0.1 ps [113]. We store the atomic coordinates of the ions each 4 ps for further analysis.

The Particle-Mesh Ewald method is corrected for slab geometry using the 3dc corrections [210].

Matlab [115] is applied for mathematical operations and plotting.

Results of the Method

The result for pure water is presented in Tab. 4.21. The model underestimates the experimentally measured surface tension, but is in agreement with the literature reference for the same model [197].

In Fig. 4.44 we present the result of a surface tension simulation of a 1 M NaCl salt solution. It is visible, that the surface tension equilibrates quickly in the used setup ($\leq$10 ns for a difference of less than 1 % from the final mean). This fast equilibration behaviour is reflected in the small standard deviation of 2.1 mN/m, which is less than 4 % of the actual result.

The SPC/E model in conjunction with the KBFF ion model clearly exclude the ions from the air/water interface as reported by Chen and Smith [198].

We will not further elaborate on the setup but will proceed with the polarizable model evaluation. The general setup has been thoroughly tested by Mikhail Stukan [3].

Table 4.21: **(25 °C neat SPC/E water)** Simulation results of pure SPC/E water in comparison with results obtained by computer simulation by Chen and Smith [197] and experimental values.

	this work	lit. reference [197]	experiment
γ (mN/m)	62.2 ± 0.6	61.3	72.0

[3] Personal communication.

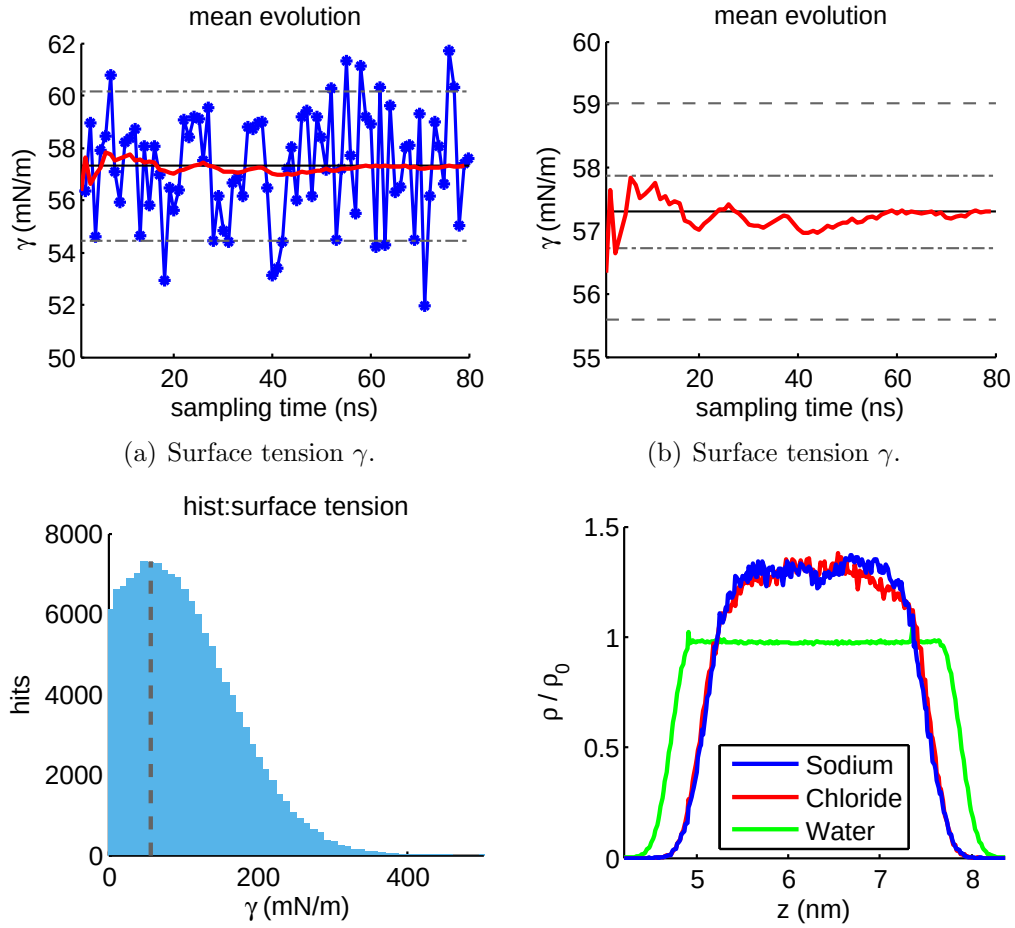

(a) Surface tension γ.

(b) Surface tension γ.

(c) Histogram of γ.

(d) Normalised density ρ/ρ_0.

Figure 4.44: **(1M NaCl SPC/E Solution)** Summary of results obtained from a surface tension calculation. 18 NaCl ion pairs are dissolved in 1024 SPC/E water molecules, resulting in a salt concentration of roughly 1 M. The solution forms a slab of roughly 3 nm width, which is positioned in the centre of a simulation box of over 12 nm length. The corrected surface tension is 61.7 ± 0.5 mN/m. The temperature is 298.15 K. The total duration of the simulation is 80 ns including 1 ns equilibration time. a) Block average of the surface tension with 1 ns sampling time (blue line with asterisks) and running average of the surface tension (red line). The horizontal lines mark the mean surface tension (solid) and a $\pm 5\,\%$ interval around it (grey dashed lines). b) Running average of the surface tension at 1 ns intervals (red line). The horizontal lines mark the mean surface tension (solid), a $\pm 1\,\%$ interval around it (grey dashed-dotted lines) and a $\pm 3\,\%$ interval around it (grey dashed lines). c) Histogram of the surface tension. The vertical dashed line marks the mean surface tension. d) Normalised density distribution of ionic species and water in the box.

4.7.5 Performance of the Polarizable Model

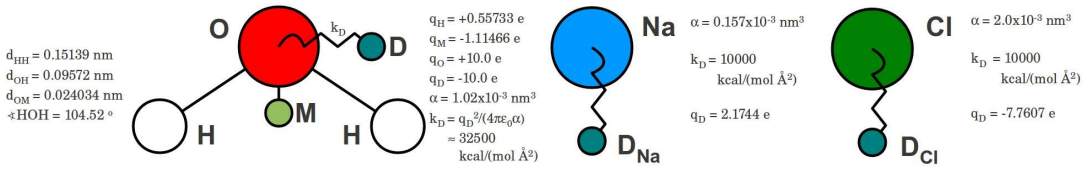

Figure 4.45: Schematic representations of the SW10e water and ion models developed by Lamoureux et al [25] and Yu et al [102], respectively and modified by Mikhail Stukan.

Simulation Setup

The simulations are performed with Gromacs 4.5.5 [110] in double precision.

Neat water A pre-equilibrated box of 1024 SW10e water molecules is prolonged in z-direction by a factor of 5, resulting in a box size of $x \times y \times z = 3.12 \times 3.12 \times 15.58\,\mathrm{nm}^3$ with a vacuum slab of roughly 12.5 nm length.

A simulation within the NVT ensemble is performed for 4 ns. For evaluation, the first 400 ps of the simulation are omitted to ensure good equilibration. The temperature is maintained at 298.15 K.

In addition a pure water box with a variation of the SW10e model with a small Drude charge $q_\mathrm{D} = 1.88\,\mathrm{e}$ is simulated.

Finite salt concentrations For simulations at different salt concentrations and different temperatures the tool Packmol [111] is used to create boxes of 1024 SW10e water molecules including 19, 38, 76 and 94 ion pairs respectively. The ion model with a Drude force constant $k_\mathrm{D} = 10 \cdot 10^3\,\mathrm{kcal}/\left(\mathrm{mol} \cdot \mathrm{Å}^2\right)$ and a polarizability of chloride $\alpha_\mathrm{Cl} = 2.0 \cdot 10^{-3}\mathrm{nm}^3$ is used.

The boxes are equilibrated in the NPT ensemble for 300 ps at 4 different temperatures: 298.15 K, 313.15 K, 333.15 K and 353.15 K. The equilibrated boxes are prolonged in z-direction by a factor of 4, resulting in a vacuum slab of roughly 9 nm length. The simulations are run in the NVT ensemble for 20 ns at 1 M salt concentration and ambient temperature and for 10 ns else.

Periodic boundary conditions are applied in all directions. The cutoff of the Lennard-Jones interactions is taken to be 1.2 nm with shifted potential taken from 1.0 nm. The long-range Coulomb interactions are handled by the Particle-Mesh Ewald method [112] with a cutoff of 1.5 nm and a grid spacing of 0.1 nm. The neighbour list for non-bonded interactions is updated every 10th integration step. We use the leap-frog algorithm for integrating Newton's equations of motion with 0.001 ps time step. All simulations are performed at fixed temperature. Velocity

rescaling is used with a temperature coupling constant of 0.1 ps [113]. We store the atomic coordinates of the ions each 5 ps for further analysis.

The Particle-Mesh Ewald method is corrected for slab geometry using the 3dc corrections [210].

Matlab [115] is applied for mathematical operations and plotting.

Results

Neat water Table 4.22 presents the results of simulated pure water for the polarizable model with a Drude charge of 1.88 e (Low Charge), the SW10e model and the original SW4-NDP model by Lamoureux et al [25]. As visible, the differences between the water models in terms of surface tension of the Low Charge model and the SW10e model are small. All models underestimate the experimental reference of 72.0 mN/m. We note, that Lamoureux et al [25] used the droplet method [84].

Table 4.22: **(25 °C neat SW10e water)** Simulation results of pure SW10e water and a modification with a Drude particle charge of 1.88 e (Low Charge) in comparison with results obtained by computer simulation by Lamoureux et al [25] with the SW4-NDP model and an experimental value, taken from Horibe et al [200]. The temperature is set to 298.15 K.

	Low Charge	SW10e	SW4-NDP [25]	experiment [200]
γ (mN/m)	69.8 ± 0.6	70.4 ± 0.8	67	72.0

Low concentration at ambient temperature Our special interest lies in the performance of our ion and water model at interfaces. Our model with a chloride polarizability of $\alpha_{\mathrm{Cl}} = 2.0 \cdot 10^{-3}\mathrm{nm}^3$ proved capable of reproducing the osmotic pressure. Using this specific model we hope to predict a realistic behaviour of the ions at the solution/air interface and to correctly reproduce experimental values for the surface tension.

Figure 4.46 provides an illustration of the simulation result for a simulation at 1 M salt concentration and ambient temperature. The chosen setup shows fast equilibration behaviour, see Fig. 4.46(a) and 4.46(b), and a small scattering of data points with a standard deviation of $S_{\mathrm{N}} = 1.89$ mN/m. Accordingly, the error estimate of the result of this 20 ns simulation is quite small: $\gamma = 73.2 \pm 0.90$ mN/m ($\leq 1.5\,\%$). The simulated result deviates only 0.7 mN/m from the experimental reference value of 73.9 mN/m [200], which is an exceedingly high agreement. We emphasis, that the model is not tuned to reproduce the surface tension but to reproduce the osmotic pressure!

The ions are well dissolved in the bulk phase of the SW10e water slab and thereby excluded from the water/air interface. This becomes apparent in the density profile of water and ions in the box, see Fig. 4.46(d): the ion density profile declines the same way as water, but the water density profile reaches farther out into the vacuum slab. The covering of the air/water surface by water

molecules only is confirmed by visual analysis of the surface. This behaviour of the ions in the solution is in agreement with the intuitive picture of strongly hydrated ions and with the result of Chen and Smith [198]. The exclusion of the ions from the surface conjures the picture of a brine slab separated from the vacuum slab by an ion-impenetrable water wall. We want to investigate this picture more thoroughly.

As the slope of the density profile of ions and water at the brine/air interface is nearly identical, we can determine the distance between the "outermost" chloride and sodium ions to the solution surface defined by the position of the outermost oxygen atoms. This distance is $d_{\mathrm{ion-surface}} = 2\,\text{Å}$.

We want to compare the $d_{\mathrm{ion-surface}} = 2\,\text{Å}$ distance with the pairing distance $r_{\mathrm{ion-oxygen}}$ of ions and water in bulk: the position of the first maximum in the RDF between sodium and oxygen and chloride and oxygen in bulk is $r_{\mathrm{Na-O}} = 2.4\,\text{Å}$ and $r_{\mathrm{Cl-O}} = 3.2\,\text{Å}$, respectively. See more details about the RDF in Sec. 4.3.

The fact, that the pairing distances $r_{\mathrm{ion-oxygen}}$ of the ions with water are larger than their separation $d_{\mathrm{ion-surface}}$ from the interface contradicts the picture of the ion-impenetrable water wall. A more reasonable explanation would be, that the ions are not excluded from the surface by a layer of water molecules, but by their respective hydration shell. Or in other words, the ions form specific ion-water structures that can reach the solution/air interface without direct ion-air contact.

At 1 M salt concentration and ambient temperature, the influence of the ions on the surface is captured in the increase of the surface tension to 73.2 mN/m compared to the result for pure SW10e water of 70.4 mN/m.

Beside their smaller ion size, the sodium ions are excluded from the surface in the same lengthscale as chloride ions, or even farther away, see again Fig. 4.46(d). This is an interesting fact, as it points to at least one additional mechanism at the surface, possibly a restructuring of the sodium hydration shell.

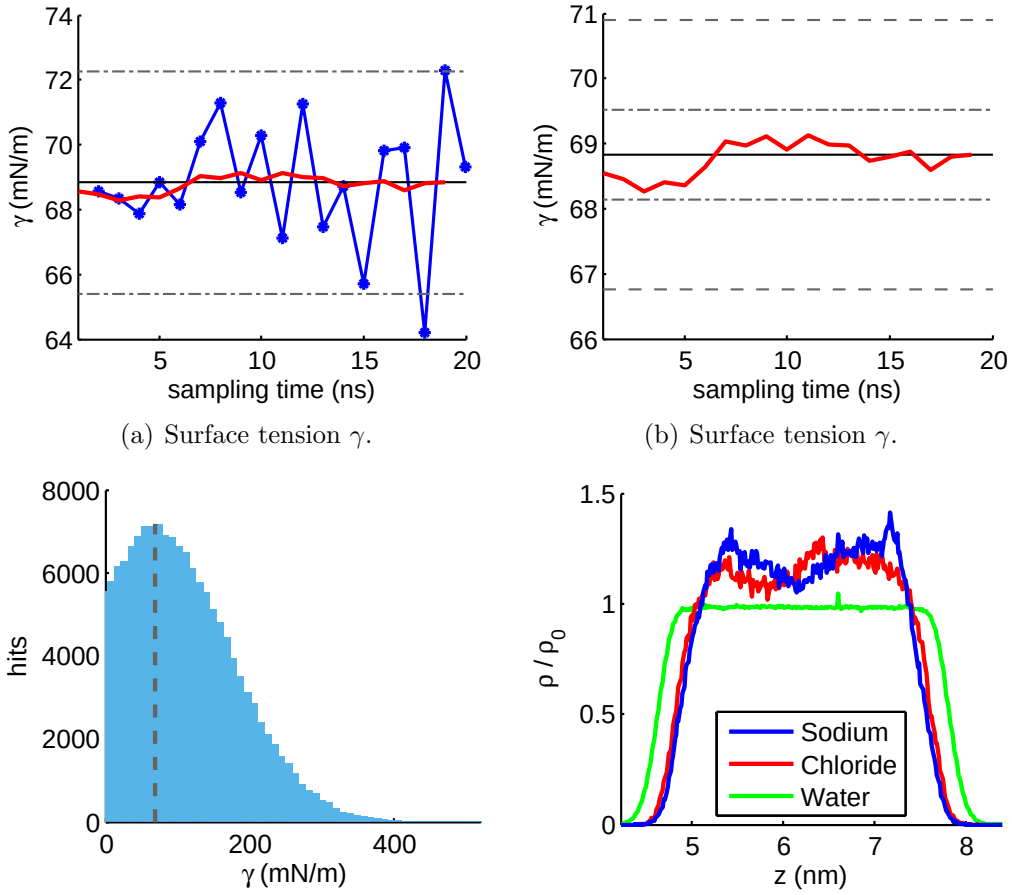

(a) Surface tension γ.

(b) Surface tension γ.

(c) Histogram of γ.

(d) Normalised density ρ/ρ_0.

Figure 4.46: **(1 M 25 °C NaCl SW10e solution)** Summary of results obtained from a surface tension calculation. 19 NaCl ion pairs are dissolved in 1024 SW10e water molecules, resulting in a salt concentration of roughly 1 M. The solution forms a slab of roughly 3 nm width, which is positioned in the centre of a simulation box of over 12 nm length. The corrected surface tension is 73.2 ± 0.90 mN/m. Further results are shown in Tab. 4.24. The temperature is 298.15 K. The total duration of the simulation is 20 ns including 1 ns equilibration time. a) Block average of the surface tension with 1 ns sampling time (blue line with asterisks) and running average of the surface tension (red line). The horizontal lines mark the mean surface tension (solid) and a ±5 % interval around it (grey dashed lines). b) Running average of the surface tension at 1 ns intervals (red line). The horizontal lines mark the mean surface tension (solid), a ±1 % interval around it (grey dashed-dotted lines) and a ±3 % interval around it (grey dashed lines). c) Histogram of the surface tension. The vertical dashed line marks the mean surface tension. d) Normalised density distribution of ionic species and water in the box.

High concentration - high temperature As the simulation with 1 M salt concentration at 298.15 K shows a good performance, we expand our discussion on the behaviour at higher salt concentrations and higher temperatures. Experimental studies indicate an increasing surface tension with increasing salt concentration and decreasing temperature.

The results of simulations at concentrations of roughly 1, 2, 4 and 5 M and 25, 40, 60 and 80 °C are presented in Tab. 4.24 and in the Fig. 4.47. We decreased the simulation time to 10 ns. A different representation of the results is shown in Fig. 4.23.

Among the simulations, there are two to be mentioned separately. First, a simulation at 80 °C and a salt concentration of 3.6 M that crashed. Secondly, a simulation at 1 M salt concentration and 60 °C, which shows an unusual behaviour: the chloride and sodium ions are unevenly distributed in the solution bulk, see Fig. C.3. We exclude these simulations from further discussions.

In general, the experimental concentration and temperature dependency is not reproduced by the model liquid. The increase in surface tension with the concentration is only slightly visible. A dependency from temperature is not visible at all, a trend, that is similarly found for the osmotic pressure.

Table 4.23: **Surface Tension** Summary of surface tensions γ of NaCl salt solutions under variation of temperature T and salt concentration c. Experimental reference values γ_{ref} are taken from Horibe et al [200].

c (M)	γ_{ref} (mN/m)	γ (mN/m)	c (M)	γ_{ref} (mN/m)	γ (mN/m)	c (M)	γ_{ref} (mN/m)	γ (mN/m)	c (M)	γ_{ref} (mN/m)	γ (mN/m)
	$T = 25\,°\text{C}$			$T = 40\,°\text{C}$			$T = 60\,°\text{C}$			$T = 80\,°\text{C}$	
1.0112	73.9	73.2	1.0017	71.8	72.5	0.9855	69.0	90.8	0.9705	66.2	65.8
1.9654	75.6	75.0	1.9468	73.5	71.7	1.9214	70.7	73.6	1.8866	67.8	74.6
3.7188	78.5	77.0	3.6804	76.4	72.2	3.6327	73.5	76.1	3.5753	70.6	—
4.4778	79.7	77.3	4.4392	77.5	73.3	4.3638	74.6	76.7	4.2996	71.7	76.5

Table 4.24: **Surface Tension with Figure Reference and Error Estimation** Summary of surface tensions γ of NaCl salt solutions under variation of temperature T and salt concentration c. Experimental reference values γ_{ref} are taken from Horibe et al [200]. The measured surface tension is given with an error estimate from block average with 95% confidence. S_{N} denotes the standard deviation.

T K	Fig.	c (M)	γ_{ref} (mN/m)	γ (mN/m)	S_{N} (mN/m)
298.15	4.46	1.0112	73.9	73.2 ± 0.90	1.89
313.15	C.2	1.0017	71.8	72.5 ± 1.01	1.45
333.15	C.3	0.9855	69.0	90.8 ± 5.82(‡)	7.89
353.15	C.4	0.9705	66.2	65.8 ± 0.90	1.30
298.15	C.5	1.9654	75.6	75.0 ± 0.90	1.29
313.15	C.6	1.9468	73.5	71.7 ± 0.89	1.28
333.15	C.7	1.9214	70.7	73.6 ± 2.34	3.37
353.15	C.8	1.8866	67.8	74.6 ± 1.11	1.59
298.15	C.9	3.7188	78.5	77.0 ± 1.49	2.14
313.15	C.10	3.6804	76.4	72.2 ± 0.98	1.41
333.15	C.11	3.6327	73.5	76.1 ± 1.66	2.39
353.15	—	3.5753	70.6	— ± —(*)	—
298.15	C.12	4.4778	79.7	77.3 ± 1.43	2.05
313.15	C.13	4.4392	77.5	73.3 ± 1.28	1.84
333.15	C.14	4.3638	74.6	76.7 ± 1.49	2.14
353.15	C.15	4.2996	71.7	76.5 ± 1.23	1.77

(‡) The simulation is not trustworthy.
(*) The simulation crashed.

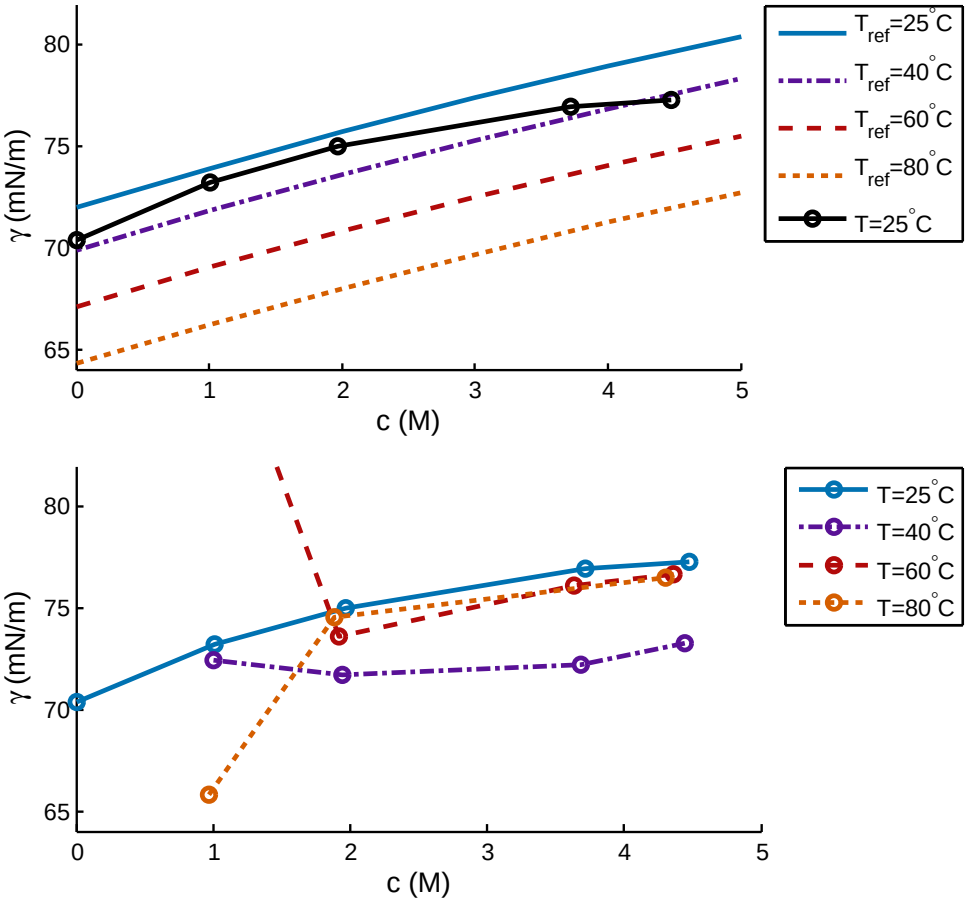

Figure 4.47: **(Overview)** Overview of the surface tensions γ of NaCl salt solutions under variation of temperature T and salt concentration c. Experimental reference values γ_{ref} for temperatures $T_{\text{ref}} = 25\,^{\circ}\text{C}$ to $T_{\text{ref}} = 80\,^{\circ}\text{C}$ are taken from Horibe et al [200].

4.7.6 Conclusion and Outlook

The surface tension is, as the osmotic pressure, an interfacial property. It can be measured experimentally with great precision and over a wide range of ion concentrations. Its importance for characterising interfacial phenomena makes it a valuable property for computational study. Also the behaviour of ions at water/air interfaces has drawn an increasing interest of scientist over the last years [27].

We calculated the surface tension for our polarizable model with $\alpha_{\mathrm{Cl}} = 2.0 \cdot 10^{-3}\mathrm{nm}^3$ at four different salt concentrations and four different temperatures, respectively.

We discussed, that ions are not excluded from the surface by a layer of water molecules, but by their respective hydration shell and that they form specific ion-water structures that can reach the solution/air interface without direct ion-air contact. We point to the surprising fact, that sodium ions are excluded from the surface in the same lengthscale as chloride ions, or even farther away, beside their smaller ion size. This points to at least one additional mechanism at the surface, possibly a restructuring of the sodium hydration shell, and gives a first thread for further research.

The ions have a distinct influence on the surface tension. At 1 M salt concentration, the surface tension is increased in comparison with results of pure water. Beside the good performance at the low concentration of 1 M and beside our efforts to adapt our model to high salt concentrations using the osmotic pressure, the current model is not able to reproduce experimentally shown trends for the surface tension at higher salt concentrations and higher temperatures.

The incapacity of the model at high concentrations and high temperatures emphasises again the need for greater attention of these respective conditions for model development.

Chapter 5

Summarising the Results - the Performance of our Model

We identified the ion model with a Drude force constant

$$k_{\mathrm{D}} = 10 \cdot 10^3 \,\mathrm{kcal}/\left(\mathrm{mol} \cdot \mathrm{\AA}^2\right)$$

and a polarizability of chloride

$$\alpha_{\mathrm{Cl}} = 2.0 \cdot 10^{-3} \mathrm{nm}^3$$

as promising. In this chapter, we will present a summary of properties of neat bulk SW10e water and the performance of the identified sodium-chloride ion model solution in SW10e.

5.1 Neat SW10e Water

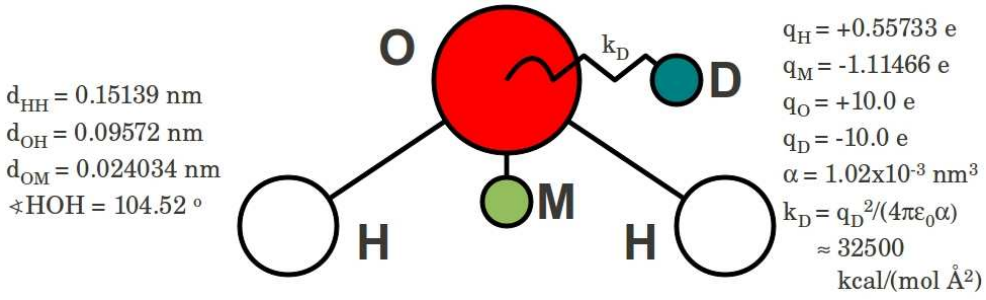

Figure 5.1: Schematic representations of the SW10e water model developed by Lamoureux et al [25] and modified by Mikhail Stukan.

Table 5.1: **Neat SW10e water** Summary of neat SW10e water properties. The diffusivity D is measured and corrected by the method proposed by Yeh and Hummer [211].

quantity	symbol	this work	experiment
density	ρ (kg/m^3)	1001.3	997.1[106]
diffusivity	D (10^{-5}cm^{2}s^{-1})	2.55	2.3 [25]
dielectric constant	ε	77.2	78.5 [212]
surface tension	γ (mN m^{-1})	70.4	72 [25]
hydration enthalpy	ΔH (kJ/mol)	-34.2	-41.5 [25]
hydration free energy	ΔG (kJ/mol)	-34.9	-18.4 to -26.5 [25]
residence time	τ (ps)	2.49	2.0 [144]
RDF	c_n	4.4	
	$r^1_{\max}$ (nm)	0.280	0.2875 [143]
	$r_{\min}$ (nm)	0.334	0.3325 [143]
	$r^2_{\max}$ (nm)	0.446	0.4475 [143]

5.2 Sodium-Chloride SW10e Solution

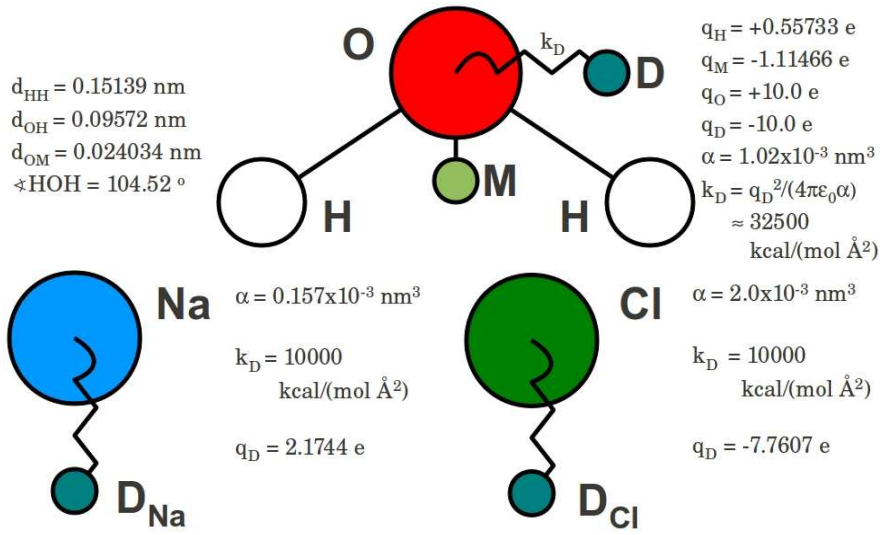

Figure 5.2: Schematic representations of the SW10e water and ion models developed by Lamoureux et al [25] and Yu et al [102], respectively and modified by Mikhail Stukan.

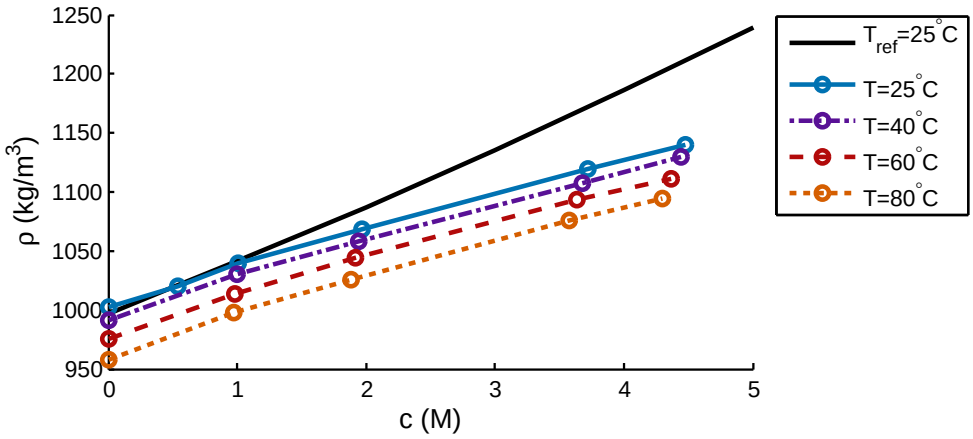

Figure 5.3: **Density** Summary of densities ρ of NaCl salt solutions under variation of temperature T and salt concentration c. Experimental reference values at $T_{\text{ref}} = 25\,\circ$C are taken from Millero et al [106].

Table 5.2: **Density** Summary of densities ρ of NaCl salt solutions under variation of temperature T and salt concentration c. Experimental reference values ρ_{ref} are taken from Millero et al [106].

c (M)	ρ ($\text{kg} \cdot \text{m}^{-3}$)	c (M)	ρ ($\text{kg} \cdot \text{m}^{-3}$)	c (M)	ρ ($\text{kg} \cdot \text{m}^{-3}$)	c (M)	ρ ($\text{kg} \cdot \text{m}^{-3}$)	c (M)	ρ_{ref} ($\text{kg} \cdot \text{m}^{-3}$)	ρ_{ref} ($\text{kg} \cdot \text{m}^{-3}$)
$T = 25\,°\text{C}$		$T = 40\,°\text{C}$		$T = 60\,°\text{C}$		$T = 80\,°\text{C}$		$T = 25\,°\text{C}$		$T = 80\,°\text{C}$
0.0	1002.50	0.0	991.22	0.0	975.68	0.0	957.81	0.0	997.075	971.722
0.5362	1019.70	—	—	—	—	—	—	0.5	1019.009	993.763
1.0112	1040.09	1.0017	1030.32	0.9855	1013.58	0.9705	998.194	1.0	1041.218	1015.564
1.9654	1068.18	1.9468	1058.09	1.9214	1044.25	1.8866	1025.38	2.0	1087.105	1059.696
3.7188	1119.24	3.6804	1107.67	3.6327	1093.32	3.5753	1076.03	4.0	1185.938	1152.357
4.4778	1139.71	4.4392	1129.90	4.3638	1110.70	4.2996	1094.36	5.0	1239.188	1201.478

Table 5.3: **Energetic properties** The de-hydration free energy $-\Delta G_{\text{hyd}}$ and the de-hydration enthalpy $-\Delta H_{\text{hyd}}$ for sodium and chloride and a sodium-Chlorde ion pair in SW10e water, respectively.

	$-\Delta G_{\text{hyd}}$ (kcal/mol)	
	this work	experiment [128]
Na	64.4	88.7
Cl	69.2	89.1

	$-\Delta H_{\text{hyd}}$ (kcal/mol)	
	this work	experiment [123]
Na-Cl	186.1	187

Table 5.4: **Dynamic properties** Residence times τ of water molecules around sodium and chloride ions and diffusivity D of sodium and chloride ions at a salt concentration of 0.5 M. The experimental reference values for the diffusivity D_{ref} are taken from Yu et al [102]. The residence time τ is measured by tracking the stay times of water molecules and fit them to an exponential decay. The diffusivity D is measured and corrected by the method proposed by Yeh and Hummer [211].

	τ	D	D_{ref}
	(ps)	($10^{-5}\,\text{cm}^2 \cdot \text{s}^{-}1$)	
Na	20.0	1.02	1.33
Cl	20.0	2.30	2.03

Table 5.5: **Structural properties** Characteristic values of the hydration shell of sodium and chloride and of sodium around chloride. Presented are the cumulative numbers c_n, positions of the first maximum $r^1_{\max}$ and positions of the first minimum $r_{\min}$ of the indicated RDFs in conjunction with experimental values taken from Patra and Karttunen [44]. For the sodium-chloride RDF no experimental data with reasonable accuracy is available.

pair	symbol	this work	experiment
Cl-O	c_n	7.0	
	$r^1_{\max}$	0.320	0.30-0.32
	$r_{\min}$	0.386	0.375-0.440
Na-O	c_n	5.5	
	$r^1_{\max}$	0.236	0.23-0.24
	$r_{\min}$	0.316	0.305-0.340
Na-Cl	c_n	0.07	
	$r^1_{\max}$	0.272	—
	$r_{\min}$	0.364	—

Table 5.6: **Osmotic pressure** Summary of osmotic pressure Π simulation results under variation of temperature T and salt concentration c. For a visualisation of the equilibration behaviour and the concentration profile, see the respective figures indicated in the second column.

T (K)	Fig.	c (M)	Π_{ref} (bar)	Π_{measured} (bar)
298.15	B.43	0.493	22.5	26.5 ± 4.6
298.15	B.44	0.995	46.18	48.23 ± 4.0
298.15	B.45	1.994	97.21	95.36 ± 5.9
298.15	B.46	3.025	157.0	165.27 ± 11.4
298.15	B.47	4.047	224.6	214.2 ± 9.6
313.15	B.48	4.029	234.6	225.0 ± 9.6
333.15	B.49	4.049	251.2	217.6 ± 9.5
353.15	B.50	4.072	268.1	211.8 ± 6.4
298.15	B.51	5.097	302.9	249.7 ± 12.8
313.15	B.52	5.072	316.1	265.8 ± 15.2
333.15	B.53	5.100	338.8	257.0 ± 10.3
353.15	B.54	5.093	358.4	259.5 ± 9.3
298.15	B.55	8.493	—	272.3 ± 18.9

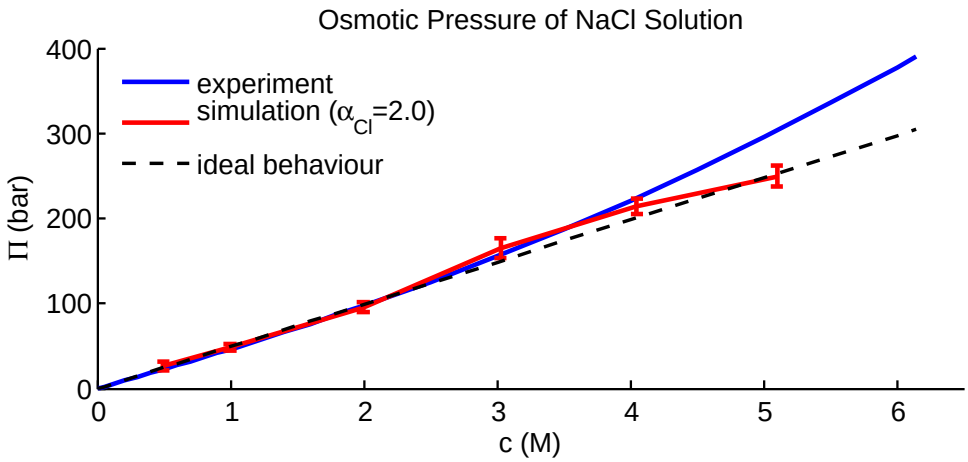

Figure 5.4: **Osmotic pressure** Overview of the results of osmotic pressure calculations (red line with error-bars). The blue line shows experimental reference values supplied by Hamer and Yung-Chi [189]. The black dashed line shows the concentration dependency of the osmotic pressure for an ideal solution according to the Van't Hoff equation.

Table 5.7: **Surface Tension** Summary of surface tensions γ of NaCl salt solutions under variation of temperature T and salt concentration c. For a visualisation of the equilibration behaviour and the concentration profile, see the respective figures indicated in the second column.

T K	Fig.	c (M)	γ_{ref} (mN/m)	γ (mN/m)	S_{N} (mN/m)
298.15	4.46	1.0112	73.9	73.2 ± 0.90	1.89
313.15	C.2	1.0017	71.8	72.5 ± 1.01	1.45
333.15	C.3	0.9855	69.0	90.8 ± 5.82(‡)	7.89
353.15	C.4	0.9705	66.2	65.8 ± 0.90	1.30
298.15	C.5	1.9654	75.6	75.0 ± 0.90	1.29
313.15	C.6	1.9468	73.5	71.7 ± 0.89	1.28
333.15	C.7	1.9214	70.7	73.6 ± 2.34	3.37
353.15	C.8	1.8866	67.8	74.6 ± 1.11	1.59
298.15	C.9	3.7188	78.5	77.0 ± 1.49	2.14
313.15	C.10	3.6804	76.4	72.2 ± 0.98	1.41
333.15	C.11	3.6327	73.5	76.1 ± 1.66	2.39
353.15	—	3.5753	70.6	— ± —(*)	—
298.15	C.12	4.4778	79.7	77.3 ± 1.43	2.05
313.15	C.13	4.4392	77.5	73.3 ± 1.28	1.84
333.15	C.14	4.3638	74.6	76.7 ± 1.49	2.14
353.15	C.15	4.2996	71.7	76.5 ± 1.23	1.77

(‡) The simulation is not trustworthy.
(*) The simulation crashed.

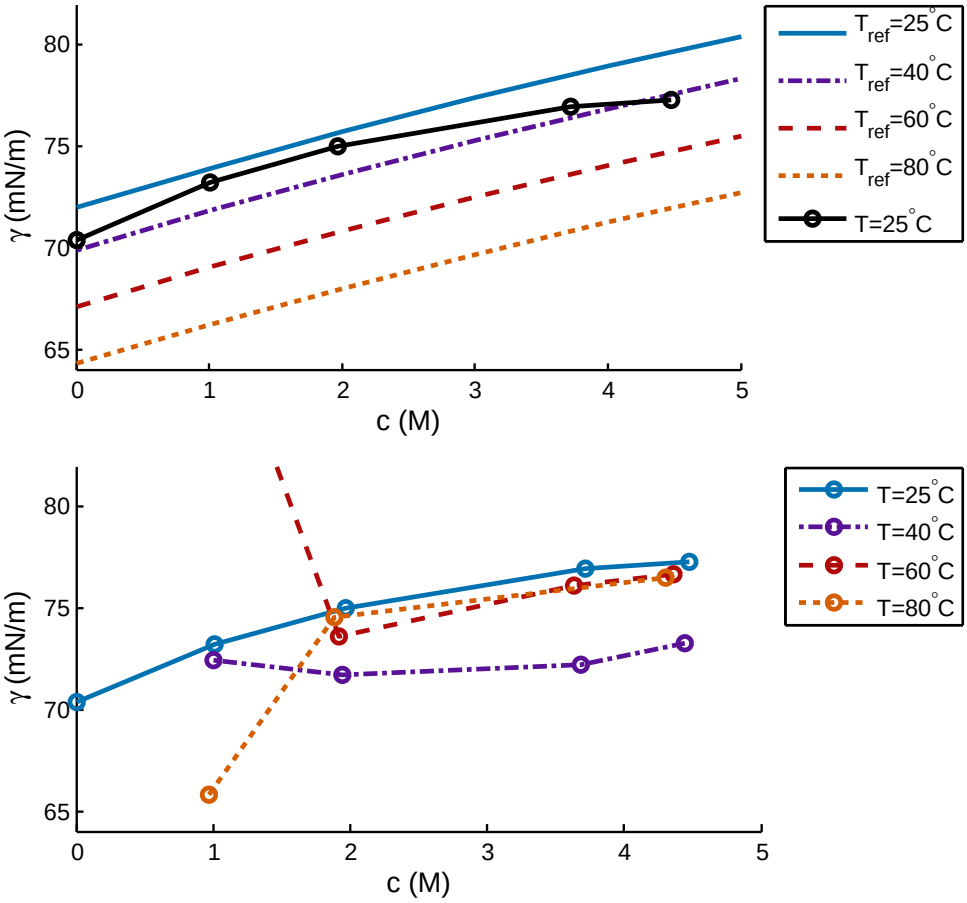

Figure 5.5: **(Overview)** Overview of the surface tensions γ of NaCl salt solutions under variation of temperature T and salt concentration c. Experimental reference values γ_{ref} for temperatures $T_{\text{ref}} = 25\,^{\circ}\text{C}$ to $T_{\text{ref}} = 80\,^{\circ}\text{C}$ are taken from Horibe et al [200].

Chapter 6

Conclusion and Outlook

Water and ions at an interface are characterised by a distortion of their original boundary formed by the solution. Especially the inclusion of polarization effects in the water-ion models is considered as a useful approach in modelling their interfaces [18, 24].

Polarizable force fields are the state of the art in computational molecular science. The SWM4-NDP created by Lamoureux et al [25] in conjunction with the ion force field developed by Yu et al [26] is the most recent. A number of recent publications [27, 28, 12, 29, 30] shows its great success.

Our goal is the further development of water and ion models to predict interfacial properties of brines. We have a special interest in solutions at high ion concentrations and the osmotic pressure as means to identify a good set of force field parameter. However, we found an essential gap in the development and improvement of computational models: *Criteria for the quality of computational models are not well defined.*

We critically discussed several physical quantities that might solve as criteria for force field evaluation of water and ions. The cheap and well characterised SPC/E water model with classical ion models proved useful for this task. The gathered knowledge is put to use on a polarizable water and ion model. In a novel approach, we used the polarizability as a variable to adjust the force field to reproduce the experimental osmotic pressure at high ion concentration. We developed an ion and water model with correct solution behaviour over a wide range of ion concentrations.

The results of our work will be presented below divided into the methodological conclusions concerning force field development and physical conclusions concerning the performance of the polarizable force field. In addition, we discuss a selection of possible extensions to the work.

6.1 Methodological Conclusion: Criteria for Evaluating Computational Water and Ion Models

We want to close the gap between model characterisation and model development by a critical discussions of the meaningfulness, experimental measurability and the measurability by computer simulation. The main conclusions are presented for the quantities investigated in this work.

The Macroscopic Density The density can be measured experimentally with great accuracy and confidence. The same is true for simulations. Therefore the quick estimation of the density provides a valuable tool for testing the simulation setup and force field before expanding the computational effort for the analysis of more sophisticated quantities.

Energetic Properties of Solvation The quantification of the hydration process in terms of energetic properties might provide physical insights. However, experimental references are based on strong assumptions, that influence the resulting values. Large deviations between reported values for the hydration free energies of ions are found [40]. Thus a comparison of experimental references and simulated quantities is difficult.

However, very accurate methods for calculating the hydration free energy have been developed in the past years. We tested the thermodynamic integration with the Bennetts Acceptance Ratio evaluation method. Although the comparison with experimental references might not be reasonable, discussions of the influence of model parameter or different models on solvation properties are promising. The determination of energetic properties is still a useful way for describing and characterising the solution model under study.

Structural Properties - Radial Distribution Functions We present a method for sampling RDFs using bulk simulations of water molecules and ions. Whereas the method is cheap and straightforward, it exhibits difficulties in sampling the ion-ion RDFs. This problem becomes more pronounced at low ion concentrations and at ion-ion distances of low probability.

To benchmark ion and water models on the real world, ion-ion RDFs are of minor interest, as they are not measurable by experiments. In terms of peak position, water-ion RDFs can be measured experimentally with good accuracy

and show good agreement with simulated results. We improved the computational performance by simulating at a finite concentration and confirmed the validity of our results, by crosschecking with results obtained at the diluted concentration limit.

Residence Time The residence time is a promising quantity in revealing dynamic properties of ion solvation and ion interaction with interfaces [144, 145, 146, 147, 43, 148]. In our opinion, the residence time is underutilised in modern computational science. The method of determining the residence time needs rigorous investigation before it can be used.

Potential of Mean Force The full form of the PMF is experimentally not accessible, however features of the PMF curve like the difference between maxima and minima might be associated with experimentally measurable energies. Still, from a molecular point of view it provides a useful tool to characterise intermolecular interaction.

Using advanced sampling techniques based on the Bennetts Acceptance Ratio, the PMF between infinitely diluted ions can be obtained with high accuracy. At finite salt concentration, three different methods for calculating the PMF are investigated:

(a) explicit calculation using the biased potential method,

(b) scaling of the PMF at infinite dilution and

(c) Boltzmann inversion of the RDF.

Method (a) and (b) *depend on strong assumptions* which lead to a wrong offset of the PMF for method (a) and a wrong offset and form of the PMF for method (b). The Boltzmann inversion (c) proved to be the most robust method, but lacks the high accuracy of method (a).

Osmotic Pressure The osmotic pressure can be measured experimentally with very high precision. As the osmotic pressure strongly depends on the ion-ion and ion-water interaction and can be measured at very high ion concentration, the quantity proved to be a valuable benchmark for force field development.

We put the membrane method for determining the osmotic pressure of aqueous solutions to a careful methodological investigation. Special emphasis was set to the calculation of the ion concentration inside the ion domain with anisotropic periodic boundary conditions, an issue often neglected in scientific literature.

The membrane method proved to be a robust and straightforward method. The membrane method is applicable without further assumptions or corrections to the full range of ion concentrations, from high degree of dilution to the solubility limit. As our main aim is to describe the behaviour of solutions at high concentrations, the applicability at high ion concentrations is emphasised. For our aims, the advantages outweight the relatively high computational costs.

Surface Tension The surface tension is, as the osmotic pressure, an interfacial property. It can be measured experimentally with great precision and over a wide range of ion concentrations. Its importance for characterising interfacial phenomena makes it a valuable property for computational study. Also the behaviour of ions at water/air interfaces has drawn an increasing interest of scientist over the last years [27].

Upon simulating liquid/vapour interfaces by computer simulations, current research on pure water with different molecular models has been controversial [197, 207, 208]. By avoiding unfeasible setups, we are able to calculate reproducible surface tensions of neat water and ion solutions.

6.2 Physical Conclusion: Reproduction of Macroscopic Phenomena of Brines

We aim to **develop a new brine model** of water and sodium-chloride. As starting point, we used the water and ion model originally developed by Lamoureux et al [25] and Yu et al [102], which was modified by Mikhail Stukan. The so-called SW10e water model is a rigid five-point water model using a Drude oscillator [104] to introduce polarizability to the model. The polarizability of the ions is realised in the same way.

By **using the polarizability as variable** we apply an unique approach for tuning the model to reproduce important physical properties. We started with a small range of polarizabilities of $\alpha_{\mathrm{Cl}} = 3.5 \cdot 10^{-3}\mathrm{nm}^3$ to $\alpha_{\mathrm{Cl}} = 4.0 \cdot 10^{-3}\mathrm{nm}^3$ and extended it to $\alpha_{\mathrm{Cl}} = 2.0 \cdot 10^{-3}\mathrm{nm}^3$. The study is supported by an investigation on possible influences of the Drude force constant k.

Whereas the the Drude force constant has only minor influence, *the variation of the ion polarizability proved to be a suitable tool* for tuning model parameter and the model with $\alpha_{\mathrm{Cl}} = 2.0 \cdot 10^{-3}\mathrm{nm}^3$ is able to reproduce experimental values over a large range of concentrations.

The following results have been obtained for the physical properties under study:

Bulk Properties

(A) The **density** of pure SW10e water and of diluted NaCl solutions are in good agreement with experimental data. At higher salt concentrations, the density is exceeded by the experimental reference values. This points to a weakened ion hydration at higher ion concentration.

(B) We calculated the **hydration enthalpy** of ions for different parameter and ion concentrations. All measured values lie in the range of experimental references. An increasing polarizability of chloride does slightly increase the solvation enthalpy. Results for the hydration free energy of sodium and chloride underestimate the free energy by 20 kcal/mol. As the discrepancy between calculated and experimental values is notable, we discussed possible reasons in the respective chapter.

(C) Structural properties of polarizable ions in SW10e water were investigated using **radial distribution functions**. The peak positions are in range of experimental data for all parameter tested. Whereas the polarizability of chloride has a minor influence on the chloride-water interaction, it plays a dominant role in the sodium-chloride coupling: while increasing the polarizability from $\alpha_{\mathrm{Cl}} = 3.5$ to $\alpha_{\mathrm{Cl}} = 4.0 \cdot 10^{-3}\,\mathrm{nm}^3$ the **coordination number** increases by a factor of 2(!), thereby replacing water molecules in the proximity of chloride by sodium ions.

(D) We are able to provide the SW10e water-water **residence time** of 2.5 ps, which is consistent with literature values [144]. The ion-water residence times are estimated with 20 ps with a deviation of 10 ps between independent simulations. We suggest further research on the method to give a physical interpretation of our model performance.

(E) For simple non-polarizable water models, the calculation of the **potential of mean force (PMF)** is doable with reasonable computer time. However, the inclusion of polarization effects in the model force field increases drastically the computational costs. Therefore, results for the polarizable model are not produced. Optimisation of the simulation routine or more computational power might provide us in the future with the possibility to calculate the PMF for polarizable ions.

Former model development concentrated on bulk properties of water and ion models at low concentrations. In contrast to that, we want to follow the *trend in recent publications in emphasising surface effects of high concentration solutions* [40, 41, 42, 30].

Interfacial Properties

(F) We calculated the **osmotic pressure** for the polarizable SW10e water model and polarizable ion models in a wide range of ion concentrations, polarizabilities and temperatures. The variation of the ion polarizability proved to be a suitable variable to reproduce experimental values of the osmotic pressure. The apparent underestimation of the osmotic pressure at high ion concentrations can be counteracted by a decrease of the polarizability. The maximum effect is anticipated to be at or close to $\alpha_{\mathrm{Cl}} = 2.0 \cdot 10^{-3}\mathrm{nm}^3$.

Finally, *the goal of reproducing the osmotic pressure over the whole range of concentrations is achieved*. The new model proved a good performance for an interface property far away from the dilution limit.

The experimental temperature behaviour is not reproduced by our model. Some possible reasons are discussed but will be further investigated in a future work.

(G) We calculated the **surface tension** for our polarizable model with $\alpha_{\mathrm{Cl}} = 2.0 \cdot 10^{-3}\mathrm{nm}^3$ at four different salt concentrations and four different temperatures, respectively.

We discussed, that ions are not excluded from the surface by a layer of water molecules, but by their respective hydration shell and that they form specific ion-water structures that can reach the solution/air interface without direct ion-air contact. We point to the surprising fact, that sodium ions are excluded from the surface in the same length scale as chloride ions, or even farther away, beside their smaller ion size. This points to at least one additional mechanism at the surface, possibly a restructuring of the sodium hydration shell, and gives a first thread for further research.

The *ions have a distinct influence on the surface tension*. Beside the good performance at low concentrations of 1 M and beside our efforts to adapt our model to high salt concentrations using the osmotic pressure, the current model is not able to reproduce experimentally shown trends at higher salt concentrations and higher temperatures.

At ambient temperature, pressure and physiological salt concentrations, the developed water model behaves well. The incapacity of the model at high concentrations and high temperatures emphasises again the need for greater attention of these respective conditions for model development.

6.3 Outlook

This work is not exhausting. The fruitfulness of the topic under study – ions in aqueous solutions – occupies scientists since decades [84]. In this section, we want to discuss some possible threads for the expansion and continuation of the presented study.

Obviously, the chloride-water and the chloride-sodium interactions play a complex role in influencing macroscopic interfacial properties as the surface tension and the osmotic pressure but also bulk properties as the density. The task of model tuning becomes even more difficult upon introducing different salt concentrations and upon varying the temperature.

This outlook is organised following two separate questions:

(1) Which scientific problems have been revealed upon studying physical properties of our brine model?

(2) The dynamics and energetic properties of the hydration shell: A gateway for understanding and solving the problems revealed in (1)?

(1) Which scientific problems have been revealed upon studying physical properties of a brine model?

Osmotic Pressure Our preferred brine model reproduces experimental osmotic pressure values over a wide range of salt concentrations, but at the highest concentration under study (5.1 M) the experimental osmotic pressure surpasses the simulated value. At this concentration, we suspect the model to be near or at the solubility limit but we were not yet able to reliably determine the reason for the drop.

Upon heating, the osmotic pressure should increase linear with temperature but the temperature dependency is not reproduced in the osmotic pressure calculations for our model.

Surface Tension In our model, ions have a noteworthy influence on the surface tension. At 1 M salt concentration, the surface tension is increased in comparison with results of pure water. Beside the good performance at the low concentration of 1 M and beside our efforts to adapt our model to high salt concentrations using the osmotic pressure, the current model is not able to reproduce experimentally shown trends for the surface tension at higher salt concentrations and higher temperatures.

Density Upon heating, the density decreases stronger than anticipated by experiment and at higher salt concentrations, the density is more and more exceeded by the experimental reference values. These effects point to 1) a weakened ion hydration at higher ion concentration with a too large ion-ion interaction energy and 2) a too small water-water interaction energy.

(2) The dynamics and energetic properties of the hydration shell: A gateway for understanding and solving the problems revealed in (1)?

We assume that the structure and dynamics of the hydration shell are of major importance for the interfacial but also bulk properties of brine solutions. Mechanisms of hydration shell formation, strength of ion-water interaction, exchange rates for water molecules and diffusion are coupled [213]. By future work on energetic properties like the *Samoilov Energy* and dynamic properties like the *Residence Time*, we hope to gain a better understanding of underlying mechanisms of ion hydration. Moreover, investigating the performance of several models with different polarizabilities for these physical properties might lead to improved brine models and help us to understand the manifold effects caused by the polarizability.

Residence Time To our opinion, the residence time is underutilised in modern computational science. The determination of the quantity revealed two possible mechanisms of water-water neighbour interaction: a fast and a slow one. It would be interesting to further investigate on these two processes.

The computational data is not sufficient to determine the ion-water and ion-ion residence time. A careful study of the polarizable models would include the calculation of the residence time of water around water or ions and of ions around ions at different concentrations (especially at the precipitation limit), temperatures and in different geometries, e.g. in bulk and in slabs. The influence of the polarizability on the ion-ion residence time would be of major interest.

As anticipated, there are numerous variables in the evaluation of the residence time. Further research on the method might increase the acceptance of the quantity in the scientific community.

Samoilov Energy In 1957, Samoilov [173] developed a theory to calculate the activation energy $\Delta E_{\text{Samoilov}}$ of water molecules in the hydration shell of ions

in bulk. Samoilov used experimental data of self-diffusion and the temperature coefficients of the ion mobilities in solutions.

The activation energy $\Delta E_{\text{Samoilov}}$ of water around ions and of ions around ions is accessible to computational scientists by means of calculating the PMF [174]. In this way, principally, many dynamic properties of ions and water can be calculated using the reverse path of Samoilov, as done by Fedorov et al [62].

6.4 Final Words

Our aim in the work was twofold: to start a critical discussion on force field development and the development and characterisation of a new water and ion force field. We tried to provoke in the reader the need to question his methods and to provide useful information and suggestions. We want to emphasise the hope, that the osmotic pressure as means to benchmark new ion and water models will play an increasing role in further studies.

The newly presented SW10e model in conjunction with the parametrised ion models is promising. Naturally, it is the wish of every scientist, that his model proves useful in future works and that further investigations confirm the good performance of the model or lead to better ones.

Bibliography

[1] K. Kirchner and M. Fedorov. NaRIBaS: A scripting framework for computational modelling of Nanomaterials and Room Temperature Ionic Liquids in Bulk and Slab. sourceforge.net/projects/naribas/, 2013.

[2] B. Corry. Designing carbon nanotube membranes for efficient water desalination. *Journal of Physical Chemistry B*, 112(5):1427–1434, February 2008.

[3] J. Cotruvo, N. Voutchkov, J. Fawell, P. Payment, D. Cunliffe, and S. Lattemann. Desalination: Technology, Health and Environment. In *Encyclopedia of Life Support Systems (EOLSS)*, chapter Water and Wastewater Treatment Technologies. Eolss Publishers, Oxford ,UK, 2011.

[4] Encyclopedia of Desalination and Water Resources.

[5] A. Achilli, T. Y. Cath, and A. E. Childress. Power generation with pressure retarded osmosis: An experimental and theoretical investigation. *Journal of Membrane Science*, 343(1-2):42–52, November 2009.

[6] W. A. Phillip, J. S. Yong, and M. Elimelech. Reverse Draw Solute Permeation in Forward Osmosis: Modeling and Experiments. *Environmental Science & Technology*, 44(13):5170–5176, July 2010.

[7] R. E. Terry. Enhanced Oil Recovery. In R. A. Meyers, editor, *Encyclopedia of Physical Science and Technology*, volume 18. Academic Press, 3 edition, 2001.

[8] F. G. Moore and G. L. Richmond. Integration or segregation: How do molecules behave at oil/water interfaces? *Accounts of Chemical Research*, 41(6):739–748, June 2008.

[9] D. Chandler. Interfaces and the driving force of hydrophobic assembly. *Nature*, 437(7059):640–647, September 2005.

[10] C. L. McFearin, D. K. Beaman, F. G. Moore, and G. L. Richmond. From Franklin to Today: Toward a Molecular Level Understanding of Bonding and Adsorption at the Oil-Water Interface. *Journal of Physical Chemistry C*, 113(4):1171–1188, January 2009.

[11] A. Warshel, P. K. Sharma, M. Kato, and W. W. Parson. Modeling electrostatic effects in proteins. *Biochimica et Biophysica Acta-Proteins and Proteomics*, 1764(11):1647–1676, November 2006.

[12] I. Vorobyov and T. W. Allen. The electrostatics of solvent and membrane interfaces and the role of electronic polarizability. *Journal of Chemical Physics*, 132(18):185101, May 2010.

[13] A. A. Chialvo and J. M. Simonson. Aqueous Na+Cl- pair association from liquidlike to steamlike densities along near-critical isotherms. *Journal of Chemical Physics*, 118(17):7921–7929, May 2003.

[14] G. C. Schatz. Using theory and computation to model nanoscale properties. *Proceedings of the National Academy of Sciences of the United States of America*, 104(17):6885–6892, April 2007.

[15] W. F. van Gunsteren, D. Bakowies, R. Baron, I. Chandrasekhar, M. Christen, X. Daura, P. Gee, D. P. Geerke, A. Glättli, P. H. Hünenberger, M. A. Kastenholz, C. Oostenbrink, M. Schenk, D. Trzesniak, N. F. A. van der Vegt, and H. B. Yu. Biomolecular modelling: Goals, problems, perspectives. *Angewandte Chemie International Edition*, 45:4064–4092, 2006.

[16] S. Aparicio, R. Alcalde, M. J. Davila, B. Garcia, and J. M. Leal. Measurements and predictive models for the N-methyl-2-pyrrolidone/water/methanol system. *Journal of Physical Chemistry B*, 112(36):11361–11373, September 2008.

[17] V. Mile, L. Pusztai, H. Dominguez, and O. Pizio. Understanding the Structure of Aqueous Cesium Chloride Solutions by Combining Diffraction Experiments, Molecular Dynamics Simulations, and Reverse Monte Carlo Modeling. *Journal of Physical Chemistry B*, 113(31):10760–10769, August 2009.

[18] J. Noah-Vanhoucke and P. L. Geissler. On the fluctuations that drive small ions toward, and away from, interfaces between polar liquids and their vapors. *Proceedings of the National Academy of Sciences of the United States of America*, 106(36):15125–15130, September 2009.

[19] T. Y. Yan, C. J. Burnham, M. G. Del Popolo, and G. A. Voth. Molecular dynamics simulation of ionic liquids: The effect of electronic polarizability. *Journal of Physical Chemistry B*, 108(32):11877–11881, August 2004.

[20] P. Cieplak, F. Y. Dupradeau, Y. Duan, and J. M. Wang. Polarization effects in molecular mechanical force fields. *Journal of Physics-condensed Matter*, 21(33):333102, August 2009.

[21] O. Borodin. Polarizable Force Field Development and Molecular Dynamics Simulations of Ionic Liquids. *Journal of Physical Chemistry B*, 113(33):11463–11478, August 2009.

[22] T. Y. Yan, Y. T. Wang, and C. Knox. On the Structure of Ionic Liquids: Comparisons between Electronically Polarizable and Nonpolarizable Models I. *Journal of Physical Chemistry B*, 114(20):6905–6921, May 2010.

[23] O. N. Starovoytov, O. Borodin, D. Bedrov, and G. D. Smith. Development of a Polarizable Force Field for Molecular Dynamics Simulations of Poly (Ethylene Oxide) in Aqueous Solution. *Journal of Chemical Theory and Computation*, 7(6):1902–1915, June 2011.

[24] B. W. Ninham, T. T. Duignan, and D. F. Parsons. Approaches to hydration, old and new: Insights through Hofmeister effects. *Current Opinion in Colloid & Interface Science*, 16(6):612–617, 2011.

[25] G. Lamoureux, E. Harder, I. V. Vorobyov, B. Roux, and A. D. MacKerell. A polarizable model of water for molecular dynamics simulations of biomolecules. *Chemical Physics Letters*, 418(1-3):245–249, January 2006.

[26] H. Yu and S. W. Rick. Free Energy, Entropy, and Enthalpy of a Water Molecule in Various Protein Environments. *Journal of Physical Chemistry B*, 114(35):11552–11560, 2010.

[27] C. Caleman, J. S. Hub, P. J. van Maaren, and D. van der Spoel. Atomistic simulation of ion solvation in water explains surface preference of halides. *Proceedings of the National Academy of Sciences of the United States of America*, 108(17):6838–6842, April 2011.

[28] D. E. Jiang, D. Meng, and J. Z. Wu. Density functional theory for differential capacitance of planar electric double layers in ionic liquids. *Chemical Physics Letters*, 504(4-6):153–158, March 2011.

[29] O. Gereben and L. Pusztai. On the accurate calculation of the dielectric constant and the diffusion coefficient from molecular dynamics simulations: the case of SPC/E water. Research Institute for Solid State Physics and Optics, Hungarian Academy of Sciences.

[30] Y. Luo, W. Jiang, H. Yu, A. D. MacKerell, and B. Roux. Simulation study of ion pairing in concentrated aqueous salt solutions with a polarizable force field. *Faraday Discussions*, 160:135–149, 2013.

[31] W. F. van Gunsteren and H. J. C. Berendsen. Computer-simulation of Molecular-dynamics - Methodology, Applications, and Perspectives In Chemistry. *Angewandte Chemie-international Edition in English*, 29(9):992–1023, September 1990.

[32] M. C. Stumpe, N. Blinov, D. Wishart, A. Kovalenko, and V. S. Pande. Calculation of Local Water Densities in Biological Systems: A Comparison of Molecular Dynamics Simulations and the 3D-RISM-KH Molecular Theory of Solvation. *Journal of Physical Chemistry B*, 115(2):319–328, January 2011.

[33] L. S. Ornstein and F. Zernike. Acculental deviations of density and opalescence at the critical point of a simple substance. *Proceedings of the Koninklijke Akademie Van Wetenschappen Te Amsterdam*, 17:793–806, 1914.

[34] D. Chandler and H. C. Andersen. Optimized cluster expansions for classical fluids. 2. Theory of molecular liquids. *Journal of Chemical Physics*, 57(5):1930–1937, 1972.

[35] C. M. Cortis, P. J. Rossky, and R. A. Friesner. A three-dimensional reduction of the Ornstein-Zernicke equation for molecular liquids. *Journal of Chemical Physics*, 107:6400–6414, 1997.

[36] V. P. Sergiievskyi, W. Hackbusch, and M. V. Fedorov. Multigrid Solver for the Reference Interaction Site Model of Molecular Liquids Theory. *Journal of Computational Chemistry*, 32(9):1982–1992, 2011.

[37] V. P. Sergiievskyi and M. V. Fedorov. 3DRISM Multigrid Algorithm for Fast Solvation Free Energy Calculations. *Journal of Chemical Theory and Computation*, 8(6):2062–2070, June 2012.

[38] R. A. Kuharski and D. Chandler. Solvation of Multiply Charged Ions - Predictions Using the Reference Interaction Site Method With Hypernetted Chain Closure. *Journal of Physical Chemistry*, 91(11):2978–2981, May 1987.

[39] O. Gereben and L. Pusztai. System size and trajectory length dependence of the static structure factor and the diffusion coefficient as calculated from molecular dynamics simulations: The case of SPC/E water. *Journal of Molecular Liquids*, 161(1):36–40, June 2011.

[40] B. Hess, C. Holm, and N. van der Vegt. Osmotic coefficients of atomistic NaCl (aq) force fields. *Journal of Chemical Physics*, 124(16):164509, April 2006.

[41] P. J. Dyer, H. Docherty, and P. T. Cummings. The importance of polarizability in the modeling of solubility: Quantifying the effect of solute polarizability on the solubility of small nonpolar solutes in popular models of water. *Journal of Chemical Physics*, 129(2):024508, 2008.

[42] Y. Luo and B. Roux. Simulation of Osmotic Pressure in Concentrated Aqueous Salt Solutions. *Journal of Physical Chemistry Letters*, 1(1):183–189, January 2010.

[43] A. I. Frolov, A. G. Rozhin, and M. V. Fedorov. Ion Interactions with the Carbon Nanotube Surface in Aqueous Solutions: Understanding the Molecular Mechanisms. *ChemPhysChem*, 11(12):2612–2616, 2010.

[44] M. Patra and M. Karttunen. Systematic comparison of force fields for microscopic simulations of NaCl in aqueous solutions: Diffusion, free energy of hydration, and structural properties. *Journal of Computational Chemistry*, 25(5):678–689, April 2004.

[45] K. D. Collins, G. W. Neilson, and J. E. Enderby. Ions in water: Characterizing the forces that control chemical processes and biological structure. *Biophysical Chemistry*, 128(2-3):95–104, July 2007.

[46] F. Hofmeister. Zur Lehre von der Wirkung der Salze. *Naunyn-Schmiedeberg's Archives of Pharmacology*, 24(4-5):247–260, 1988.

[47] M. G. Cacace, E. M. Landau, and J. J. Ramsden. The Hofmeister series: Salt and solvent effects on interfacial phenomena. *Quarterly Reviews of Biophysics*, 30(3):241–277, August 1997.

[48] K. D. Collins. Ions from the Hofmeister series and osmolytes: effects on proteins in solution and in the crystallization process. *Methods*, 34(3):300–311, November 2004.

[49] W. Kunz. Specific ion effects in liquids, in biological systems, and at interfaces. *Pure and Applied Chemistry*, 78(8):1611–1617, August 2006.

[50] C. L. Henry and V. S. J. Craig. The Link between Ion Specific Bubble Coalescence and Hofmeister Effects Is the Partitioning of Ions within the Interface. *Langmuir*, 26(9):6478–6483, May 2010.

[51] A. Pertsin and M. Grunze. Computer simulations of water-mediated force between phospholipid membranes. *Current Opinion in Colloid & Interface Science*, 16(6):534–541, 2011.

[52] B. Bagchi. Water dynamics in the hydration layer around proteins and micelles. *Chemical Reviews*, 105(9):3197–3219, September 2005.

[53] S. Nihonyanagi, T. Ishiyama, T. Lee, S. Yamaguchi, M. Bonn, A. Morita, and T. Tahara. Unified Molecular View of the Air/Water Interface Based on Experimental and Theoretical chi((2)) Spectra of an Isotopically Diluted Water Surface. *Journal of the American Chemical Society*, 133(42):16875–16880, October 2011.

[54] D. Stacchiola, J. B. Park, P. Liu, S. Ma, F. Yang, D. E. Starr, E. Muller, P. Sutter, and J. Hrbek. Water Nucleation on Gold: Existence of a Unique Double Bilayer. *Journal of Physical Chemistry C*, 113(34):15102–15105, August 2009.

[55] J. A. Thomas and A. J. H. McGaughey. Density, distribution, and orientation of water molecules inside and outside carbon nanotubes. *Journal of Chemical Physics*, 128(8):084715, February 2008.

[56] G. Hummer, J. C. Rasaiah, and J. P. Noworyta. Water conduction through the hydrophobic channel of a carbon nanotube. *Nature*, 414(6860):188–190, November 2001.

[57] T. A. Pascal, W. A. Goddard, and Y. Jung. Entropy and the driving force for the filling of carbon nanotubes with water. *Proceedings of the National Academy of Sciences of the United States of America*, 108(29):11794–11798, July 2011.

[58] P. Jungwirth and D. J. Tobias. Specific ion effects at the air/water interface. *Chemical Reviews*, 106(4):1259–1281, April 2006.

[59] P. Jungwirth and D. J. Tobias. Molecular structure of salt solutions: A new view of the interface with implications for heterogeneous atmospheric chemistry. *Journal of Physical Chemistry B*, 105(43):10468–10472, November 2001.

[60] B. L. Eggimann and J. I. Siepmann. Size effects on the solvation of anions at the aqueous liquid-vapor interface. *Journal of Physical Chemistry C*, 112(1):210–218, January 2008.

[61] R. L. Baldwin. How Hofmeister ion interactions affect protein stability. *Biophysical Journal*, 71(4):2056–2063, October 1996.

[62] M.V. Fedorov, J.M. Goodman, and S. Schumm. Solvent effects and hydration of a tripeptide in sodium halide aqueous solutions: an in silico study. *Physical Chemistry Chemical Physics*, 9(40):5423–5435, 2007.

[63] M. V. Fedorov, J. M. Goodman, and S. Schumm. The effect of sodium chloride on poly-L-glutamate conformation. *Chemical Communications*, (8):896–898, 2009.

[64] M. V. Fedorov, J. M. Goodman, and S. Schumm. To Switch or Not To Switch: The Effects of Potassium and Sodium Ions on alpha-Poly-L-glutamate Conformations in Aqueous Solutions. *Journal of the American Chemical Society*, 131(31):10854–10856, August 2009.

[65] M. V. Fedorov, J. M. Goodman, V. V. Kolombet, S. Schumm, and I. M. Socorro. Conformational changes of trialanine in sodium halide solutions: An in silico study. *Journal of Molecular Liquids*, 147(1-2):117–123, July 2009.

[66] M. V. Fedorov, A. I. Frolov, A. O. Romanova, K. Kirchner, and I. V. Terekhova. Ion effects on biomolecule conformation and complex formation in water. *Abstracts of Papers of the American Chemical Society*, 241, March 2011.

[67] R. Piazza and M. Pierno. Protein interactions near crystallization: A microscopic approach to the Hofmeister series. *Journal of Physics: Condensed Matter*, 12(8A):A443–A449, February 2000.

[68] L. M. Pegram and M. T. Record. Thermodynamic origin of Hofmeister ion effects. *Journal of Physical Chemistry B*, 112(31):9428–9436, August 2008.

[69] M. Lund, R. Vacha, and P. Jungwirth. Specific ion binding to macromolecules: Effects of hydrophobicity and ion pairing. *Langmuir*, 24(7):3387–3391, April 2008.

[70] M. Sammalkorpi, M. Karttunen, and M. Haataja. Ionic Surfactant Aggregates in Saline Solutions: Sodium Dodecyl Sulfate (SDS) in the Presence of Excess Sodium Chloride (NaCl) or Calcium Chloride (CaCl2). *Journal of Physical Chemistry B*, 113(17):5863–5870, April 2009.

[71] S. Niyogi, S. Boukhalfa, S. B. Chikkannanavar, T. J. McDonald, M. J. Heben, and S. K. Doorn. Selective aggregation of single-walled carbon nanotubes via salt addition. *Journal of the American Chemical Society*, 129(7):1898–1899, February 2007.

[72] S. Niyogi, C. G. Densmore, and S. K. Doom. Electrolyte Tuning of Surfactant Interfacial Behavior for Enhanced Density-Based Separations of Single-Walled Carbon Nanotubes. *Journal of the American Chemical Society*, 131(3):1144–1153, January 2009.

[73] J.J. Brege, C. Gallaway, and A.R. Barron. Fluorescence Quenching of Single-Walled Carbon Nanotubes in SDBS Surfactant Suspension by Metal Ions: Quenching Efficiency as a Function of Metal and Nanotube Identity. *Journal of Physical Chemistry C*, 111:17812–17820, 2007.

[74] J. J. Brege, C. Gallaway, and A. R. Barron. Fluorescence Quenching of Single-Walled Carbon Nanotubes with Transition-Metal Ions. *Journal of Physical Chemistry C*, 113(11):4270–4276, March 2009.

[75] K. D. Ausman, R. Piner, O. Lourie, R. S. Ruoff, and M. Korobov. Organic solvent dispersions of single-walled carbon nanotubes: Toward solutions of pristine nanotubes. *Journal of Physical Chemistry B*, 104(38):8911–8915, September 2000.

[76] M. J. O'Connell, S. M. Bachilo, C. B. Huffman, V. C. Moore, M. S. Strano, E. H. Haroz, K. L. Rialon, P. J. Boul, W. H. Noon, C. Kittrell, J. P. Ma, R. H. Hauge, R. B. Weisman, and R. E. Smalley. Band gap fluorescence from individual single-walled carbon nanotubes. *Science*, 297(5581):593–596, July 2002.

[77] P. H. Tan, A. G. Rozhin, T. Hasan, P. Hu, V. Scardaci, W. I. Milne, and A. C. Ferrari. Photoluminescence spectroscopy of carbon nanotube bundles: Evidence for exciton energy transfer. *Physical Review Letters*, 99(13):137402, September 2007.

[78] T. Hasan, Z. P. Sun, F. Q. Wang, F. Bonaccorso, P. H. Tan, A. G. Rozhin, and A. C. Ferrari. Nanotube-Polymer Composites for Ultrafast Photonics. *Advanced Materials*, 21(38-39):3874–3899, October 2009.

[79] Z. P. Liu, X. P. Wu, and W. C. Wang. A novel united-atom force field for imidazolium-based ionic liquids. *Physical Chemistry Chemical Physics*, 8(9):1096–1104, 2006.

[80] Y. Xu and N. R. Aluru. Carbon nanotube screening effects on the water-ion channels. *Applied Physics Letters*, 93(4):043122, July 2008.

[81] H. W. Horn, W. C. Swope, J. W. Pitera, J. D. Madura, T. J. Dick, G. L. Hura, and T. Head-Gordon. Development of an improved four-site water model for biomolecular simulations: TIP4P-Ew. *Journal of Chemical Physics*, 120(20):9665–9678, May 2004.

[82] K. P. Jensen and W. L. Jorgensen. Halide, ammonium, and alkali metal ion parameters for modeling aqueous solutions. *Journal of Chemical Theory and Computation*, 2(6):1499–1509, November 2006.

[83] M. Fyta, I. Kalcher, J. Dzubiella, L. Vrbka, and R. R. Netz. Ionic force field optimization based on single-ion and ion-pair solvation properties. *Journal of Chemical Physics*, 132(2):024911, January 2010.

[84] M. P. Allen and D. J. Tildesley. *Computer Simulation of Liquids*. Oxford University Press; Clarendon Press, 1989.

[85] F. Jensen. *Introduction to Computational Chemistry*. Wiley, 2006.

[86] J. P. Ryckaert, G. Ciccotti, and H. J. C. Berendsen. Numerical-integration of Cartesian Equations of Motion of A System With Constraints - Molecular-dynamics of N-alkanes. *Journal of Computational Physics*, 23(3):327–341, 1977.

[87] H. C. Andersen. Rattle - a Velocity Version of the Shake Algorithm for Molecular-Dynamics Calculations. *Journal of Computational Physics*, 52(1):24–34, 1983.

[88] B. Hess, H. Bekker, H. J. C. Berendsen, and J. G. E. M. Fraaije. LINCS: A linear constraint solver for molecular simulations. *Journal of Computational Chemistry*, 18(12):1463–1472, September 1997.

[89] J. E. Lennard-Jones. Cohesion. *Proceedings of the Physical Society*, 43:461–482, January 1931.

[90] D. M. Duh and D. Henderson. Integral equation theory for Lennard-Jones fluids: The bridge function and applications to pure fluids and mixtures. *Journal of Chemical Physics*, 104(17):6742–6754, May 1996.

[91] D. Boda and D. Henderson. The effects of deviations from Lorentz-Berthelot rules on the properties of a simple mixture. *Molecular Physics*, 106(20):2367–2370, 2008.

[92] A. G. Donchev, V. D. Ozrin, M. V. Subbotin, O. V. Tarasov, and V. I. Tarasov. A quantum mechanical polarizable force field for biomolecular interactions. *Proceedings of the National Academy of Sciences of the United States of America*, 102(22):7829–7834, May 2005.

[93] H. J. C. Berendsen, J. R. Grigera, and T. P. Straatsma. The missing term in effective pair potentials. *Journal of Physical Chemistry*, 91(24):6269–6271, November 1987.

[94] S. Weerasinghe and P. E. Smith. A Kirkwood-Buff derived force field for sodium chloride in water, journal = Journal of Chemical Physics. 119(21):11342–11349, December 2003.

[95] I. S. Joung and T. E. Cheatham. Determination of alkali and halide monovalent ion parameters for use in explicitly solvated biomolecular simulations. *Journal of Physical Chemistry B*, 112(30):9020–9041, July 2008.

[96] W. L. Jorgensen, J. P. Ulmschneider, and J. Tirado-Rives. Free energies of hydration from a generalized Born model and an ALL-atom force field. *Journal of Physical Chemistry B*, 108(41):16264–16270, October 2004.

[97] D. A. Case, T. A. Darden, T. E. Cheatham III, C. L. Simmerling, J. Wang, R.E. Duke, R. Luo, R. C. Walker, W. Zhang, K. M. Merz, B. Roberts, B. Wang, S. Hayik, A. Roitberg, G. Seabra, I. Kolossvary, K. F. Wong, F. Paesani, J. Vanicek, J. Liu, X. Wu, S. R. Brozell, T. Steinbrecher, H. Gohlke, Q. Cai, X. Ye, J. Wang, M.-J. Hsieh, G. Cui, D. R. Roe, D. H.

Mathews, M. G. Seetin, C. Sagui, V. Babin, T. Luchko, S. Gusarov, A. Kovalenko, and P. A. Kollman.

[98] L. X. Dang. Mechanism and Thermodynamics of Ion Selectivity In Aqueous-solutions of 18-crown-6 Ether - A Molecular-dynamics Study. *Journal of the American Chemical Society*, 117(26):6954–6960, July 1995.

[99] G. Lamoureux and B. Roux. Modeling induced polarization with classical Drude oscillators: Theory and molecular dynamics simulation algorithm. *Journal of Chemical Physics*, 119(6):3025–3039, August 2003.

[100] G. Lamoureux, A. D. MacKerell, and B. Roux. A simple polarizable model of water based on classical Drude oscillators. *Journal of Chemical Physics*, 119(10):5185–5197, September 2003.

[101] G. Lamoureux and B. Roux. Absolute hydration free energy scale for alkali and halide ions established from simulations with a polarizable force field. *Journal of Physical Chemistry B*, 110(7):3308–3322, February 2006.

[102] H. B. Yu, T. W. Whitfield, E. Harder, G. Lamoureux, I. Vorobyov, V. M. Anisimov, A. D. MacKerell, and B. Roux. Simulating Monovalent and Divalent Ions in Aqueous Solution Using a Drude Polarizable Force Field. *Journal of Chemical Theory and Computation*, 6(3):774–786, March 2010.

[103] P. J. van Maaren and D. van der Spoel. Molecular dynamics simulations of water with novel shell-model potentials. *Journal of Physical Chemistry B*, 105(13):2618–2626, April 2001.

[104] P. Drude. *The Theory of Optics*. Longmans, Green, and Co., London New York, 1902.

[105] W. L. Jorgensen, J. Chandrasekhar, J. D. Madura, R. W. Impey, and M. L. Klein. Comparison Of Simple Potential Functions For Simulating Liquid Water. *Journal of Chemical Physics*, 79(2):926–935, 1983.

[106] F. J. Millero, C. T. Chen, K. Schleicher, and A. Bradshaw. A New High-pressure Equation of State For Seawater. *Deep-sea Research Part A-oceanographic Research Papers*, 27(3-4):255–264, 1980.

[107] C. T. A. Chen, J. H. Chen, and F. J. Millero. Densities of $NaCl$, $MgCl_2$, Na_2SO_4, and $MgSO_4$ Aqueous-solutions At 1 Atm From 0-degrees-c To 50-degrees-c and From 0.001 To 1.5 M. *Journal of Chemical and Engineering Data*, 25(4):307–310, 1980.

[108] J. Safarov, F. Millero, R. Feistel, A. Heintz, and E. Hassel. Thermodynamic properties of standard seawater: extensions to high temperatures and pressures. *Ocean Science*, 5(3):235–246, 2009.

[109] Unknown. The Alfred Wegener Institute, Helmholtz Centre for Polar and Marine Research - CTD Instrument and Water Sampler. www.awi.de/en/research/, April 2013.

[110] B. Hess, C. Kutzner, D. van der Spoel, and E. Lindahl. GROMACS 4: Algorithms for highly efficient, load-balanced, and scalable molecular simulation. *Journal of Chemical Theory and Computation*, 4(3):435–447, March 2008.

[111] L. Martínez, R. Andrade, E. G. Birgin, and J. M. Martínez. PACKMOL: A Package for Building Initial Configurations for Molecular Dynamics Simulations. *Journal of Computational Chemistry*, 30(13):2157–2164, October 2009.

[112] U. Essmann, L. Perera, M. L. Berkowitz, T. Darden, H. Lee, and L. G. Pedersen. A Smooth Particle Mesh Ewald Method. *Journal of Chemical Physics*, 103(19):8577–8593, November 1995.

[113] G. Bussi, D. Donadio, and M. Parrinello. Canonical sampling through velocity rescaling. *The Journal of Chemical Physics*, 126(1):014101, January 2007.

[114] H. J. C. Berendsen, J. P. M. Postma, W. F. van Gunsteren, A. Dinola, and J. R. Haak. Molecular dynamics with coupling to an external bath. *Journal of Chemical Physics*, 81(8):3684–3690, 1984.

[115] http://mathworks.com/.

[116] D. R. Lide. *CRC Handbook of Chemistry and Physics, (Internet Version 2008)*. CRC Press/Taylor and Francis, Boca Raton, FL, 2008.

[117] J. L. Knight and C. L. Brooks. lambda-Dynamics Free Energy Simulation Methods. *Journal of Computational Chemistry*, 30(11):1692–1700, August 2009.

[118] A. Ben-Naim. *Molecular Theory of Water and Aqueous Solutions. Part 1 - Understanding Water*. World Scientific Publishing Co., 2009.

[119] D. S. Palmer, A. Llinas, I. Morao, G. M. Day, J. M. Goodman, R. C. Glen, and J. B. O. Mitchell. Predicting intrinsic aqueous solubility by a thermodynamic cycle. *Molecular Pharmaceutics*, 5(2):266–279, March 2008.

[120] M. M. Kubo, E. Gallicchio, and R. M. Levy. Thermodynamic decomposition of hydration free energies by computer simulation: Application to amines, oxides, and sulfides. *Journal of Physical Chemistry B*, 101(49):10527–10534, December 1997.

[121] W. R. Fawcett. Thermodynamic parameters for the solvation of monatomic ions in water. *Journal of Physical Chemistry B*, 103(50):11181–11185, December 1999.

[122] A. Cooper. Heat capacity effects in protein folding and ligand binding: a re-evaluation of the role of water in biomolecular thermodynamics. *Biophysical Chemistry*, 115(2-3):89–97, April 2005.

[123] Y. Marcus. The Thermodynamics of Solvation of Ions. 2. the Enthalpy of Hydration At 298.15K. *Journal of the Chemical Society-faraday Transactions I*, 83:339–349, 1987.

[124] D. S. Palmer, J. L. McDonagh, J. B. O. Mitchell, T. van Mourik, and M. V. Fedorov. First-Principles Calculation of the Intrinsic Aqueous Solubility of Crystalline Druglike Molecules. *Journal of Chemical Theory and Computation*, 8(9):3322–3337, September 2012.

[125] P. G. Karamertzanis, P. Raiteri, and A. Galindo. The Use of Anisotropic Potentials in Modeling Water and Free Energies of Hydration. *Journal of Chemical Theory and Computation*, 6(5):1590–1607, May 2010.

[126] D. van der Spoel, E. Lindahl, B. Hess, A. R. van Buuren, E. Apol, P. J. Meulenhoff, D. P. Tieleman, A. L. T. M. Sijbers, K. A. Feenstra, R. van Drunen, and H. J. C. Berendsen. *Gromacs User Manual version 4.5*, 2010. GROMACS - Groningen Machine for Chemical Simulations; User Manual.

[127] C. H. Bennett. Efficient Estimation of Free-energy Differences From Monte-carlo Data. *Journal of Computational Physics*, 22(2):245–268, 1976.

[128] R. Schmid, A. M. Miah, and V. N. Sapunov. A new table of the thermodynamic quantities of ionic hydration: values and some applications (enthalpy-entropy compensation and Born radii). *Physical Chemistry Chemical Physics*, 2(1):97–102, 2000.

[129] Y. Marcus. A Simple Empirical-model Describing the Thermodynamics of Hydration of Ions of Widely Varying Charges, Sizes, and Shapes. *Biophysical Chemistry*, 51(2-3):111–127, August 1994.

[130] G. N. Chuev, M. V. Fedorov, S. Chiodo, N. Russo, and E. Sicilia. Hydration of ionic species studied by the reference interaction site model with a repulsive bridge correction. *Journal of Computational Chemistry*, 29(14):2406–2415, 2008.

[131] M. Schmidt, H. Loewen, J. M. Brader, and R. Evans. Density Functional for a Model Colloid-Polymer Mixture. *Physical Review Letters*, 85:1934–1937, 2000.

[132] B. Hess and N. F. A. van der Vegt. Hydration thermodynamic properties of amino acid analogues: A systematic comparison of biomolecular force fields and water models. *Journal of Physical Chemistry B*, 110(35):17616–17626, September 2006.

[133] S. Koneshan, J. C. Rasaiah, R. M. Lynden-Bell, and S. H. Lee. Solvent structure, dynamics, and ion mobility in aqueous solutions at 25°C. *Journal of Physical Chemistry B*, 102(21):4193–4204, May 1998.

[134] I. Waluyo, C. C. Huang, D. Nordlund, U. Bergmann, T. M. Weiss, L. G. M. Pettersson, and A. Nilsson. The structure of water in the hydration shell of cations from x-ray Raman and small angle x-ray scattering measurements. *Journal of Chemical Physics*, 134(6):064513, February 2011.

[135] J.-P. Hansen and I. R. McDonald. *Theory of Simple Liquids, 4th ed.* Elsevier Academic Press, Amsterdam, The Netherlands, 2000.

[136] Yizhak Marcus. *Ion solvation.* John Wiley & Sons, Chichester, UK, 1985.

[137] A. A. Chialvo, P. T. Cummings, J. M. Simonson, and R. E. Mesmer. Solvation in high-temperature electrolyte solutions. I. Hydration shell behavior from molecular simulation. *Journal of Chemical Physics*, 110(2):1064–1074, January 1999.

[138] A. A. Chialvo and J. M. Simonson. The structure of $CaCl_2$ aqueous solutions over a wide range of concentration. Interpretation of diffraction experiments via molecular simulation. *Journal of Chemical Physics*, 119(15):8052–8061, October 2003.

[139] A. Botti, F. Bruni, S. Imberti, M. A. Ricci, and A. K. Soper. Ions in water: The microscopic structure of a concentrated HCl solution. *Journal of Chemical Physics*, 121(16):7840–7848, October 2004.

[140] I. Harsanyi, P. A. Bopp, A. Vrhovsek, and L. Pusztai. On the hydration structure of LiCl aqueous solutions: A Reverse Monte Carlo based combination of diffraction data and Molecular Dynamics simulations. *Journal of Molecular Liquids*, 158(1):61–67, January 2011.

[141] I. Harsanyi, L. Temleitner, B. Beuneu, and L. Pusztai. Neutron and X-ray diffraction measurements on highly concentrated aqueous LiCl solutions. *Journal of Molecular Liquids*, 165:94–100, January 2012.

[142] J. Mahler and I. Persson. A Study of the Hydration of the Alkali Metal Ions in Aqueous Solution. *Inorganic Chemistry*, 51(1):425–438, January 2012.

[143] A. K. Soper and M. G. Phillips. A New Determination of the Structure of Water At 25-degrees-c. *Chemical Physics*, 107(1):47–60, August 1986.

[144] R. W. Impey, P. A. Madden, and I. R. Mcdonald. Hydration And Mobility Of Ions In Solution. *Journal of Physical Chemistry*, 87(25):5071–5083, 1983.

[145] E. Guàrdia and J. A. Padró. Molecular Dynamics Simulation of Single Ions In Aqueous-solutions - Effects of the Flexibility of the Water-molecules. *Journal of Physical Chemistry*, 94(15):6049–6055, July 1990.

[146] D. E. Smith and L. X. Dang. Computer-simulations of Nacl Association In Polarizable Water. *Journal of Chemical Physics*, 100(5):3757–3766, March 1994.

[147] S. H. Lee and J. C. Rasaiah. Molecular-dynamics Simulation of Ionic Mobility. I. Alkali metal Cations in Water At 25°C. *Journal of Chemical Physics*, 101(8):6964–6974, October 1994.

[148] I. S. Joung and T. E. Cheatham. Molecular Dynamics Simulations of the Dynamic and Energetic Properties of Alkali and Halide Ions Using Water-Model-Specific Ion Parameters. *Journal of Physical Chemistry B*, 113(40):13279–13290, October 2009.

[149] H. Ohtaki and T. Radnai. Structure and Dynamics of Hydrated Ions. *Chemical Reviews*, 93(3):1157–1204, May 1993.

[150] D. Laage and J. T. Hynes. On the Molecular Mechanism of Water Reorientation. *Journal of Physical Chemistry B*, 112(45):14230–14242, November 2008.

[151] S. H. Northrup and J. T. Hynes. The Stable States Picture Of Chemical Reactions .1. Formulation For Rate Constants And Initial Condition Effects. *Journal of Chemical Physics*, 73(6):2700–2714, 1980.

[152] J. G. Kirkwood. Statistical Mechanics of Fluid Mixtures. *Journal of Chemical Physics*, 3:300–313, 1935.

[153] M. Kinoshita and Y. Harano. Potential of mean force between solute atoms in salt solution: Effects due to salt species and relevance to conformational transition of biomolecules. *Bulletin of the Chemical Society of Japan*, 78(8):1431–1441, August 2005.

[154] R. Akiyama, N. Fujino, K. Kaneda, and M. Kinoshita. Interaction between like-charged colloidal particles in aqueous electrolyte solution: Attractive component arising from solvent granularity. *Condensed Matter Physics*, 10(4):587–596, 2007.

[155] E. Sobolewski, M. Makowski, C. Czaplewski, A. Liwo, S. Oldziej, and H. A. Scheraga. Potential of mean force of hydrophobic association: Dependence on solute size. *Journal of Physical Chemistry B*, 111(36):10765–10774, September 2007.

[156] S. Phongphanphanee, N. Yoshida, and F. Hirata. The potential of mean force of water and ions in aquaporin channels investigated by the 3D-RISM method. *Journal of Molecular Liquids*, 147(1-2):107–111, July 2009.

[157] C. J. Fennell, A. Bizjak, V. Vlachy, and K. A. Dill. Ion Pairing in Molecular Simulations of Aqueous Alkali Halide Solutions. *Journal of Physical Chemistry B*, 113(19):6782–6791, May 2009.

[158] Y. Q. Deng and B. Roux. Computations of Standard Binding Free Energies with Molecular Dynamics Simulations. *Journal of Physical Chemistry B*, 113(8):2234–2246, February 2009.

[159] J. Mondal, X. A. Zhu, Q. A. Cui, and A. Yethiraj. Self-Assembly of beta-Peptides: Insight from the Pair and Many-Body Free Energy of Association. *Journal of Physical Chemistry C*, 114(32):13551–13556, August 2010.

[160] S. C. Lin and D. Blankschtein. Role of the Bile Salt Surfactant Sodium Cholate in Enhancing the Aqueous Dispersion Stability of Single-Walled Carbon Nanotubes: A Molecular Dynamics Simulation Study. *Journal of Physical Chemistry B*, 114(47):15616–15625, December 2010.

[161] B. Egwolf, Y. Luo, D. E. Walters, and B. Roux. Ion Selectivity of alpha-Hemolysin with beta-Cyclodextrin Adapter. II. Multi-Ion Effects Studied with Grand Canonical Monte Carlo/Brownian Dynamics Simulations. *Journal of Physical Chemistry B*, 114(8):2901–2909, March 2010.

[162] T. Miyata, Y. Ikuta, and F. Hirata. Free energy calculation using molecular dynamics simulation combined with the three-dimensional reference interaction site model theory. II. Thermodynamic integration along a spatial reaction coordinate. *Journal of Chemical Physics*, 134(4):044127, January 2011.

[163] B. A. Bauer, S. C. Ou, and S. Patel. Role of spatial ionic distribution on the energetics of hydrophobic assembly and properties of the water/hydrophobe interface. *Physical Chemistry Chemical Physics*, 14(6):1892–1906, 2012.

[164] R. M. Lynden-Bell, A. I. Frolov, and M. V. Fedorov. Electrode screening by ionic liquids. *Physical Chemistry Chemical Physics*, 2012.

[165] D. A. McQuarrie. *Statistical Mechanics*. University Science Books, 1 edition, May 2000.

[166] J. G. Kirkwood and F. P. Buff. The Statistical Mechanical Theory Of Solutions .1. *Journal of Chemical Physics*, 19(6):774–777, 1951.

[167] A. Ben-Naim. *Molecular Theory of Solutions*. Oxford University Press, USA, 2006.

[168] S. Shimizu, W. M. McLaren, and N. Matubayasi. The Hofmeister series and protein-salt interactions. *Journal of Chemical Physics*, 124(23):234905, June 2006.

[169] V. Pierce, M. Kang, M. Aburi, S. Weerasinghe, and P. E. Smith. Recent applications of Kirkwood-Buff theory to biological systems. *Cell Biochemistry and Biophysics*, 50(1):1–22, 2008.

[170] M. B. Gee and P. E. Smith. Kirkwood-Buff theory of molecular and protein association, aggregation, and cellular crowding. *Journal of Chemical Physics*, 131(16):165101, October 2009.

[171] M. B. Gee, N. R. Cox, Y. Jiao, N. Bentenitis, S. Weerasinghe, and P. E. Smith. A Kirkwood-Buff Derived Force Field for Aqueous Alkali Halides. *Journal of Chemical Theory and Computation*, 7(5):1369–1380, 2011.

[172] J. R. Gullingsrud, R. Braun, and K. Schulten. Reconstructing potentials of mean force through time series analysis of steered molecular dynamics simulations. *Journal of Computational Physics*, 151(1):190–211, May 1999.

[173] O. Ya. Samoilov. A new approach to the study of hydration of ions in aqueous solutions. *Discussions of the Faraday Society*, 24:141–146, 1957.

[174] S. H. Chong and F. Hirata. Ion hydration: Thermodynamic and structural analysis with an integral equation theory of liquids. *Journal of Physical Chemistry B*, 101(16):3209–3220, April 1997.

[175] Y. V. Kalyuzhnyi, V. Vlachy, and K. A. Dill. Hydration of simple ions. Effect of the charge density. *Acta Chimica Slovenica*, 48(3):309–316, 2001.

[176] M. V. Fedorov and A. A. Kornyshev. Unravelling the solvent response to neutral and charged solutes. *Molecular Physics*, 105(1):1–16, January 2007.

[177] M. Neumann. Dipole-moment Fluctuation Formulas In Computer-simulations of Polar Systems. *Molecular Physics*, 50(4):841–858, 1983.

[178] B. Van der Bruggen, C. Vandecasteele, T. Van Gestel, W. Doyen, and R. Leysen. A review of pressure-driven membrane processes in wastewater treatment and drinking water production. *Environmental Progress*, 22(1):46–56, April 2003.

[179] K. Haerens, S. Van Deuren, E. Matthijs, and B. Van der Bruggen. Challenges for recycling ionic liquids by using pressure driven membrane processes. *Green Chemistry*, 12(12):2182–2188, December 2010.

[180] M. Z. Bazant, M. S. Kilic, B. D. Storey, and A. Ajdari. Towards an understanding of induced-charge electrokinetics at large applied voltages in concentrated solutions. *Advances in Colloid and Interface Science*, 152(1-2):48–88, November 2009.

[181] A. P. Lyubartsev and A. Laaksonen. Osmotic and activity coefficients from effective potentials for hydrated ions. *Physical Review E*, 55(5):5689–5696, May 1997.

[182] I. Kalcher and J. Dzubiella. Structure-thermodynamics relation of electrolyte solutions. *Journal of Chemical Physics*, 130(13):134507, April 2009.

[183] A. D. McNaught and A. Wilkinson. *Compendium of chemical terminology : IUPAC recommendations*. Blackwell Science, Oxford, 2 edition, 1997.

[184] Berkeley E. and E. G. J. Hartley. A method of measuring directly high osmotic pressures. *Proceedings of the Royal Society of London*, 73(495):436–443, June 1904.

[185] Berkeley Earl and E. G. J. Hartley. The determination of the osmotic pressures of solutions by the measurement of their vapour pressures. *Proceedings of the Royal Society of London Series A-containing Papers of A Mathematical and Physical Character*, 77(515):156–169, February 1906.

[186] R. A. Robinson. The vapour pressures of solutions of potassium chloride and sodium chloride. *Transactions of the Royal Society of New Zealand*, 75((2)):203–217, 1946.

[187] A. Grattoni, G. Canavese, F. M. Montevecchi, and M. Ferrari. Fast membrane osmometer as alternative to freezing point and vapor pressure osmometry. *Analytical Chemistry*, 80(7):2617–2622, April 2008.

[188] R. A. Robinson and R. H. Stokes. *Electrolyte Solutions*. Dover Publications, Inc., Mineola, NY, 2002.

[189] W. J. Hamer and Y-C. Wu. Osmotic Coefficients And Mean Activity Coefficients Of Uni-univalent Electrolytes In Water At 25 Degrees. *Journal of Physical and Chemical Reference Data*, 1:1047–1100, 1972.

[190] D. G. Archer. Thermodynamic Properties of the $NaCl + H_2O$ System. 2. Thermodynamic Properties of $NaCl$(aq), $NaCl.2H_2O$(cr), and Phase-equilibria. *Journal of Physical and Chemical Reference Data*, 21(4):793–829, July 1992.

[191] C. T. Liu and W. T. Lindsay. Osmotic Coefficients of Aqueous Sodium Chloride Solutions From 125 Degrees To 130 Degrees. *Journal of Physical Chemistry*, 74(2):341–346, 1970.

[192] A. P. Lyubartsev and A. Laaksonen. Calculation of Effective Interaction Potentials From Radial-distribution Functions - A Reverse Monte-carlo Approach. *Physical Review E*, 52(4):3730–3737, October 1995.

[193] A. P. Lyubartsev and A. Laaksonen. Concentration effects in aqueous NaCl solutions. A molecular dynamics simulation. *Journal of Physical Chemistry*, 100(40):16410–16418, October 1996.

[194] A. P. Lyubartsev and A. Laaksonen. Reconstruction of pair interaction potentials from radial distribution functions. *Computer Physics Communications*, 121:57–59, September 1999.

[195] B. Hess, C. Holm, and N. van der Vegt. Modeling multibody effects in ionic solutions with a concentration dependent dielectric permittivity. *Physical Review Letters*, 96(14):147801, April 2006.

[196] W. Humphrey, A. Dalke, and K. Schulten. VMD: Visual molecular dynamics. *Journal of Molecular Graphics*, 14(1):33–38, February 1996.

[197] F. Chen and P. E. Smith. Simulated surface tensions of common water models. *Journal of Chemical Physics*, 126(22):221101, June 2007.

[198] F. Chen and P. E. Smith. Theory and computer simulation of solute effects on the surface tension of liquids. *Journal of Physical Chemistry B*, 112(30):8975–8984, July 2008.

[199] R. F. Probstein. *Physicochemical Hydrodynamics: An Introduction*. John Wiley & Sons, 2 edition, 1994.

[200] A. Horibe, S. Fukusako, and M. Yamada. Surface tension of low-temperature aqueous solutions. *International Journal of Thermophysics*, 17(2):483–493, March 1996.

[201] P. L. du Nouy. An interfacial tensiometer for universal use. *Journal of General Physiology*, 7(5):625–U53, May 1925.

[202] E. Rame. The interpretation of dynamic contact angles measured by the Wilhelmy plate method. *Journal of Colloid and Interface Science*, 185(1):245–251, January 1997.

[203] G. Macdougall and C. Ockrent. Surface energy relations in liquid/solid systems I. The adhesion of liquids to solids and a new method of determining the surface tension of liquids. *Proceedings of the Royal Society of London Series A-mathematical and Physical Sciences*, 180(A981):0151–0173, June 1942.

[204] T. W. Richards and E. K. Carver. A critical study of the capillary rise method of determining surface tension, with data for water, benzene, toluene, chloroform, carbon tetrachloride, ether and dimethyl aniline. [Second paper.]. *Journal of the American Chemical Society*, 43:827–847, April 1921.

[205] W. Wagner and A. Pruss. The IAPWS formulation 1995 for the thermodynamic properties of ordinary water substance for general and scientific use. *Journal of Physical and Chemical Reference Data*, 31(2):387–535, June 2002.

[206] N. B. Vargaftik, B. N. Volkov, and L. D. Voljak. International Tables of the Surface-tension of Water. *Journal of Physical and Chemical Reference Data*, 12(3):817–820, 1983.

[207] F. N. Mendoza, J. Lopez-Lemus, G. A. Chapela, and J. Alejandre. The Wolf method applied to the liquid-vapor interface of water. *Journal of Chemical Physics*, 129(2):024706, July 2008.

[208] P. K. Yuet and D. Blankschtein. Molecular Dynamics Simulation Study of Water Surfaces: Comparison of Flexible Water Models. *Journal of Physical Chemistry B*, 114(43):13786–13795, October 2010.

[209] E. Spohr. Effect of electrostatic boundary conditions and system size on the interfacial properties of water and aqueous solutions. *Journal of Chemical Physics*, 107(16):6342–6348, 1997.

[210] I.C. Yeh and M.L. Berkowitz. Ewald summation for systems with slab geometry. *Journal of Chemical Physics*, 111:3155–3162, 1999.

[211] I. C. Yeh and G. Hummer. System-size dependence of diffusion coefficients and viscosities from molecular dynamics simulations with periodic boundary conditions. *Journal of Physical Chemistry B*, 108(40):15873–15879, October 2004.

[212] G. Raabe and R. J. Sadus. Molecular dynamics simulation of the dielectric constant of water: The effect of bond flexibility. *Journal of Chemical Physics*, 134(23):234501, June 2011.

[213] E. Spohr. Molecular dynamics simulations of water and ion dynamics in the electrochemical double layer. *Solid State Ionics*, 150(1-2):1–12, 2002.

[214] C. Schröder and O. Steinhauser. Using fit functions in computational dielectric spectroscopy. *Journal of Chemical Physics*, 132(24):244109, June 2010.

Appendix A

Frequency Dependent Dielectric Function $\varepsilon(\omega)$ of Neat SW10e Water

The frequency dependent dielectric function $\epsilon(f)$ provides useful insights into some dynamic and static properties of the water model. As a natural consequence of the model character of simulations, not all physical features of real water can be reproduced, as for example the vibrational modes of water are not reproduced by a rigid water model. Figure A.1 shows the result obtained with the SW10e water model in conjunction with the experimental curve of real water. As can be seen, in the region of dipolar movement, the model reproduces the behaviour of real water.

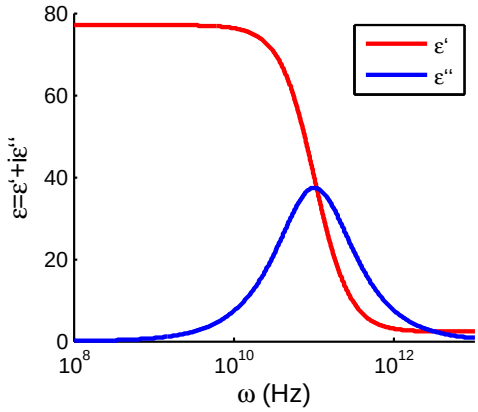

Figure A.1: Frequence dependent dielectric function $\varepsilon(\omega)$ of the SW10e water model. $\omega = 2\pi f$ denotes the angular frequency.

A Comment on the Method The method of calculating the frequency dependent dielectric function $\varepsilon(\omega)$ is taken from the work of Schröder and Steinhauser [214].

We are calculating the dielectric function for neat water. As neat water does not contain charged molecules, many formulas simplify. We will only consider here this simplified calculation.

The collective dipole moment $\vec{M}_{\mathrm{tot}}(t)$ of the simulation box

$$\vec{M}_{\mathrm{tot}}(t) = \sum_i \sum_\alpha q_{i,\alpha} \cdot \vec{r}_{i,\alpha}(t),$$

is the sum over all dipoles created by the atoms α of all molecules i. As the water molecules are neutral, we can write the total dipole moment as sum of all dipoles of the molecules

$$\vec{M}_{\mathrm{tot}}(t) = \vec{M}_{\mathrm{D}}(t) = \sum_i \sum_\alpha q_{i,\alpha}(\vec{r}_{i,\alpha}(t) - \vec{r}_{cm,i}(t)),$$

with $r_{cm,i}$ being the centre of mass of molecule i. $\vec{M}_{\mathrm{D}}(t)$ denotes the rotational part of the total dipole moment, which for neat water is identical with the total dipole moment.

The time correlation function or auto correlation function (ACF)

$$\phi(t) = \langle \vec{M}_{\mathrm{D}}(0) \cdot \vec{M}_{\mathrm{D}}(t) \rangle$$

of the total dipole is fitted to the function $A \cdot \exp(-t/\tau)$. The normalised ACF and the fit are presented in Fig. A.2.

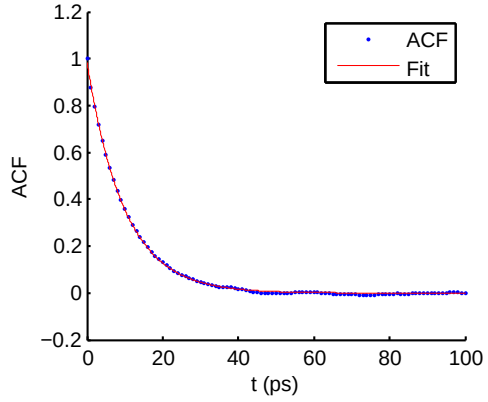

Figure A.2: Normalised ACF of the total dipole of a simulation box with SW10e water. The blue dots show the ACF, the red line shows a fit to the function $A \cdot \exp(-t/\tau)$.

Schröder and Steinhauser [214] normalised the ACF with $\langle \vec{M}_{\mathrm{D}}^2 \rangle$. To be exact, the factor $\langle \vec{M}_{\mathrm{D}}^2 \rangle - \langle \vec{M}_{\mathrm{D}} \rangle^2$ would be correct [177]. As $\langle \vec{M}_{\mathrm{D}} \rangle^2$ is usually several magnitudes smaller than $\langle \vec{M}_{\mathrm{D}}^2 \rangle$, often only $\langle \vec{M}_{\mathrm{D}} \rangle^2$ is evaluated.

The ACF converts via a Fourier-Laplace transformation $L[f(t)] = \int_0^\infty f(t) e^{i\omega t} \mathrm{d}t$ into a function called L_{DD}:

$$L_{DD}(\omega) = L[\langle \vec{M}_{\mathrm{D}}(0) \cdot \vec{M}_{\mathrm{D}}(t) \rangle] = \langle \vec{M}_{\mathrm{D}}^2 \rangle \cdot \frac{A \cdot \tau}{1 - i\omega\tau}.$$

The function L_{DD} provides us with the frequency dependent dielectric function:

$$\varepsilon(\omega) = 1 + \frac{4\pi}{3Vk_{\mathrm{B}}T} \left(\langle \vec{M}_{\mathrm{D}}^2 \rangle + i\omega L_{DD} \right).$$

Once again, we want to stress the point, that this calculation is only valid for systems without charged particles. Up to now, Gaussian units were applied, in SI units the real part ε' and the imaginary part ε'' of the frequency dependent dielectric function calculate:

$$\varepsilon' = 1 + \frac{1}{4\pi\varepsilon_0} \cdot \frac{4\pi}{3Vk_{\mathrm{B}}T} \cdot \langle \vec{M}_{\mathrm{D}}^2 \rangle \cdot \left(1 - \frac{A \cdot \omega^2\tau^2}{\omega^2\tau^2 + 1} \right),$$

$$\varepsilon'' = \frac{1}{4\pi\varepsilon_0} \cdot \frac{4\pi}{3Vk_{\mathrm{B}}T} \cdot \langle \vec{M}_{\mathrm{D}}^2 \rangle \cdot \left(\frac{A \cdot \omega\tau}{\omega\tau + 1} \right).$$

ε' and ε'' are presented in Fig. A.1 for SW10e water.

Appendix B

Osmotic Pressure

B.1 Osmotic Pressure - non-Polarizable Force Field

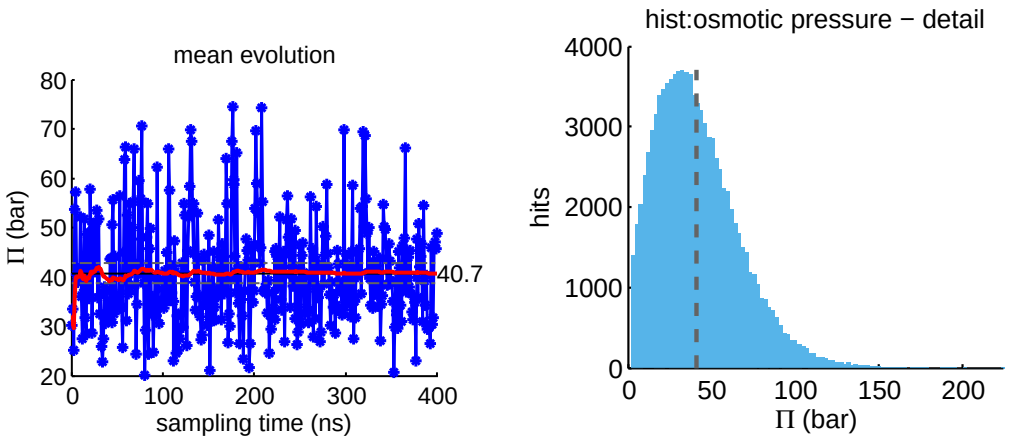

(a) Osmotic pressure Π.

(b) Close-up histogram of Π.

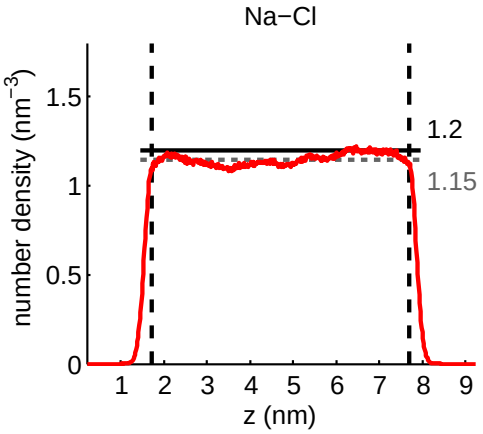

(c) Number density distribution ρ_N.

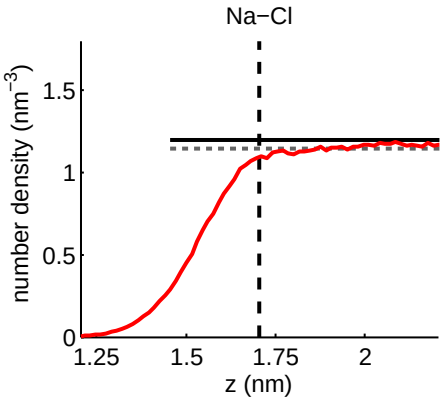

(d) Close-up of the ρ_N.

Figure B.1: **(long)** Summary of results obtained from an osmotic pressure calculation using membrane walls with a force constant k of 100 kJ/(mol·nm^2). 36 NaCl ion pairs are dissolved in 3072 SW10e water molecules and are confined in a 6 nm slab, resulting in a salt concentration of 0.95 M inside the ion domain. The box was allowed to change its size in z-direction to maintain the pressure, namely a NPAT ensemble was applied. Further results are shown in Tab. 4.14. The temperature is 298.15 K and the pressure 1 bar. The total duration of the simulation was 400 ns including 1 ns equilibration time. a) Block average of the osmotic pressure with 1 ns sampling time (blue line with asterisks) and running average of the osmotic pressure (red line). The horizontal lines mark the mean osmotic pressure (solid) and a ±5 % interval around it (grey dashed lines). b) Close-up of the histogram of the osmotic pressure. The bin at $\Pi = 0$ was not printed. The vertical dashed line marks the mean osmotic pressure. c) Number density distribution of ion species in the box. The vertical dashed line marks the position of the membrane. The horizontal line marks the position of the target concentration with 'hard' membrane walls (black solid), and of the actual concentration between the membrane walls (grey dashed line). d) Close-up of the number density distribution at the membrane wall.

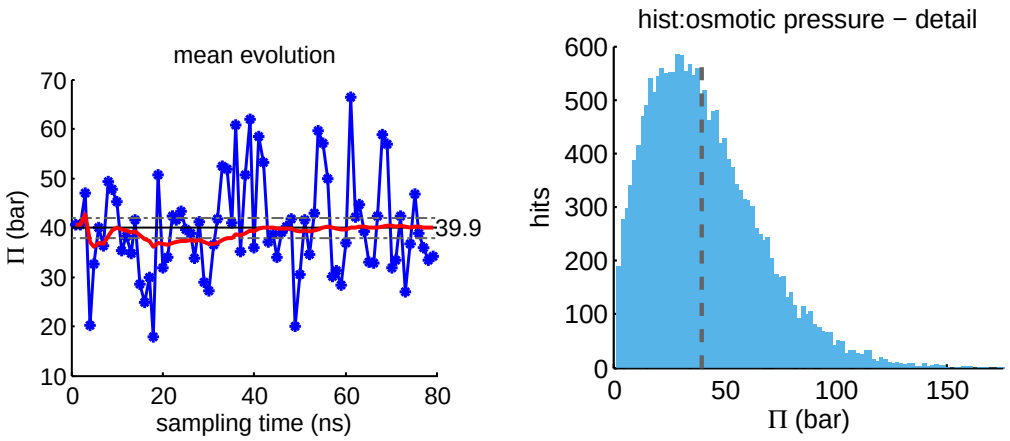

(a) Osmotic pressure Π.

(b) Close-up histogram of Π.

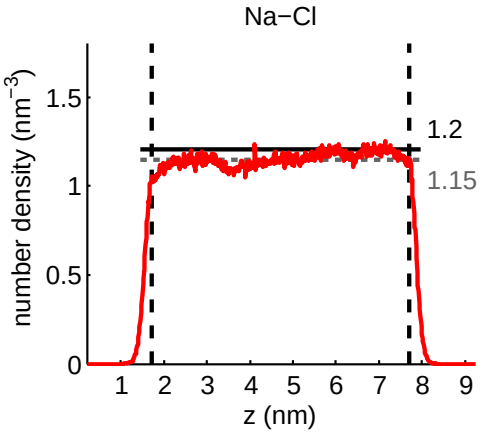

(c) Number density distribution ρ_N.

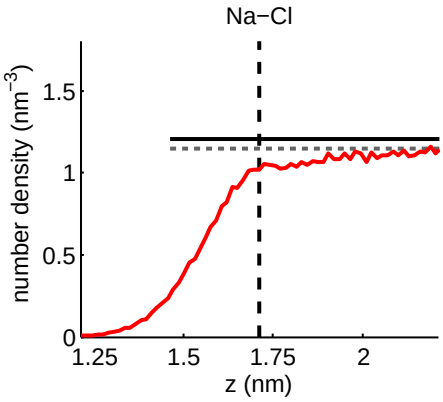

(d) Close-up of the ρ_N.

Figure B.2: **(NVT)** Summary of results obtained from an osmotic pressure calculation using membrane walls with a force constant k of 100 kJ/(mol·nm^2). 36 NaCl ion pairs are dissolved in 3072 SW10e water molecules and are confined in a 6 nm slab, resulting in a salt concentration of 0.95 M inside the ion domain. The volume of the box was kept constant after a 400 ps equilibration time in an NPT ensemble at 1 bar, namely a NVT ensemble was applied. Further results are shown in Tab. 4.14. The temperature is 298.15 K. The total duration of the simulation was 80 ns including 1 ns equilibration time. a) Block average of the osmotic pressure with 1 ns sampling time (blue line with asterisks) and running average of the osmotic pressure (red line). The horizontal lines mark the mean osmotic pressure (solid) and a ±5 % interval around it (grey dashed lines). b) Close-up of the histogram of the osmotic pressure. The bin at $\Pi = 0$ was not printed. The vertical dashed line marks the mean osmotic pressure. c) Number density distribution of ion species in the box. The vertical dashed line marks the position of the membrane. The horizontal line marks the position of the target concentration with 'hard' membrane walls (black solid), and of the actual concentration between the membrane walls (grey dashed line). d) Close-up of the number density distribution at the membrane wall.

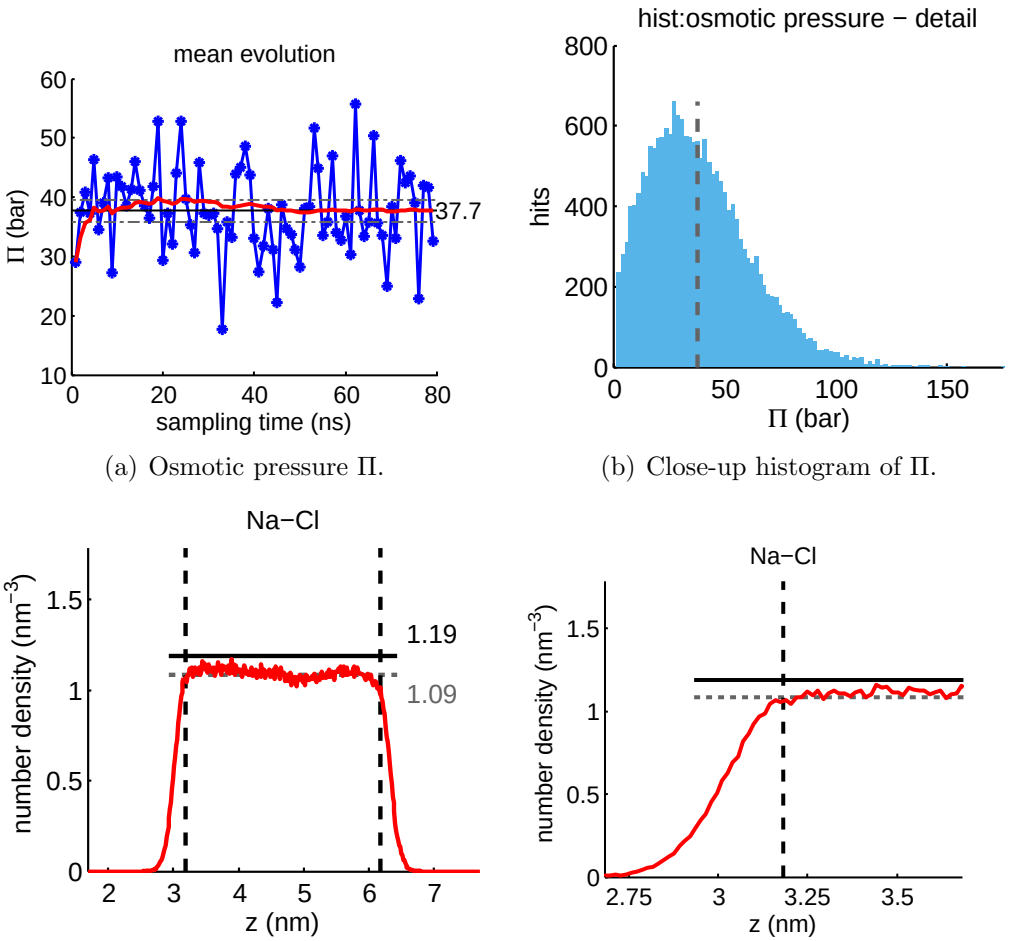

(a) Osmotic pressure Π.

(b) Close-up histogram of Π.

(c) Number density distribution ρ_N.

(d) Close-up of the ρ_N.

Figure B.3: **(small domain)** Summary of results obtained from an osmotic pressure calculation using membrane walls with a force constant k of 100 kJ/(mol·nm^2). 18 NaCl ion pairs are dissolved in 3072 SW10e water molecules and are confined in a 3 nm slab, resulting in a salt concentration of 0.9 M inside the ion domain. The box was allowed to change its size in z-direction to maintain the pressure, namely a NPAT ensemble was applied. Further results are shown in Tab. 4.14. The temperature is 298.15 K and the pressure 1 bar. The total duration of the simulation was 80 ns including 1 ns equilibration time. a) Block average of the osmotic pressure with 1 ns sampling time (blue line with asterisks) and running average of the osmotic pressure (red line). The horizontal lines mark the mean osmotic pressure (solid) and a ±5 % interval around it (grey dashed lines). b) Close-up of the histogram of the osmotic pressure. The bin at $\Pi = 0$ was not printed. The vertical dashed line marks the mean osmotic pressure. c) Number density distribution of ion species in the box. The vertical dashed line marks the position of the membrane. The horizontal line marks the position of the target concentration with 'hard' membrane walls (black solid), and of the actual concentration between the membrane walls (grey dashed line). d) Close-up of the number density distribution at the membrane wall.

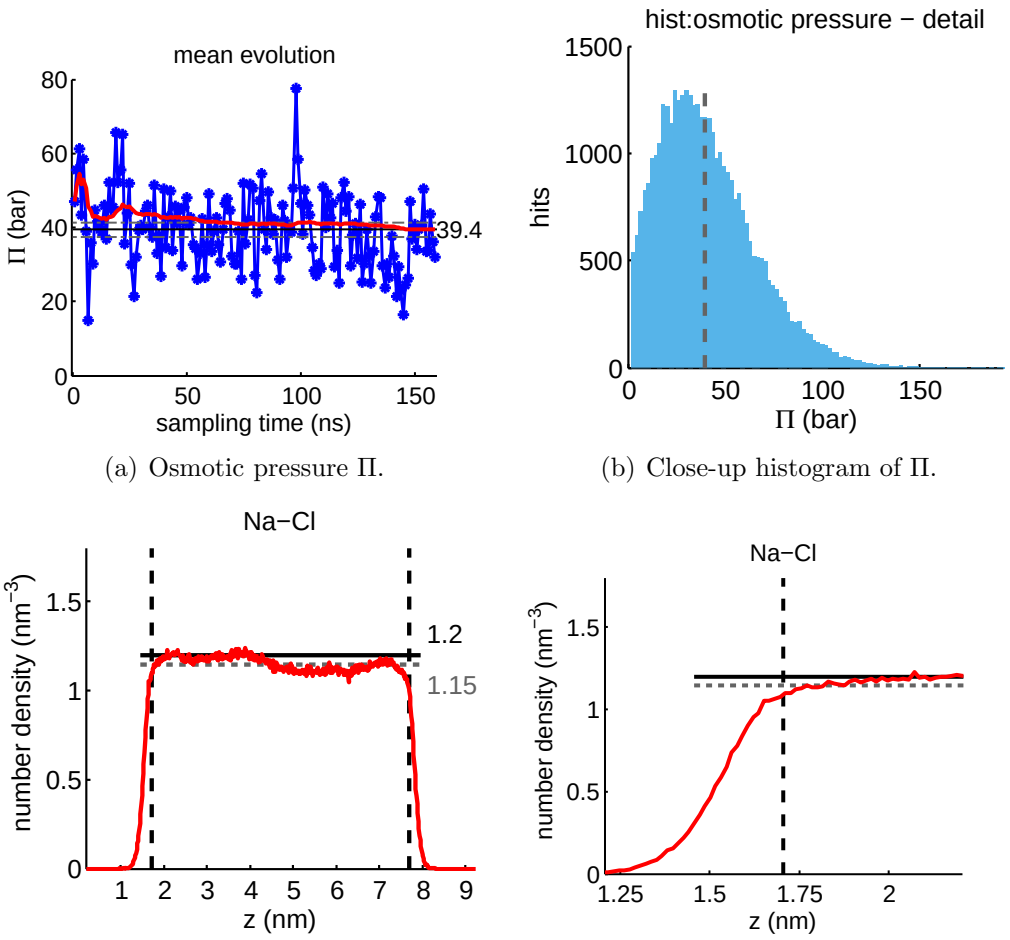

(a) Osmotic pressure Π.

(b) Close-up histogram of Π.

(c) Number density distribution ρ_N.

(d) Close-up of the ρ_N.

Figure B.4: **(coupled ions)** Summary of results obtained from an osmotic pressure calculation using membrane walls with a force constant k of 100 kJ/(mol·nm^2). The ions were coupled to the thermostat. 36 NaCl ion pairs are dissolved in 3072 SW10e water molecules and are confined in a 6 nm slab, resulting in a salt concentration of 0.95 M inside the ion domain. The box was allowed to change its size in z-direction to maintain the pressure, namely a NPAT ensemble was applied. Further results are shown in Tab. 4.14. The temperature is 298.15 K and the pressure 1 bar. The total duration of the simulation was 160 ns including 1 ns equilibration time. a) Block average of the osmotic pressure with 1 ns sampling time (blue line with asterisks) and running average of the osmotic pressure (red line). The horizontal lines mark the mean osmotic pressure (solid) and a ±5 % interval around it (grey dashed lines). b) Close-up of the histogram of the osmotic pressure. The bin at $\Pi = 0$ was not printed. The vertical dashed line marks the mean osmotic pressure. c) Number density distribution of ion species in the box. The vertical dashed line marks the position of the membrane. The horizontal line marks the position of the target concentration with 'hard' membrane walls (black solid), and of the actual concentration between the membrane walls (grey dashed line). d) Close-up of the number density distribution at the membrane wall.

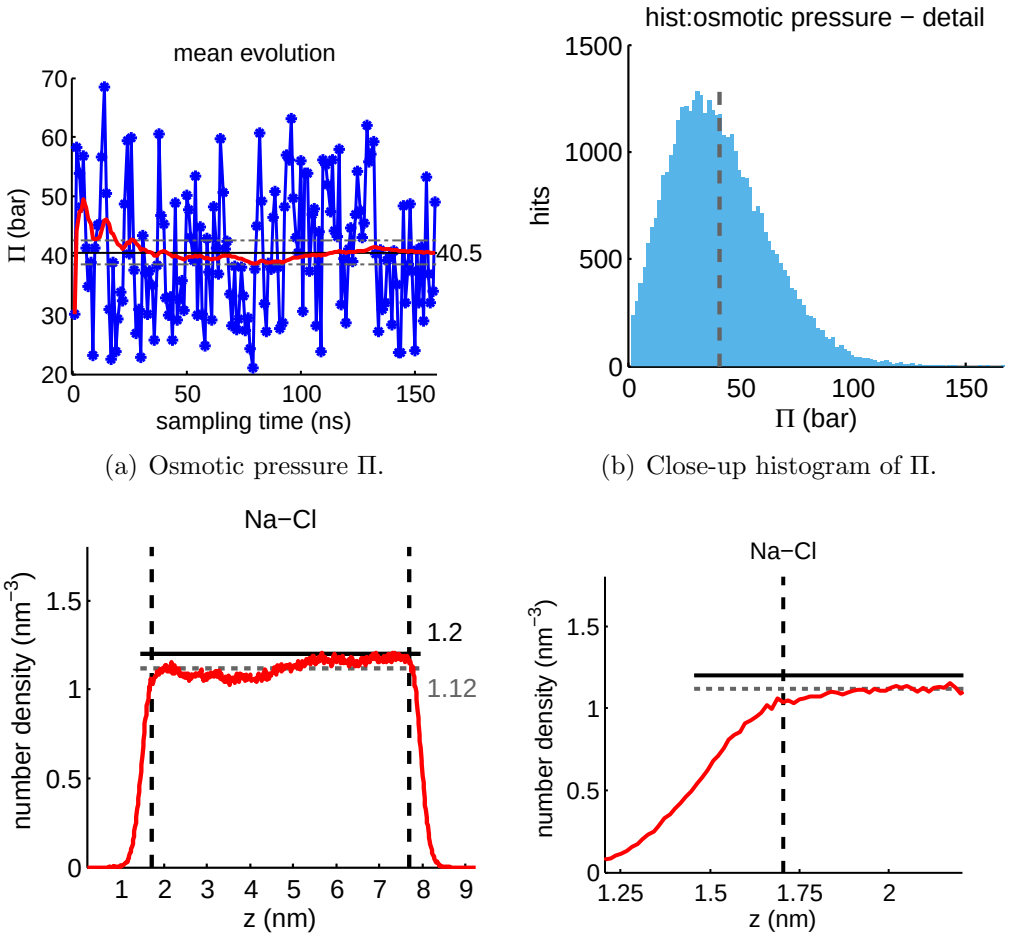

(a) Osmotic pressure Π.

(b) Close-up histogram of Π.

(c) Number density distribution ρ_N.

(d) Close-up of the ρ_N.

Figure B.5: **(k=50 kJ/(mol·nm^2))** Summary of results obtained from an osmotic pressure calculation using membrane walls with a force constant k of 200 kJ/(mol·nm^2). 36 NaCl ion pairs are dissolved in 3072 SW10e water molecules and are confined in a 6 nm slab, resulting in a salt concentration of 0.93 M inside the ion domain. The box was allowed to change its size in z-direction to maintain the pressure, namely a NPAT ensemble was applied. Further results are shown in Tab. 4.15. The temperature is 298.15 K and the pressure 1 bar. The total duration of the simulation was 160 ns including 1 ns equilibration time. a) Block average of the osmotic pressure with 1 ns sampling time (blue line with asterisks) and running average of the osmotic pressure (red line). The horizontal lines mark the mean osmotic pressure (solid) and a ±5 % interval around it (grey dashed lines). b) Close-up of the histogram of the osmotic pressure. The bin at $\Pi = 0$ was not printed. The vertical dashed line marks the mean osmotic pressure. c) Number density distribution of ion species in the box. The vertical dashed line marks the position of the membrane. The horizontal line marks the position of the target concentration with 'hard' membrane walls (black solid), and of the actual concentration between the membrane walls (grey dashed line). d) Close-up of the number density distribution at the membrane wall.

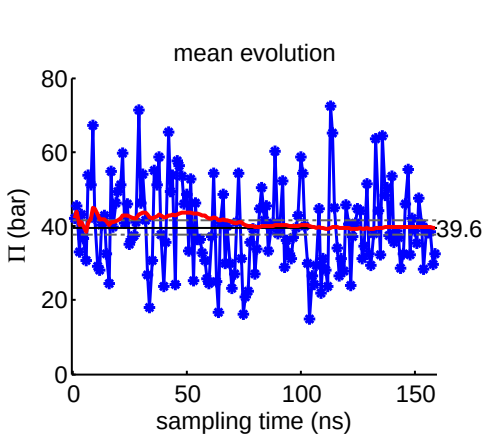

(a) Osmotic pressure Π.

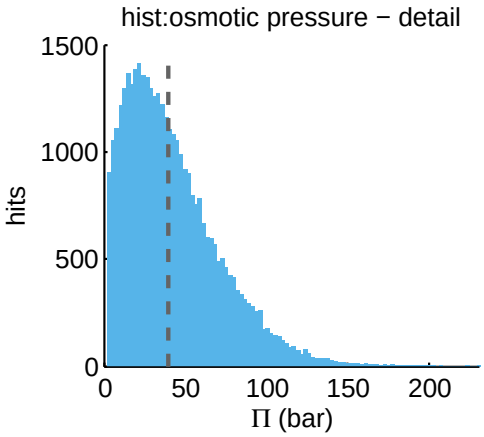

(b) Close-up histogram of Π.

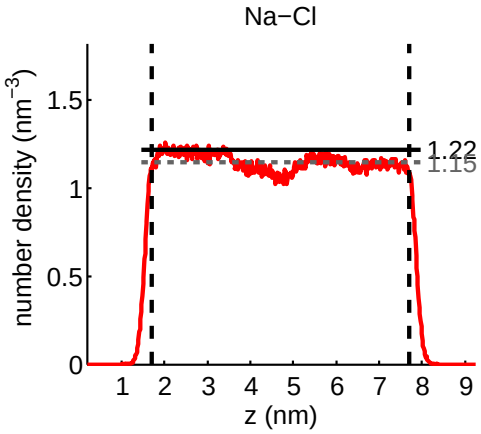

(c) Number density distribution ρ_N.

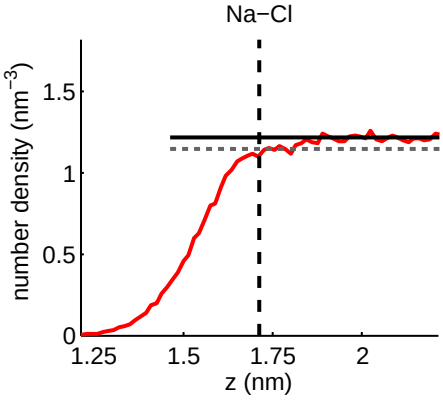

(d) Close-up of the ρ_N.

Figure B.6: **(k=100 kJ/(mol·nm^2))** Summary of results obtained from an osmotic pressure calculation using membrane walls with a force constant k of 100 kJ/(mol·nm^2). 36 NaCl ion pairs are dissolved in 3072 SW10e water molecules and are confined in a 6 nm slab, resulting in a salt concentration of 0.95 M inside the ion domain. The box was allowed to change its size in z-direction to maintain the pressure, namely a NPAT ensemble was applied. Further results are shown in Tab. 4.15. The temperature is 298.15 K and the pressure 1 bar. The total duration of the simulation was 160 ns including 1 ns equilibration time. a) Block average of the osmotic pressure with 1 ns sampling time (blue line with asterisks) and running average of the osmotic pressure (red line). The horizontal lines mark the mean osmotic pressure (solid) and a ±5 % interval around it (grey dashed lines). b) Close-up of the histogram of the osmotic pressure. The bin at $\Pi = 0$ was not printed. The vertical dashed line marks the mean osmotic pressure. c) Number density distribution of ion species in the box. The vertical dashed line marks the position of the membrane. The horizontal line marks the position of the target concentration with 'hard' membrane walls (black solid), and of the actual concentration between the membrane walls (grey dashed line). d) Close-up of the number density distribution at the membrane wall.

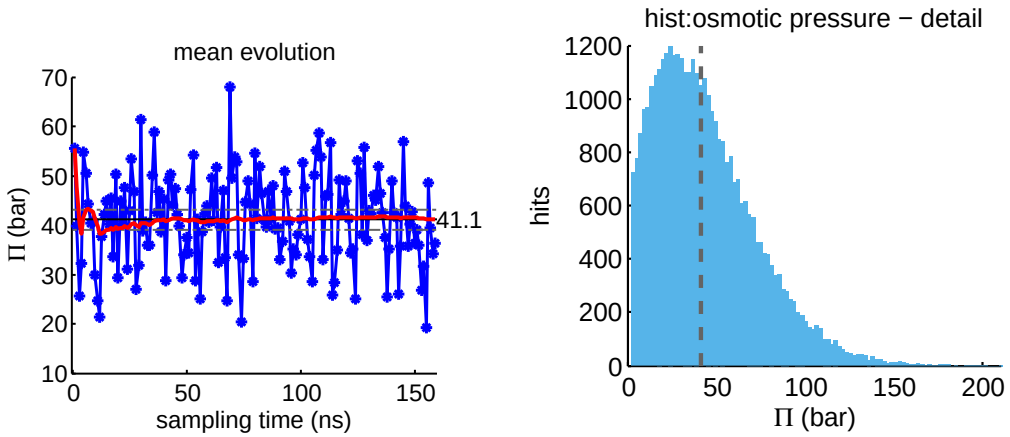

(a) Osmotic pressure Π.

(b) Close-up histogram of Π.

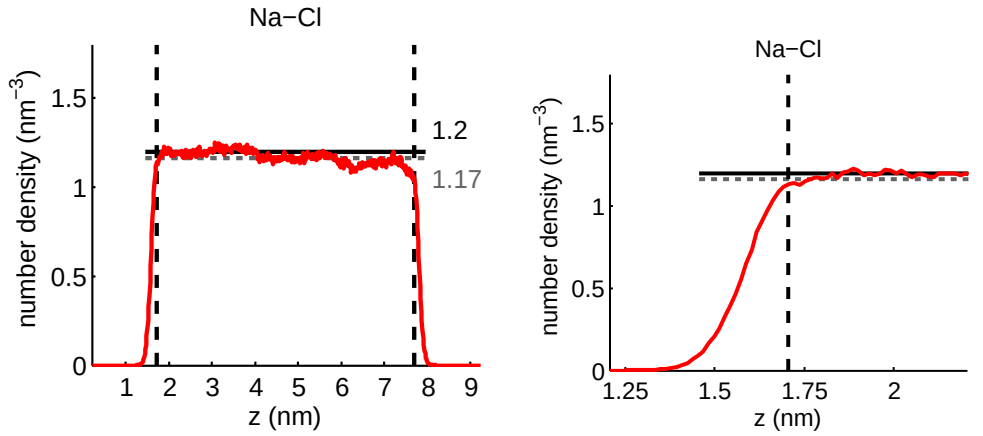

(c) Number density distribution ρ_N.

(d) Close-up of the ρ_N.

Figure B.7: **(k=200 kJ/(mol·nm^2))** Summary of results obtained from an osmotic pressure calculation using membrane walls with a force constant k of 200 kJ/(mol·nm^2). 36 NaCl ion pairs are dissolved in 3072 SW10e water molecules and are confined in a 6 nm slab, resulting in a salt concentration of 0.97 M inside the ion domain. The box was allowed to change its size in z-direction to maintain the pressure, namely a NPAT ensemble was applied. Further results are shown in Tab. 4.15. The temperature is 298.15 K and the pressure 1 bar. The total duration of the simulation was 160 ns including 1 ns equilibration time. a) Block average of the osmotic pressure with 1 ns sampling time (blue line with asterisks) and running average of the osmotic pressure (red line). The horizontal lines mark the mean osmotic pressure (solid) and a ±5 % interval around it (grey dashed lines). b) Close-up of the histogram of the osmotic pressure. The bin at $\Pi = 0$ was not printed. The vertical dashed line marks the mean osmotic pressure. c) Number density distribution of ion species in the box. The vertical dashed line marks the position of the membrane. The horizontal line marks the position of the target concentration with 'hard' membrane walls (black solid), and of the actual concentration between the membrane walls (grey dashed line). d) Close-up of the number density distribution at the membrane wall.

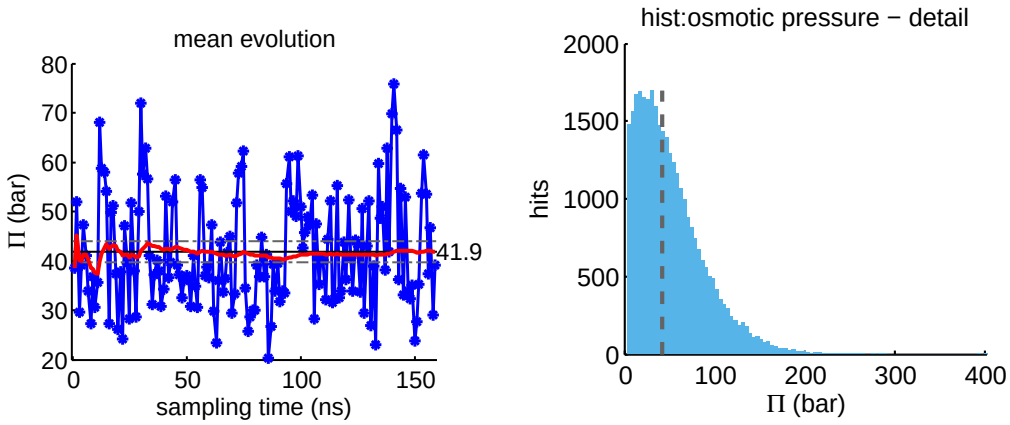

(a) Osmotic pressure Π.

(b) Close-up histogram of Π.

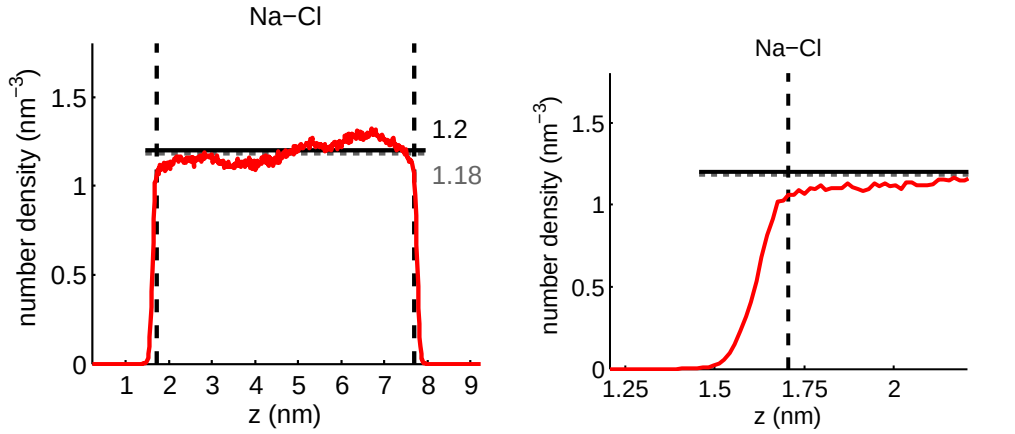

(c) Number density distribution ρ_N.

(d) Close-up of the ρ_N.

Figure B.8: **(k=500 kJ/(mol·nm^2))** Summary of results obtained from an osmotic pressure calculation using membrane walls with a force constant k of 500 kJ/(mol·nm^2). 36 NaCl ion pairs are dissolved in 3072 SW10e water molecules and are confined in a 6 nm slab, resulting in a salt concentration of 0.98 M inside the ion domain. The box was allowed to change its size in z-direction to maintain the pressure, namely a NPAT ensemble was applied. Further results are shown in Tab. 4.15. The temperature is 298.15 K and the pressure 1 bar. The total duration of the simulation was 160 ns including 1 ns equilibration time. a) Block average of the osmotic pressure with 1 ns sampling time (blue line with asterisks) and running average of the osmotic pressure (red line). The horizontal lines mark the mean osmotic pressure (solid) and a ±5 % interval around it (grey dashed lines). b) Close-up of the histogram of the osmotic pressure. The bin at $\Pi = 0$ was not printed. The vertical dashed line marks the mean osmotic pressure. c) Number density distribution of ion species in the box. The vertical dashed line marks the position of the membrane. The horizontal line marks the position of the target concentration with 'hard' membrane walls (black solid), and of the actual concentration between the membrane walls (grey dashed line). d) Close-up of the number density distribution at the membrane wall.

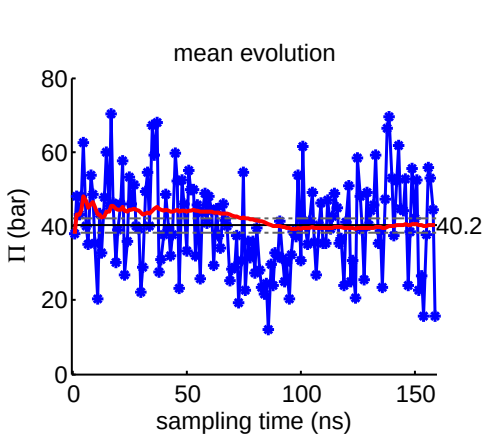

(a) Osmotic pressure Π.

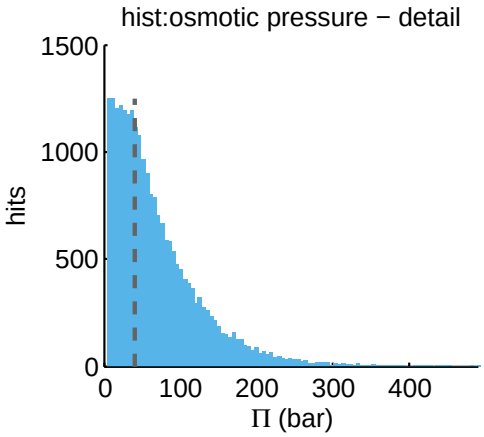

(b) Close-up histogram of Π.

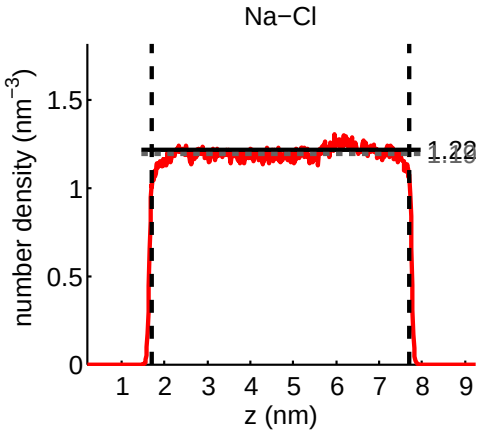

(c) Number density distribution ρ_N.

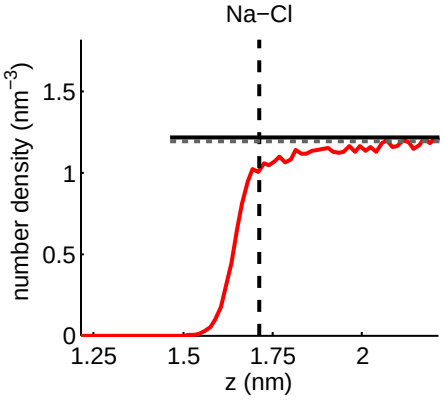

(d) Close-up of the ρ_N.

Figure B.9: **(k=1000 kJ/(mol·nm^2))** Summary of results obtained from an osmotic pressure calculation using membrane walls with a force constant k of 1'000 kJ/(mol·nm^2). 36 NaCl ion pairs are dissolved in 3072 SW10e water molecules and are confined in a 6 nm slab, resulting in a salt concentration of 0.99 M inside the ion domain. The box was allowed to change its size in z-direction to maintain the pressure, namely a NPAT ensemble was applied. Further results are shown in Tab. 4.15. The temperature is 298.15 K and the pressure 1 bar. The total duration of the simulation was 160 ns including 1 ns equilibration time. a) Block average of the osmotic pressure with 1 ns sampling time (blue line with asterisks) and running average of the osmotic pressure (red line). The horizontal lines mark the mean osmotic pressure (solid) and a ±5 % interval around it (grey dashed lines). b) Close-up of the histogram of the osmotic pressure. The bin at $\Pi = 0$ was not printed. The vertical dashed line marks the mean osmotic pressure. c) Number density distribution of ion species in the box. The vertical dashed line marks the position of the membrane. The horizontal line marks the position of the target concentration with 'hard' membrane walls (black solid), and of the actual concentration between the membrane walls (grey dashed line). d) Close-up of the number density distribution at the membrane wall.

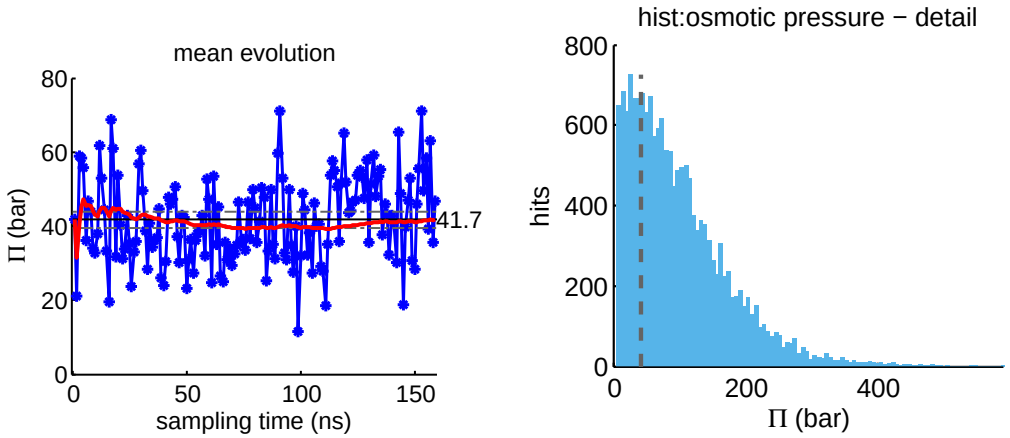

(a) Osmotic pressure Π.

(b) Close-up histogram of Π.

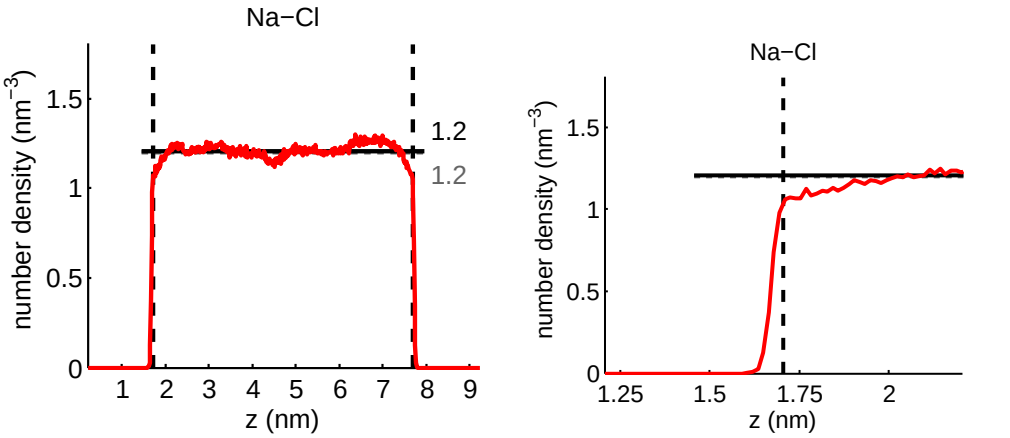

(c) Number density distribution ρ_N.

(d) Close-up of the ρ_N.

Figure B.10: **(k=5000 kJ/(mol·nm^2))** Summary of results obtained from an osmotic pressure calculation using membrane walls with a force constant k of 5000 kJ/(mol·nm^2). 36 NaCl ion pairs are dissolved in 3072 SW10e water molecules and are confined in a 6 nm slab, resulting in a salt concentration of 0.99 M inside the ion domain. The box was allowed to change its size in z-direction to maintain the pressure, namely a NPAT ensemble was applied. Further results are shown in Tab. 4.15. The temperature is 298.15 K and the pressure 1 bar. The total duration of the simulation was 160 ns including 1 ns equilibration time. a) Block average of the osmotic pressure with 1 ns sampling time (blue line with asterisks) and running average of the osmotic pressure (red line). The horizontal lines mark the mean osmotic pressure (solid) and a ±5 % interval around it (grey dashed lines). b) Close-up of the histogram of the osmotic pressure. The bin at $\Pi = 0$ was not printed. The vertical dashed line marks the mean osmotic pressure. c) Number density distribution of ion species in the box. The vertical dashed line marks the position of the membrane. The horizontal line marks the position of the target concentration with 'hard' membrane walls (black solid), and of the actual concentration between the membrane walls (grey dashed line). d) Close-up of the number density distribution at the membrane wall.

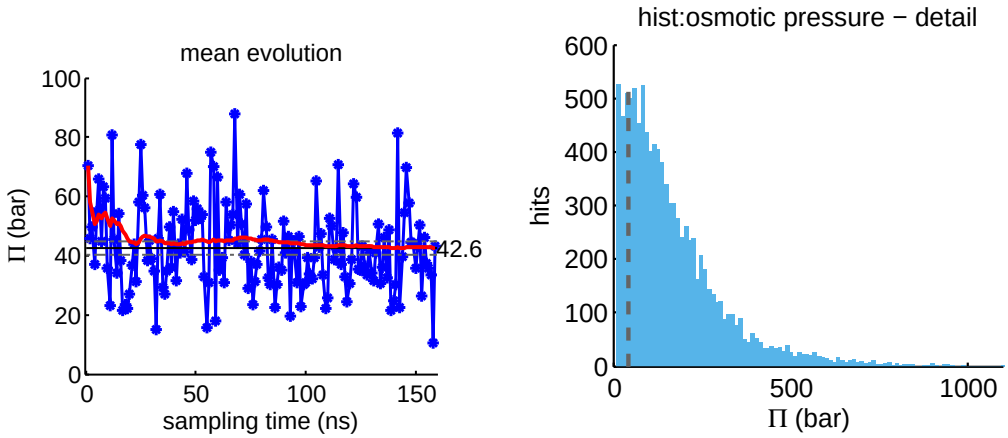

(a) Osmotic pressure Π.

(b) Close-up histogram of Π.

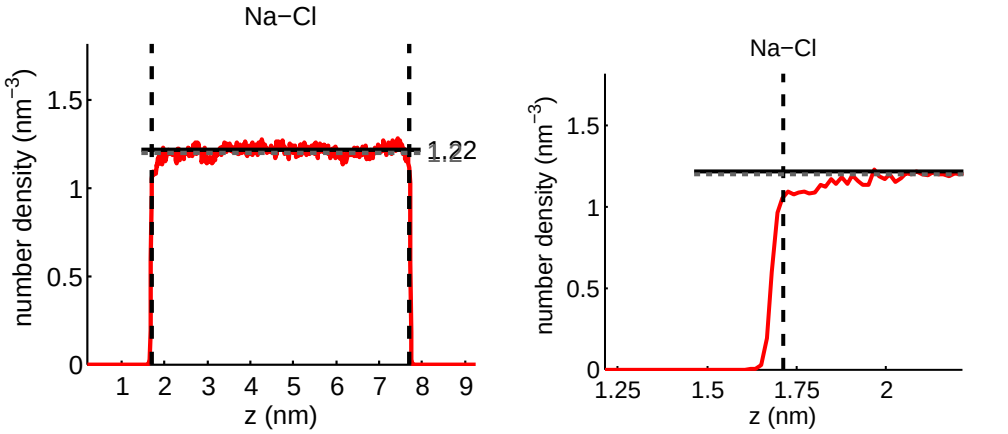

(c) Number density distribution ρ_N.

(d) Close-up of the ρ_N.

Figure B.11: **(k=10000 kJ/(mol·nm^2))** Summary of results obtained from an osmotic pressure calculation using membrane walls with a force constant k of 10'000 kJ/(mol·nm^2). 36 NaCl ion pairs are dissolved in 3072 SW10e water molecules and are confined in a 6 nm slab, resulting in a salt concentration of 1.00 M inside the ion domain. The box was allowed to change its size in z-direction to maintain the pressure, namely a NPAT ensemble was applied. Further results are shown in Tab. 4.15. The temperature is 298.15 K and the pressure 1 bar. The total duration of the simulation was 160 ns including 1 ns equilibration time. a) Block average of the osmotic pressure with 1 ns sampling time (blue line with asterisks) and running average of the osmotic pressure (red line). The horizontal lines mark the mean osmotic pressure (solid) and a ±5 % interval around it (grey dashed lines). b) Close-up of the histogram of the osmotic pressure. The bin at $\Pi = 0$ was not printed. The vertical dashed line marks the mean osmotic pressure. c) Number density distribution of ion species in the box. The vertical dashed line marks the position of the membrane. The horizontal line marks the position of the target concentration with 'hard' membrane walls (black solid), and of the actual concentration between the membrane walls (grey dashed line). d) Close-up of the number density distribution at the membrane wall.

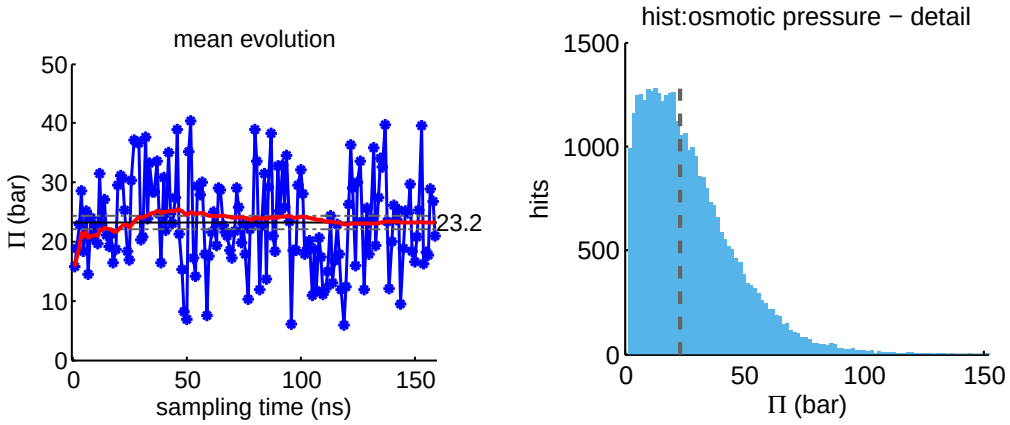

(a) Osmotic pressure Π.

(b) Close-up histogram of Π.

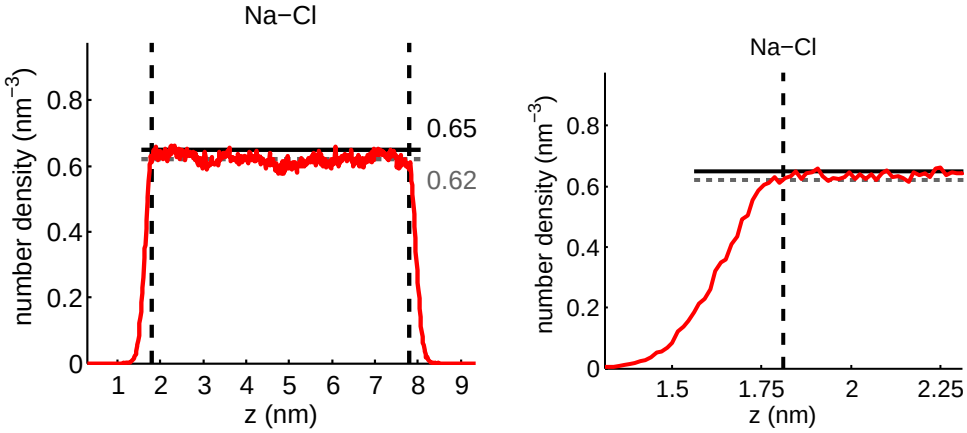

(c) Number density distribution ρ_N.

(d) Close-up of the ρ_N.

Figure B.12: **(0.5 M)** Summary of results obtained from an osmotic pressure calculation using membrane walls with a force constant k of 100 kJ/(mol·nm^2). 19 NaCl ion pairs are dissolved in 3072 SPC/E water molecules and are confined in a 6 nm slab, resulting in a salt concentration of 0.5 M inside the ion domain. The volume of the box was kept constant after a 300 ps equilibration time in a NPAT ensemble at 1 bar, namely a NVT ensemble was applied. Further results are shown in Tab. 4.16. The temperature is 298.15 K. The total duration of the simulation was 160 ns including 1 ns equilibration time. a) Block average of the osmotic pressure with 1 ns sampling time (blue line with asterisks) and running average of the osmotic pressure (red line). The horizontal lines mark the mean osmotic pressure (solid) and a ±5 % interval around it (grey dashed lines). b) Close-up of the histogram of the osmotic pressure. The bin at $\Pi = 0$ was not printed. The vertical dashed line marks the mean osmotic pressure. c) Number density distribution of ion species in the box. The vertical dashed lines mark the position of the membrane. The horizontal lines mark the position of the target concentration with 'hard' membrane walls (black solid), and of the actual concentration between the membrane walls (grey dashed line). d) Close-up of the number density distribution at the membrane wall.

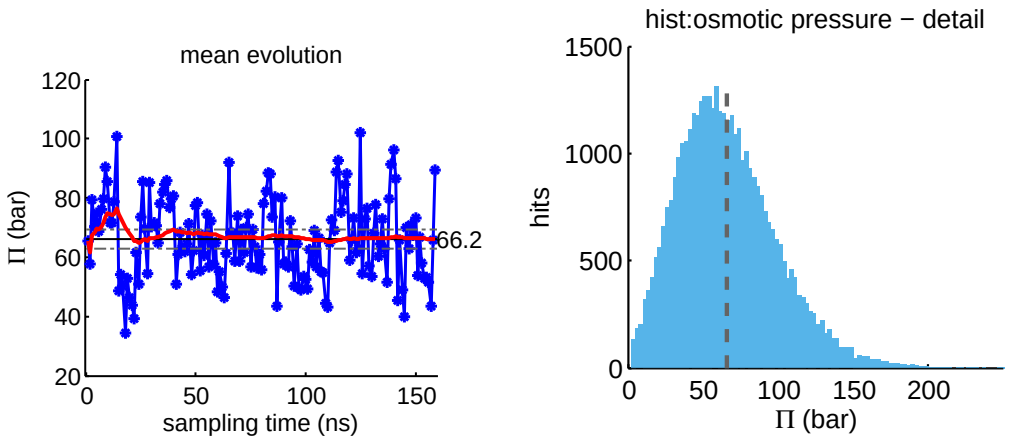

(a) Osmotic pressure Π.

(b) Close-up histogram of Π.

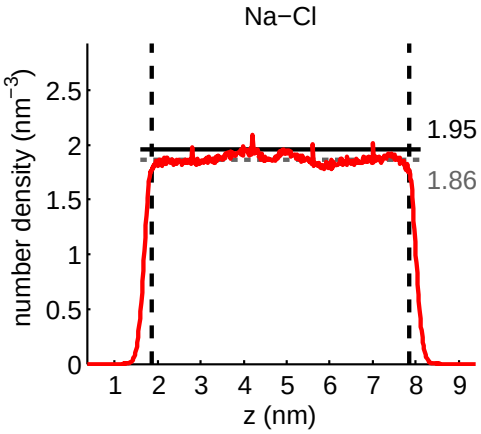

(c) Number density distribution ρ_N.

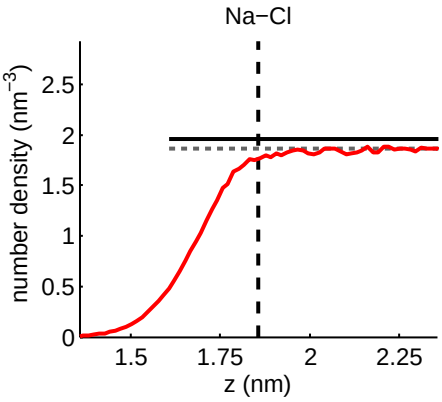

(d) Close-up of the ρ_N.

Figure B.13: **(1.5 M)** Summary of results obtained from an osmotic pressure calculation using membrane walls with a force constant k of 100 kJ/(mol·nm^2). 57 NaCl ion pairs are dissolved in 3072 SPC/E water molecules and are confined in a 6 nm slab, resulting in a salt concentration of 1.5 M inside the ion domain. The volume of the box was kept constant after a 300 ps equilibration time in a NPAT ensemble at 1 bar, namely a NVT ensemble was applied. Further results are shown in Tab. 4.16. The temperature is 298.15 K. The total duration of the simulation was 160 ns including 1 ns equilibration time. a) Block average of the osmotic pressure with 1 ns sampling time (blue line with asterisks) and running average of the osmotic pressure (red line). The horizontal lines mark the mean osmotic pressure (solid) and a ±5 % interval around it (grey dashed lines). b) Close-up of the histogram of the osmotic pressure. The bin at $\Pi = 0$ was not printed. The vertical dashed line marks the mean osmotic pressure. c) Number density distribution of ion species in the box. The vertical dashed lines mark the position of the membrane. The horizontal lines mark the position of the target concentration with 'hard' membrane walls (black solid), and of the actual concentration between the membrane walls (grey dashed line). d) Close-up of the number density distribution at the membrane wall.

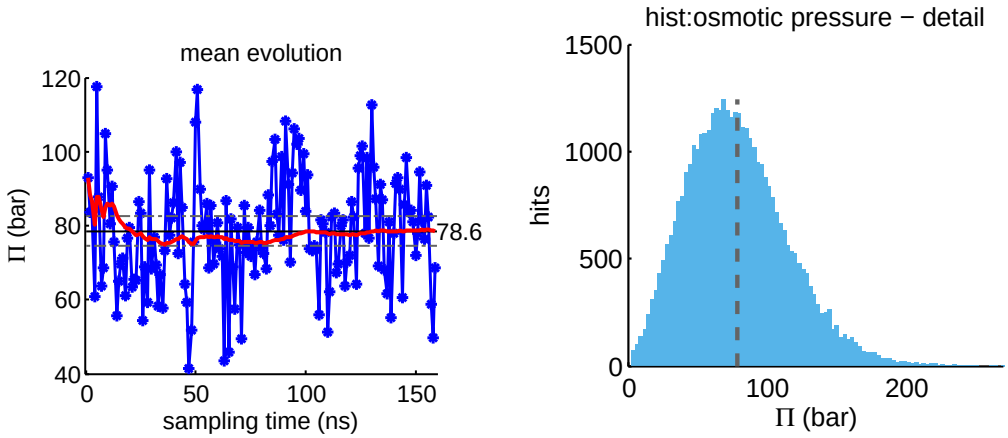

(a) Osmotic pressure Π.

(b) Close-up histogram of Π.

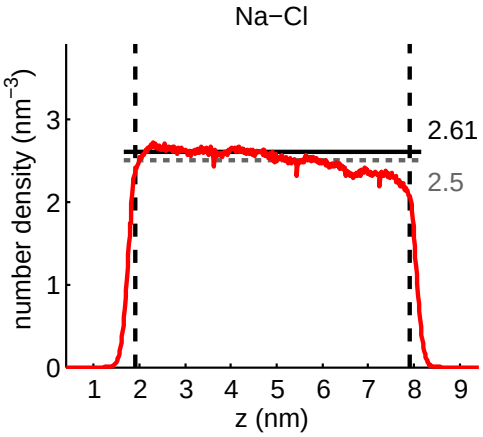

(c) Number density distribution ρ_N.

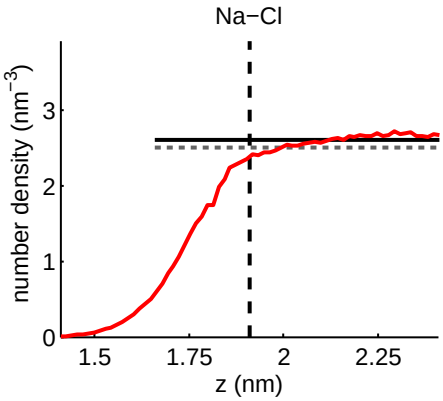

(d) Close-up of the ρ_N.

Figure B.14: **(2.0 M)** Summary of results obtained from an osmotic pressure calculation using membrane walls with a force constant k of 100 kJ/(mol·nm^2). 76 NaCl ion pairs are dissolved in 3072 SPC/E water molecules and are confined in a 6 nm slab, resulting in a salt concentration of 2.1 M inside the ion domain. The volume of the box was kept constant after a 300 ps equilibration time in a NPAT ensemble at 1 bar, namely a NVT ensemble was applied. Further results are shown in Tab. 4.16. The temperature is 298.15 K. The total duration of the simulation was 160 ns including 1 ns equilibration time. a) Block average of the osmotic pressure with 1 ns sampling time (blue line with asterisks) and running average of the osmotic pressure (red line). The horizontal lines mark the mean osmotic pressure (solid) and a ±5 % interval around it (grey dashed lines). b) Close-up of the histogram of the osmotic pressure. The bin at $\Pi = 0$ was not printed. The vertical dashed line marks the mean osmotic pressure. c) Number density distribution of ion species in the box. The vertical dashed lines mark the position of the membrane. The horizontal lines mark the position of the target concentration with 'hard' membrane walls (black solid), and of the actual concentration between the membrane walls (grey dashed line). d) Close-up of the number density distribution at the membrane wall.

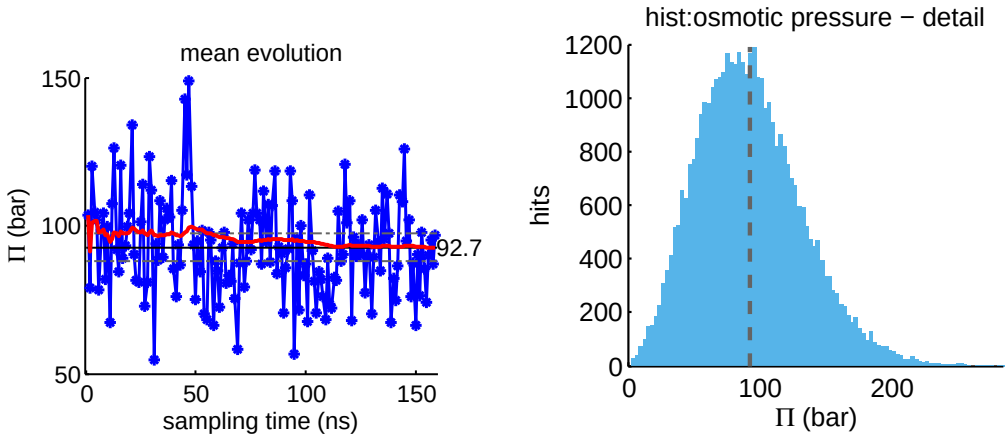

(a) Osmotic pressure Π.

(b) Close-up histogram of Π.

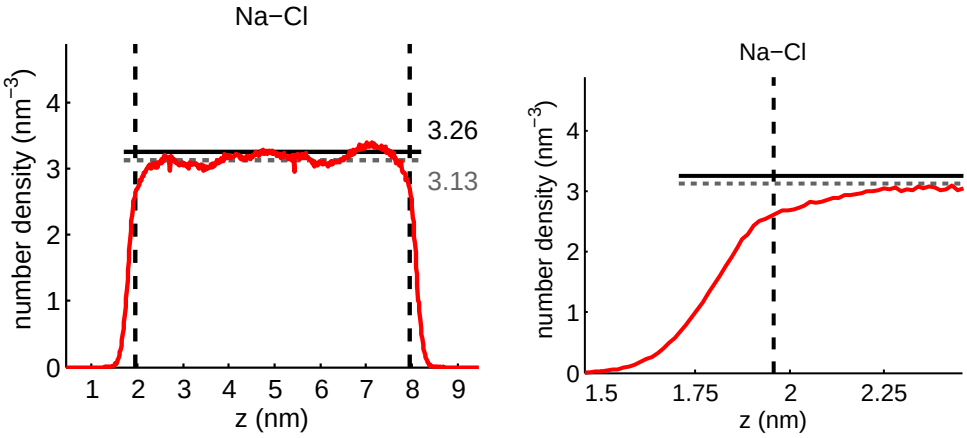

(c) Number density distribution ρ_N.

(d) Close-up of the ρ_N.

Figure B.15: **(2.5 M)** Summary of results obtained from an osmotic pressure calculation using membrane walls with a force constant k of 100 kJ/(mol·nm^2). 95 NaCl ion pairs are dissolved in 3072 SPC/E water molecules and are confined in a 6 nm slab, resulting in a salt concentration of 2.6 M inside the ion domain. The volume of the box was kept constant after a 300 ps equilibration time in a NPAT ensemble at 1 bar, namely a NVT ensemble was applied. Further results are shown in Tab. 4.16. The temperature is 298.15 K. The total duration of the simulation was 160 ns including 1 ns equilibration time. a) Block average of the osmotic pressure with 1 ns sampling time (blue line with asterisks) and running average of the osmotic pressure (red line). The horizontal lines mark the mean osmotic pressure (solid) and a ±5 % interval around it (grey dashed lines). b) Close-up of the histogram of the osmotic pressure. The bin at $\Pi = 0$ was not printed. The vertical dashed line marks the mean osmotic pressure. c) Number density distribution of ion species in the box. The vertical dashed lines mark the position of the membrane. The horizontal lines mark the position of the target concentration with 'hard' membrane walls (black solid), and of the actual concentration between the membrane walls (grey dashed line). d) Close-up of the number density distribution at the membrane wall.

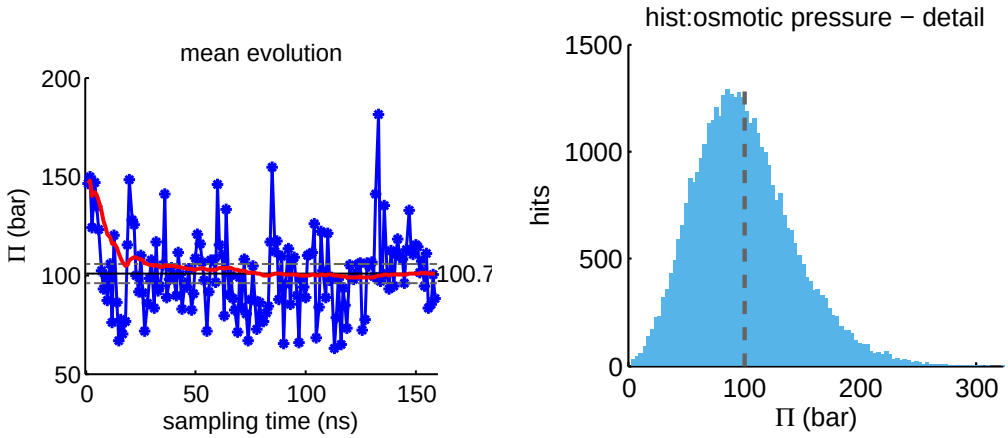

(a) Osmotic pressure Π.

(b) Close-up histogram of Π.

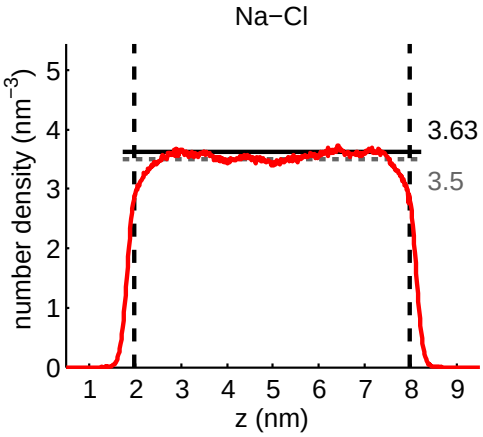

(c) Number density distribution ρ_N.

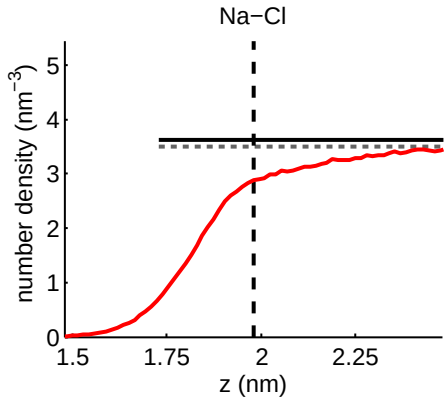

(d) Close-up of the ρ_N.

Figure B.16: **(2.8 M)** Summary of results obtained from an osmotic pressure calculation using membrane walls with a force constant k of 100 kJ/(mol·nm^2). 106 NaCl ion pairs are dissolved in 3072 SPC/E water molecules and are confined in a 6 nm slab, resulting in a salt concentration of 2.9 M inside the ion domain. The volume of the box was kept constant after a 300 ps equilibration time in a NPAT ensemble at 1 bar, namely a NVT ensemble was applied. Further results are shown in Tab. 4.16. The temperature is 298.15 K. The total duration of the simulation was 160 ns including 1 ns equilibration time. a) Block average of the osmotic pressure with 1 ns sampling time (blue line with asterisks) and running average of the osmotic pressure (red line). The horizontal lines mark the mean osmotic pressure (solid) and a ±5 % interval around it (grey dashed lines). b) Close-up of the histogram of the osmotic pressure. The bin at $\Pi = 0$ was not printed. The vertical dashed line marks the mean osmotic pressure. c) Number density distribution of ion species in the box. The vertical dashed lines mark the position of the membrane. The horizontal lines mark the position of the target concentration with 'hard' membrane walls (black solid), and of the actual concentration between the membrane walls (grey dashed line). d) Close-up of the number density distribution at the membrane wall.

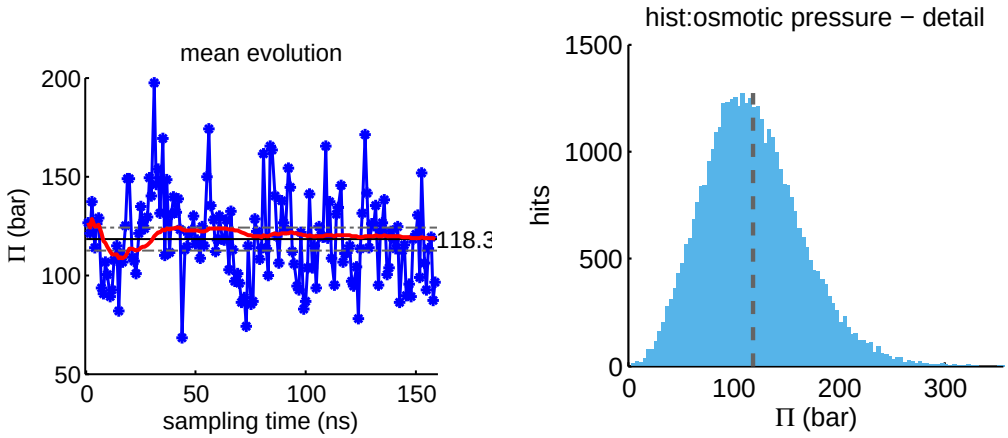

(a) Osmotic pressure Π.

(b) Close-up histogram of Π.

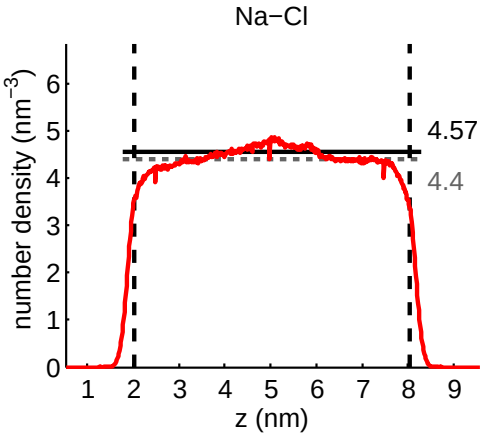

(c) Number density distribution ρ_N.

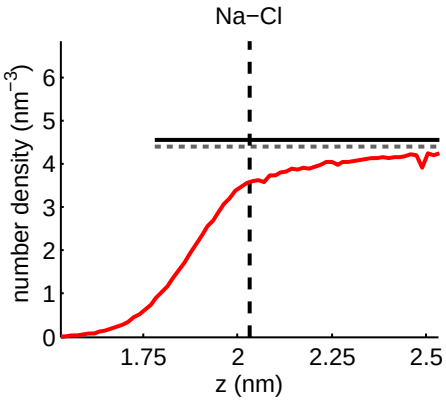

(d) Close-up of the ρ_N.

Figure B.17: **(3.5 M)** Summary of results obtained from an osmotic pressure calculation using membrane walls with a force constant k of 100 kJ/(mol·nm^2). 133 NaCl ion pairs are dissolved in 3072 SPC/E water molecules and are confined in a 6 nm slab, resulting in a salt concentration of 3.7 M inside the ion domain. The volume of the box was kept constant after a 300 ps equilibration time in a NPAT ensemble at 1 bar, namely a NVT ensemble was applied. Further results are shown in Tab. 4.16. The temperature is 298.15 K. The total duration of the simulation was 160 ns including 1 ns equilibration time. a) Block average of the osmotic pressure with 1 ns sampling time (blue line with asterisks) and running average of the osmotic pressure (red line). The horizontal lines mark the mean osmotic pressure (solid) and a ±5 % interval around it (grey dashed lines). b) Close-up of the histogram of the osmotic pressure. The bin at $\Pi = 0$ was not printed. The vertical dashed line marks the mean osmotic pressure. c) Number density distribution of ion species in the box. The vertical dashed lines mark the position of the membrane. The horizontal lines mark the position of the target concentration with 'hard' membrane walls (black solid), and of the actual concentration between the membrane walls (grey dashed line). d) Close-up of the number density distribution at the membrane wall.

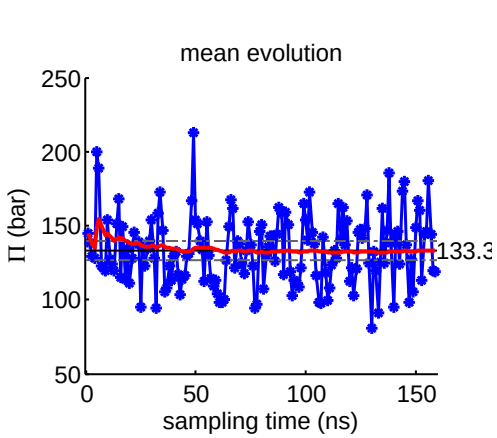

(a) Osmotic pressure Π.

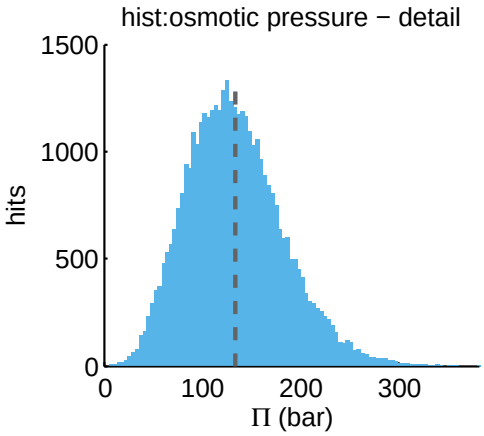

(b) Close-up histogram of Π.

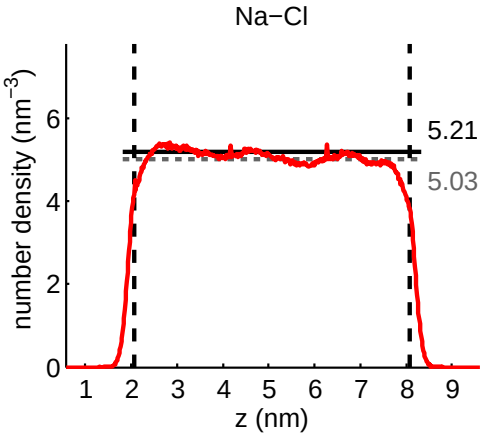

(c) Number density distribution ρ_N.

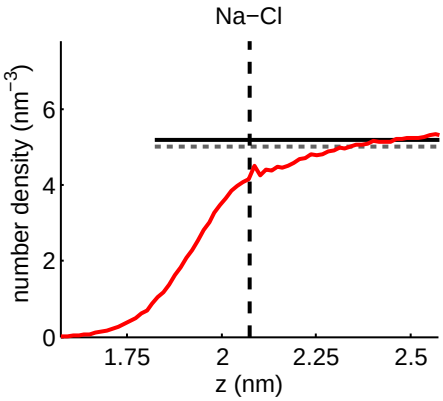

(d) Close-up of the ρ_N.

Figure B.18: **(4.0 M)** Summary of results obtained from an osmotic pressure calculation using membrane walls with a force constant k of 100 kJ/(mol·nm^2). 152 NaCl ion pairs are dissolved in 3072 SPC/E water molecules and are confined in a 6 nm slab, resulting in a salt concentration of 4.2 M inside the ion domain. The volume of the box was kept constant after a 300 ps equilibration time in a NPAT ensemble at 1 bar, namely a NVT ensemble was applied. Further results are shown in Tab. 4.16. The temperature is 298.15 K. The total duration of the simulation was 160 ns including 1 ns equilibration time. a) Block average of the osmotic pressure with 1 ns sampling time (blue line with asterisks) and running average of the osmotic pressure (red line). The horizontal lines mark the mean osmotic pressure (solid) and a ±5 % interval around it (grey dashed lines). b) Close-up of the histogram of the osmotic pressure. The bin at $\Pi = 0$ was not printed. The vertical dashed line marks the mean osmotic pressure. c) Number density distribution of ion species in the box. The vertical dashed lines mark the position of the membrane. The horizontal lines mark the position of the target concentration with 'hard' membrane walls (black solid), and of the actual concentration between the membrane walls (grey dashed line). d) Close-up of the number density distribution at the membrane wall.

B.2 Osmotic Pressure - $\alpha_{\mathrm{Cl}} \neq 2.0 \cdot 10^{-3}\mathrm{nm}^3$

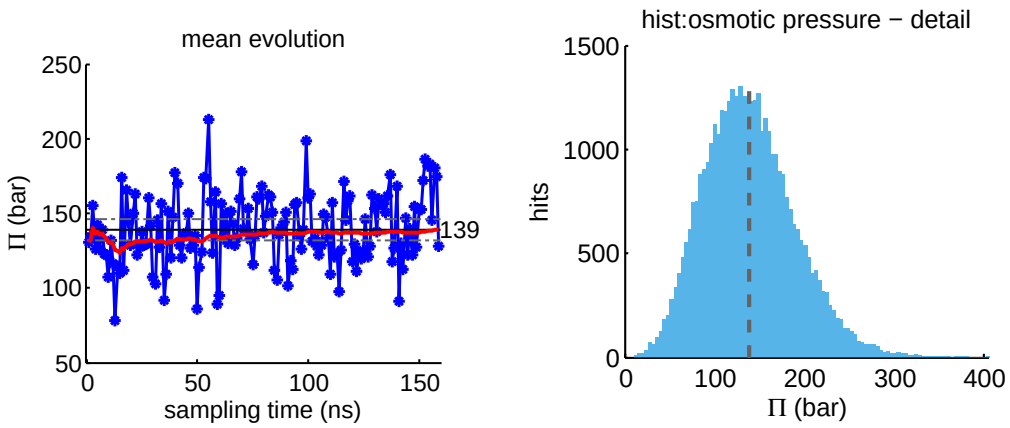

(a) Osmotic pressure Π.

(b) Close-up histogram of Π.

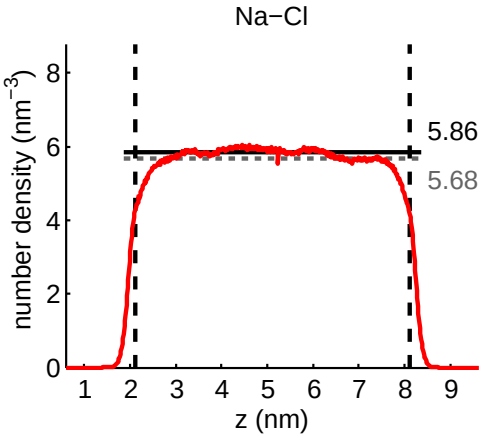

(c) Number density distribution ρ_N.

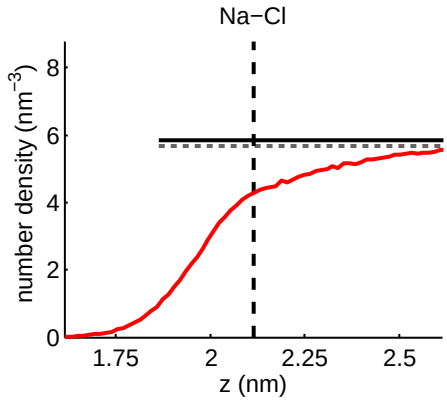

(d) Close-up of the ρ_N.

Figure B.19: **(4.5 M)** Summary of results obtained from an osmotic pressure calculation using membrane walls with a force constant k of 100 kJ/(mol·nm^2). 171 NaCl ion pairs are dissolved in 3072 SPC/E water molecules and are confined in a 6 nm slab, resulting in a salt concentration of 4.7 M inside the ion domain. The volume of the box was kept constant after a 300 ps equilibration time in a NPAT ensemble at 1 bar, namely a NVT ensemble was applied. Further results are shown in Tab. 4.16. The temperature is 298.15 K. The total duration of the simulation was 160 ns including 1 ns equilibration time. a) Block average of the osmotic pressure with 1 ns sampling time (blue line with asterisks) and running average of the osmotic pressure (red line). The horizontal lines mark the mean osmotic pressure (solid) and a ±5 % interval around it (grey dashed lines). b) Close-up of the histogram of the osmotic pressure. The bin at $\Pi = 0$ was not printed. The vertical dashed line marks the mean osmotic pressure. c) Number density distribution of ion species in the box. The vertical dashed lines mark the position of the membrane. The horizontal lines mark the position of the target concentration with 'hard' membrane walls (black solid), and of the actual concentration between the membrane walls (grey dashed line). d) Close-up of the number density distribution at the membrane wall.

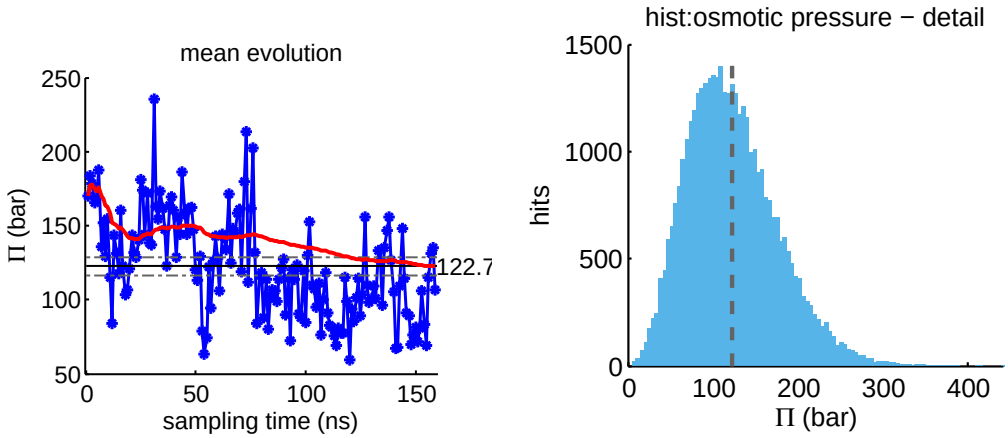

(a) Osmotic pressure Π.

(b) Close-up histogram of Π.

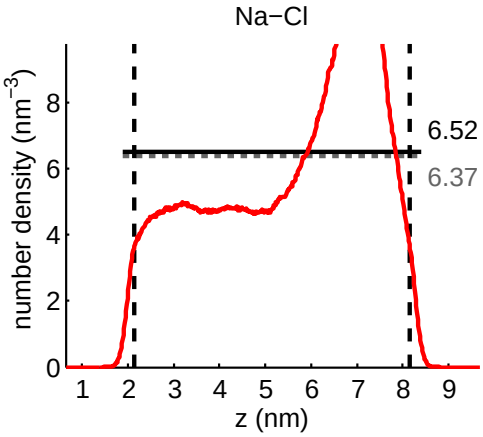

(c) Number density distribution ρ_N.

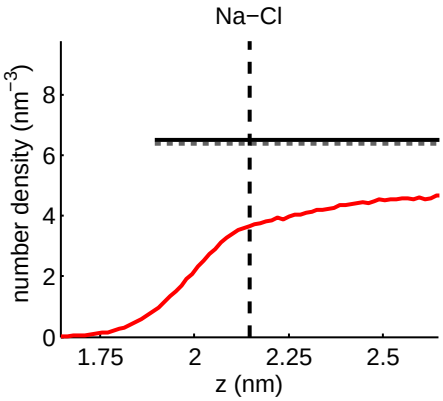

(d) Close-up of the ρ_N.

Figure B.20: **(5.0 M)** Summary of results obtained from an osmotic pressure calculation using membrane walls with a force constant k of 100 kJ/(mol·nm^2). 190 NaCl ion pairs are dissolved in 3072 SPC/E water molecules and are confined in a 6 nm slab, resulting in a salt concentration of 5.3 M inside the ion domain. The volume of the box was kept constant after a 300 ps equilibration time in a NPAT ensemble at 1 bar, namely a NVT ensemble was applied. Further results are shown in Tab. 4.16. The temperature is 298.15 K. The total duration of the simulation was 160 ns including 1 ns equilibration time. a) Block average of the osmotic pressure with 1 ns sampling time (blue line with asterisks) and running average of the osmotic pressure (red line). The horizontal lines mark the mean osmotic pressure (solid) and a ±5 % interval around it (grey dashed lines). b) Close-up of the histogram of the osmotic pressure. The bin at $\Pi = 0$ was not printed. The vertical dashed line marks the mean osmotic pressure. c) Number density distribution of ion species in the box. The vertical dashed lines mark the position of the membrane. The horizontal lines mark the position of the target concentration with 'hard' membrane walls (black solid), and of the actual concentration between the membrane walls (grey dashed line). d) Close-up of the number density distribution at the membrane wall.

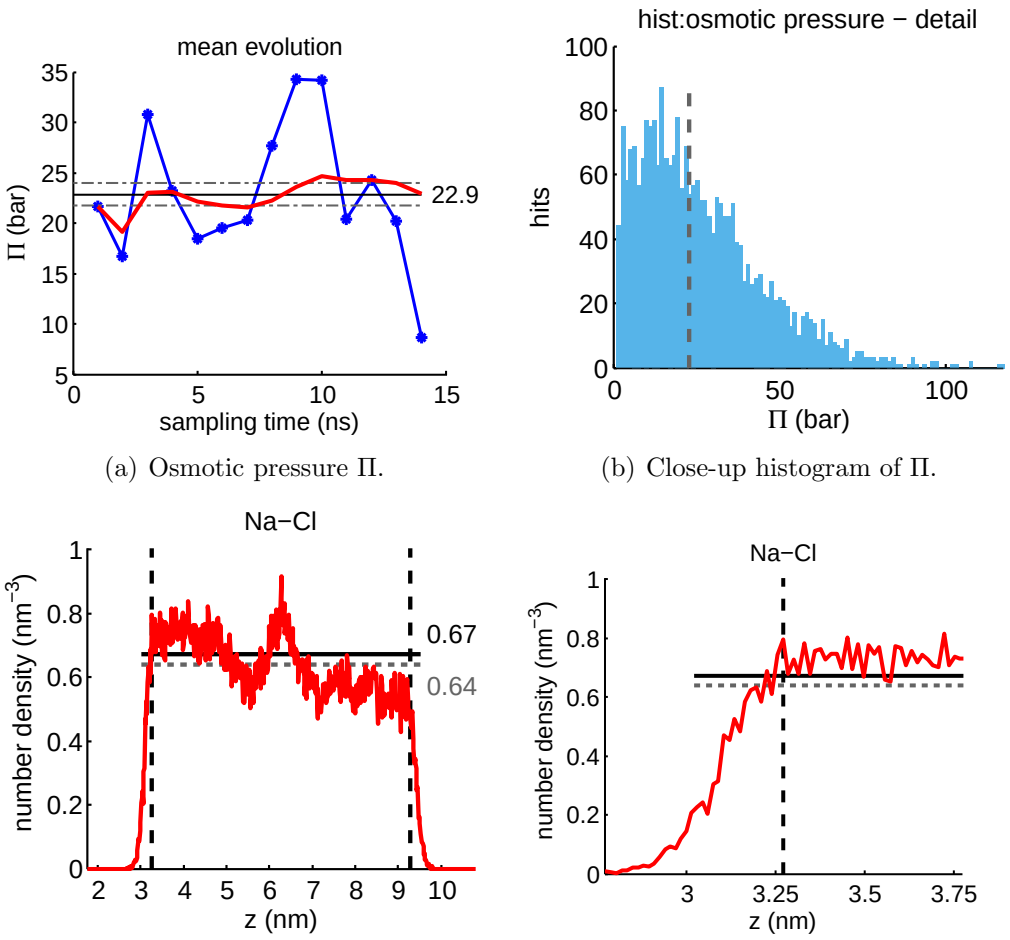

(a) Osmotic pressure Π.

(b) Close-up histogram of Π.

(c) Number density distribution ρ_N.

(d) Close-up of the ρ_N.

Figure B.21: **(big domain)** Summary of results obtained from an osmotic pressure calculation using membrane walls with a force constant k of 100 kJ/(mol·nm^2). 20 NaCl ion pairs are dissolved in 4096 SW10e water molecules and are confined in a 6 nm slab, resulting in a salt concentration of 0.53 M inside the ion domain. The NVT ensemble was applied after 300 ps of equilibration in a NPT ensemble at a pressure of 1 bar. Further results are shown in Tab. 4.17. The simulation was performed for an ion model with $\alpha_{\mathrm{Cl}} = 4.0 \cdot 10^{-3}\mathrm{nm}^3$. The temperature is 298.15 K. The total duration of the simulation was 15 ns including 1 ns equilibration time. a) Block average of the osmotic pressure with 1 ns sampling time (blue line with asterisks) and running average of the osmotic pressure (red line). The horizontal lines mark the mean osmotic pressure (solid) and a ±5 % interval around it (grey dashed lines). b) Close-up of the histogram of the osmotic pressure. The bin at $\Pi = 0$ was not printed. The vertical dashed line marks the mean osmotic pressure. c) Number density distribution of ion species in the box. The vertical dashed line marks the position of the membrane. The horizontal line marks the position of the ideal concentration with 'hard' membrane walls (black solid), and of the actual concentration between the membrane walls (grey dashed line). d) Close-up of the number density distribution at the membrane wall.

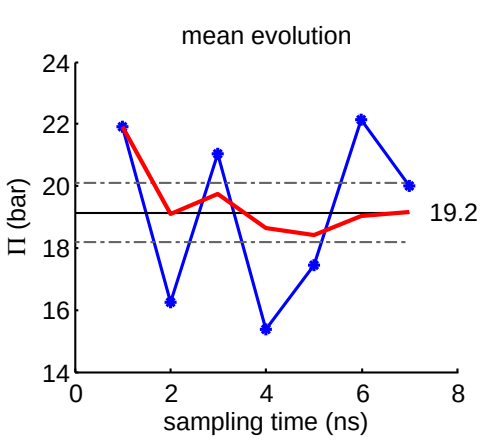

(a) Osmotic pressure Π.

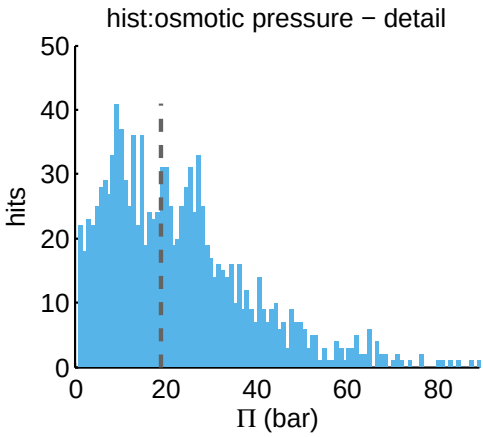

(b) Close-up histogram of Π.

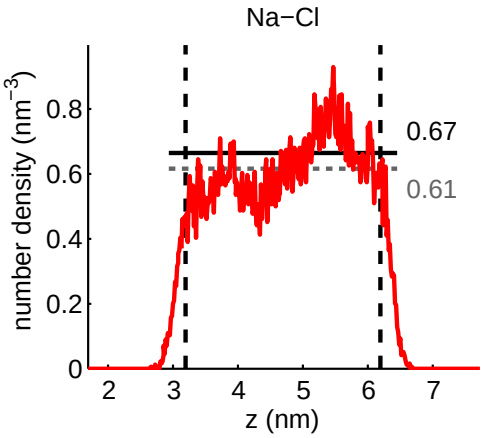

(c) Number density distribution ρ_N.

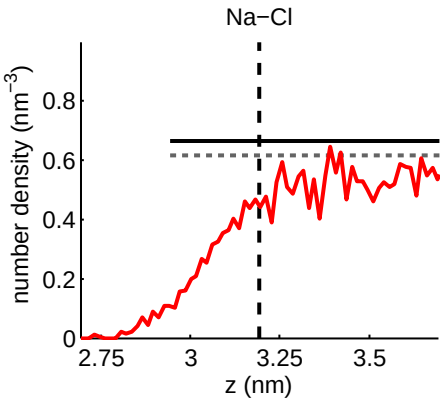

(d) Close-up of the ρ_N.

Figure B.22: **(big polar)** Summary of results obtained from an osmotic pressure calculation using membrane walls with a force constant k of 100 kJ/(mol·nm^2). 10 NaCl ion pairs are dissolved in 4096 SW10e water molecules and are confined in a 3 nm slab, resulting in a salt concentration of 0.51 M inside the ion domain. The NVT ensemble was applied after 300 ps of equilibration in a NPT ensemble at a pressure of 1 bar. Further results are shown in Tab. 4.17. The simulation was performed for an ion model with $\alpha_{\mathrm{Cl}} = 4.0 \cdot 10^{-3}\mathrm{nm}^3$. The temperature is 298.15 K. The total duration of the simulation was 8 ns including 1 ns equilibration time. a) Block average of the osmotic pressure with 1 ns sampling time (blue line with asterisks) and running average of the osmotic pressure (red line). The horizontal lines mark the mean osmotic pressure (solid) and a ±5 % interval around it (grey dashed lines). b) Close-up of the histogram of the osmotic pressure. The bin at $\Pi = 0$ was not printed. The vertical dashed line marks the mean osmotic pressure. c) Number density distribution of ion species in the box. The vertical dashed line marks the position of the membrane. The horizontal line marks the position of the ideal concentration with 'hard' membrane walls (black solid), and of the actual concentration between the membrane walls (grey dashed line). d) Close-up of the number density distribution at the membrane wall.

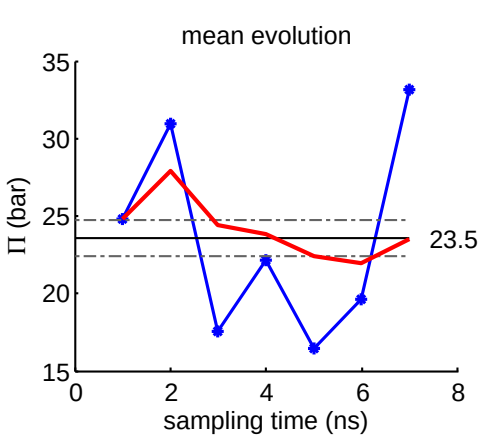

(a) Osmotic pressure Π.

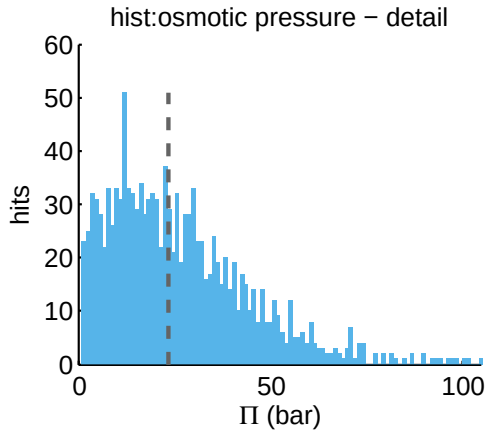

(b) Close-up histogram of Π.

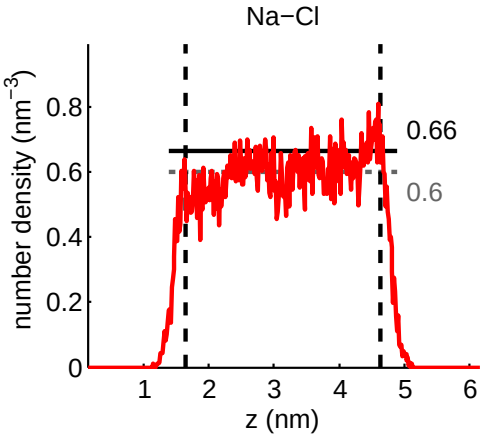

(c) Number density distribution ρ_N.

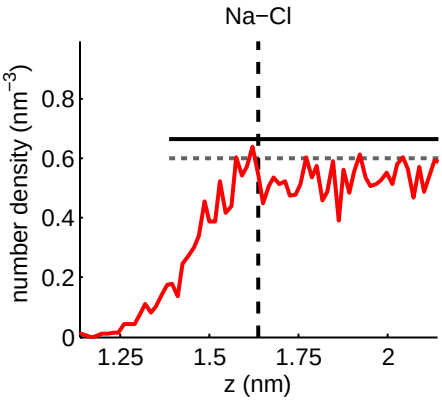

(d) Close-up of the ρ_N.

Figure B.23: **(small box)** Summary of results obtained from an osmotic pressure calculation using membrane walls with a force constant k of 100 kJ/(mol·nm^2). 10 NaCl ion pairs are dissolved in 2048 SW10e water molecules and are confined in a 3 nm slab, resulting in a salt concentration of 0.50 M inside the ion domain. The NVT ensemble was applied after 300 ps of equilibration in a NPT ensemble at a pressure of 1 bar. Further results are shown in Tab. 4.17. The simulation was performed for an ion model with $\alpha_{\mathrm{Cl}} = 4.0 \cdot 10^{-3}\mathrm{nm}^3$. The temperature is 298.15 K. The total duration of the simulation was 8 ns including 1 ns equilibration time. a) Block average of the osmotic pressure with 1 ns sampling time (blue line with asterisks) and running average of the osmotic pressure (red line). The horizontal lines mark the mean osmotic pressure (solid) and a ±5 % interval around it (grey dashed lines). b) Close-up of the histogram of the osmotic pressure. The bin at $\Pi = 0$ was not printed. The vertical dashed line marks the mean osmotic pressure. c) Number density distribution of ion species in the box. The vertical dashed line marks the position of the membrane. The horizontal line marks the position of the ideal concentration with 'hard' membrane walls (black solid), and of the actual concentration between the membrane walls (grey dashed line). d) Close-up of the number density distribution at the membrane wall.

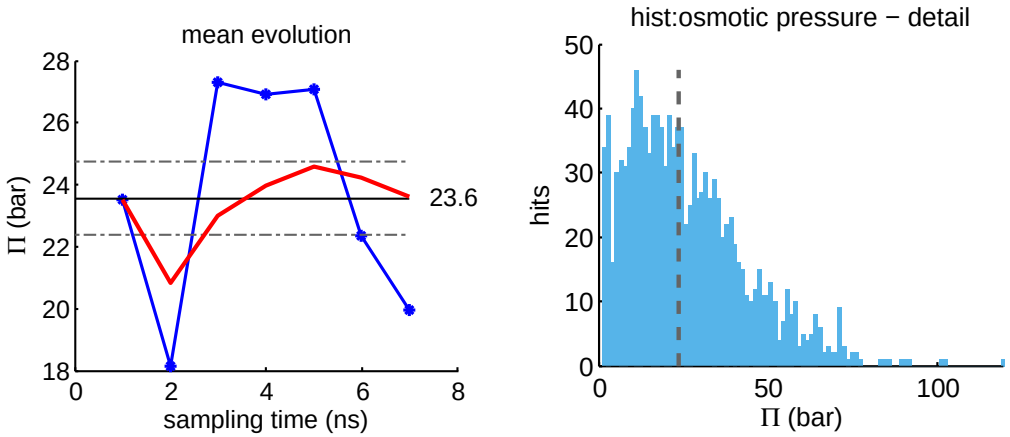

(a) Osmotic pressure Π.

(b) Close-up histogram of Π.

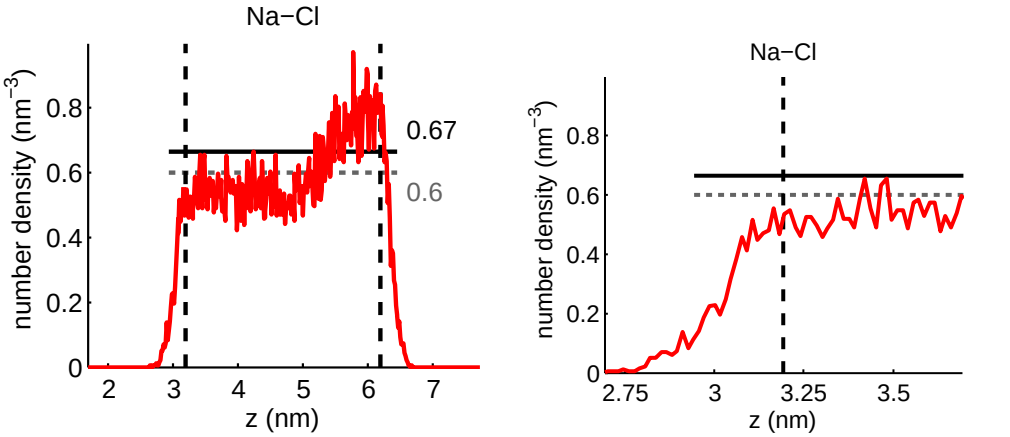

(c) Number density distribution ρ_N.

(d) Close-up of the ρ_N.

Figure B.24: **(small polar)** Summary of results obtained from an osmotic pressure calculation using membrane walls with a force constant k of 100 kJ/(mol·nm^2). 10 NaCl ion pairs are dissolved in 4096 SW10e water molecules and are confined in a 3 nm slab, resulting in a salt concentration of 0.50 M inside the ion domain. The NVT ensemble was applied after 300 ps of equilibration in a NPT ensemble at a pressure of 1 bar. Further results are shown in Tab. 4.17. The simulation was performed for an ion model with $\alpha_{\mathrm{Cl}} = 3.5 \cdot 10^{-3}\mathrm{nm}^3$. The temperature is 298.15 K. The total duration of the simulation was 8 ns including 1 ns equilibration time. a) Block average of the osmotic pressure with 1 ns sampling time (blue line with asterisks) and running average of the osmotic pressure (red line). The horizontal lines mark the mean osmotic pressure (solid) and a ±5 % interval around it (grey dashed lines). b) Close-up of the histogram of the osmotic pressure. The bin at $\Pi = 0$ was not printed. The vertical dashed line marks the mean osmotic pressure. c) Number density distribution of ion species in the box. The vertical dashed line marks the position of the membrane. The horizontal line marks the position of the ideal concentration with 'hard' membrane walls (black solid), and of the actual concentration between the membrane walls (grey dashed line). d) Close-up of the number density distribution at the membrane wall.

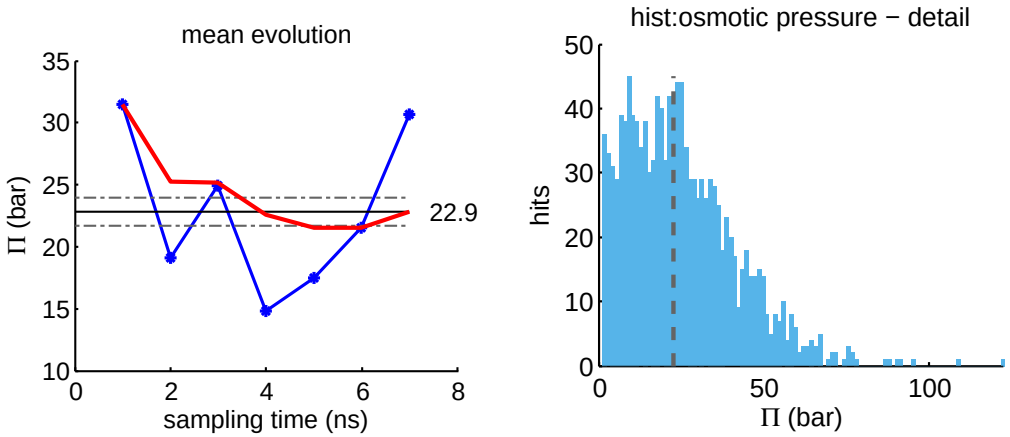

(a) Osmotic pressure Π.

(b) Close-up histogram of Π.

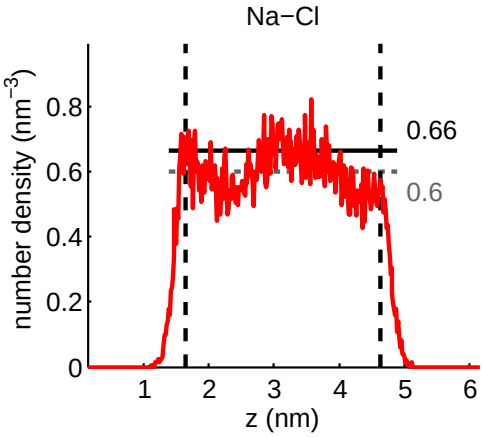

(c) Number density distribution ρ_N.

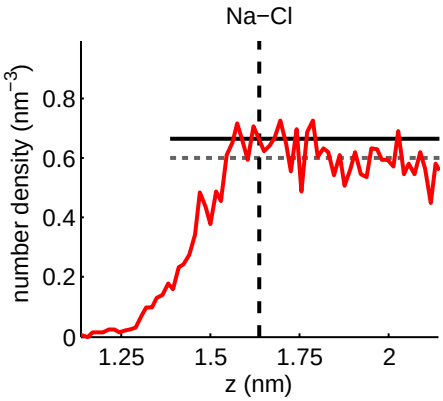

(d) Close-up of the ρ_N.

Figure B.25: **(small box alpha 3.0)** Summary of results obtained from an osmotic pressure calculation using membrane walls with a force constant k of 100 kJ/(mol·nm^2). 10 NaCl ion pairs are dissolved in 2048 SW10e water molecules and are confined in a 3 nm slab, resulting in a salt concentration of 0.50 M inside the ion domain. The NVT ensemble was applied after 300 ps of equilibration in a NPT ensemble at a pressure of 1 bar. Further results are shown in Tab. 4.17. The simulation was performed for an ion model with $\alpha_{\mathrm{Cl}} = 3.0 \cdot 10^{-3}\mathrm{nm}^3$. The temperature is 298.15 K. The total duration of the simulation was 8 ns including 1 ns equilibration time. a) Block average of the osmotic pressure with 1 ns sampling time (blue line with asterisks) and running average of the osmotic pressure (red line). The horizontal lines mark the mean osmotic pressure (solid) and a ±5 % interval around it (grey dashed lines). b) Close-up of the histogram of the osmotic pressure. The bin at $\Pi = 0$ was not printed. The vertical dashed line marks the mean osmotic pressure. c) Number density distribution of ion species in the box. The vertical dashed line marks the position of the membrane. The horizontal line marks the position of the ideal concentration with 'hard' membrane walls (black solid), and of the actual concentration between the membrane walls (grey dashed line). d) Close-up of the number density distribution at the membrane wall.

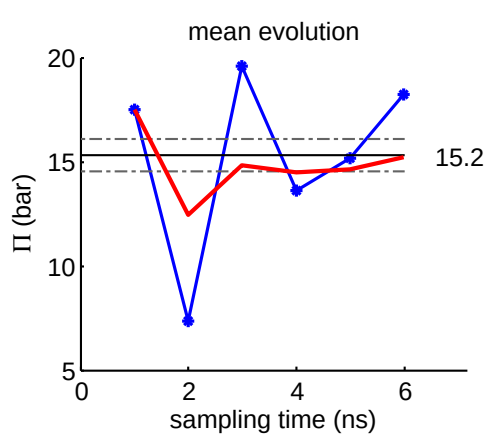

(a) Osmotic pressure Π.

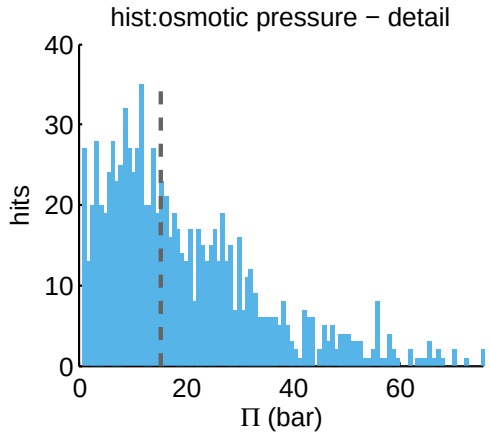

(b) Close-up histogram of Π.

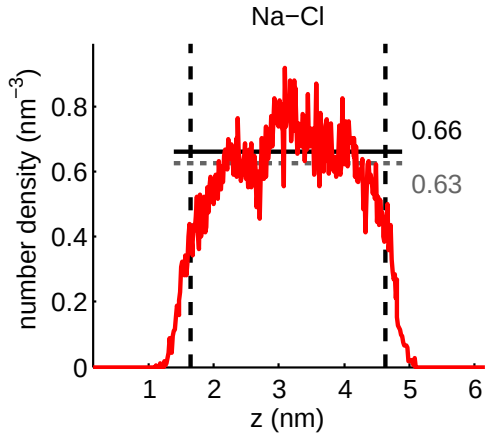

(c) Number density distribution ρ_N.

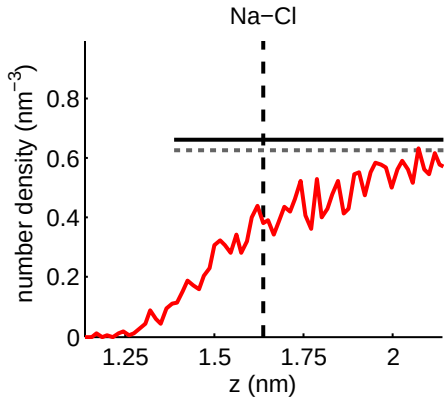

(d) Close-up of the ρ_N.

Figure B.26: **(small box alpha 2.5)** Summary of results obtained from an osmotic pressure calculation using membrane walls with a force constant k of 100 kJ/(mol·nm^2). 10 NaCl ion pairs are dissolved in 2048 SW10e water molecules and are confined in a 3 nm slab, resulting in a salt concentration of 0.52 M inside the ion domain. The NVT ensemble was applied after 300 ps of equilibration in a NPT ensemble at a pressure of 1 bar. Further results are shown in Tab. 4.17. The simulation was performed for an ion model with $\alpha_{\mathrm{Cl}} = 2.5 \cdot 10^{-3}\mathrm{nm}^3$. The temperature is 298.15 K. The total duration of the simulation was 8 ns including 1 ns equilibration time. a) Block average of the osmotic pressure with 1 ns sampling time (blue line with asterisks) and running average of the osmotic pressure (red line). The horizontal lines mark the mean osmotic pressure (solid) and a ±5 % interval around it (grey dashed lines). b) Close-up of the histogram of the osmotic pressure. The bin at $\Pi = 0$ was not printed. The vertical dashed line marks the mean osmotic pressure. c) Number density distribution of ion species in the box. The vertical dashed line marks the position of the membrane. The horizontal line marks the position of the ideal concentration with 'hard' membrane walls (black solid), and of the actual concentration between the membrane walls (grey dashed line). d) Close-up of the number density distribution at the membrane wall.

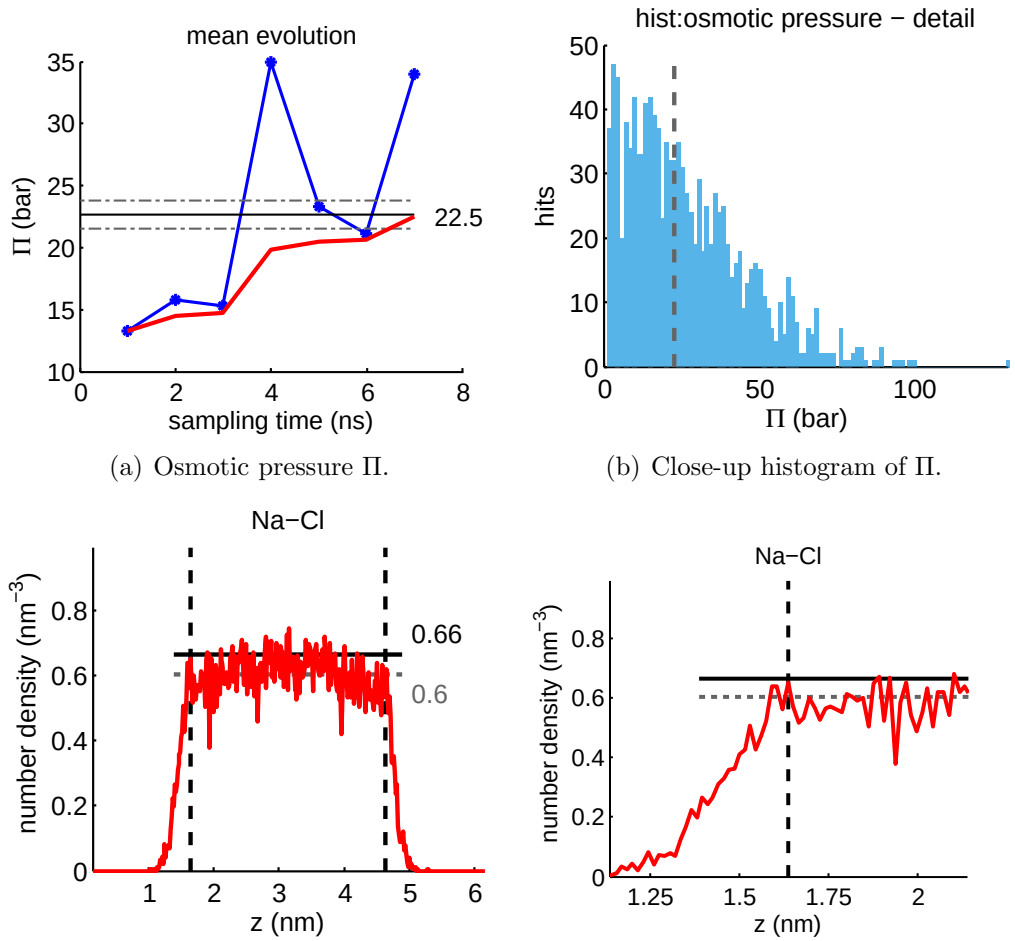

(a) Osmotic pressure Π.

(b) Close-up histogram of Π.

(c) Number density distribution ρ_N.

(d) Close-up of the ρ_N.

Figure B.27: **(diff wall k100)** Summary of results obtained from an osmotic pressure calculation using membrane walls with a force constant k of 100 kJ/(mol·nm^2). 10 NaCl ion pairs are dissolved in 2048 SW10e water molecules and are confined in a 3 nm slab, resulting in a salt concentration of 0.50 M inside the ion domain. The NVT ensemble was applied after 300 ps of equilibration in a NPT ensemble at a pressure of 1 bar. Further results are shown in Tab. 4.17 or Tab. 4.17. The simulation was performed for an ion model with $\alpha_{\mathrm{Cl}} = 3.5 \cdot 10^{-3}\mathrm{nm}^3$. The temperature is 298.15 K. The total duration of the simulation was 8 ns including 1 ns equilibration time. a) Block average of the osmotic pressure with 1 ns sampling time (blue line with asterisks) and running average of the osmotic pressure (red line). The horizontal lines mark the mean osmotic pressure (solid) and a ±5 % interval around it (grey dashed lines). b) Close-up of the histogram of the osmotic pressure. The bin at $\Pi = 0$ was not printed. The vertical dashed line marks the mean osmotic pressure. c) Number density distribution of ion species in the box. The vertical dashed line marks the position of the membrane. The horizontal line marks the position of the ideal concentration with 'hard' membrane walls (black solid), and of the actual concentration between the membrane walls (grey dashed line). d) Close-up of the number density distribution at the membrane wall.

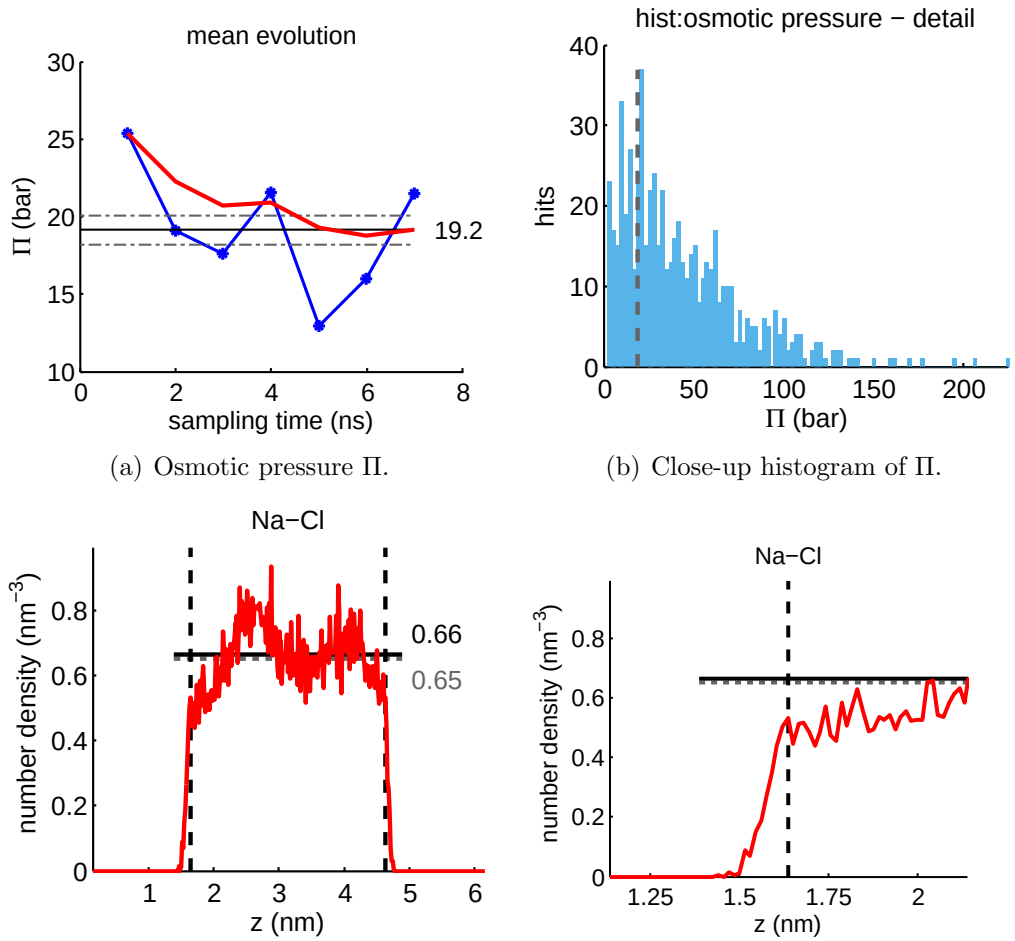

(a) Osmotic pressure Π.

(b) Close-up histogram of Π.

(c) Number density distribution ρ_N.

(d) Close-up of the ρ_N.

Figure B.28: **(diff wall k1000)** Summary of results obtained from an osmotic pressure calculation using membrane walls with a force constant k of 1'000 kJ/(mol·nm^2). 10 NaCl ion pairs are dissolved in 2048 SW10e water molecules and are confined in a 3 nm slab, resulting in a salt concentration of 0.54 M inside the ion domain. The NVT ensemble was applied after 300 ps of equilibration in a NPT ensemble at a pressure of 1 bar. Further results are shown in Tab. 4.17. The simulation was performed for an ion model with $\alpha_{\mathrm{Cl}} = 3.5 \cdot 10^{-3}\mathrm{nm}^3$. The temperature is 298.15 K. The total duration of the simulation was 8 ns including 1 ns equilibration time. a) Block average of the osmotic pressure with 1 ns sampling time (blue line with asterisks) and running average of the osmotic pressure (red line). The horizontal lines mark the mean osmotic pressure (solid) and a ±5 % interval around it (grey dashed lines). b) Close-up of the histogram of the osmotic pressure. The bin at $\Pi = 0$ was not printed. The vertical dashed line marks the mean osmotic pressure. c) Number density distribution of ion species in the box. The vertical dashed line marks the position of the membrane. The horizontal line marks the position of the ideal concentration with 'hard' membrane walls (black solid), and of the actual concentration between the membrane walls (grey dashed line). d) Close-up of the number density distribution at the membrane wall.

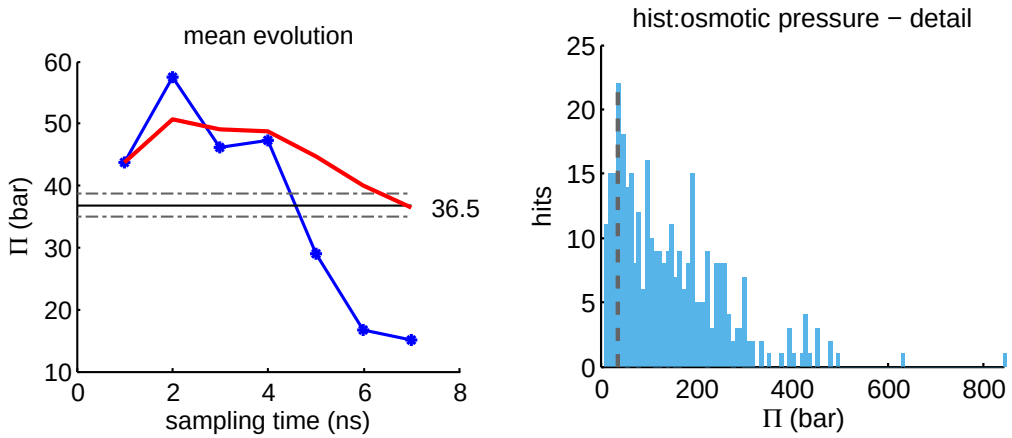

(a) Osmotic pressure Π.

(b) Close-up histogram of Π.

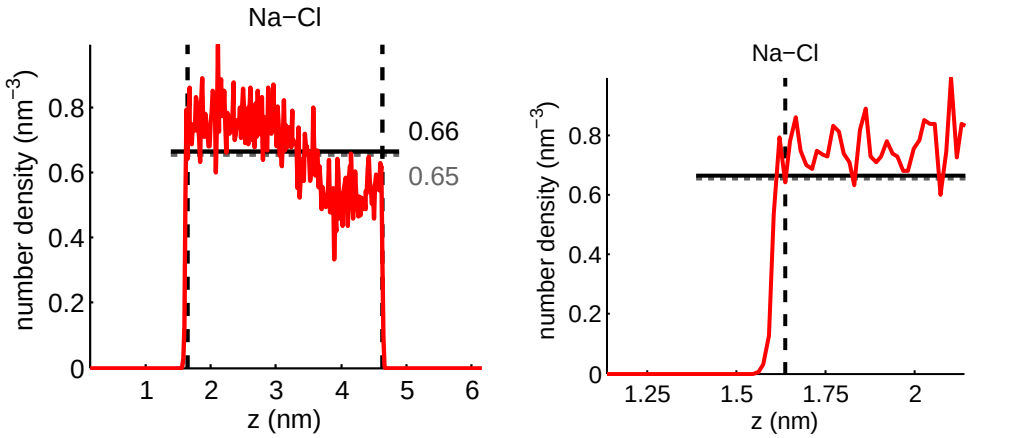

(c) Number density distribution ρ_N.

(d) Close-up of the ρ_N.

Figure B.29: **(diff wall k10000)** Summary of results obtained from an osmotic pressure calculation using membrane walls with a force constant k of 10'000 kJ/(mol·nm^2). 10 NaCl ion pairs are dissolved in 2048 SW10e water molecules and are confined in a 3 nm slab, resulting in a salt concentration of 0.54 M inside the ion domain. The NVT ensemble was applied after 300 ps of equilibration in a NPT ensemble at a pressure of 1 bar. Further results are shown in Tab. 4.17. The simulation was performed for an ion model with $\alpha_{\mathrm{Cl}} = 3.5 \cdot 10^{-3}\mathrm{nm}^3$. The temperature is 298.15 K. The total duration of the simulation was 8 ns including 1 ns equilibration time. a) Block average of the osmotic pressure with 1 ns sampling time (blue line with asterisks) and running average of the osmotic pressure (red line). The horizontal lines mark the mean osmotic pressure (solid) and a ±5 % interval around it (grey dashed lines). b) Close-up of the histogram of the osmotic pressure. The bin at $\Pi = 0$ was not printed. The vertical dashed line marks the mean osmotic pressure. c) Number density distribution of ion species in the box. The vertical dashed line marks the position of the membrane. The horizontal line marks the position of the ideal concentration with 'hard' membrane walls (black solid), and of the actual concentration between the membrane walls (grey dashed line). d) Close-up of the number density distribution at the membrane wall.

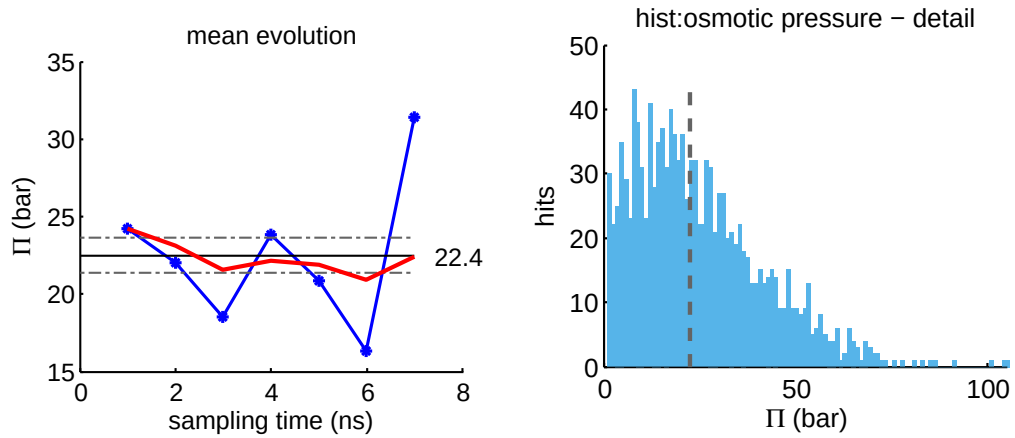

(a) Osmotic pressure Π.

(b) Close-up histogram of Π.

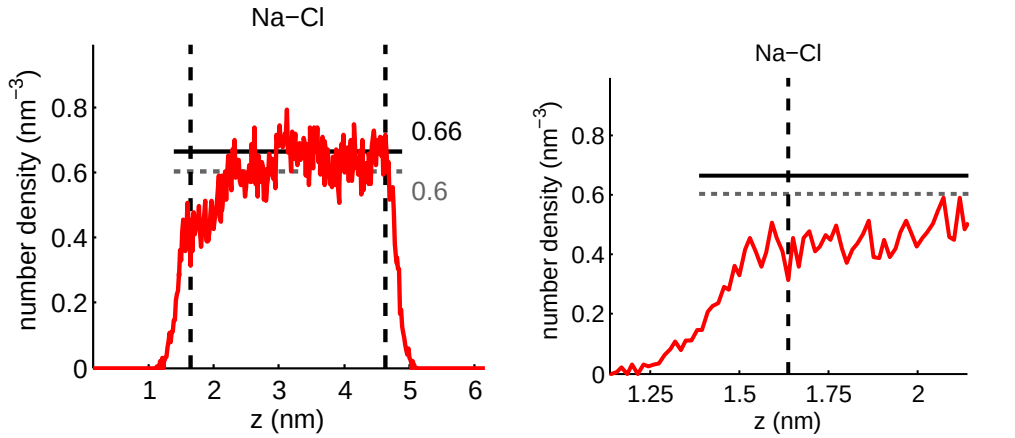

(c) Number density distribution ρ_N.

(d) Close-up of the ρ_N.

Figure B.30: **(diff wall decoupl k100)** Summary of results obtained from an osmotic pressure calculation using membrane walls with a force constant k of 100 kJ/(mol·nm^2). The ions were decoupled from the thermostat. 10 NaCl ion pairs are dissolved in 2048 SW10e water molecules and are confined in a 3 nm slab, resulting in a salt concentration of 0.50 M inside the ion domain. The NVT ensemble was applied after 300 ps of equilibration in a NPT ensemble at a pressure of 1 bar. Further results are shown in Tab. 4.17. The simulation was performed for an ion model with $\alpha_{\mathrm{Cl}} = 3.5 \cdot 10^{-3}\mathrm{nm}^3$. The temperature is 298.15 K. The total duration of the simulation was 8 ns including 1 ns equilibration time. a) Block average of the osmotic pressure with 1 ns sampling time (blue line with asterisks) and running average of the osmotic pressure (red line). The horizontal lines mark the mean osmotic pressure (solid) and a ±5 % interval around it (grey dashed lines). b) Close-up of the histogram of the osmotic pressure. The bin at $\Pi = 0$ was not printed. The vertical dashed line marks the mean osmotic pressure. c) Number density distribution of ion species in the box. The vertical dashed line marks the position of the membrane. The horizontal line marks the position of the ideal concentration with 'hard' membrane walls (black solid), and of the actual concentration between the membrane walls (grey dashed line). d) Close-up of the number density distribution at the membrane wall.

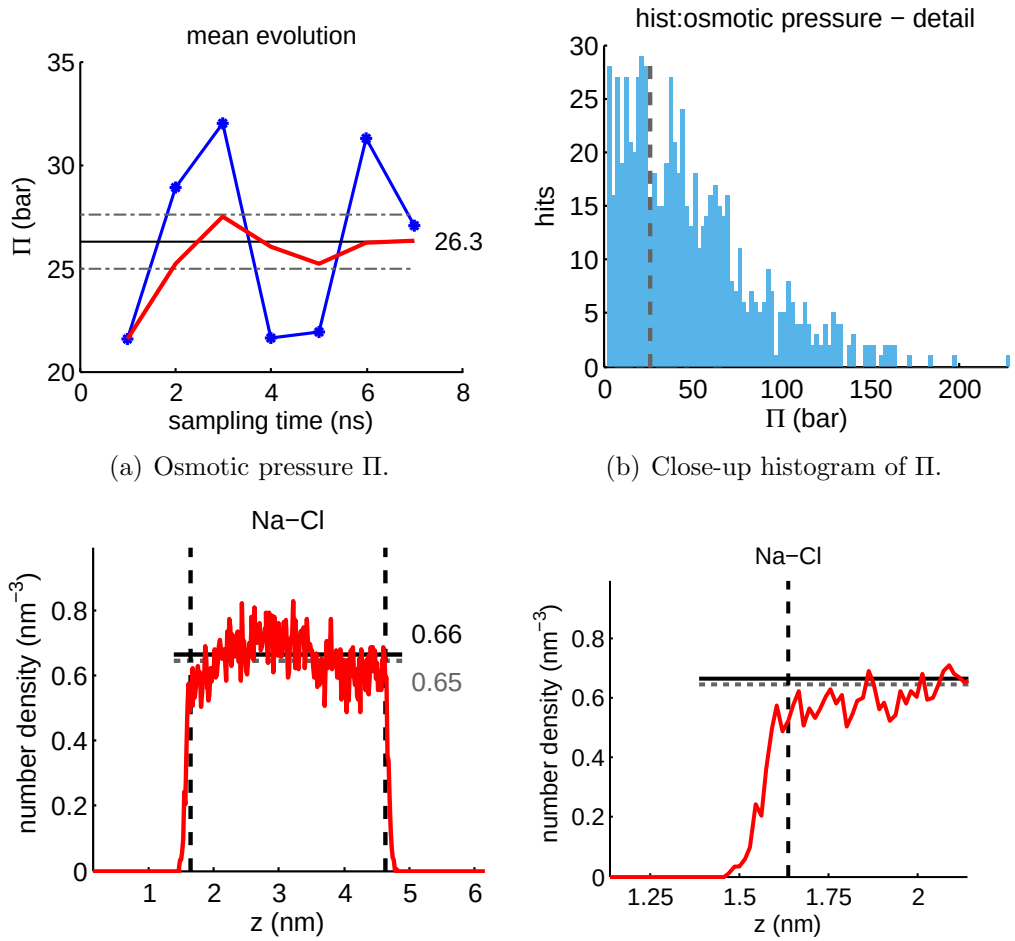

(a) Osmotic pressure Π.

(b) Close-up histogram of Π.

(c) Number density distribution ρ_N.

(d) Close-up of the ρ_N.

Figure B.31: **(diff wall decoupl k1'000)** Summary of results obtained from an osmotic pressure calculation using membrane walls with a force constant k of 1'000 kJ/(mol·nm^2). The ions were decoupled from the thermostat. 10 NaCl ion pairs are dissolved in 2048 SW10e water molecules and are confined in a 3 nm slab, resulting in a salt concentration of 0.54 M inside the ion domain. The NVT ensemble was applied after 300 ps of equilibration in a NPT ensemble at a pressure of 1 bar. Further results are shown in Tab. 4.17. The simulation was performed for an ion model with $\alpha_{\mathrm{Cl}} = 3.5 \cdot 10^{-3}\mathrm{nm}^3$. The temperature is 298.15 K. The total duration of the simulation was 8 ns including 1 ns equilibration time. a) Block average of the osmotic pressure with 1 ns sampling time (blue line with asterisks) and running average of the osmotic pressure (red line). The horizontal lines mark the mean osmotic pressure (solid) and a ±5 % interval around it (grey dashed lines). b) Close-up of the histogram of the osmotic pressure. The bin at $\Pi = 0$ was not printed. The vertical dashed line marks the mean osmotic pressure. c) Number density distribution of ion species in the box. The vertical dashed line marks the position of the membrane. The horizontal line marks the position of the ideal concentration with 'hard' membrane walls (black solid), and of the actual concentration between the membrane walls (grey dashed line). d) Close-up of the number density distribution at the membrane wall.

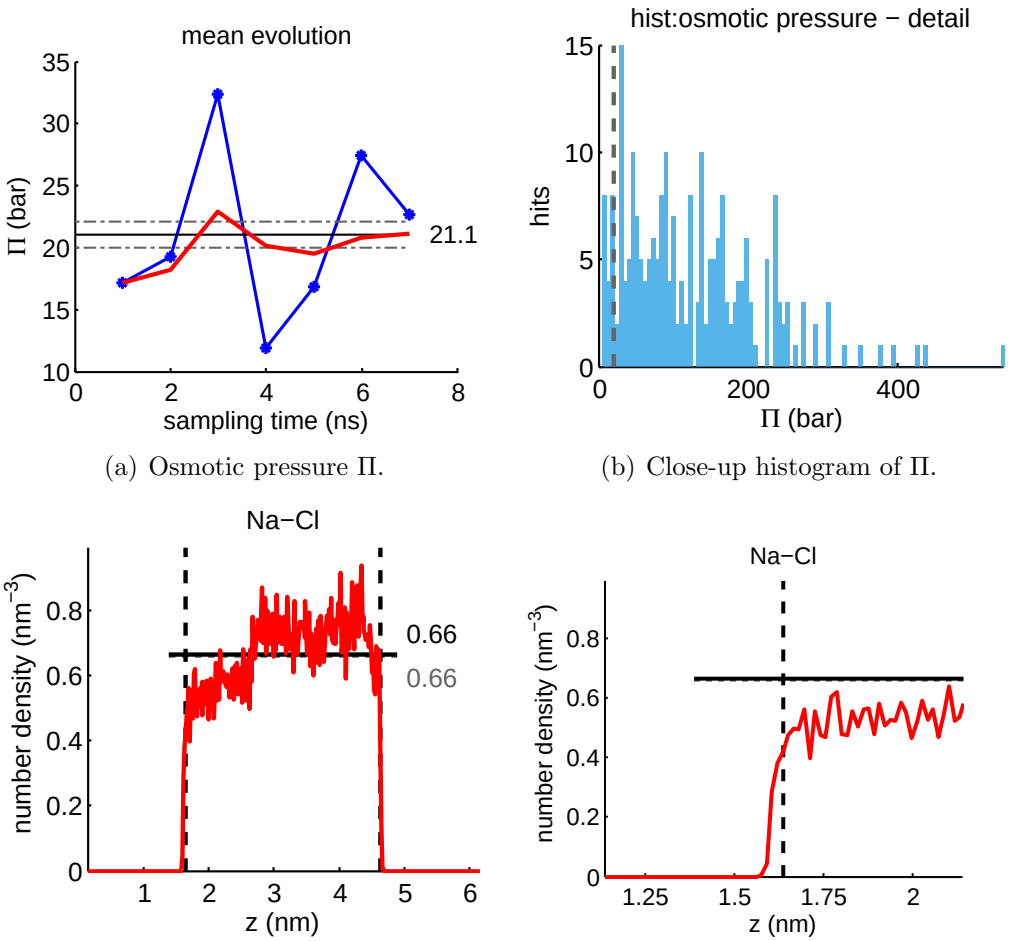

(a) Osmotic pressure Π.

(b) Close-up histogram of Π.

(c) Number density distribution ρ_N.

(d) Close-up of the ρ_N.

Figure B.32: **(diff wall decoupl k10'000)** Summary of results obtained from an osmotic pressure calculation using membrane walls with a force constant k of 10'000 kJ/(mol·nm^2). The ions were decoupled from the thermostat. 10 NaCl ion pairs are dissolved in 2048 SW10e water molecules and are confined in a 3 nm slab, resulting in a salt concentration of 0.55 M inside the ion domain. The NVT ensemble was applied after 300 ps of equilibration in a NPT ensemble at a pressure of 1 bar. Further results are shown in Tab. 4.17. The simulation was performed for an ion model with $\alpha_{\mathrm{Cl}} = 3.5 \cdot 10^{-3}\mathrm{nm}^3$. The temperature is 298.15 K. The total duration of the simulation was 8 ns including 1 ns equilibration time. a) Block average of the osmotic pressure with 1 ns sampling time (blue line with asterisks) and running average of the osmotic pressure (red line). The horizontal lines mark the mean osmotic pressure (solid) and a ±5 % interval around it (grey dashed lines). b) Close-up of the histogram of the osmotic pressure. The bin at $\Pi = 0$ was not printed. The vertical dashed line marks the mean osmotic pressure. c) Number density distribution of ion species in the box. The vertical dashed line marks the position of the membrane. The horizontal line marks the position of the ideal concentration with 'hard' membrane walls (black solid), and of the actual concentration between the membrane walls (grey dashed line). d) Close-up of the number density distribution at the membrane wall.

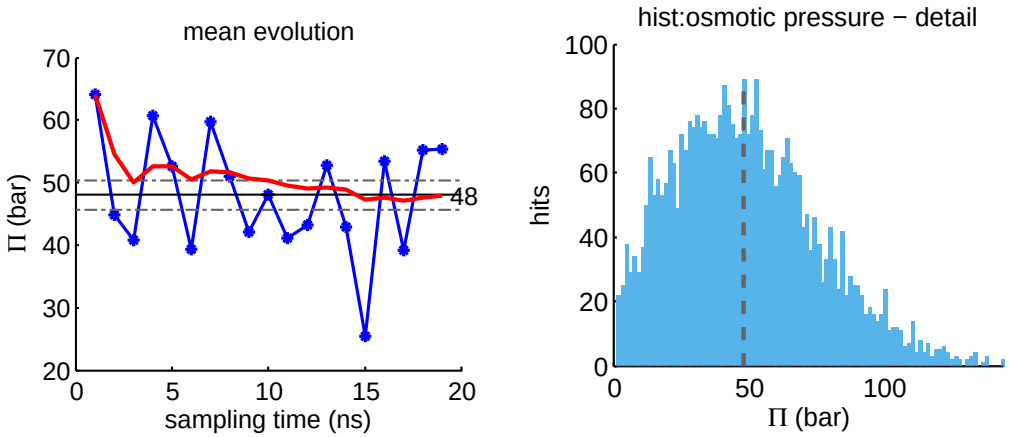

(a) Osmotic pressure Π.

(b) Close-up histogram of Π.

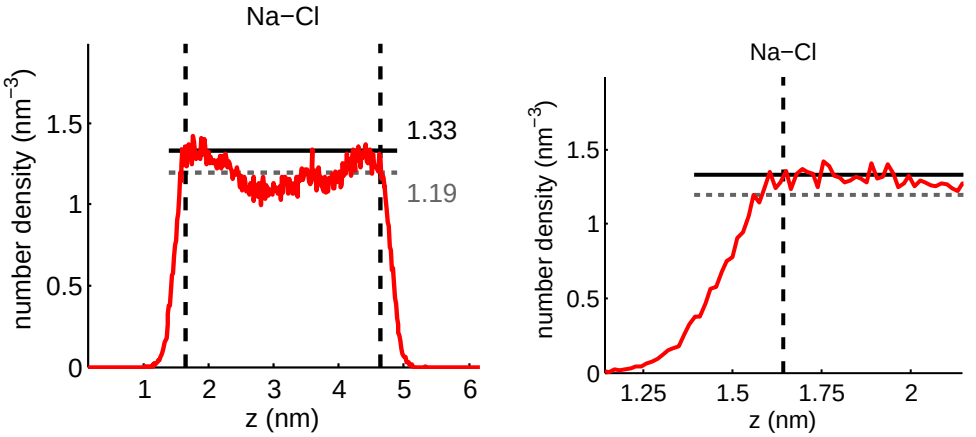

(c) Number density distribution ρ_N.

(d) Close-up of the ρ_N.

Figure B.33: **(1 M, $\alpha_{Cl} = 3.5$)** Summary of results obtained from an osmotic pressure calculation using membrane walls with a force constant k of 100 kJ/(mol·nm^2). 20 NaCl ion pairs are dissolved in 2048 SW10e water molecules and are confined in a 3 nm slab, resulting in a salt concentration of 0.99 M inside the ion domain. The NVT ensemble was applied after 300 ps of equilibration in a NAPT ensemble at a pressure of 1 bar. Further results are shown in Tab. 4.18. The simulation was performed for an ion model with $\alpha_{Cl} = 3.5 \cdot 10^{-3}$nm^3. The temperature is 298.15 K. The total duration of the simulation was 20 ns including 1 ns equilibration time. a) Block average of the osmotic pressure with 1 ns sampling time (blue line with asterisks) and running average of the osmotic pressure (red line). The horizontal lines mark the mean osmotic pressure (solid) and a ±5 % interval around it (grey dashed lines). b) Close-up of the histogram of the osmotic pressure. The bin at $\Pi = 0$ was not printed. The vertical dashed line marks the mean osmotic pressure. c) Number density distribution of ion species in the box. The vertical dashed line marks the position of the membrane. The horizontal line marks the position of the ideal concentration with 'hard' membrane walls (black solid), and of the actual concentration between the membrane walls (grey dashed line). d) Close-up of the number density distribution at the membrane wall.

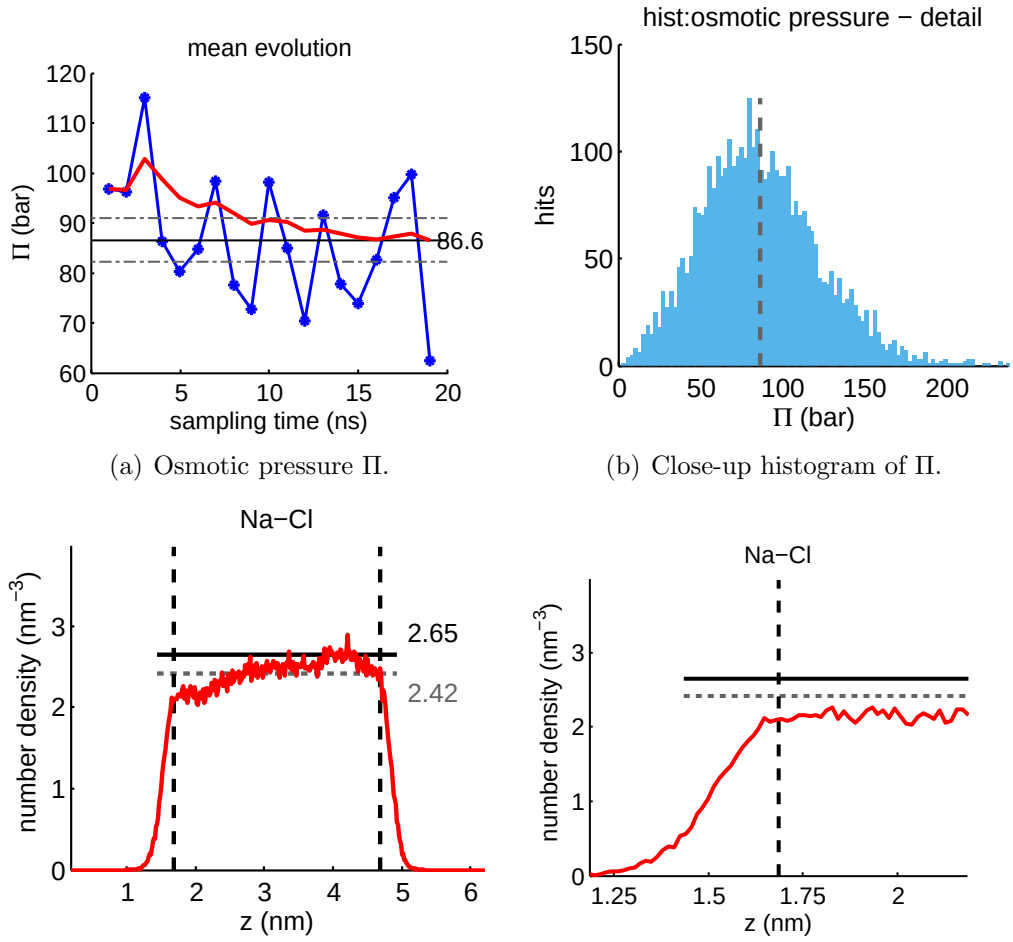

(a) Osmotic pressure Π.

(b) Close-up histogram of Π.

(c) Number density distribution ρ_N.

(d) Close-up of the ρ_N.

Figure B.34: **(1 M, $\alpha_{Cl} = 3.5$)** Summary of results obtained from an osmotic pressure calculation using membrane walls with a force constant k of 100 kJ/(mol·nm^2). 40 NaCl ion pairs are dissolved in 2048 SW10e water molecules and are confined in a 3 nm slab, resulting in a salt concentration of 2.01 M inside the ion domain. The NVT ensemble was applied after 300 ps of equilibration in a NAPT ensemble at a pressure of 1 bar. Further results are shown in Tab. 4.18. The simulation was performed for an ion model with $\alpha_{Cl} = 3.5 \cdot 10^{-3}$nm^3. The temperature is 298.15 K. The total duration of the simulation was 20 ns including 1 ns equilibration time. a) Block average of the osmotic pressure with 1 ns sampling time (blue line with asterisks) and running average of the osmotic pressure (red line). The horizontal lines mark the mean osmotic pressure (solid) and a ±5 % interval around it (grey dashed lines). b) Close-up of the histogram of the osmotic pressure. The bin at $\Pi = 0$ was not printed. The vertical dashed line marks the mean osmotic pressure. c) Number density distribution of ion species in the box. The vertical dashed line marks the position of the membrane. The horizontal line marks the position of the ideal concentration with 'hard' membrane walls (black solid), and of the actual concentration between the membrane walls (grey dashed line). d) Close-up of the number density distribution at the membrane wall.

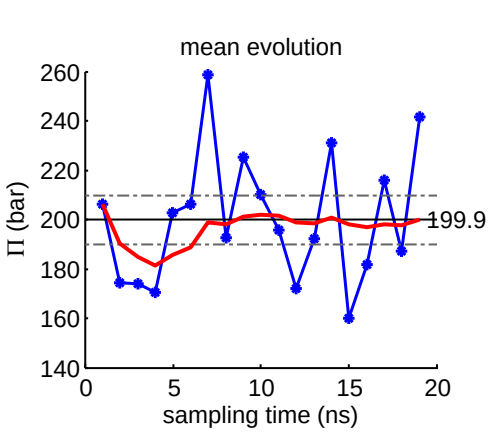

(a) Osmotic pressure Π.

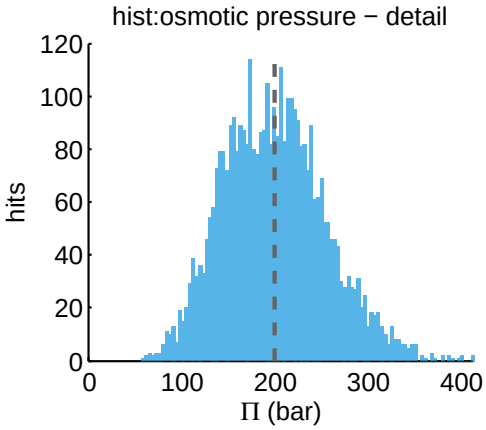

(b) Close-up histogram of Π.

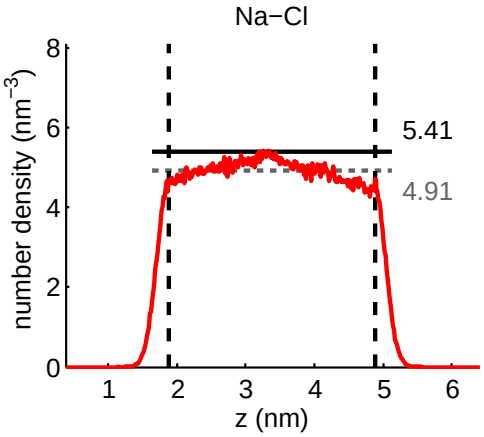

(c) Number density distribution ρ_N.

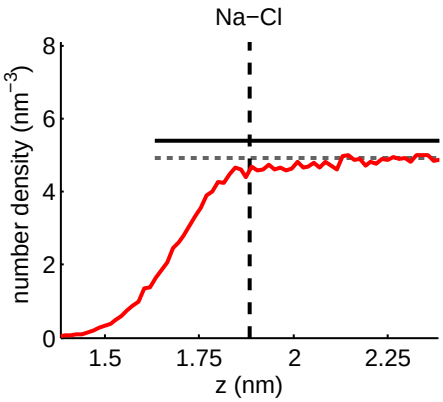

(d) Close-up of the ρ_N.

Figure B.35: **(4 M, $\alpha_{Cl} = 2.5$)** Summary of results obtained from an osmotic pressure calculation using membrane walls with a force constant k of 100 kJ/(mol·nm^2). The ions were decoupled from the thermostat. 80 NaCl ion pairs are dissolved in 2048 SW10e water molecules and are confined in a 3 nm slab, resulting in a salt concentration of 4.08 M inside the ion domain. The NVT ensemble was applied after 300 ps of equilibration in a NAPT ensemble at a pressure of 1 bar. Further results are shown in Tab. 4.18. The simulation was performed for an ion model with $\alpha_{Cl} = 2.5 \cdot 10^{-3}$nm^3. The temperature is 298.15 K. The total duration of the simulation was 20 ns including 1 ns equilibration time. a) Block average of the osmotic pressure with 1 ns sampling time (blue line with asterisks) and running average of the osmotic pressure (red line). The horizontal lines mark the mean osmotic pressure (solid) and a ±5 % interval around it (grey dashed lines). b) Close-up of the histogram of the osmotic pressure. The bin at $\Pi = 0$ was not printed. The vertical dashed line marks the mean osmotic pressure. c) Number density distribution of ion species in the box. The vertical dashed line marks the position of the membrane. The horizontal line marks the position of the ideal concentration with 'hard' membrane walls (black solid), and of the actual concentration between the membrane walls (grey dashed line). d) Close-up of the number density distribution at the membrane wall.

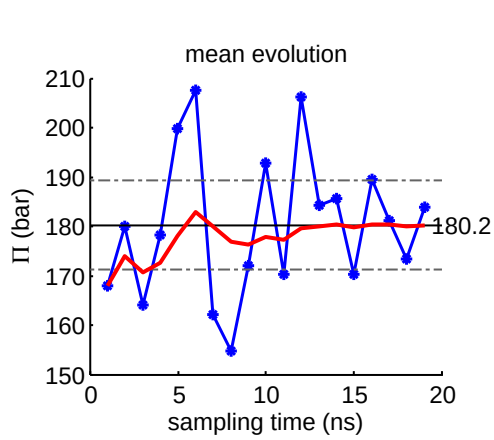

(a) Osmotic pressure Π.

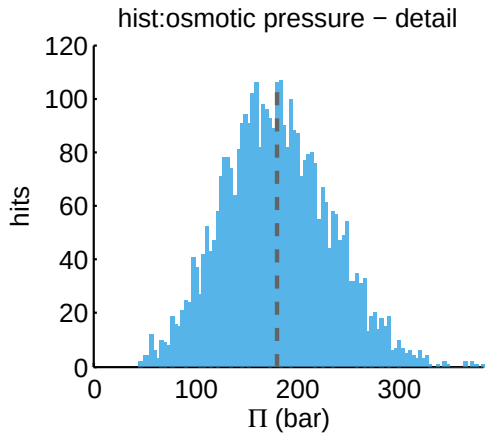

(b) Close-up histogram of Π.

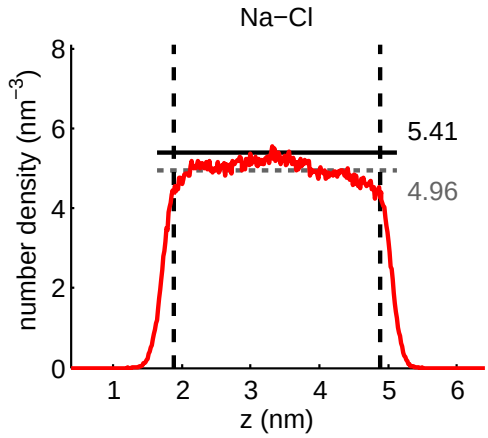

(c) Number density distribution ρ_N.

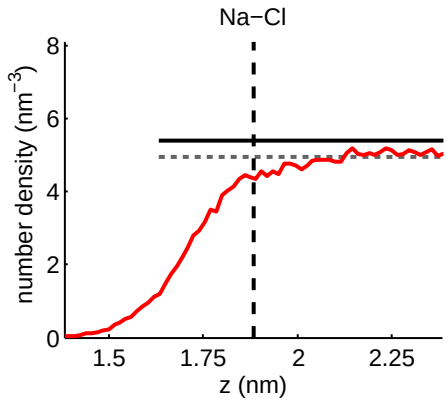

(d) Close-up of the ρ_N.

Figure B.36: **(4 M, $\alpha_{Cl} = 3.0$)** Summary of results obtained from an osmotic pressure calculation using membrane walls with a force constant k of 100 kJ/(mol·nm^2). The ions were decoupled from the thermostat. 80 NaCl ion pairs are dissolved in 2048 SW10e water molecules and are confined in a 3 nm slab, resulting in a salt concentration of 4.12 M inside the ion domain. The NVT ensemble was applied after 300 ps of equilibration in a NAPT ensemble at a pressure of 1 bar. Further results are shown in Tab. 4.18. The simulation was performed for an ion model with $\alpha_{Cl} = 3.0 \cdot 10^{-3}$nm^3. The temperature is 298.15 K. The total duration of the simulation was 20 ns including 1 ns equilibration time. a) Block average of the osmotic pressure with 1 ns sampling time (blue line with asterisks) and running average of the osmotic pressure (red line). The horizontal lines mark the mean osmotic pressure (solid) and a ±5 % interval around it (grey dashed lines). b) Close-up of the histogram of the osmotic pressure. The bin at $\Pi = 0$ was not printed. The vertical dashed line marks the mean osmotic pressure. c) Number density distribution of ion species in the box. The vertical dashed line marks the position of the membrane. The horizontal line marks the position of the ideal concentration with 'hard' membrane walls (black solid), and of the actual concentration between the membrane walls (grey dashed line). d) Close-up of the number density distribution at the membrane wall.

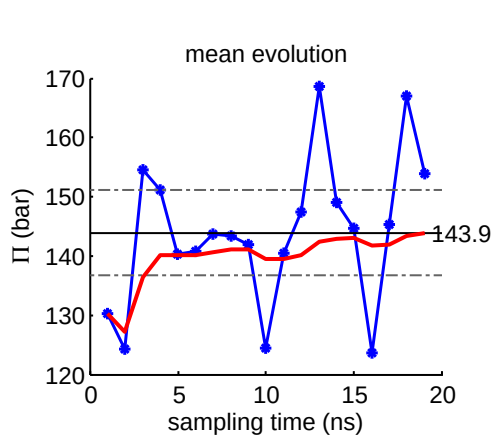

(a) Osmotic pressure Π.

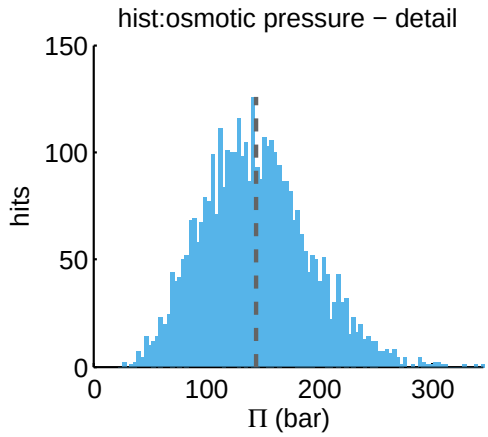

(b) Close-up histogram of Π.

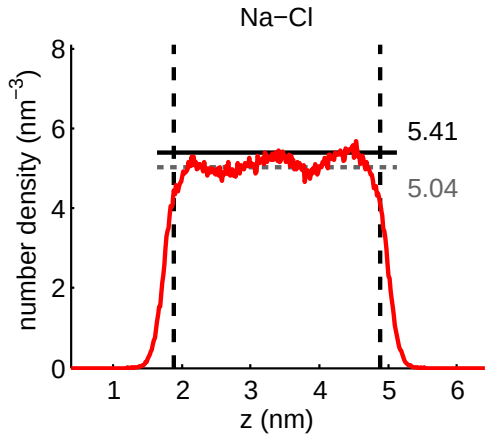

(c) Number density distribution ρ_N.

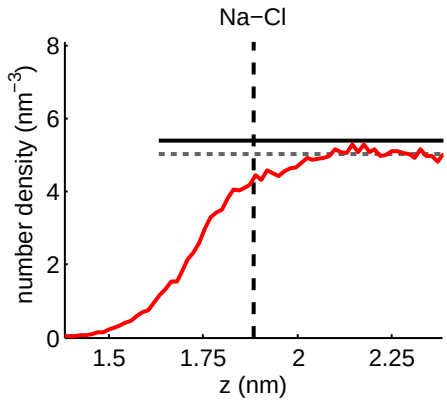

(d) Close-up of the ρ_N.

Figure B.37: **(4 M, $\alpha_{\mathrm{Cl}} = 3.5$)** Summary of results obtained from an osmotic pressure calculation using membrane walls with a force constant k of 100 kJ/(mol·nm^2). The ions were decoupled from the thermostat. 80 NaCl ion pairs are dissolved in 2048 SW10e water molecules and are confined in a 3 nm slab, resulting in a salt concentration of 4.18 M inside the ion domain. The NVT ensemble was applied after 300 ps of equilibration in a NAPT ensemble at a pressure of 1 bar. Further results are shown in Tab. 4.18. The simulation was performed for an ion model with $\alpha_{\mathrm{Cl}} = 3.5 \cdot 10^{-3}\mathrm{nm}^3$. The temperature is 298.15 K. The total duration of the simulation was 20 ns including 1 ns equilibration time. a) Block average of the osmotic pressure with 1 ns sampling time (blue line with asterisks) and running average of the osmotic pressure (red line). The horizontal lines mark the mean osmotic pressure (solid) and a ±5 % interval around it (grey dashed lines). b) Close-up of the histogram of the osmotic pressure. The bin at $\Pi = 0$ was not printed. The vertical dashed line marks the mean osmotic pressure. c) Number density distribution of ion species in the box. The vertical dashed line marks the position of the membrane. The horizontal line marks the position of the ideal concentration with 'hard' membrane walls (black solid), and of the actual concentration between the membrane walls (grey dashed line). d) Close-up of the number density distribution at the membrane wall.

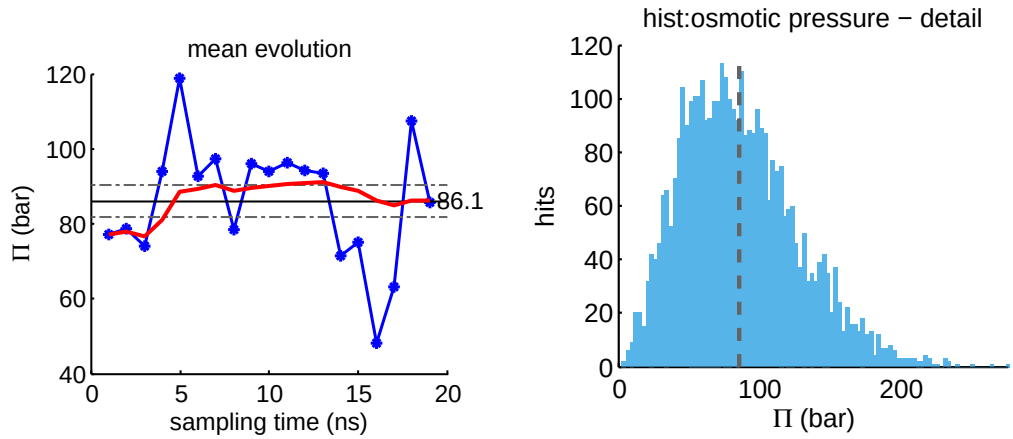

(a) Osmotic pressure Π.

(b) Close-up histogram of Π.

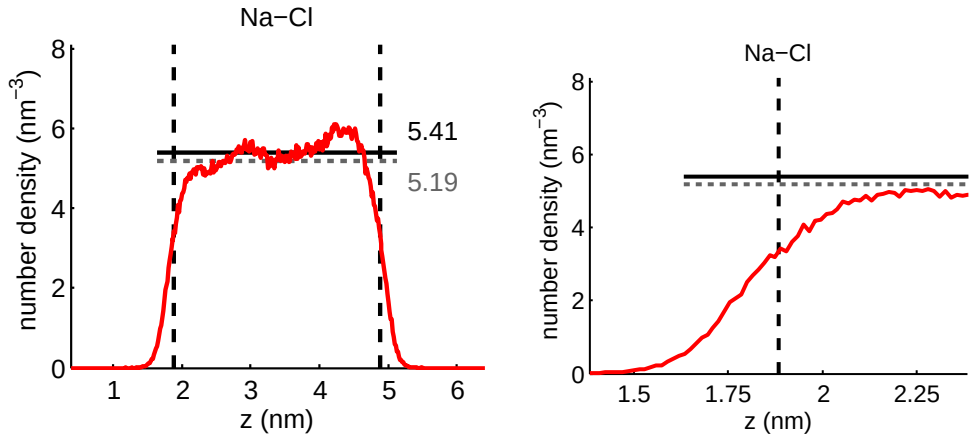

(c) Number density distribution ρ_N.

(d) Close-up of the ρ_N.

Figure B.38: **(4 M, $\alpha_{\mathrm{Cl}} = 4.0$)** Summary of results obtained from an osmotic pressure calculation using membrane walls with a force constant k of 100 kJ/(mol·nm^2). The ions were decoupled from the thermostat. 80 NaCl ion pairs are dissolved in 2048 SW10e water molecules and are confined in a 3 nm slab, resulting in a salt concentration of 4.31 M inside the ion domain. The NVT ensemble was applied after 300 ps of equilibration in a NAPT ensemble at a pressure of 1 bar. Further results are shown in Tab. 4.18. The simulation was performed for an ion model with $\alpha_{\mathrm{Cl}} = 4.0 \cdot 10^{-3}\mathrm{nm}^3$. The temperature is 298.15 K. The total duration of the simulation was 20 ns including 1 ns equilibration time. a) Block average of the osmotic pressure with 1 ns sampling time (blue line with asterisks) and running average of the osmotic pressure (red line). The horizontal lines mark the mean osmotic pressure (solid) and a ±5 % interval around it (grey dashed lines). b) Close-up of the histogram of the osmotic pressure. The bin at $\Pi = 0$ was not printed. The vertical dashed line marks the mean osmotic pressure. c) Number density distribution of ion species in the box. The vertical dashed line marks the position of the membrane. The horizontal line marks the position of the ideal concentration with 'hard' membrane walls (black solid), and of the actual concentration between the membrane walls (grey dashed line). d) Close-up of the number density distribution at the membrane wall.

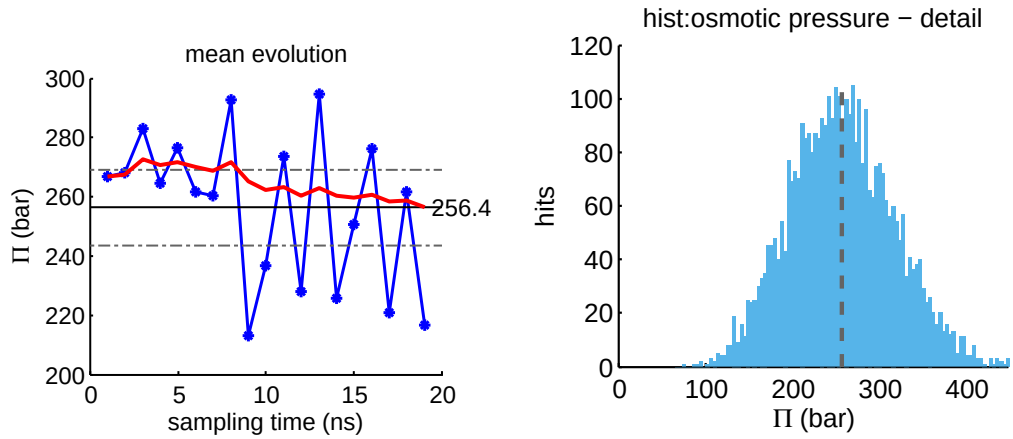

(a) Osmotic pressure Π.

(b) Close-up histogram of Π.

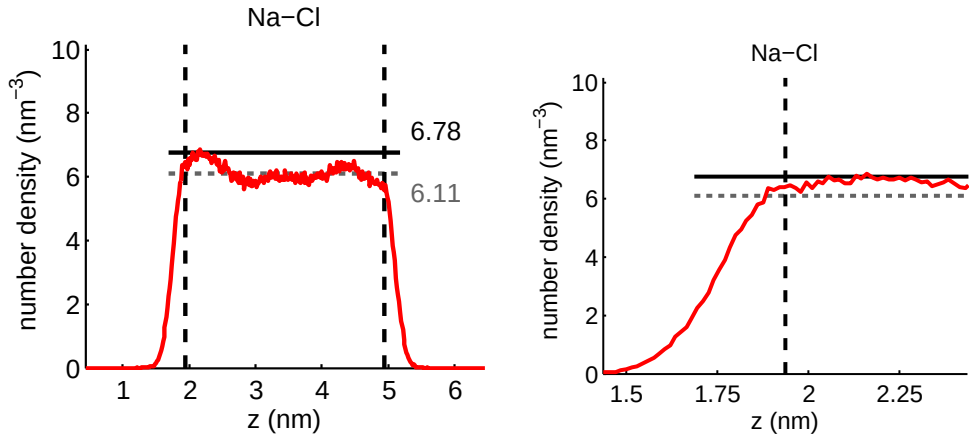

(c) Number density distribution ρ_N.

(d) Close-up of the ρ_N.

Figure B.39: **(5 M, $\alpha_{Cl} = 2.5$)** Summary of results obtained from an osmotic pressure calculation using membrane walls with a force constant k of 100 kJ/(mol·nm^2). The ions were decoupled from the thermostat. 100 NaCl ion pairs are dissolved in 2048 SW10e water molecules and are confined in a 3 nm slab, resulting in a salt concentration of 5.07 M inside the ion domain. The NVT ensemble was applied after 300 ps of equilibration in a NAPT ensemble at a pressure of 1 bar. Further results are shown in Tab. 4.18. The simulation was performed for an ion model with $\alpha_{Cl} = 2.5 \cdot 10^{-3}$nm^3. The temperature is 298.15 K. The total duration of the simulation was 20 ns including 1 ns equilibration time. a) Block average of the osmotic pressure with 1 ns sampling time (blue line with asterisks) and running average of the osmotic pressure (red line). The horizontal lines mark the mean osmotic pressure (solid) and a ±5 % interval around it (grey dashed lines). b) Close-up of the histogram of the osmotic pressure. The bin at $\Pi = 0$ was not printed. The vertical dashed line marks the mean osmotic pressure. c) Number density distribution of ion species in the box. The vertical dashed line marks the position of the membrane. The horizontal line marks the position of the ideal concentration with 'hard' membrane walls (black solid), and of the actual concentration between the membrane walls (grey dashed line). d) Close-up of the number density distribution at the membrane wall.

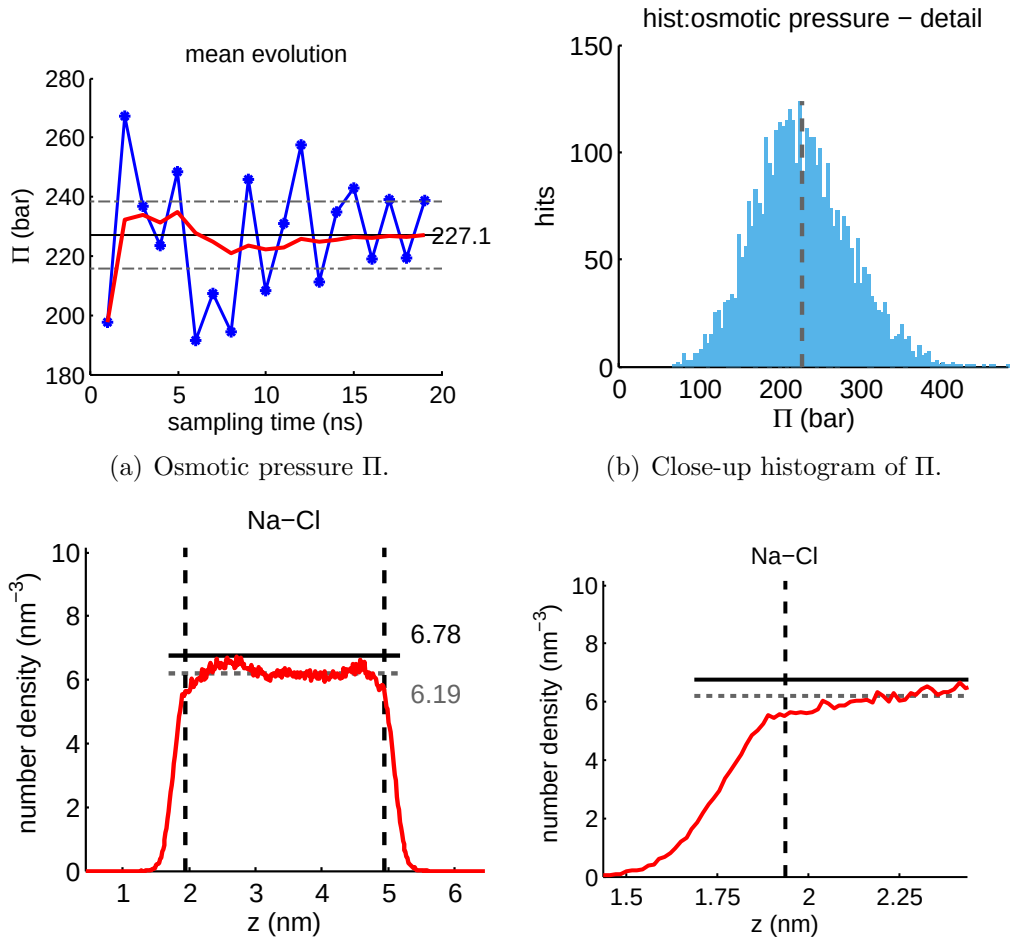

(a) Osmotic pressure Π.

(b) Close-up histogram of Π.

(c) Number density distribution ρ_N.

(d) Close-up of the ρ_N.

Figure B.40: **(5 M, $\alpha_{\mathrm{Cl}} = 3.0$)** Summary of results obtained from an osmotic pressure calculation using membrane walls with a force constant k of 100 kJ/(mol·nm^2). The ions were decoupled from the thermostat. 100 NaCl ion pairs are dissolved in 2048 SW10e water molecules and are confined in a 3 nm slab, resulting in a salt concentration of 5.14 M inside the ion domain. The NVT ensemble was applied after 300 ps of equilibration in a NAPT ensemble at a pressure of 1 bar. Further results are shown in Tab. 4.18. The simulation was performed for an ion model with $\alpha_{\mathrm{Cl}} = 3.0 \cdot 10^{-3}\mathrm{nm}^3$. The temperature is 298.15 K. The total duration of the simulation was 20 ns including 1 ns equilibration time. a) Block average of the osmotic pressure with 1 ns sampling time (blue line with asterisks) and running average of the osmotic pressure (red line). The horizontal lines mark the mean osmotic pressure (solid) and a ±5 % interval around it (grey dashed lines). b) Close-up of the histogram of the osmotic pressure. The bin at $\Pi = 0$ was not printed. The vertical dashed line marks the mean osmotic pressure. c) Number density distribution of ion species in the box. The vertical dashed line marks the position of the membrane. The horizontal line marks the position of the ideal concentration with 'hard' membrane walls (black solid), and of the actual concentration between the membrane walls (grey dashed line). d) Close-up of the number density distribution at the membrane wall.

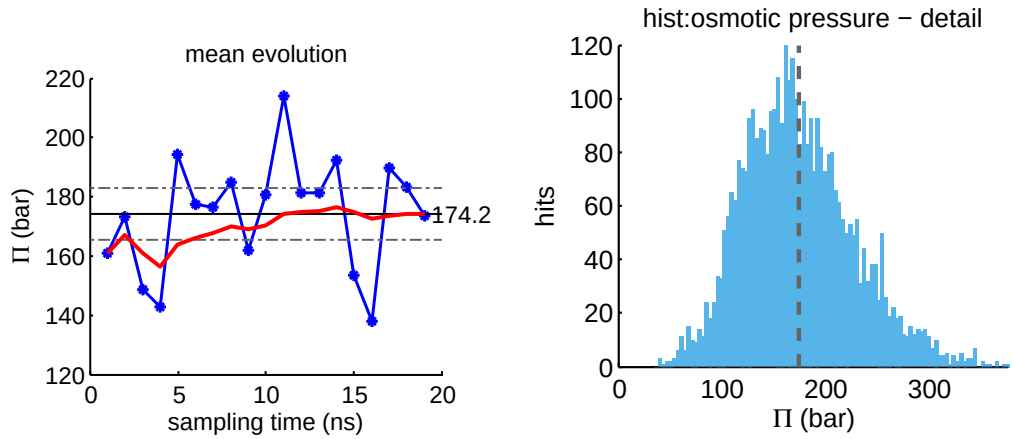

(a) Osmotic pressure Π.

(b) Close-up histogram of Π.

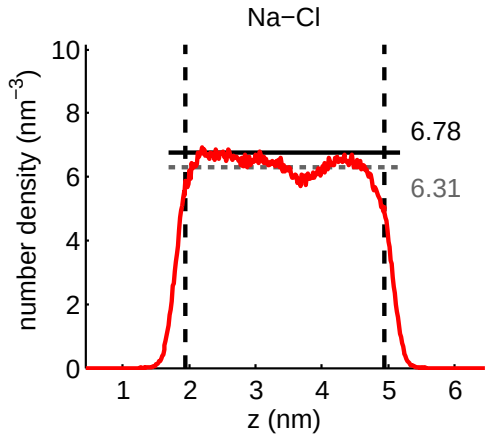

(c) Number density distribution ρ_N.

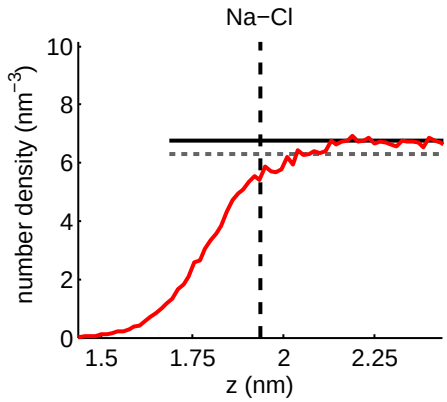

(d) Close-up of the ρ_N.

Figure B.41: **(5 M, $\alpha_{Cl} = 3.5$)** Summary of results obtained from an osmotic pressure calculation using membrane walls with a force constant k of 100 kJ/(mol·nm^2). The ions were decoupled from the thermostat. 100 NaCl ion pairs are dissolved in 2048 SW10e water molecules and are confined in a 3 nm slab, resulting in a salt concentration of 5.24 M inside the ion domain. The NVT ensemble was applied after 300 ps of equilibration in a NAPT ensemble at a pressure of 1 bar. Further results are shown in Tab. 4.18. The simulation was performed for an ion model with $\alpha_{Cl} = 3.5 \cdot 10^{-3}$nm^3. The temperature is 298.15 K. The total duration of the simulation was 20 ns including 1 ns equilibration time. a) Block average of the osmotic pressure with 1 ns sampling time (blue line with asterisks) and running average of the osmotic pressure (red line). The horizontal lines mark the mean osmotic pressure (solid) and a ±5 % interval around it (grey dashed lines). b) Close-up of the histogram of the osmotic pressure. The bin at $\Pi = 0$ was not printed. The vertical dashed line marks the mean osmotic pressure. c) Number density distribution of ion species in the box. The vertical dashed line marks the position of the membrane. The horizontal line marks the position of the ideal concentration with 'hard' membrane walls (black solid), and of the actual concentration between the membrane walls (grey dashed line). d) Close-up of the number density distribution at the membrane wall.

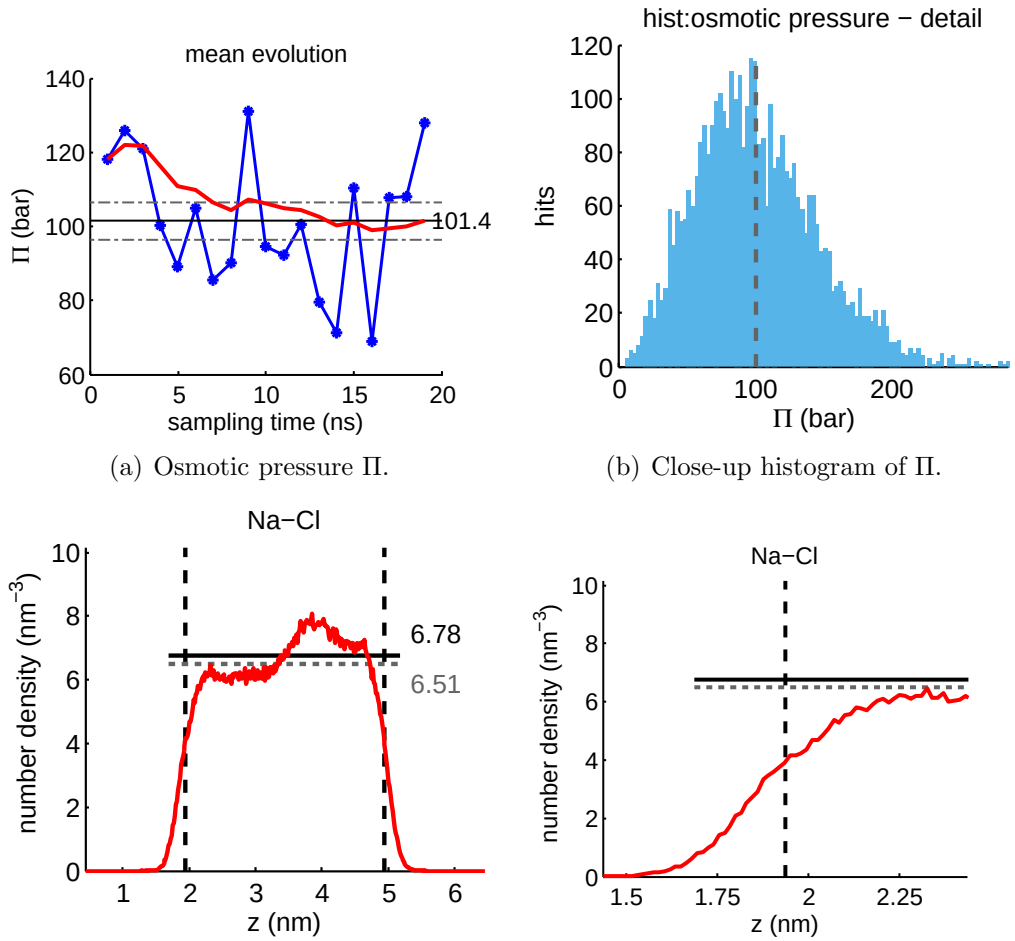

(a) Osmotic pressure Π.

(b) Close-up histogram of Π.

(c) Number density distribution ρ_N.

(d) Close-up of the ρ_N.

Figure B.42: **(5 M, $\alpha_{\mathrm{Cl}} = 4.0$)** Summary of results obtained from an osmotic pressure calculation using membrane walls with a force constant k of 100 kJ/(mol·nm^2). The ions were decoupled from the thermostat. 100 NaCl ion pairs are dissolved in 2048 SW10e water molecules and are confined in a 3 nm slab, resulting in a salt concentration of 5.41 M inside the ion domain. The NVT ensemble was applied after 300 ps of equilibration in a NAPT ensemble at a pressure of 1 bar. Further results are shown in Tab. 4.18. The simulation was performed for an ion model with $\alpha_{\mathrm{Cl}} = 4.0 \cdot 10^{-3}\mathrm{nm}^3$. The temperature is 298.15 K. The total duration of the simulation was 20 ns including 1 ns equilibration time. a) Block average of the osmotic pressure with 1 ns sampling time (blue line with asterisks) and running average of the osmotic pressure (red line). The horizontal lines mark the mean osmotic pressure (solid) and a ±5 % interval around it (grey dashed lines). b) Close-up of the histogram of the osmotic pressure. The bin at $\Pi = 0$ was not printed. The vertical dashed line marks the mean osmotic pressure. c) Number density distribution of ion species in the box. The vertical dashed line marks the position of the membrane. The horizontal line marks the position of the ideal concentration with 'hard' membrane walls (black solid), and of the actual concentration between the membrane walls (grey dashed line). d) Close-up of the number density distribution at the membrane wall.

B.3 Osmotic Pressure - $\alpha_{\mathrm{Cl}} = 2.0 \cdot 10^{-3}\mathrm{nm}^3$

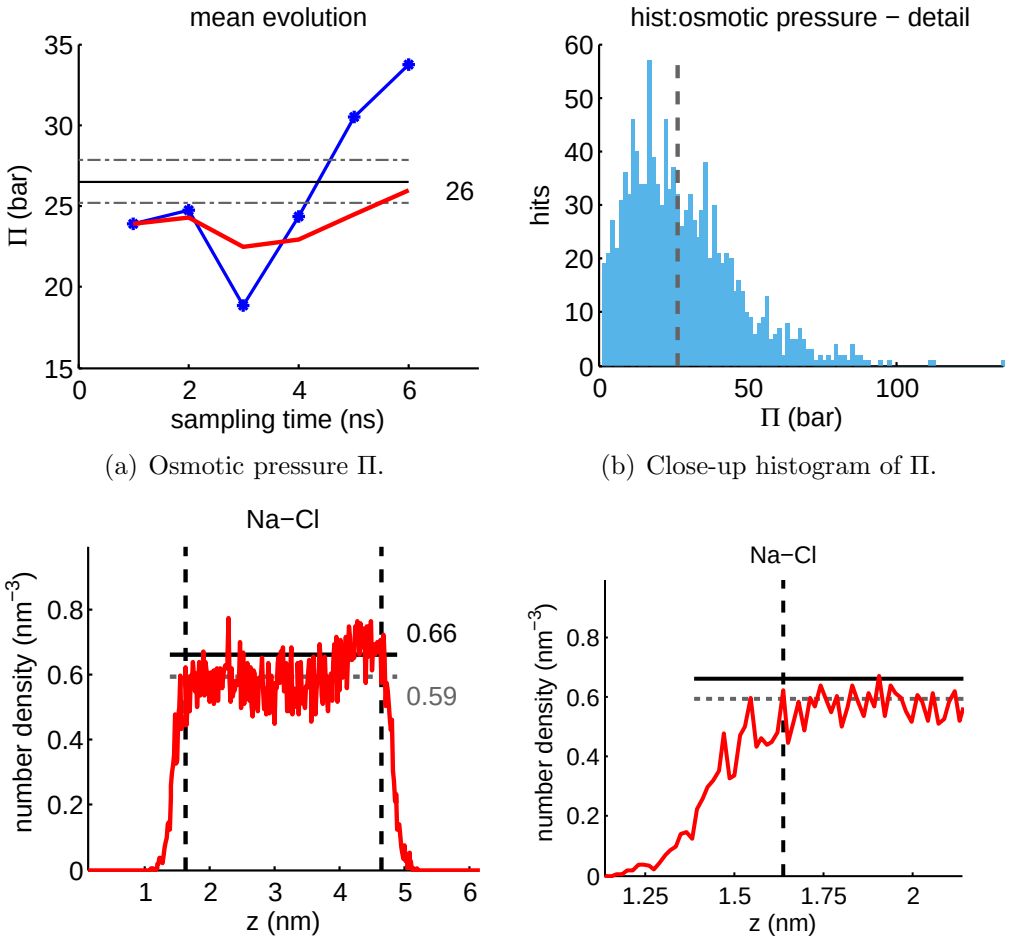

(a) Osmotic pressure Π.

(b) Close-up histogram of Π.

(c) Number density distribution ρ_N.

(d) Close-up of the ρ_N.

Figure B.43: **(0.5 M alpha 2.0)** Summary of results obtained from an osmotic pressure calculation using membrane walls with a force constant k of 100 kJ/(mol·nm^2). 10 NaCl ion pairs are dissolved in 2048 SW10e water molecules and are confined in a 3 nm slab, resulting in a salt concentration of 0.49 M inside the ion domain. The NVT ensemble was applied after 300 ps of equilibration in a NPT ensemble at a pressure of 1 bar. Further results are shown in Tab. 4.20. The simulation was performed for an ion model with $\alpha_{\mathrm{Cl}} = 2.0 \cdot 10^{-3}\mathrm{nm}^3$. The temperature is 298.15 K. The total duration of the simulation was 8 ns including 1 ns equilibration time. a) Block average of the osmotic pressure with 1 ns sampling time (blue line with asterisks) and running average of the osmotic pressure (red line). The horizontal lines mark the mean osmotic pressure (solid) and a ±5 % interval around it (grey dashed lines). b) Close-up of the histogram of the osmotic pressure. The bin at $\Pi = 0$ was not printed. The vertical dashed line marks the mean osmotic pressure. c) Number density distribution of ion species in the box. The vertical dashed line marks the position of the membrane. The horizontal line marks the position of the ideal concentration with 'hard' membrane walls (black solid), and of the actual concentration between the membrane walls (grey dashed line). d) Close-up of the number density distribution at the membrane wall.

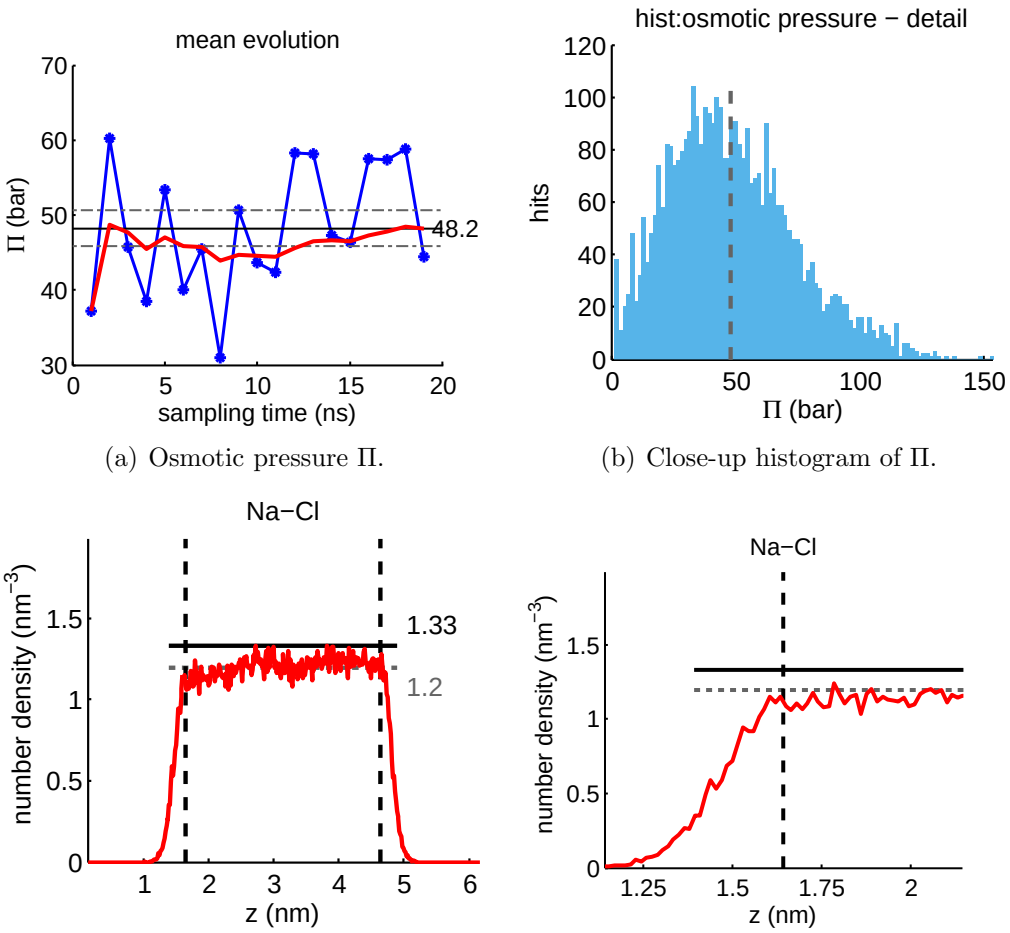

(a) Osmotic pressure Π.

(b) Close-up histogram of Π.

(c) Number density distribution ρ_N.

(d) Close-up of the ρ_N.

Figure B.44: **(1 M, $\alpha_{\mathrm{Cl}} = 2.0$)** Summary of results obtained from an osmotic pressure calculation using membrane walls with a force constant k of 100 kJ/(mol·nm^2). The ions were decoupled from the thermostat. 20 NaCl ion pairs are dissolved in 2048 SW10e water molecules and are confined in a 3 nm slab, resulting in a salt concentration of 1.00 M inside the ion domain. The NVT ensemble was applied after 300 ps of equilibration in a NAPT ensemble at a pressure of 1 bar. Further results are shown in Tab. 4.20. The simulation was performed for an ion model with $\alpha_{\mathrm{Cl}} = 2.0 \cdot 10^{-3}\mathrm{nm}^3$. The temperature is 298.15 K. The total duration of the simulation was 20 ns including 1 ns equilibration time. a) Block average of the osmotic pressure with 1 ns sampling time (blue line with asterisks) and running average of the osmotic pressure (red line). The horizontal lines mark the mean osmotic pressure (solid) and a ±5 % interval around it (grey dashed lines). b) Close-up of the histogram of the osmotic pressure. The bin at $\Pi = 0$ was not printed. The vertical dashed line marks the mean osmotic pressure. c) Number density distribution of ion species in the box. The vertical dashed line marks the position of the membrane. The horizontal line marks the position of the ideal concentration with 'hard' membrane walls (black solid), and of the actual concentration between the membrane walls (grey dashed line). d) Close-up of the number density distribution at the membrane wall.

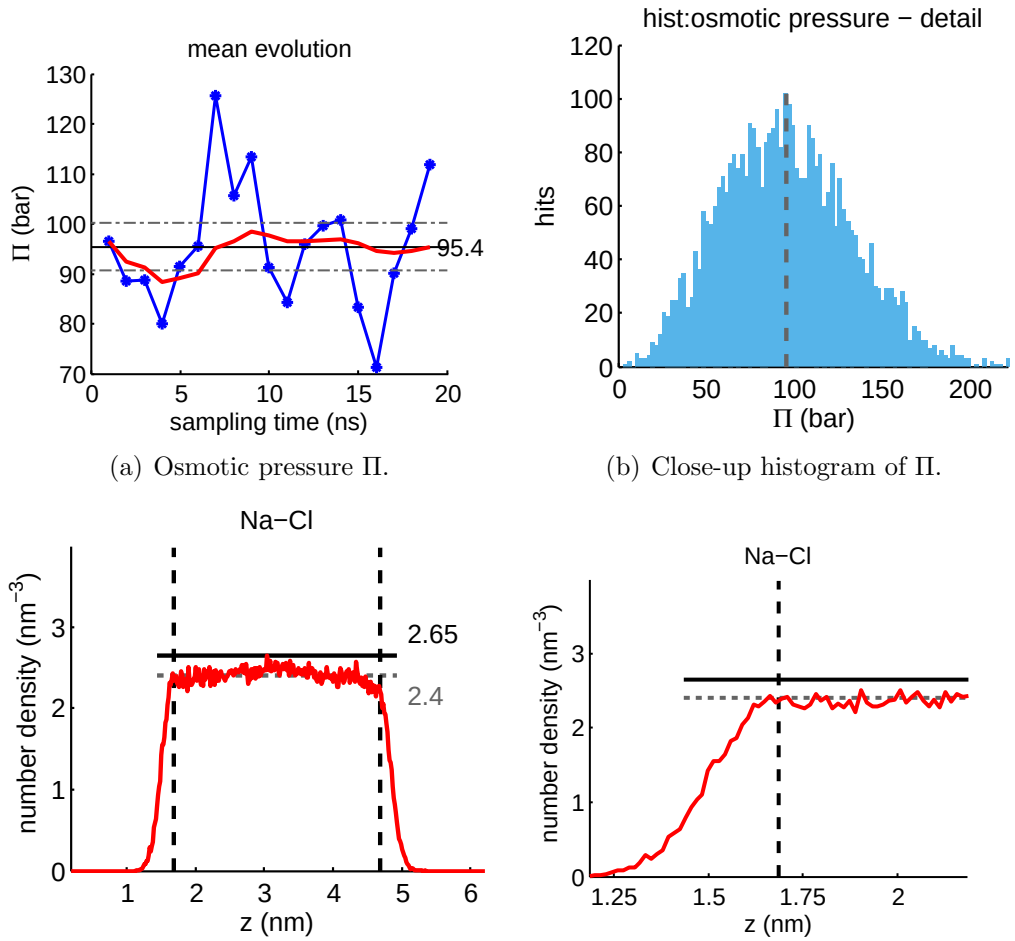

(a) Osmotic pressure Π.

(b) Close-up histogram of Π.

(c) Number density distribution ρ_N.

(d) Close-up of the ρ_N.

Figure B.45: **(2 M, $\alpha_{\mathrm{Cl}} = 2.0$)** Summary of results obtained from an osmotic pressure calculation using membrane walls with a force constant k of 100 kJ/(mol·nm^2). The ions were decoupled from the thermostat. 40 NaCl ion pairs are dissolved in 2048 SW10e water molecules and are confined in a 3 nm slab, resulting in a salt concentration of 2.00 M inside the ion domain. The NVT ensemble was applied after 300 ps of equilibration in a NAPT ensemble at a pressure of 1 bar. Further results are shown in Tab. 4.20. The simulation was performed for an ion model with $\alpha_{\mathrm{Cl}} = 2.0 \cdot 10^{-3}\mathrm{nm}^3$. The temperature is 298.15 K. The total duration of the simulation was 20 ns including 1 ns equilibration time. a) Block average of the osmotic pressure with 1 ns sampling time (blue line with asterisks) and running average of the osmotic pressure (red line). The horizontal lines mark the mean osmotic pressure (solid) and a ±5 % interval around it (grey dashed lines). b) Close-up of the histogram of the osmotic pressure. The bin at $\Pi = 0$ was not printed. The vertical dashed line marks the mean osmotic pressure. c) Number density distribution of ion species in the box. The vertical dashed line marks the position of the membrane. The horizontal line marks the position of the ideal concentration with 'hard' membrane walls (black solid), and of the actual concentration between the membrane walls (grey dashed line). d) Close-up of the number density distribution at the membrane wall.

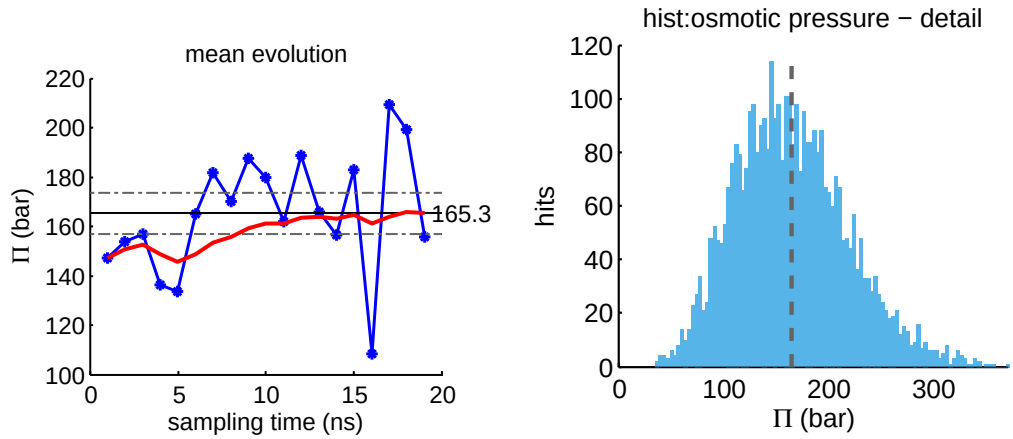

(a) Osmotic pressure Π.

(b) Close-up histogram of Π.

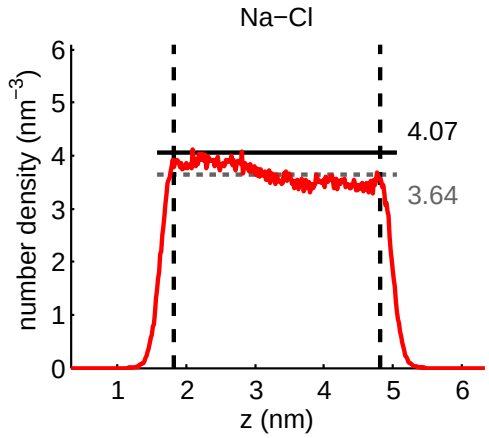

(c) Number density distribution ρ_N.

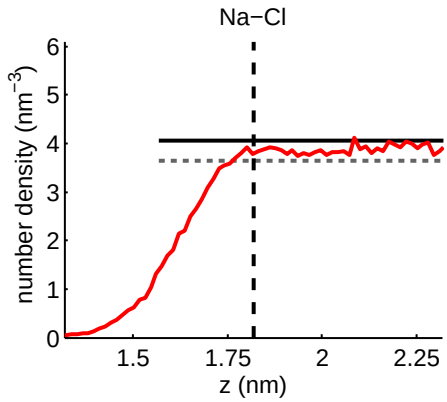

(d) Close-up of the ρ_N.

Figure B.46: **(3 M, $\alpha_{Cl} = 2.0$)** Summary of results obtained from an osmotic pressure calculation using membrane walls with a force constant k of 100 kJ/(mol·nm^2). The ions were decoupled from the thermostat. 20 NaCl ion pairs are dissolved in 2048 SW10e water molecules and are confined in a 3 nm slab, resulting in a salt concentration of 3.02 M inside the ion domain. The NVT ensemble was applied after 300 ps of equilibration in a NAPT ensemble at a pressure of 1 bar. Further results are shown in Tab. 4.20. The simulation was performed for an ion model with $\alpha_{Cl} = 2.0 \cdot 10^{-3}$nm^3. The temperature is 298.15 K. The total duration of the simulation was 20 ns including 1 ns equilibration time. a) Block average of the osmotic pressure with 1 ns sampling time (blue line with asterisks) and running average of the osmotic pressure (red line). The horizontal lines mark the mean osmotic pressure (solid) and a ±5 % interval around it (grey dashed lines). b) Close-up of the histogram of the osmotic pressure. The bin at $\Pi = 0$ was not printed. The vertical dashed line marks the mean osmotic pressure. c) Number density distribution of ion species in the box. The vertical dashed line marks the position of the membrane. The horizontal line marks the position of the ideal concentration with 'hard' membrane walls (black solid), and of the actual concentration between the membrane walls (grey dashed line). d) Close-up of the number density distribution at the membrane wall.

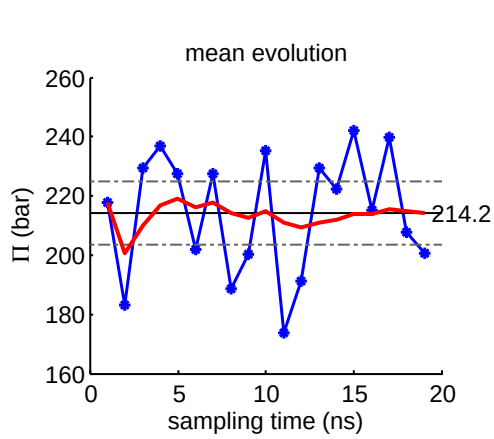

(a) Osmotic pressure Π.

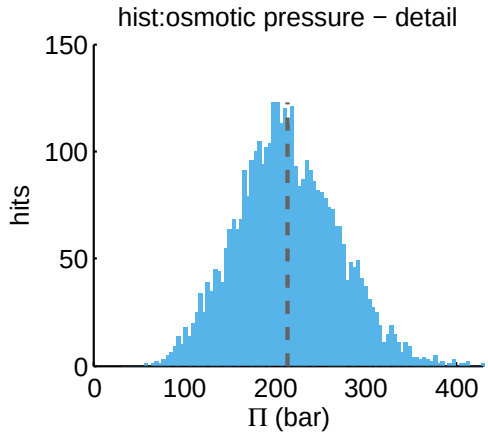

(b) Close-up histogram of Π.

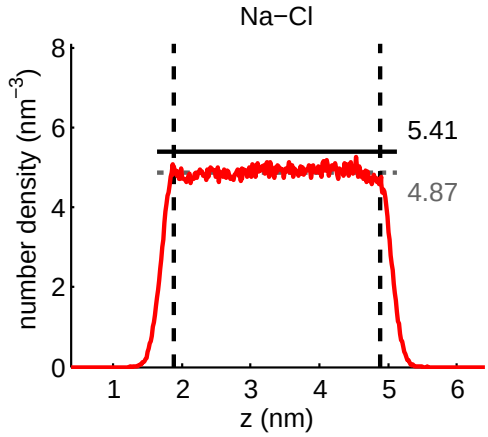

(c) Number density distribution ρ_N.

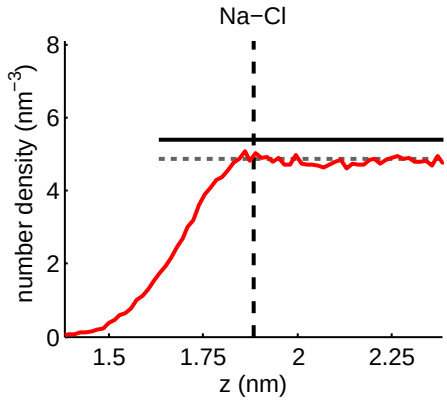

(d) Close-up of the ρ_N.

Figure B.47: **(4 M, $\alpha_{Cl} = 2.0$)** Summary of results obtained from an osmotic pressure calculation using membrane walls with a force constant k of 100 kJ/(mol·nm^2). 80 NaCl ion pairs are dissolved in 2048 SW10e water molecules and are confined in a 3 nm slab, resulting in a salt concentration of 4.05 M inside the ion domain. The NVT ensemble was applied after 300 ps of equilibration in a NAPT ensemble at a pressure of 1 bar. Further results are shown in Tab. 4.20. The simulation was performed for an ion model with $\alpha_{Cl} = 2.0 \cdot 10^{-3}$nm^3. The temperature is 298.15 K. The total duration of the simulation was 20 ns including 1 ns equilibration time. a) Block average of the osmotic pressure with 1 ns sampling time (blue line with asterisks) and running average of the osmotic pressure (red line). The horizontal lines mark the mean osmotic pressure (solid) and a ±5 % interval around it (grey dashed lines). b) Close-up of the histogram of the osmotic pressure. The bin at $\Pi = 0$ was not printed. The vertical dashed line marks the mean osmotic pressure. c) Number density distribution of ion species in the box. The vertical dashed line marks the position of the membrane. The horizontal line marks the position of the ideal concentration with 'hard' membrane walls (black solid), and of the actual concentration between the membrane walls (grey dashed line). d) Close-up of the number density distribution at the membrane wall.

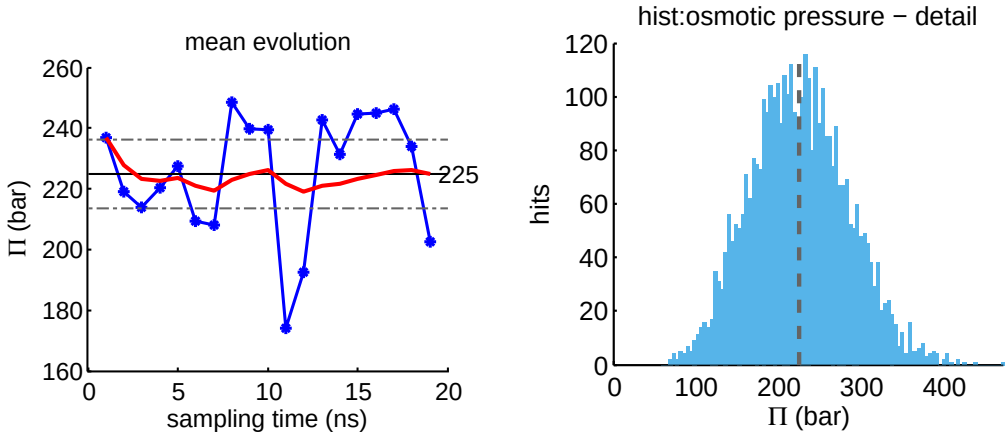

(a) Osmotic pressure Π.

(b) Close-up histogram of Π.

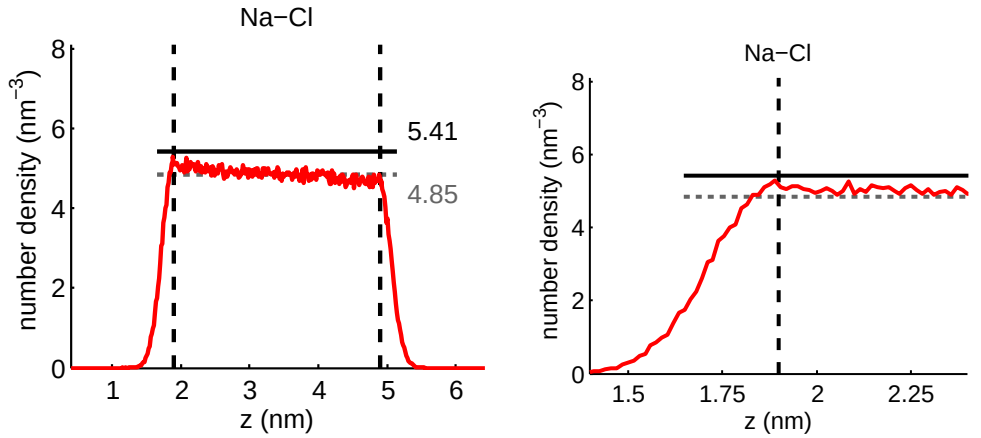

(c) Number density distribution ρ_N.

(d) Close-up of the ρ_N.

Figure B.48: **(4 M, $\alpha_{Cl} = 2.0$)** Summary of results obtained from an osmotic pressure calculation using membrane walls with a force constant k of 100 kJ/(mol·nm^2). The ions were decoupled from the thermostat. 80 NaCl ion pairs are dissolved in 2048 SW10e water molecules and are confined in a 3 nm slab, resulting in a salt concentration of 4.03 M inside the ion domain. The NVT ensemble was applied after 300 ps of equilibration in a NAPT ensemble at a pressure of 1 bar. Further results are shown in Tab. 4.20. The simulation was performed for an ion model with $\alpha_{Cl} = 2.0 \cdot 10^{-3}$nm^3. The temperature is 313.15 K. The total duration of the simulation was 20 ns including 1 ns equilibration time. a) Block average of the osmotic pressure with 1 ns sampling time (blue line with asterisks) and running average of the osmotic pressure (red line). The horizontal lines mark the mean osmotic pressure (solid) and a ±5 % interval around it (grey dashed lines). b) Close-up of the histogram of the osmotic pressure. The bin at $\Pi = 0$ was not printed. The vertical dashed line marks the mean osmotic pressure. c) Number density distribution of ion species in the box. The vertical dashed line marks the position of the membrane. The horizontal line marks the position of the ideal concentration with 'hard' membrane walls (black solid), and of the actual concentration between the membrane walls (grey dashed line). d) Close-up of the number density distribution at the membrane wall.

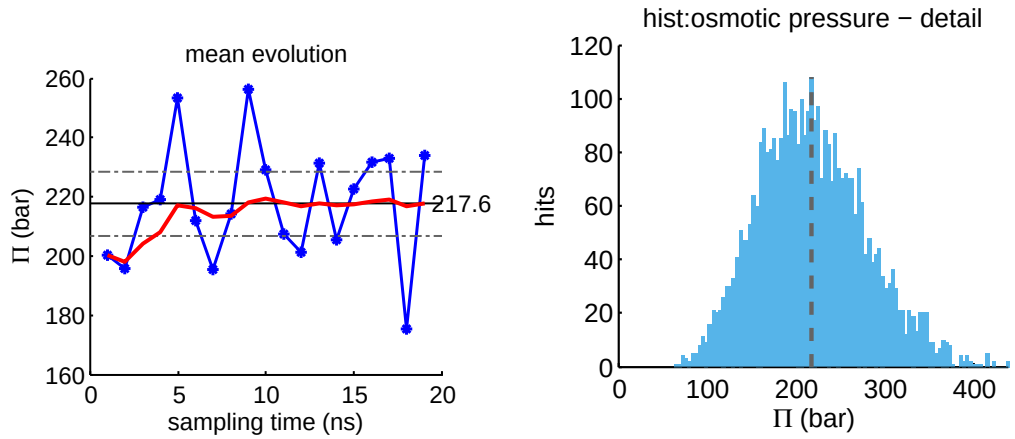

(a) Osmotic pressure Π.

(b) Close-up histogram of Π.

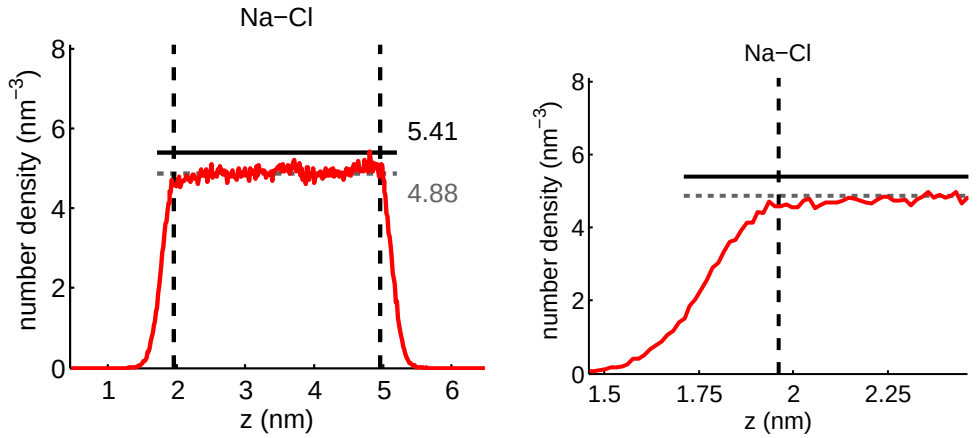

(c) Number density distribution ρ_N.

(d) Close-up of the ρ_N.

Figure B.49: **(4 M, $\alpha_{\mathrm{Cl}} = 2.0$)** Summary of results obtained from an osmotic pressure calculation using membrane walls with a force constant k of 100 kJ/(mol·nm^2). The ions were decoupled from the thermostat. 80 NaCl ion pairs are dissolved in 2048 SW10e water molecules and are confined in a 3 nm slab, resulting in a salt concentration of 4.05 M inside the ion domain. The NVT ensemble was applied after 300 ps of equilibration in a NAPT ensemble at a pressure of 1 bar. Further results are shown in Tab. 4.20. The simulation was performed for an ion model with $\alpha_{\mathrm{Cl}} = 2.0 \cdot 10^{-3}\mathrm{nm}^3$. The temperature is 333.15 K. The total duration of the simulation was 20 ns including 1 ns equilibration time. a) Block average of the osmotic pressure with 1 ns sampling time (blue line with asterisks) and running average of the osmotic pressure (red line). The horizontal lines mark the mean osmotic pressure (solid) and a ±5 % interval around it (grey dashed lines). b) Close-up of the histogram of the osmotic pressure. The bin at $\Pi = 0$ was not printed. The vertical dashed line marks the mean osmotic pressure. c) Number density distribution of ion species in the box. The vertical dashed line marks the position of the membrane. The horizontal line marks the position of the ideal concentration with 'hard' membrane walls (black solid), and of the actual concentration between the membrane walls (grey dashed line). d) Close-up of the number density distribution at the membrane wall.

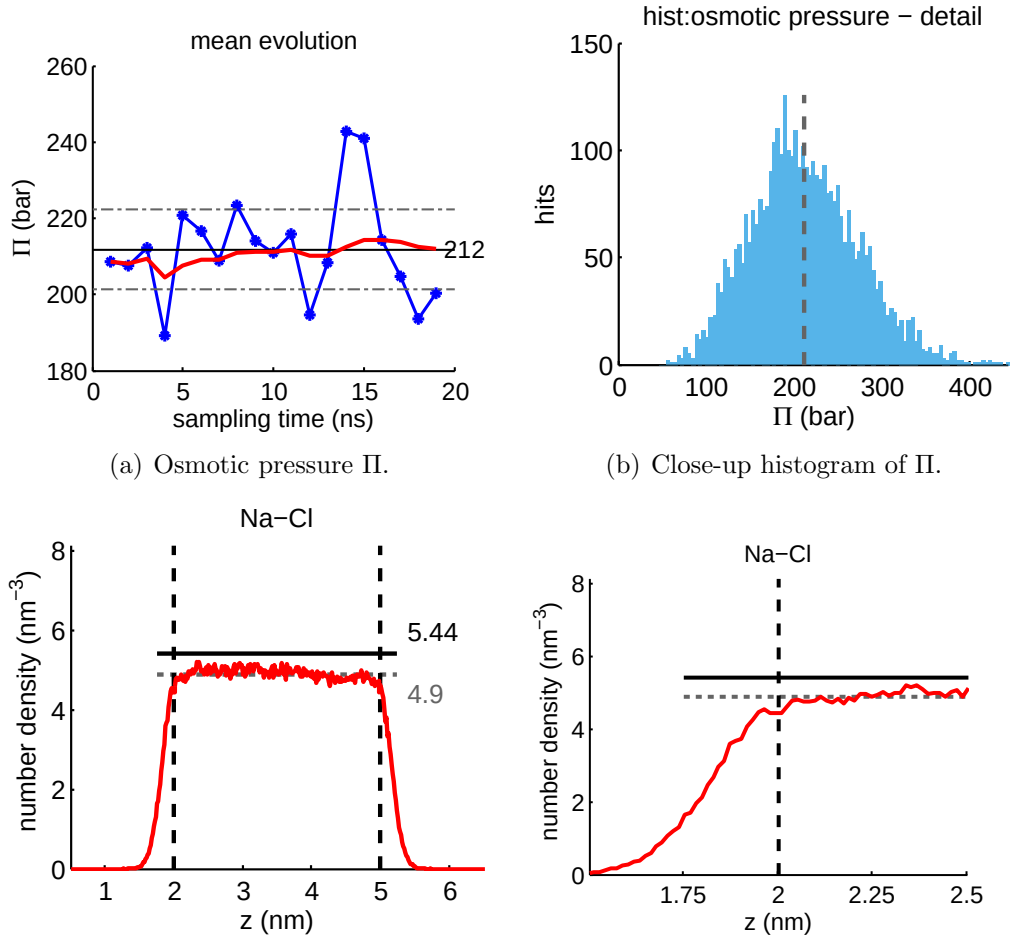

(a) Osmotic pressure Π.

(b) Close-up histogram of Π.

(c) Number density distribution ρ_N.

(d) Close-up of the ρ_N.

Figure B.50: **(4 M, $\alpha_{\mathrm{Cl}} = 2.0$)** Summary of results obtained from an osmotic pressure calculation using membrane walls with a force constant k of 100 kJ/(mol·nm^2). The ions were decoupled from the thermostat. 80 NaCl ion pairs are dissolved in 2048 SW10e water molecules and are confined in a 3 nm slab, resulting in a salt concentration of 4.07 M inside the ion domain. The NVT ensemble was applied after 300 ps of equilibration in a NAPT ensemble at a pressure of 1 bar. Further results are shown in Tab. 4.20. The simulation was performed for an ion model with $\alpha_{\mathrm{Cl}} = 2.0 \cdot 10^{-3}\mathrm{nm}^3$. The temperature is 333.15 K. The total duration of the simulation was 20 ns including 1 ns equilibration time. a) Block average of the osmotic pressure with 1 ns sampling time (blue line with asterisks) and running average of the osmotic pressure (red line). The horizontal lines mark the mean osmotic pressure (solid) and a ±5 % interval around it (grey dashed lines). b) Close-up of the histogram of the osmotic pressure. The bin at $\Pi = 0$ was not printed. The vertical dashed line marks the mean osmotic pressure. c) Number density distribution of ion species in the box. The vertical dashed line marks the position of the membrane. The horizontal line marks the position of the ideal concentration with 'hard' membrane walls (black solid), and of the actual concentration between the membrane walls (grey dashed line). d) Close-up of the number density distribution at the membrane wall.

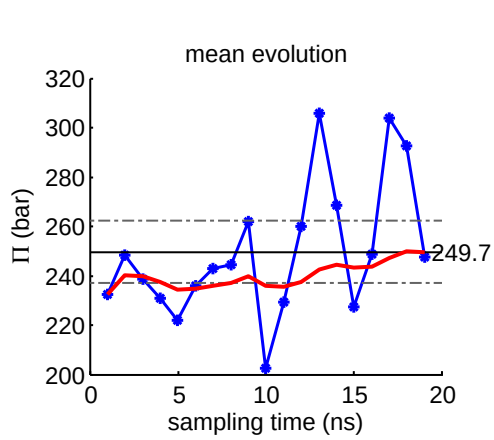

(a) Osmotic pressure Π.

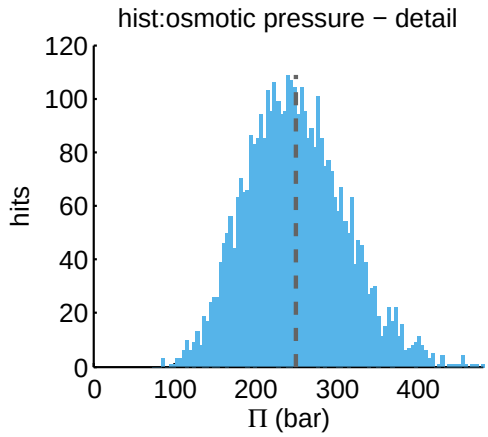

(b) Close-up histogram of Π.

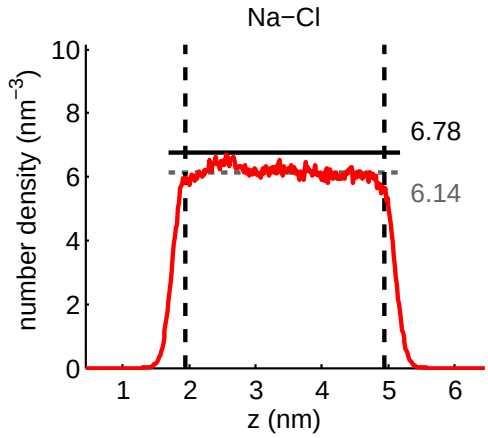

(c) Number density distribution ρ_N.

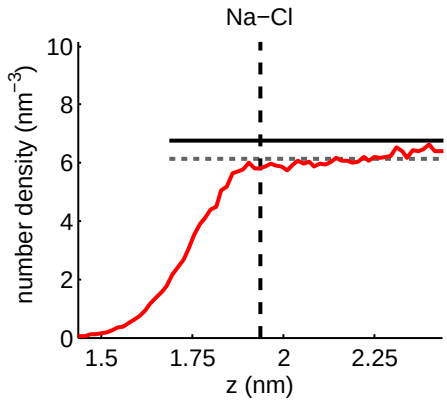

(d) Close-up of the ρ_N.

Figure B.51: **(5 M, α_{Cl} = 2.0)** Summary of results obtained from an osmotic pressure calculation using membrane walls with a force constant k of 100 kJ/(mol·nm^2). The ions were decoupled from the thermostat. 100 NaCl ion pairs are dissolved in 2048 SW10e water molecules and are confined in a 3 nm slab, resulting in a salt concentration of 5.10 M inside the ion domain. The NVT ensemble was applied after 300 ps of equilibration in a NAPT ensemble at a pressure of 1 bar. Further results are shown in Tab. 4.20. The simulation was performed for an ion model with $\alpha_{Cl} = 2.0 \cdot 10^{-3}$nm^3. The temperature is 298.15 K. The total duration of the simulation was 20 ns including 1 ns equilibration time. a) Block average of the osmotic pressure with 1 ns sampling time (blue line with asterisks) and running average of the osmotic pressure (red line). The horizontal lines mark the mean osmotic pressure (solid) and a ±5 % interval around it (grey dashed lines). b) Close-up of the histogram of the osmotic pressure. The bin at Π = 0 was not printed. The vertical dashed line marks the mean osmotic pressure. c) Number density distribution of ion species in the box. The vertical dashed line marks the position of the membrane. The horizontal line marks the position of the ideal concentration with 'hard' membrane walls (black solid), and of the actual concentration between the membrane walls (grey dashed line). d) Close-up of the number density distribution at the membrane wall.

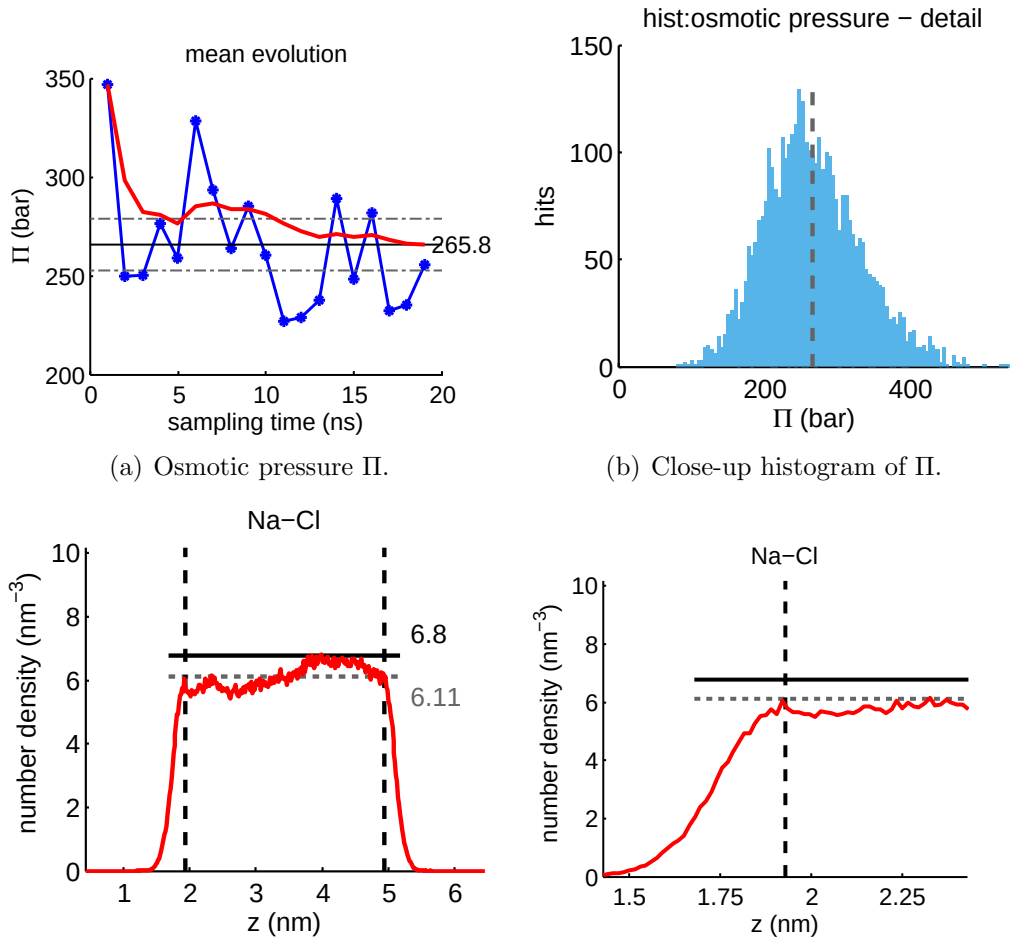

(a) Osmotic pressure Π.

(b) Close-up histogram of Π.

(c) Number density distribution ρ_N.

(d) Close-up of the ρ_N.

Figure B.52: **(5 M, $\alpha_{\mathrm{Cl}} = 2.0$)** Summary of results obtained from an osmotic pressure calculation using membrane walls with a force constant k of 100 kJ/(mol·nm^2). The ions were decoupled from the thermostat. 100 NaCl ion pairs are dissolved in 2048 SW10e water molecules and are confined in a 3 nm slab, resulting in a salt concentration of 5.07 M inside the ion domain. The NVT ensemble was applied after 300 ps of equilibration in a NAPT ensemble at a pressure of 1 bar. Further results are shown in Tab. 4.20. The simulation was performed for an ion model with $\alpha_{\mathrm{Cl}} = 2.0 \cdot 10^{-3}\mathrm{nm}^3$. The temperature is 313.15 K. The total duration of the simulation was 20 ns including 1 ns equilibration time. a) Block average of the osmotic pressure with 1 ns sampling time (blue line with asterisks) and running average of the osmotic pressure (red line). The horizontal lines mark the mean osmotic pressure (solid) and a ±5 % interval around it (grey dashed lines). b) Close-up of the histogram of the osmotic pressure. The bin at $\Pi = 0$ was not printed. The vertical dashed line marks the mean osmotic pressure. c) Number density distribution of ion species in the box. The vertical dashed line marks the position of the membrane. The horizontal line marks the position of the ideal concentration with 'hard' membrane walls (black solid), and of the actual concentration between the membrane walls (grey dashed line). d) Close-up of the number density distribution at the membrane wall.

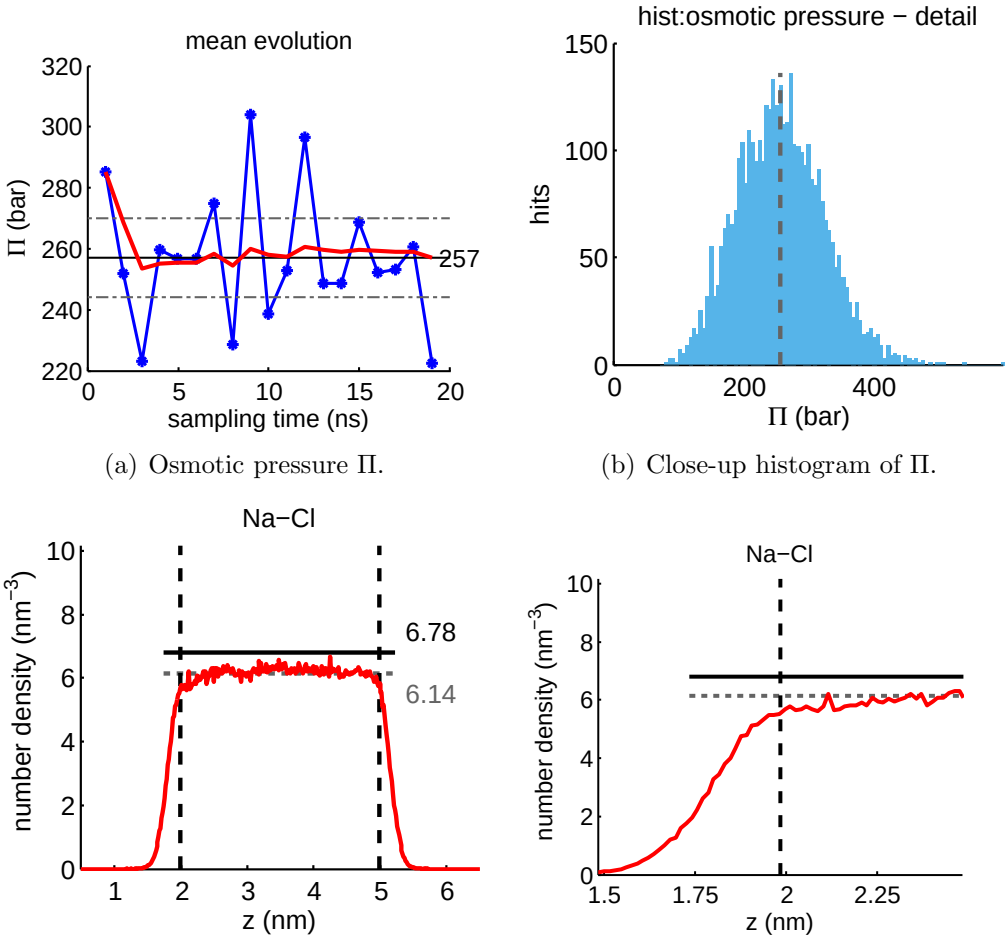

(a) Osmotic pressure Π.

(b) Close-up histogram of Π.

(c) Number density distribution ρ_N.

(d) Close-up of the ρ_N.

Figure B.53: **(5 M, $\alpha_{\mathrm{Cl}} = 2.0$)** Summary of results obtained from an osmotic pressure calculation using membrane walls with a force constant k of 100 kJ/(mol·nm^2). The ions were decoupled from the thermostat. 100 NaCl ion pairs are dissolved in 2048 SW10e water molecules and are confined in a 3 nm slab, resulting in a salt concentration of 5.10 M inside the ion domain. The NVT ensemble was applied after 300 ps of equilibration in a NAPT ensemble at a pressure of 1 bar. Further results are shown in Tab. 4.20. The simulation was performed for an ion model with $\alpha_{\mathrm{Cl}} = 2.0 \cdot 10^{-3}\mathrm{nm}^3$. The temperature is 333.15 K. The total duration of the simulation was 20 ns including 1 ns equilibration time. a) Block average of the osmotic pressure with 1 ns sampling time (blue line with asterisks) and running average of the osmotic pressure (red line). The horizontal lines mark the mean osmotic pressure (solid) and a ±5 % interval around it (grey dashed lines). b) Close-up of the histogram of the osmotic pressure. The bin at $\Pi = 0$ was not printed. The vertical dashed line marks the mean osmotic pressure. c) Number density distribution of ion species in the box. The vertical dashed line marks the position of the membrane. The horizontal line marks the position of the ideal concentration with 'hard' membrane walls (black solid), and of the actual concentration between the membrane walls (grey dashed line). d) Close-up of the number density distribution at the membrane wall.

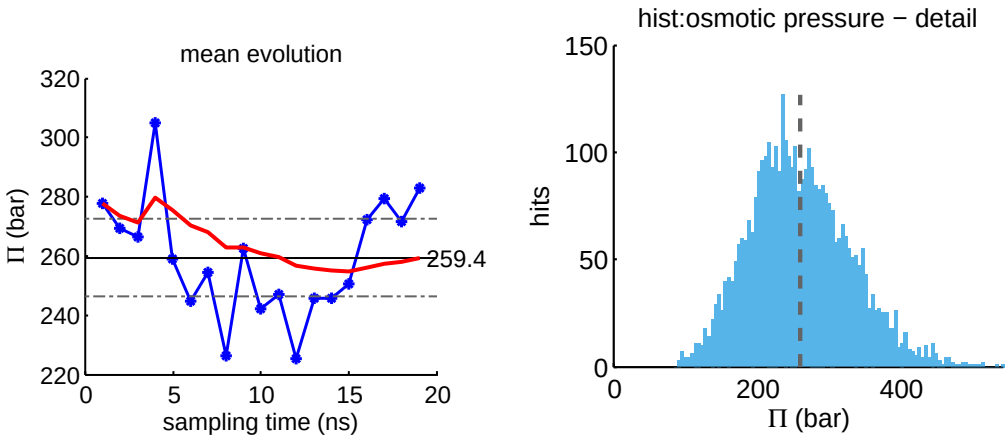

(a) Osmotic pressure Π.

(b) Close-up histogram of Π.

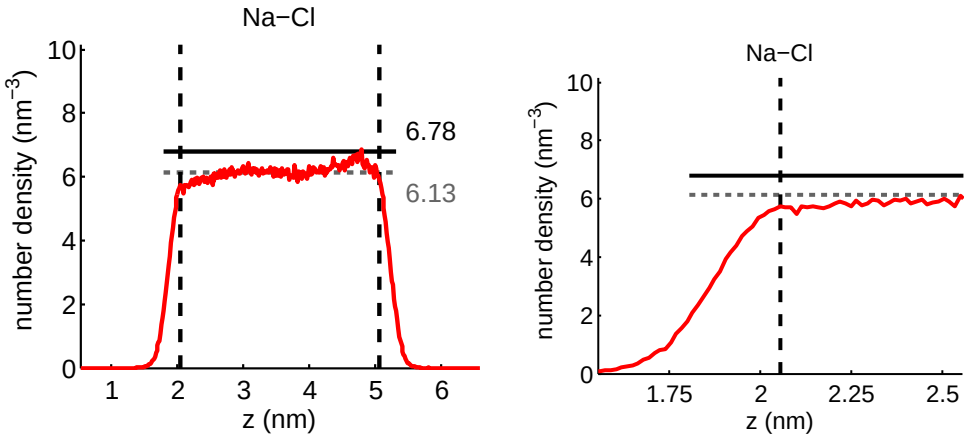

(c) Number density distribution ρ_N.

(d) Close-up of the ρ_N.

Figure B.54: **(5 M, $\alpha_{Cl} = 2.0$)** Summary of results obtained from an osmotic pressure calculation using membrane walls with a force constant k of 100 kJ/(mol·nm^2). The ions were decoupled from the thermostat. 100 NaCl ion pairs are dissolved in 2048 SW10e water molecules and are confined in a 3 nm slab, resulting in a salt concentration of 5.09 M inside the ion domain. The NVT ensemble was applied after 300 ps of equilibration in a NAPT ensemble at a pressure of 1 bar. Further results are shown in Tab. 4.19. The simulation was performed for an ion model with $\alpha_{Cl} = 2.0 \cdot 10^{-3}$nm^3. The temperature is 353.15 K. The total duration of the simulation was 20 ns including 1 ns equilibration time. a) Block average of the osmotic pressure with 1 ns sampling time (blue line with asterisks) and running average of the osmotic pressure (red line). The horizontal lines mark the mean osmotic pressure (solid) and a ±5 % interval around it (grey dashed lines). b) Close-up of the histogram of the osmotic pressure. The bin at $\Pi = 0$ was not printed. The vertical dashed line marks the mean osmotic pressure. c) Number density distribution of ion species in the box. The vertical dashed line marks the position of the membrane. The horizontal line marks the position of the ideal concentration with 'hard' membrane walls (black solid), and of the actual concentration between the membrane walls (grey dashed line). d) Close-up of the number density distribution at the membrane wall.

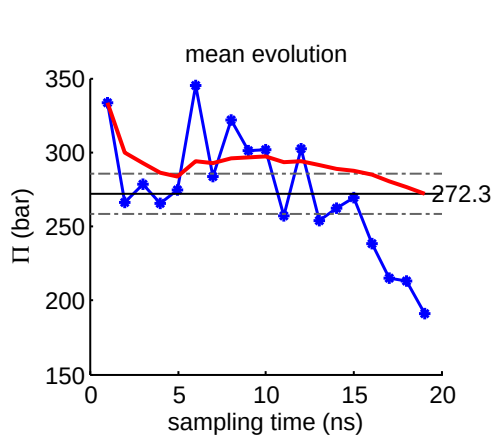

(a) Osmotic pressure Π.

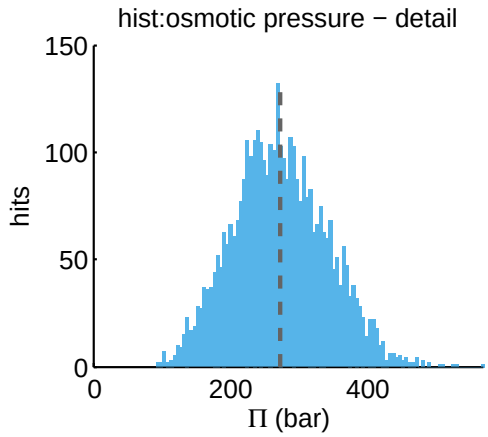

(b) Close-up histogram of Π.

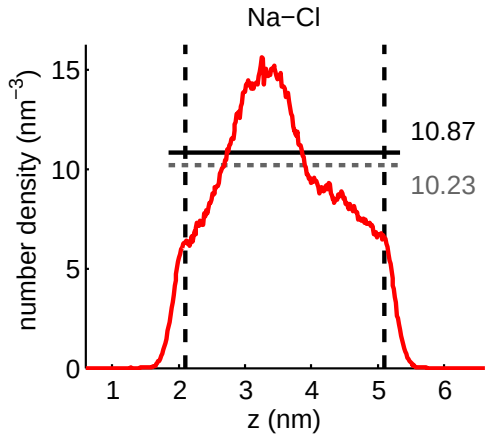

(c) Number density distribution ρ_N.

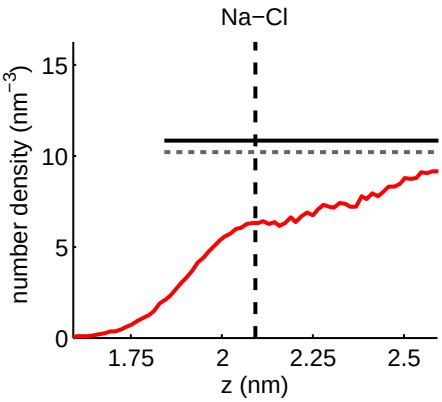

(d) Close-up of the ρ_N.

Figure B.55: **(8 M, $\alpha_{\mathrm{Cl}} = 2.0$)** Summary of results obtained from an osmotic pressure calculation using membrane walls with a force constant k of 100 kJ/(mol·nm^2). The ions were decoupled from the thermostat. 160 NaCl ion pairs are dissolved in 2048 SW10e water molecules and are confined in a 3 nm slab, resulting in a salt concentration of 8.49 M inside the ion domain. The NVT ensemble was applied after 300 ps of equilibration in a NAPT ensemble at a pressure of 1 bar. Further results are shown in Tab. 4.20. The simulation was performed for an ion model with $\alpha_{\mathrm{Cl}} = 2.0 \cdot 10^{-3}\mathrm{nm}^3$. The temperature is 298.15 K. The total duration of the simulation was 20 ns including 1 ns equilibration time. a) Block average of the osmotic pressure with 1 ns sampling time (blue line with asterisks) and running average of the osmotic pressure (red line). The horizontal lines mark the mean osmotic pressure (solid) and a ±5 % interval around it (grey dashed lines). b) Close-up of the histogram of the osmotic pressure. The bin at $\Pi = 0$ was not printed. The vertical dashed line marks the mean osmotic pressure. c) Number density distribution of ion species in the box. The vertical dashed line marks the position of the membrane. The horizontal line marks the position of the ideal concentration with 'hard' membrane walls (black solid), and of the actual concentration between the membrane walls (grey dashed line). d) Close-up of the number density distribution at the membrane wall.

Appendix C

Surface Tension

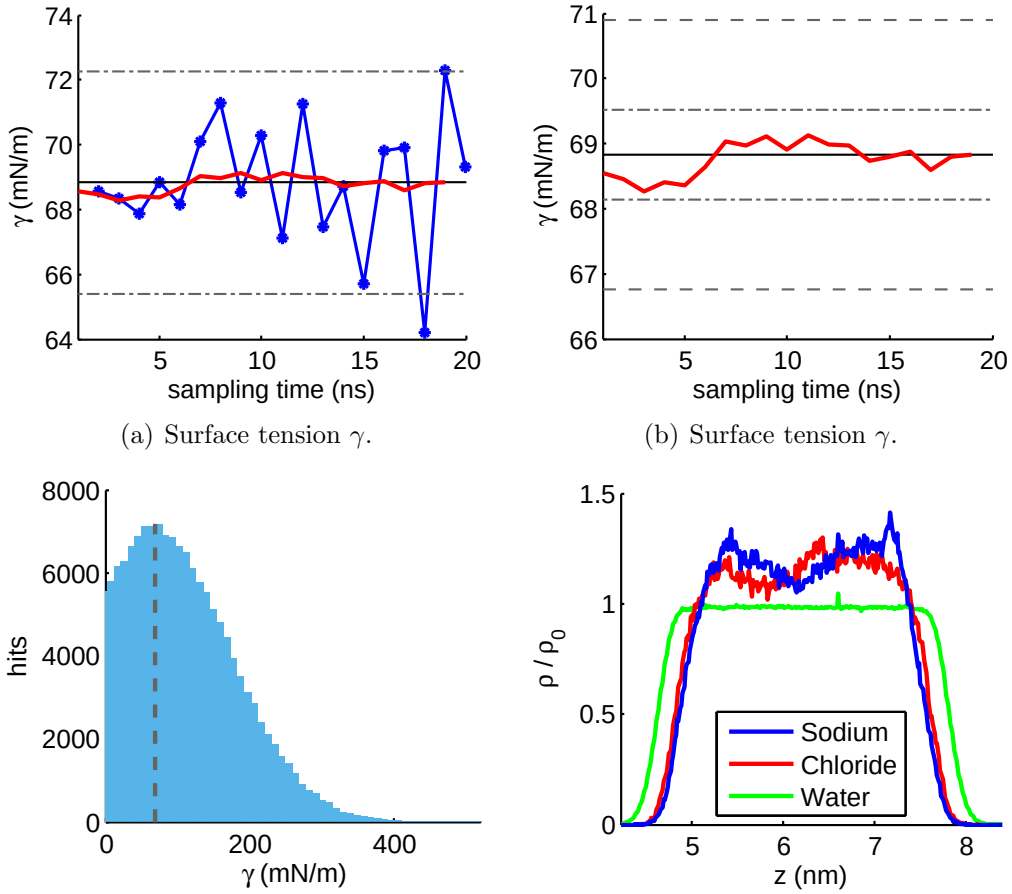

(a) Surface tension γ.

(b) Surface tension γ.

(c) Histogram of γ.

(d) Normalised density ρ/ρ_0.

Figure C.1: **(1 M 25 °C NaCl SW10e solution)** Summary of results obtained from a surface tension calculation. 19 NaCl ion pairs are dissolved in 1024 SPC/E water molecules, resulting in a salt concentration of roughly 1 M. The solution forms a slab of roughly 3 nm width, which is positioned in the centre of a simulation box of over 12 nm length. The corrected surface tension is 73.2 ± 0.90 mN/m. Further results are shown in Tab. 4.24. The temperature is 298.15 K. The total duration of the simulation is 20 ns including 1 ns equilibration time. a) Block average of the surface tension with 1 ns sampling time (blue line with asterisks) and running average of the surface tension (red line). The horizontal lines mark the mean surface tension (solid) and a ±5 % interval around it (grey dashed lines). b) Running average of the surface tension at 1 ns intervals (red line). The horizontal lines mark the mean surface tension (solid), a ±1 % interval around it (grey dashed-dotted lines) and a ±3 % interval around it (grey dashed lines). c) Histogram of the surface tension. The vertical dashed line marks the mean surface tension. d) Normalised density distribution of ionic species and water in the box.

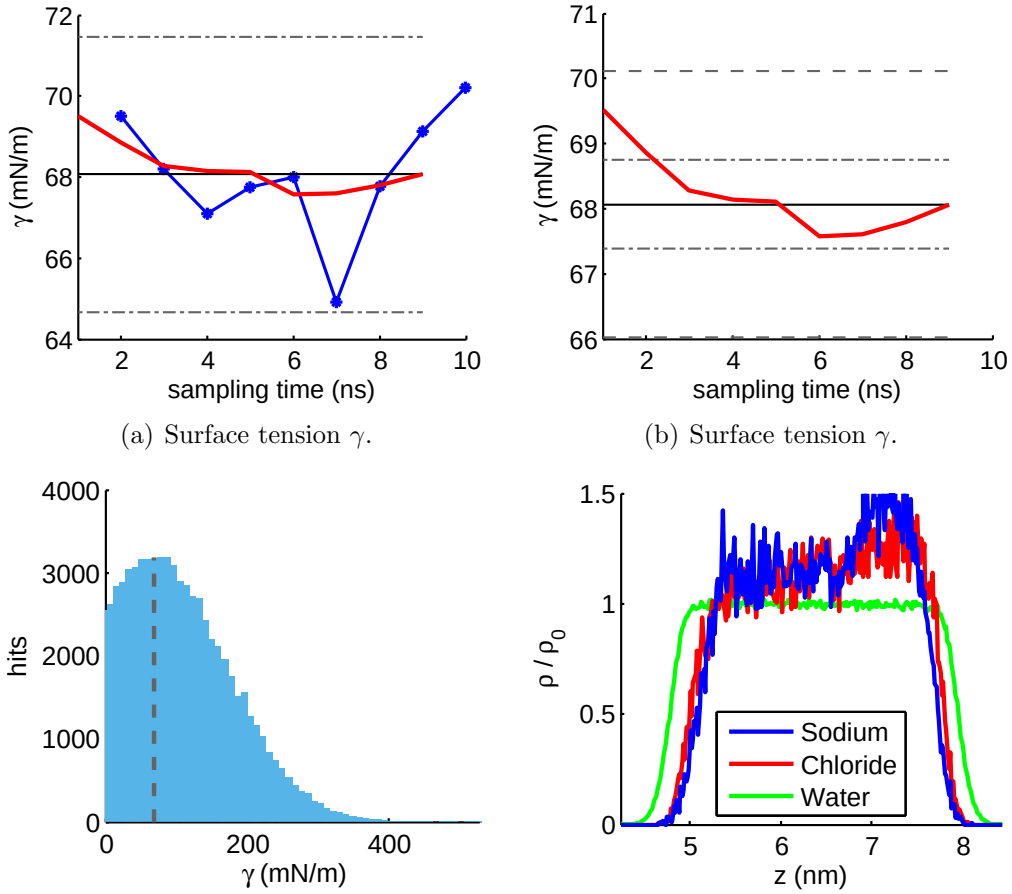

(a) Surface tension γ.

(b) Surface tension γ.

(c) Histogram of γ.

(d) Normalised density ρ/ρ_0.

Figure C.2: **(1 M 40 °C NaCl SW10e solution)** Summary of results obtained from a surface tension calculation. 19 NaCl ion pairs are dissolved in 1024 SPC/E water molecules, resulting in a salt concentration of roughly 1 M. The solution forms a slab of roughly 3 nm width, which is positioned in the centre of a simulation box of over 12 nm length. The corrected surface tension is 72.5 ± 1.01 mN/m. Further results are shown in Tab. 4.24. The temperature is 313.15 K. The total duration of the simulation is 20 ns including 1 ns equilibration time. a) Block average of the surface tension with 1 ns sampling time (blue line with asterisks) and running average of the surface tension (red line). The horizontal lines mark the mean surface tension (solid) and a $\pm 5\,\%$ interval around it (grey dashed lines). b) Running average of the surface tension at 1 ns intervals (red line). The horizontal lines mark the mean surface tension (solid), a $\pm 1\,\%$ interval around it (grey dashed-dotted lines) and a $\pm 3\,\%$ interval around it (grey dashed lines). c) Histogram of the surface tension. The vertical dashed line marks the mean surface tension. d) Normalised density distribution of ionic species and water in the box.

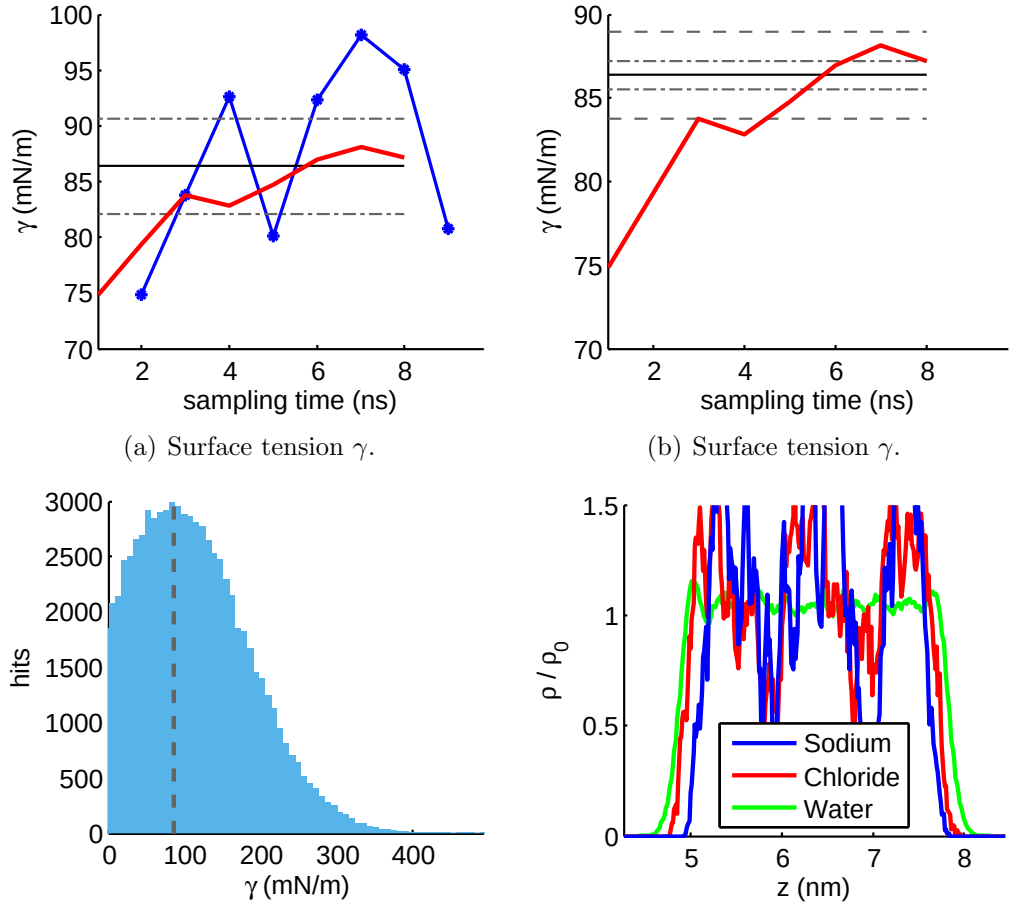

(a) Surface tension γ.

(b) Surface tension γ.

(c) Histogram of γ.

(d) Normalised density ρ/ρ_0.

Figure C.3: **(1 M 60 °C NaCl SW10e solution)** Summary of results obtained from a surface tension calculation. 19 NaCl ion pairs are dissolved in 1024 SPC/E water molecules, resulting in a salt concentration of roughly 1 M. The solution forms a slab of roughly 3 nm width, which is positioned in the centre of a simulation box of over 12 nm length. The corrected surface tension is 90.8 ± 5.82 mN/m. Further results are shown in Tab. 4.24. The temperature is 333.15 K. The total duration of the simulation is 20 ns including 1 ns equilibration time. a) Block average of the surface tension with 1 ns sampling time (blue line with asterisks) and running average of the surface tension (red line). The horizontal lines mark the mean surface tension (solid) and a ±5 % interval around it (grey dashed lines). b) Running average of the surface tension at 1 ns intervals (red line). The horizontal lines mark the mean surface tension (solid), a ±1 % interval around it (grey dashed-dotted lines) and a ±3 % interval around it (grey dashed lines). c) Histogram of the surface tension. The vertical dashed line marks the mean surface tension. d) Normalised density distribution of ionic species and water in the box.

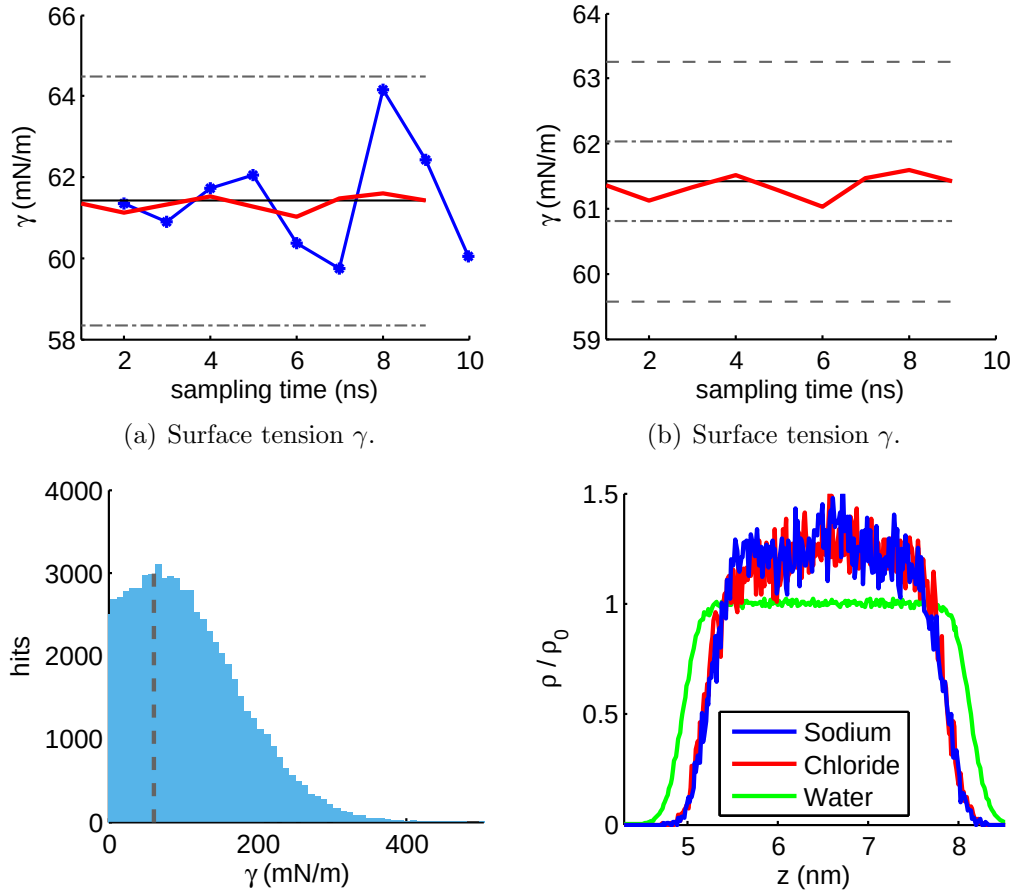

(a) Surface tension γ.

(b) Surface tension γ.

(c) Histogram of γ.

(d) Normalised density ρ/ρ_0.

Figure C.4: **(1 M 80 °C NaCl SW10e solution)** Summary of results obtained from a surface tension calculation. 19 NaCl ion pairs are dissolved in 1024 SPC/E water molecules, resulting in a salt concentration of roughly 1 M. The solution forms a slab of roughly 3 nm width, which is positioned in the centre of a simulation box of over 12 nm length. The corrected surface tension is 65.8 ± 0.90 mN/m. Further results are shown in Tab. 4.24. The temperature is 353.15 K. The total duration of the simulation is 20 ns including 1 ns equilibration time. a) Block average of the surface tension with 1 ns sampling time (blue line with asterisks) and running average of the surface tension (red line). The horizontal lines mark the mean surface tension (solid) and a $\pm 5\,\%$ interval around it (grey dashed lines). b) Running average of the surface tension at 1 ns intervals (red line). The horizontal lines mark the mean surface tension (solid), a $\pm 1\,\%$ interval around it (grey dashed-dotted lines) and a $\pm 3\,\%$ interval around it (grey dashed lines). c) Histogram of the surface tension. The vertical dashed line marks the mean surface tension. d) Normalised density distribution of ionic species and water in the box.

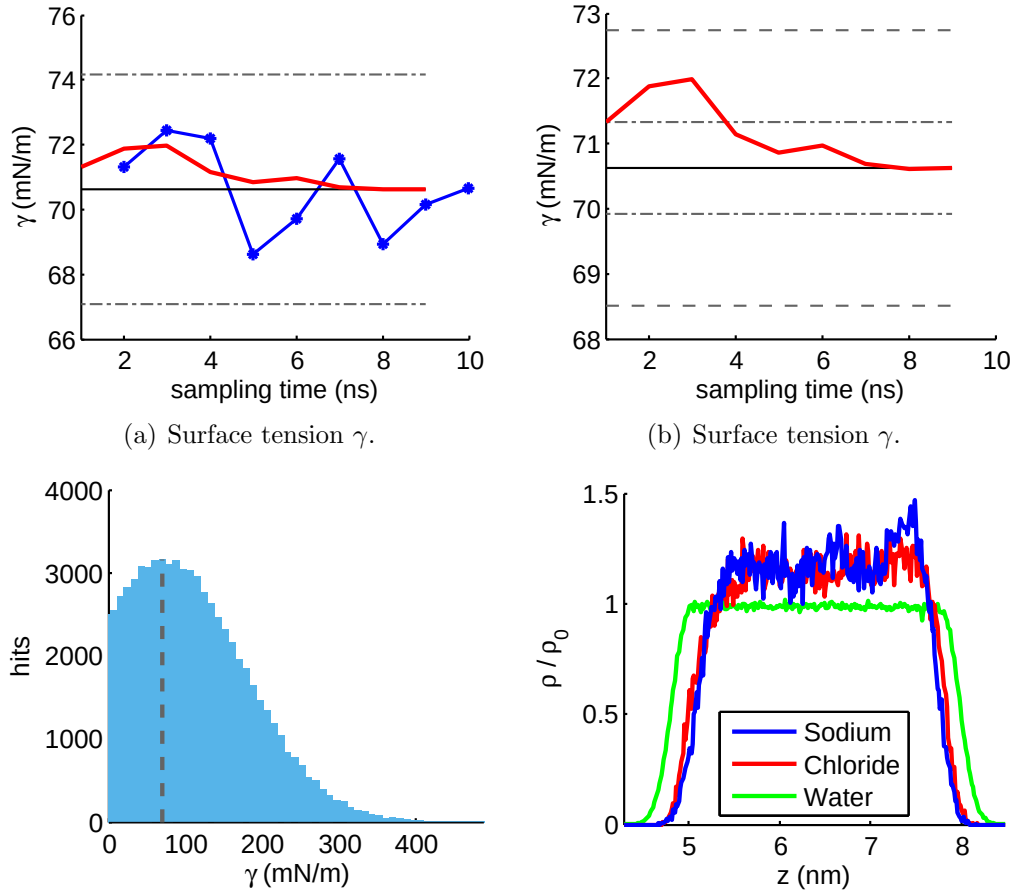

(a) Surface tension γ.

(b) Surface tension γ.

(c) Histogram of γ.

(d) Normalised density ρ/ρ_0.

Figure C.5: **(2 M 25 °C NaCl SW10e solution)** Summary of results obtained from a surface tension calculation. 38 NaCl ion pairs are dissolved in 1024 SPC/E water molecules, resulting in a salt concentration of roughly 1.9 M. The solution forms a slab of roughly 3 nm width, which is positioned in the centre of a simulation box of over 12 nm length. The corrected surface tension is 75.0 ± 0.90 mN/m. Further results are shown in Tab. 4.24. The temperature is 298.15 K. The total duration of the simulation is 20 ns including 1 ns equilibration time. a) Block average of the surface tension with 1 ns sampling time (blue line with asterisks) and running average of the surface tension (red line). The horizontal lines mark the mean surface tension (solid) and a $\pm 5\,\%$ interval around it (grey dashed lines). b) Running average of the surface tension at 1 ns intervals (red line). The horizontal lines mark the mean surface tension (solid), a $\pm 1\,\%$ interval around it (grey dashed-dotted lines) and a $\pm 3\,\%$ interval around it (grey dashed lines). c) Histogram of the surface tension. The vertical dashed line marks the mean surface tension. d) Normalised density distribution of ionic species and water in the box.

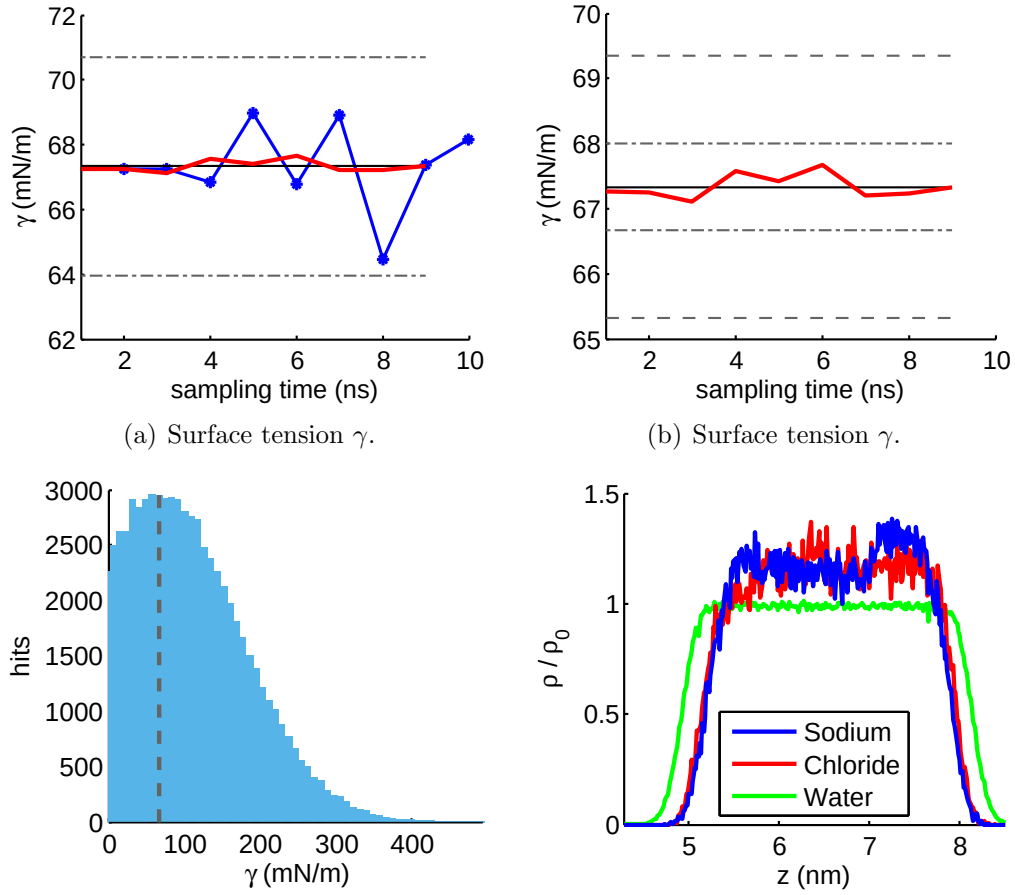

(a) Surface tension γ.

(b) Surface tension γ.

(c) Histogram of γ.

(d) Normalised density ρ/ρ_0.

Figure C.6: **(2 M 40 °C NaCl SW10e solution)** Summary of results obtained from a surface tension calculation. 38 NaCl ion pairs are dissolved in 1024 SPC/E water molecules, resulting in a salt concentration of roughly 1.9 M. The solution forms a slab of roughly 3 nm width, which is positioned in the centre of a simulation box of over 12 nm length. The corrected surface tension is 71.7 ± 0.89 mN/m. Further results are shown in Tab. 4.24. The temperature is 313.15 K. The total duration of the simulation is 20 ns including 1 ns equilibration time. a) Block average of the surface tension with 1 ns sampling time (blue line with asterisks) and running average of the surface tension (red line). The horizontal lines mark the mean surface tension (solid) and a $\pm 5\,\%$ interval around it (grey dashed lines). b) Running average of the surface tension at 1 ns intervals (red line). The horizontal lines mark the mean surface tension (solid), a $\pm 1\,\%$ interval around it (grey dashed-dotted lines) and a $\pm 3\,\%$ interval around it (grey dashed lines). c) Histogram of the surface tension. The vertical dashed line marks the mean surface tension. d) Normalised density distribution of ionic species and water in the box.

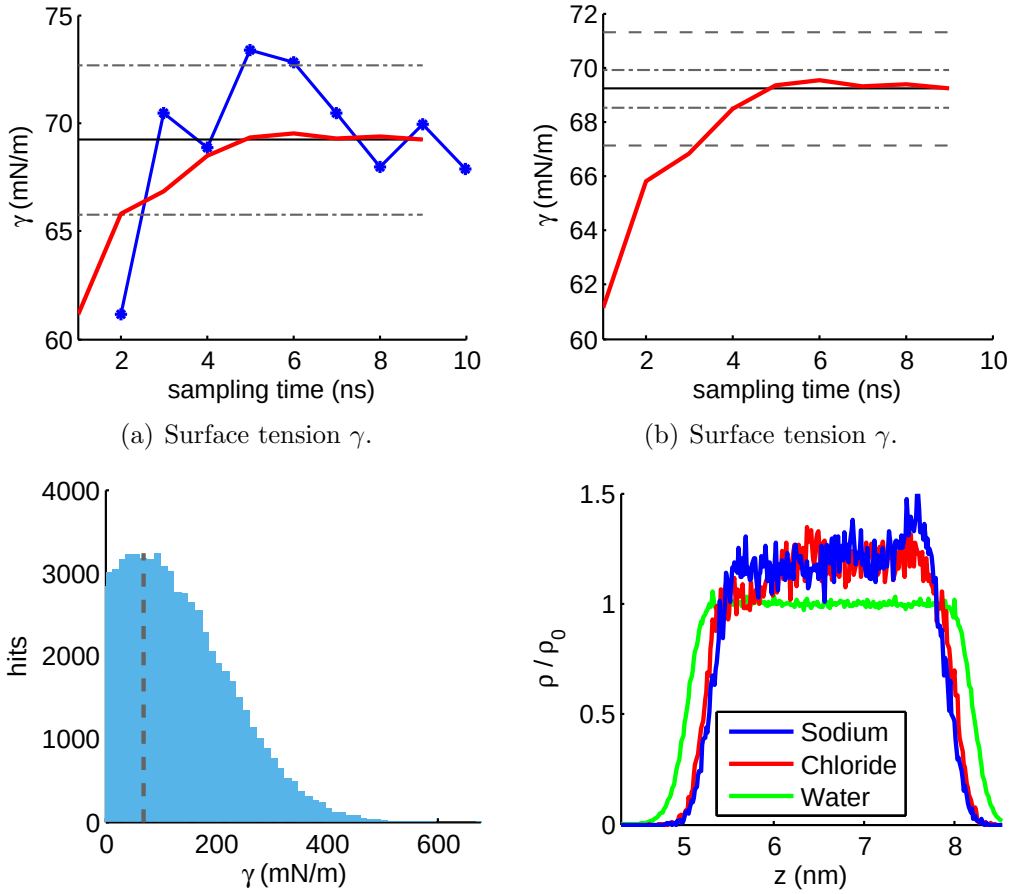

(a) Surface tension γ.

(b) Surface tension γ.

(c) Histogram of γ.

(d) Normalised density ρ/ρ_0.

Figure C.7: **(2 M 60 °C NaCl SW10e solution)** Summary of results obtained from a surface tension calculation. 38 NaCl ion pairs are dissolved in 1024 SPC/E water molecules, resulting in a salt concentration of roughly 1.9 M. The solution forms a slab of roughly 3 nm width, which is positioned in the centre of a simulation box of over 12 nm length. The corrected surface tension is 73.6 ± 2.34 mN/m. Further results are shown in Tab. 4.24. The temperature is 333.15 K. The total duration of the simulation is 20 ns including 1 ns equilibration time. a) Block average of the surface tension with 1 ns sampling time (blue line with asterisks) and running average of the surface tension (red line). The horizontal lines mark the mean surface tension (solid) and a $\pm 5\,\%$ interval around it (grey dashed lines). b) Running average of the surface tension at 1 ns intervals (red line). The horizontal lines mark the mean surface tension (solid), a $\pm 1\,\%$ interval around it (grey dashed-dotted lines) and a $\pm 3\,\%$ interval around it (grey dashed lines). c) Histogram of the surface tension. The vertical dashed line marks the mean surface tension. d) Normalised density distribution of ionic species and water in the box.

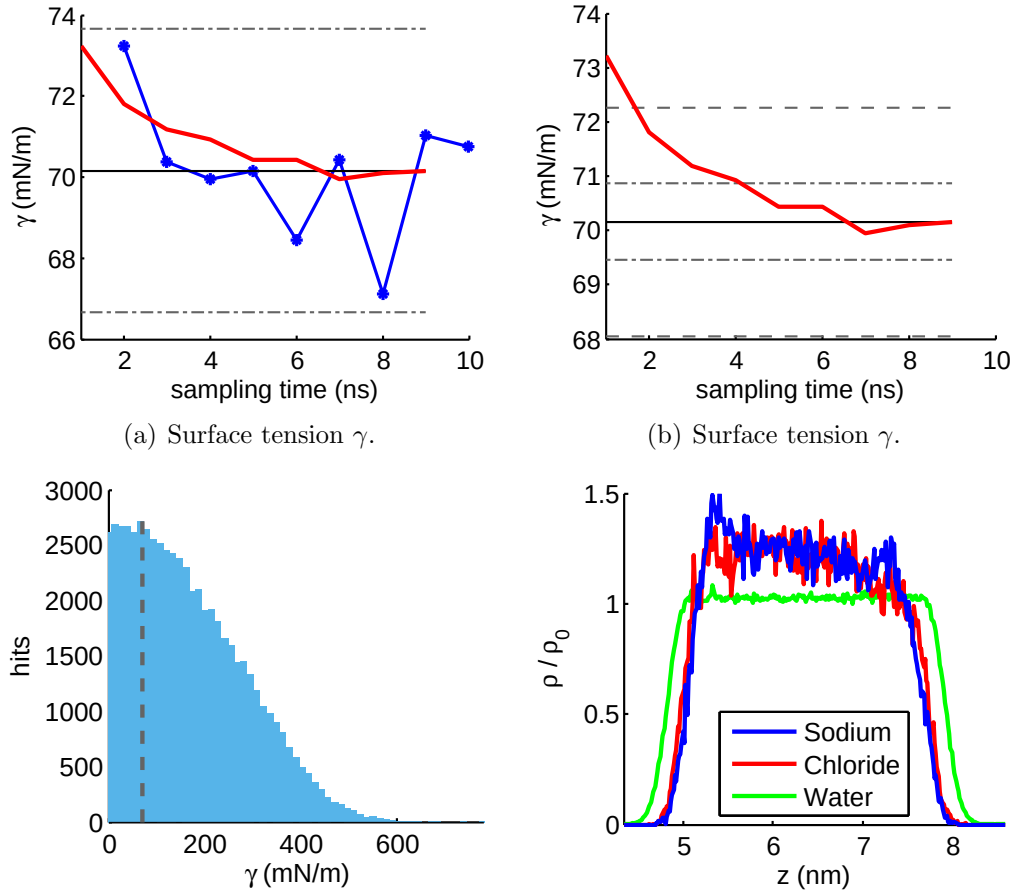

(a) Surface tension γ.

(b) Surface tension γ.

(c) Histogram of γ.

(d) Normalised density ρ/ρ_0.

Figure C.8: **(2 M 80 °C NaCl SW10e solution)** Summary of results obtained from a surface tension calculation. 38 NaCl ion pairs are dissolved in 1024 SPC/E water molecules, resulting in a salt concentration of roughly 1.9 M. The solution forms a slab of roughly 3 nm width, which is positioned in the centre of a simulation box of over 12 nm length. The corrected surface tension is 74.6 ± 1.11 mN/m. Further results are shown in Tab. 4.24. The temperature is 353.15 K. The total duration of the simulation is 20 ns including 1 ns equilibration time. a) Block average of the surface tension with 1 ns sampling time (blue line with asterisks) and running average of the surface tension (red line). The horizontal lines mark the mean surface tension (solid) and a $\pm 5\,\%$ interval around it (grey dashed lines). b) Running average of the surface tension at 1 ns intervals (red line). The horizontal lines mark the mean surface tension (solid), a $\pm 1\,\%$ interval around it (grey dashed-dotted lines) and a $\pm 3\,\%$ interval around it (grey dashed lines). c) Histogram of the surface tension. The vertical dashed line marks the mean surface tension. d) Normalised density distribution of ionic species and water in the box.

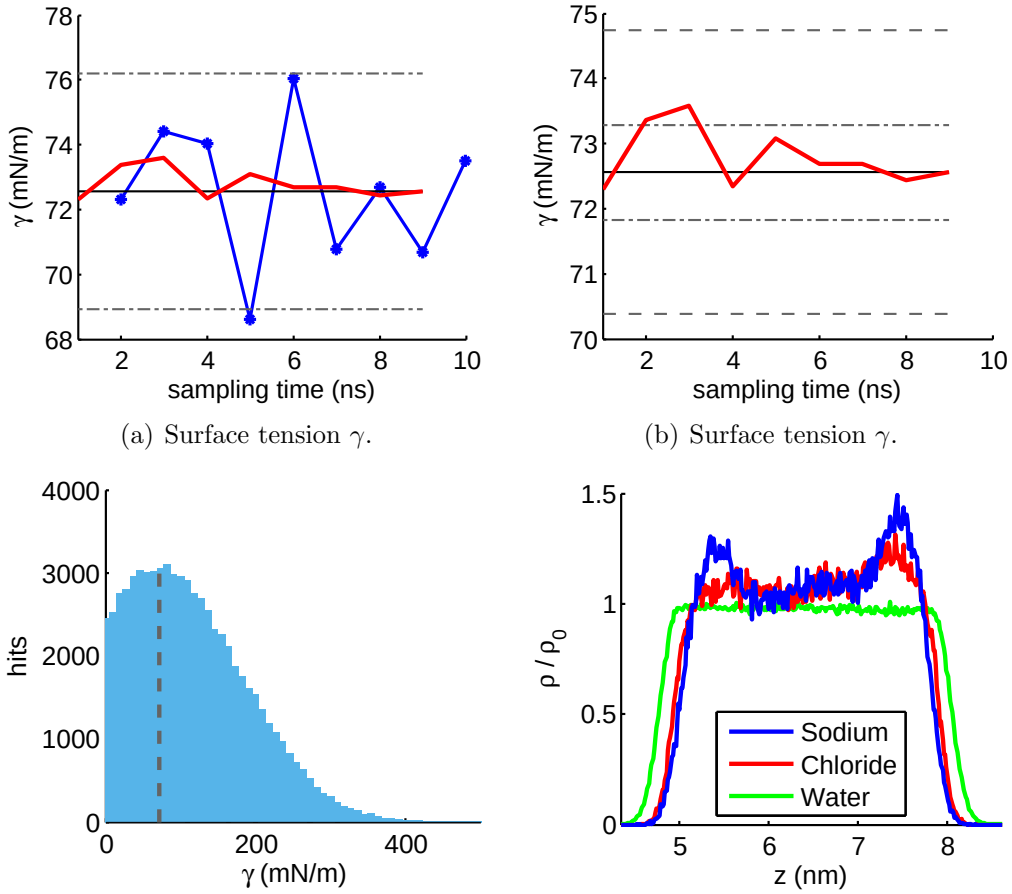

(a) Surface tension γ.

(b) Surface tension γ.

(c) Histogram of γ.

(d) Normalised density ρ/ρ_0.

Figure C.9: **(4 M 25 °C NaCl SW10e solution)** Summary of results obtained from a surface tension calculation. 76 NaCl ion pairs are dissolved in 1024 SPC/E water molecules, resulting in a salt concentration of roughly 3.6 M. The solution forms a slab of roughly 3 nm width, which is positioned in the centre of a simulation box of over 12 nm length. The corrected surface tension is 77.0 ± 1.49 mN/m. Further results are shown in Tab. 4.24. The temperature is 298.15 K. The total duration of the simulation is 20 ns including 1 ns equilibration time. a) Block average of the surface tension with 1 ns sampling time (blue line with asterisks) and running average of the surface tension (red line). The horizontal lines mark the mean surface tension (solid) and a $\pm 5\,\%$ interval around it (grey dashed lines). b) Running average of the surface tension at 1 ns intervals (red line). The horizontal lines mark the mean surface tension (solid), a $\pm 1\,\%$ interval around it (grey dashed-dotted lines) and a $\pm 3\,\%$ interval around it (grey dashed lines). c) Histogram of the surface tension. The vertical dashed line marks the mean surface tension. d) Normalised density distribution of ionic species and water in the box.

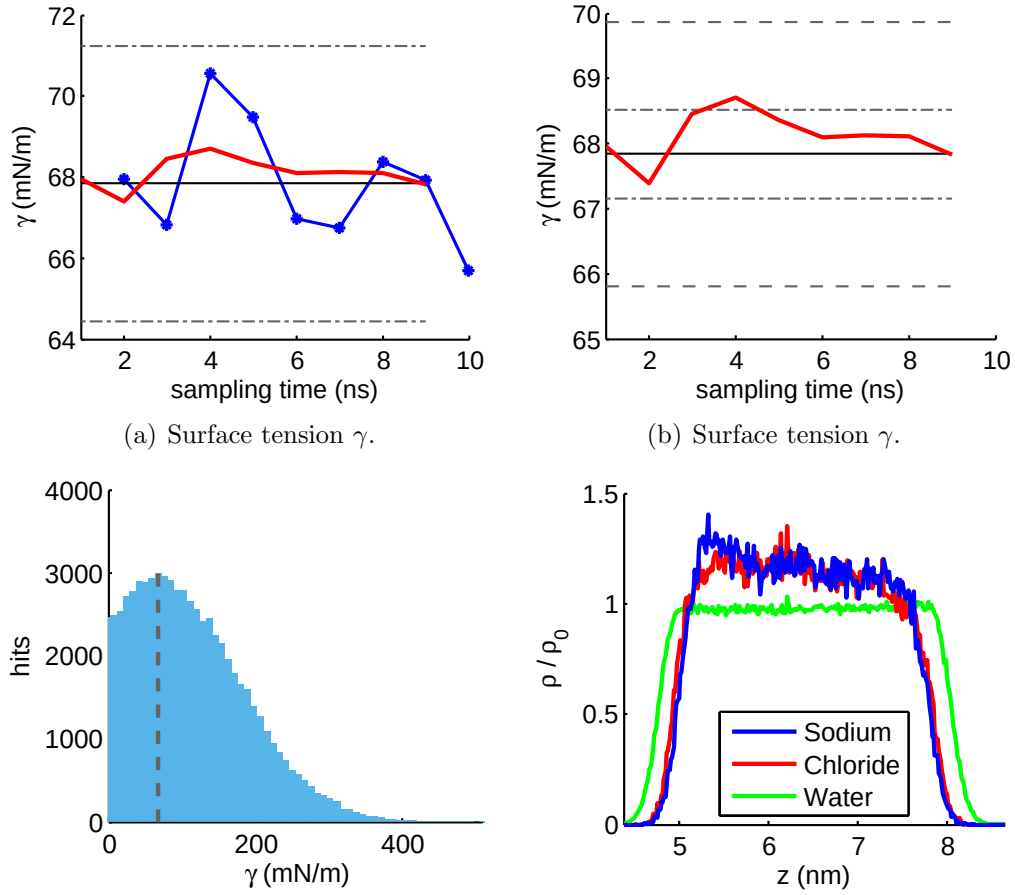

(a) Surface tension γ.

(b) Surface tension γ.

(c) Histogram of γ.

(d) Normalised density ρ/ρ_0.

Figure C.10: **(4 M 40 °C NaCl SW10e solution)** Summary of results obtained from a surface tension calculation. 76 NaCl ion pairs are dissolved in 1024 SPC/E water molecules, resulting in a salt concentration of roughly 3.6 M. The solution forms a slab of roughly 3 nm width, which is positioned in the centre of a simulation box of over 12 nm length. The corrected surface tension is 72.2 ± 0.98 mN/m. Further results are shown in Tab. 4.24. The temperature is 313.15 K. The total duration of the simulation is 20 ns including 1 ns equilibration time. a) Block average of the surface tension with 1 ns sampling time (blue line with asterisks) and running average of the surface tension (red line). The horizontal lines mark the mean surface tension (solid) and a $\pm 5\,\%$ interval around it (grey dashed lines). b) Running average of the surface tension at 1 ns intervals (red line). The horizontal lines mark the mean surface tension (solid), a $\pm 1\,\%$ interval around it (grey dashed-dotted lines) and a $\pm 3\,\%$ interval around it (grey dashed lines). c) Histogram of the surface tension. The vertical dashed line marks the mean surface tension. d) Normalised density distribution of ionic species and water in the box.

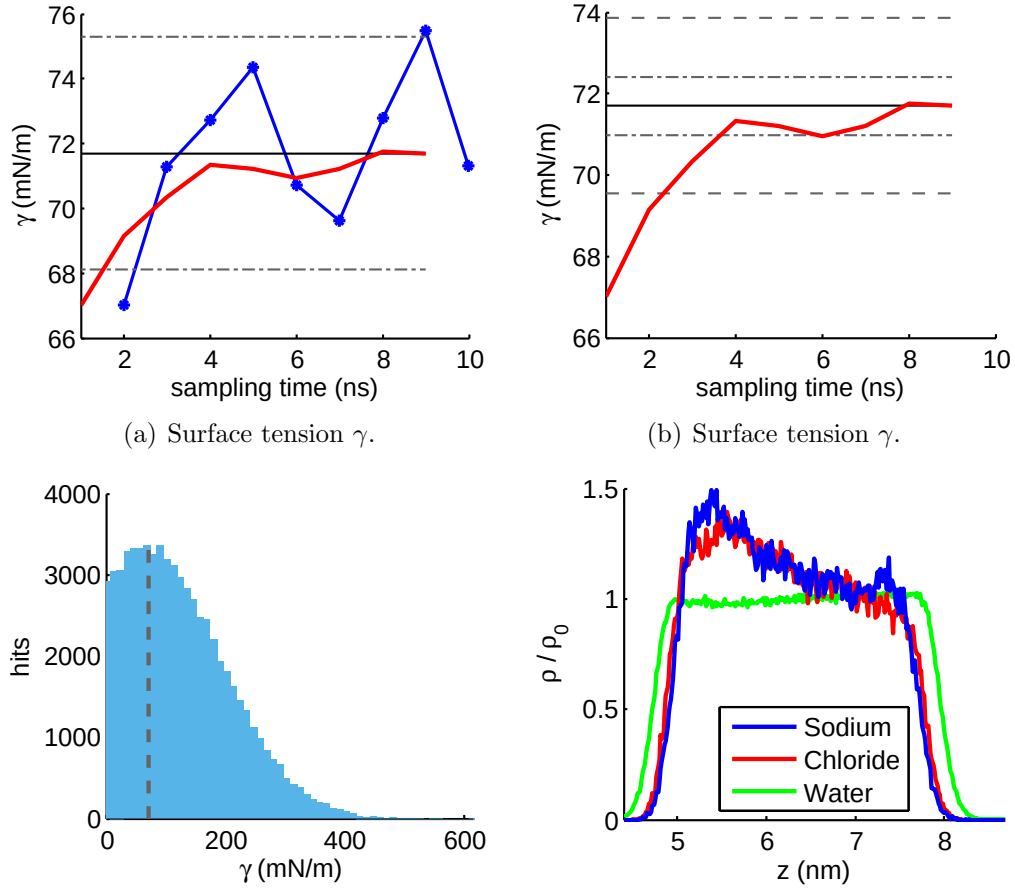

(a) Surface tension γ.

(b) Surface tension γ.

(c) Histogram of γ.

(d) Normalised density ρ/ρ_0.

Figure C.11: **(4 M 60 °C NaCl SW10e solution)** Summary of results obtained from a surface tension calculation. 76 NaCl ion pairs are dissolved in 1024 SPC/E water molecules, resulting in a salt concentration of roughly 3.6 M. The solution forms a slab of roughly 3 nm width, which is positioned in the centre of a simulation box of over 12 nm length. The corrected surface tension is 76.1 ± 1.66 mN/m. Further results are shown in Tab. 4.24. The temperature is 333.15 K. The total duration of the simulation is 20 ns including 1 ns equilibration time. a) Block average of the surface tension with 1 ns sampling time (blue line with asterisks) and running average of the surface tension (red line). The horizontal lines mark the mean surface tension (solid) and a $\pm 5\,\%$ interval around it (grey dashed lines). b) Running average of the surface tension at 1 ns intervals (red line). The horizontal lines mark the mean surface tension (solid), a $\pm 1\,\%$ interval around it (grey dashed-dotted lines) and a $\pm 3\,\%$ interval around it (grey dashed lines). c) Histogram of the surface tension. The vertical dashed line marks the mean surface tension. d) Normalised density distribution of ionic species and water in the box.

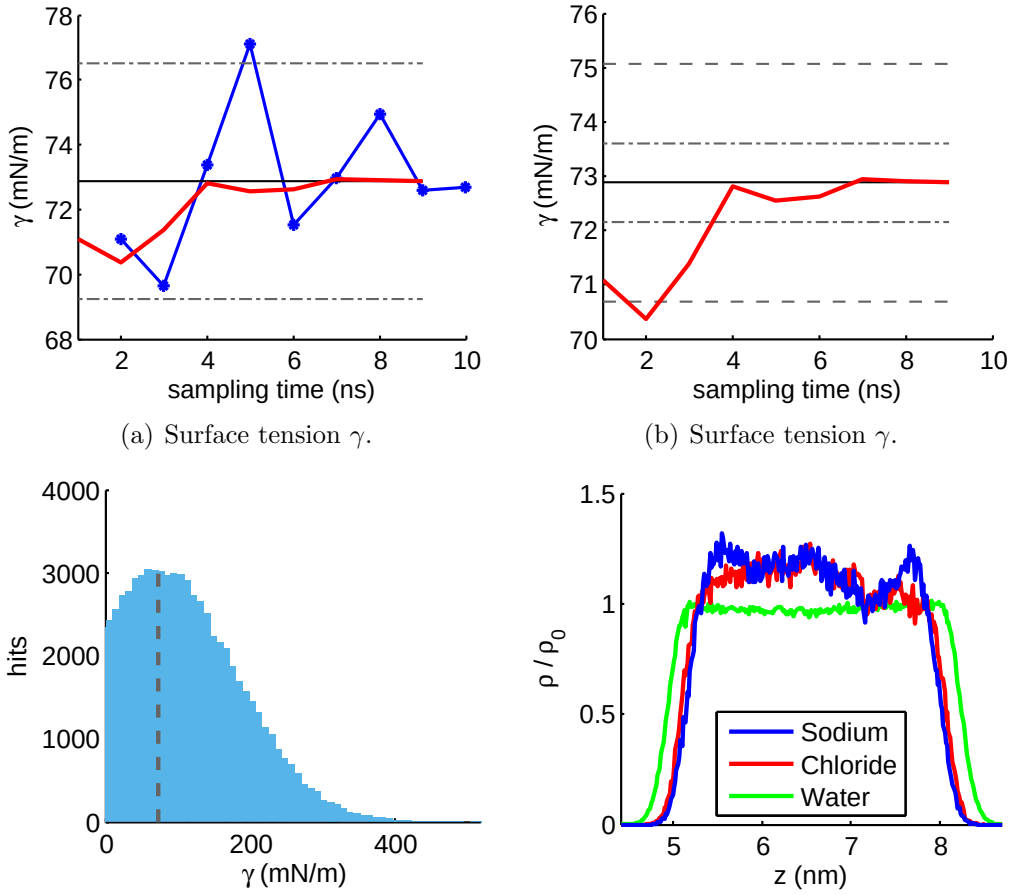

(a) Surface tension γ.

(b) Surface tension γ.

(c) Histogram of γ.

(d) Normalised density ρ/ρ_0.

Figure C.12: **(5 M 25 °C NaCl SW10e solution)** Summary of results obtained from a surface tension calculation. 94 NaCl ion pairs are dissolved in 1024 SPC/E water molecules, resulting in a salt concentration of roughly 4.3 to 4.5 M. The solution forms a slab of roughly 3 nm width, which is positioned in the centre of a simulation box of over 12 nm length. The corrected surface tension is 77.3 ± 1.43 mN/m. Further results are shown in Tab. 4.24. The temperature is 298.15 K. The total duration of the simulation is 20 ns including 1 ns equilibration time. a) Block average of the surface tension with 1 ns sampling time (blue line with asterisks) and running average of the surface tension (red line). The horizontal lines mark the mean surface tension (solid) and a ±5 % interval around it (grey dashed lines). b) Running average of the surface tension at 1 ns intervals (red line). The horizontal lines mark the mean surface tension (solid), a ±1 % interval around it (grey dashed-dotted lines) and a ±3 % interval around it (grey dashed lines). c) Histogram of the surface tension. The vertical dashed line marks the mean surface tension. d) Normalised density distribution of ionic species and water in the box.

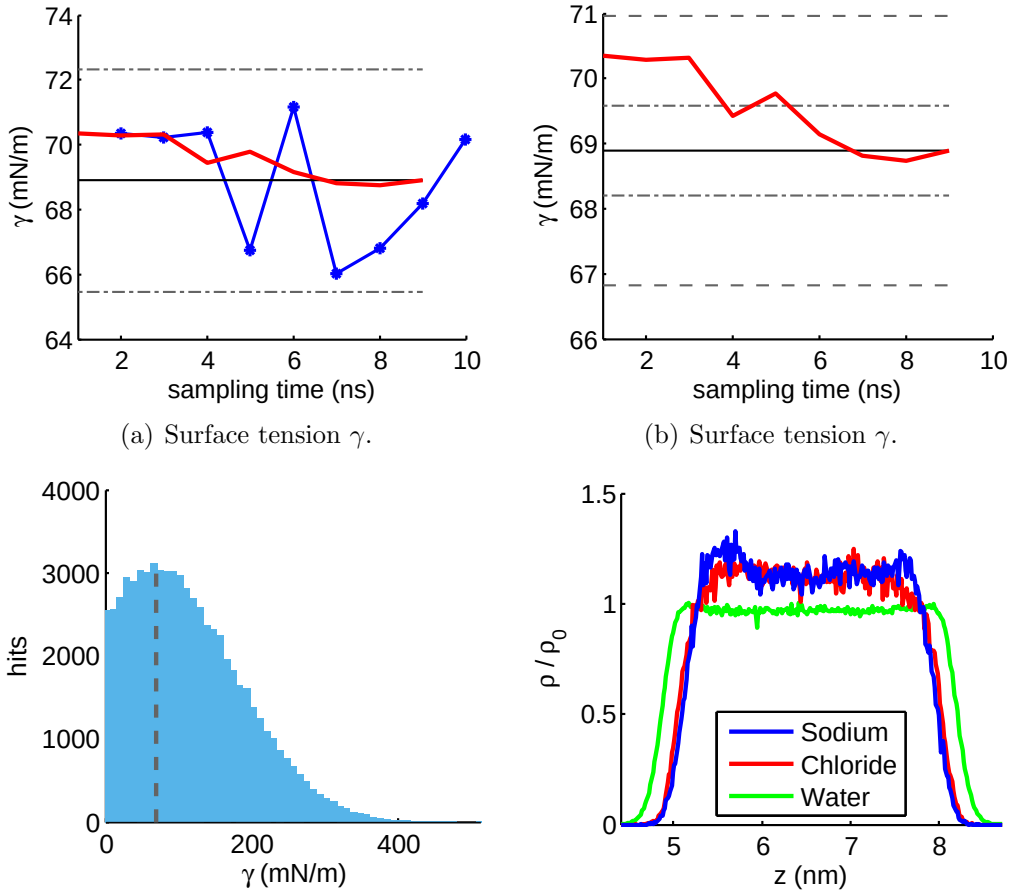

(a) Surface tension γ.

(b) Surface tension γ.

(c) Histogram of γ.

(d) Normalised density ρ/ρ_0.

Figure C.13: **(5 M 40 °C NaCl SW10e solution)** Summary of results obtained from a surface tension calculation. 94 NaCl ion pairs are dissolved in 1024 SPC/E water molecules, resulting in a salt concentration of roughly 4.3 to 4.5 M. The solution forms a slab of roughly 3 nm width, which is positioned in the centre of a simulation box of over 12 nm length. The corrected surface tension is 73.3 ± 1.28 mN/m. Further results are shown in Tab. 4.24. The temperature is 313.15 K. The total duration of the simulation is 20 ns including 1 ns equilibration time. a) Block average of the surface tension with 1 ns sampling time (blue line with asterisks) and running average of the surface tension (red line). The horizontal lines mark the mean surface tension (solid) and a ±5 % interval around it (grey dashed lines). b) Running average of the surface tension at 1 ns intervals (red line). The horizontal lines mark the mean surface tension (solid), a ±1 % interval around it (grey dashed-dotted lines) and a ±3 % interval around it (grey dashed lines). c) Histogram of the surface tension. The vertical dashed line marks the mean surface tension. d) Normalised density distribution of ionic species and water in the box.

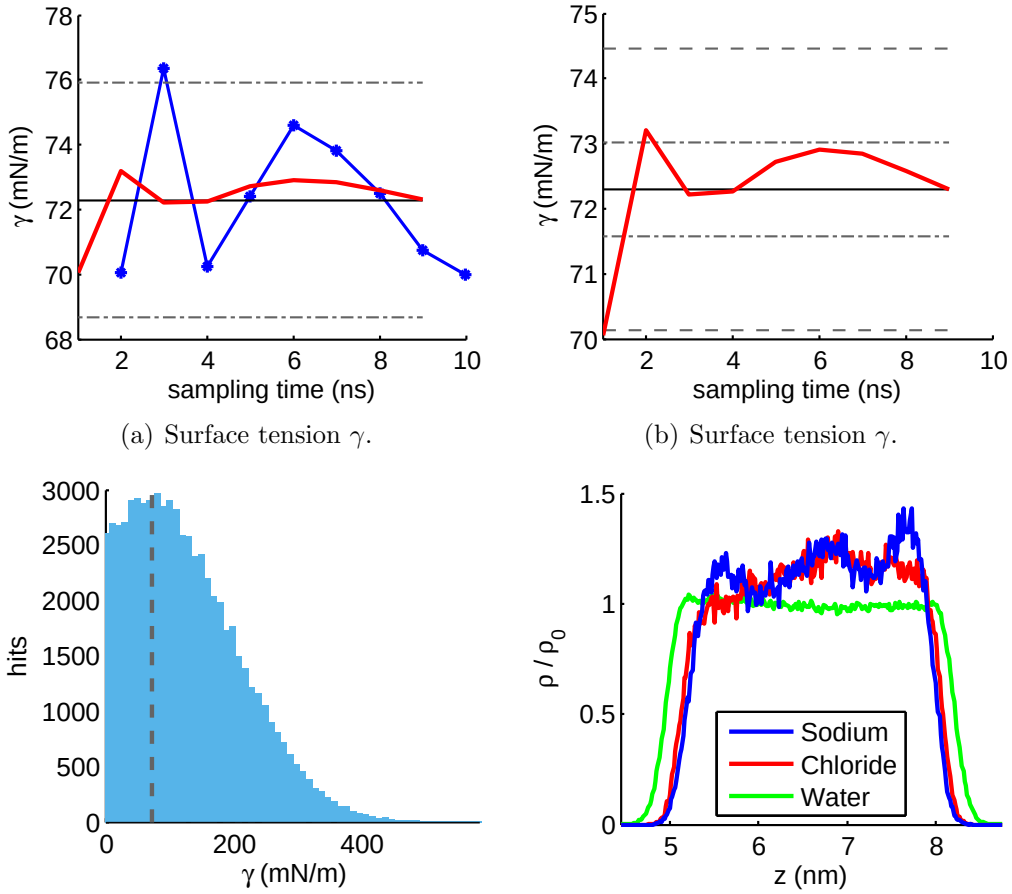

(a) Surface tension γ.

(b) Surface tension γ.

(c) Histogram of γ.

(d) Normalised density ρ/ρ_0.

Figure C.14: **(5 M 60 °C NaCl SW10e solution)** Summary of results obtained from a surface tension calculation. 94 NaCl ion pairs are dissolved in 1024 SPC/E water molecules, resulting in a salt concentration of roughly 4.3 to 4.5 M. The solution forms a slab of roughly 3 nm width, which is positioned in the centre of a simulation box of over 12 nm length. The corrected surface tension is 76.7 ± 1.49 mN/m. Further results are shown in Tab. 4.24. The temperature is 333.15 K. The total duration of the simulation is 20 ns including 1 ns equilibration time. a) Block average of the surface tension with 1 ns sampling time (blue line with asterisks) and running average of the surface tension (red line). The horizontal lines mark the mean surface tension (solid) and a ±5 % interval around it (grey dashed lines). b) Running average of the surface tension at 1 ns intervals (red line). The horizontal lines mark the mean surface tension (solid), a ±1 % interval around it (grey dashed-dotted lines) and a ±3 % interval around it (grey dashed lines). c) Histogram of the surface tension. The vertical dashed line marks the mean surface tension. d) Normalised density distribution of ionic species and water in the box.

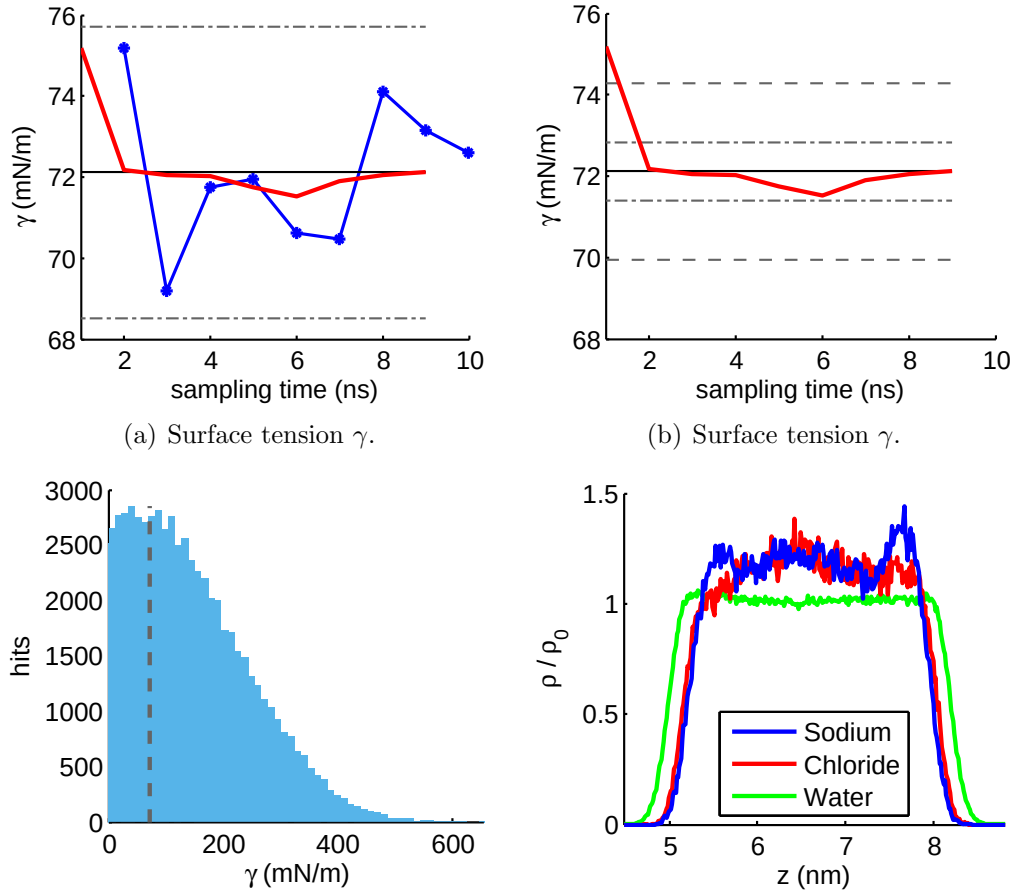

(a) Surface tension γ.

(b) Surface tension γ.

(c) Histogram of γ.

(d) Normalised density ρ/ρ_0.

Figure C.15: **(5 M 80 °C NaCl SW10e solution)** Summary of results obtained from a surface tension calculation. 94 NaCl ion pairs are dissolved in 1024 SPC/E water molecules, resulting in a salt concentration of roughly 4.3 to 4.5 M. The solution forms a slab of roughly 3 nm width, which is positioned in the centre of a simulation box of over 12 nm length. The corrected surface tension is 76.5 ± 1.23 mN/m. Further results are shown in Tab. 4.24. The temperature is 353.15 K. The total duration of the simulation is 20 ns including 1 ns equilibration time. a) Block average of the surface tension with 1 ns sampling time (blue line with asterisks) and running average of the surface tension (red line). The horizontal lines mark the mean surface tension (solid) and a ±5 % interval around it (grey dashed lines). b) Running average of the surface tension at 1 ns intervals (red line). The horizontal lines mark the mean surface tension (solid), a ±1 % interval around it (grey dashed-dotted lines) and a ±3 % interval around it (grey dashed lines). c) Histogram of the surface tension. The vertical dashed line marks the mean surface tension. d) Normalised density distribution of ionic species and water in the box.